ABSTRACT

Title of Dissertation: MULTIPLE SULFUR ISOTOPE FRACTIONATIONS IN INORGANIC AQUEOUS SYSTEMS

Daniel Lee Eldridge, Doctor of Philosophy, 2016

Dissertation directed by: Professor James Farquhar, Department of Geology

New constraints on isotope fractionation factors in inorganic aqueous sulfur systems based on theoretical and experimental techniques relevant to studies of the sulfur cycle in modern environments and the geologic rock record are presented in this dissertation. These include theoretical estimations of equilibrium isotope fractionation factors utilizing quantum mechanical software and a water cluster model approach for aqueous sulfur compounds that span the entire range of oxidation state for sulfur. These theoretical calculations generally reproduce the available experimental determinations from the literature and provide new constraints where no others are available. These theoretical calculations illustrate in detail the relationship between sulfur bonding environment and the mass dependence associated with equilibrium isotope exchange reactions involving all four isotopes of sulfur. I additionally highlight the effect of isomers of protonated compounds (compounds with the same chemical formula but different structure, where protons are bound to

either sulfur or oxygen atoms) on isotope partitioning in the sulfite (S^{4+}) and sulfoxylate (S^{2+}) systems, both of which are key intermediates in oxidation-reduction processes in the sulfur cycle. I demonstrate that isomers containing the highest degree of coordination around sulfur (where protonation occurs on the sulfur atom) have a strong influence on isotopic fractionation factors, and argue that isomerization phenomenon should be considered in models of the sulfur cycle. Additionally, experimental results of the reaction rates and isotope fractionations associated with the chemical oxidation of aqueous sulfide are presented. Sulfide oxidation is a major process in the global sulfur cycle due largely to the sulfide-producing activity of anaerobic microorganisms in organic-rich marine sediments. These experiments reveal relationships between isotope fractionations and reaction rate as a function of both temperature and trace metal (ferrous iron) catalysis that I interpret in the context of the complex mechanism of sulfide oxidation. I also demonstrate that sulfide oxidation is a process associated with a mass dependence that can be described as not conforming to the mass dependence typically associated with equilibrium isotope exchange. This observation has implications for the inclusion of oxidative processes in environmental- and global-scale models of the sulfur cycle based on the mass balance of all four isotopes of sulfur. The contents of this dissertation provide key reference information on isotopic fractionation factors in aqueous sulfur systems that will have far-reaching applicability to studies of the sulfur cycle in a wide variety of natural settings.

MULTIPLE SULFUR ISOTOPE FRACTIONATIONS IN INORGANIC AQUEOUS SYSTEMS

by

Daniel Lee Eldridge

Dissertation submitted to the Faculty of the Graduate School of the
University of Maryland, College Park, in partial fulfillment
of the requirements for the degree of
Doctor of Philosophy
2016

Advisory Committee:
Professor James Farquhar, Chair
Professor Alan Jay Kaufman
Professor Sujay Kaushal
Professor Karen Prestegaard
Professor Russell Dickerson

Foreword

The contents of Chapter 2 comprise a manuscript that has been submitted to *Geochimica et Cosmochimica Acta*:

Eldridge D.L., Guo W., and Farquhar J., Theoretical estimates of equilibrium sulfur isotope effects in aqueous sulfur systems: Highlighting the role of isomers in the sulfite and sulfoxylate systems. *Geochimica et Cosmochimica Acta* (submitted).

I constructed all molecular clusters utilizing Gaussian 09 software (Frisch et al., 2010) installed on the desktop computer in the J. Farquhar laboratory with substantial early input from J. Farquhar on cluster building methodology. I additionally ran most of the optimization and frequency calculations on this same system. Some of the calculations (those in the sulfite system, S^{4+}) were run for optimization and frequency calculations on the high performance Scylla computer cluster at WHOI with assistance from W. Guo to expedite data acquisition. I performed all data processing, prepared and analyzed results, prepared plots, and made all comparisons (and related calculations) of my theoretical calculations to experimental datasets. I wrote the manuscript with input to drafts from both W. Guo and J. Farquhar. The manuscript is "under review" at the time of the submission of this dissertation.

Acknowledgements

I acknowledge a NASA Earth and Space Sciences Fellowship (awarded 2012-2015) that supported me for much of my dissertation (NNX12AL77H). I additionally acknowledge an NSF grant (awarded to J. Farquhar) that I wrote with my advisor that supported much of the research presented in this dissertation (NSF grant 1361945: Sulfur isotope studies of sulfide oxidation).

My advisor, Professor James Farquhar, is thanked for all of his generous and thoughtful brainstorming and support over the years, especially throughout the experimental work that often seemed grueling and unrewarding. Without his enthusiastic encouragement and insight, none of the work contained in this dissertation would have been possible. I am especially grateful for his emphasis on teaching the fundamentals to his students that made the study of Chapter 2 possible.

The past and present Farquhar laboratory cohort is additionally thanked and acknowledged for friendship, moral support, and solidarity over the years (in no particular order or completeness: J. Hoek, J. Labidi, H. Oduro, J. Dottin III, M. Antonelli, E. Gautier, A. Kamyshny, A. Zerkle, Z. Mansaray, B. Harms, and so many others). I believe much of the research contained in this dissertation would not have been as much fun without their friendship and presence in the lab over the years. A. Kamyshny is thanked especially for his analytical expertise and guidance with HPLC methods and protocol, and for acting as a gracious host during my visit to Israel (and especially for introducing me to Georgian food in Jerusalem). Dr. Kamyshny is additionally acknowledged as providing the idea that the isotope effects associated with sulfide oxidation be revisited that led to the study of Chapter 3. I am also

thankful for the efforts of the high school students (Diandre Sheridan, Anisha Hosadurga) and UMD undergraduates (Noah Bowman) that I was lucky enough to act as mentor to throughout my tenure at UMD. The heroic experimental efforts of N. Bowman for his senior research thesis especially helped to improve the experimental design of the sulfide oxidation experiments presented in Chapter 3.

Conversations and input from the late John ("Jack") Tossell regarding theoretical calculations of aqueous sulfur compounds (Chapter 2) were instrumental in getting this work off of the ground.

I additionally acknowledge the never-ending support of my loving family. I especially thank my dad, Steve Eldridge, who pushed me into attending community college as a late teenager. It was at Red Rocks Community College that I discovered a love of learning, and developed my early appreciation for geology and chemistry. I learned through these experiences to open my eyes to the natural landscape of the Denver basin and surrounding foothills, and wonder what lies beneath (as it turns out, it's a bunch of rocks).

Table of Contents

List of Tables

List of Figures

Chapter 1: Introduction and Motivation

1.0 Broad Overview

The chemical elements are typically what we think of as the "stuff" that makes up the universe. They can combine to form numerous molecular, crystalline, and other substances that comprise not only our own bodies, but also the countless celestial bodies that make the day and nighttime sky shine. Chemical elements in their atomic form are comprised of a nucleus and some electrons. The nucleus is made up of a mash-up of protons and neutrons, and the number of protons in the nucleus defines the chemical element. For example, the chemical element containing 6 protons in its nucleus is known as "carbon", the chemical element containing 16 protons is known as "sulfur", the chemical element containing 26 protons is known as "iron", and so on. Elements in their atomic and neutral form have as many electrons as protons. The number of electrons an element has comprises its electronic structure, and controls the reactivity and bond-forming capability of the chemical element. Due to the systematic and periodic ways in which electrons comprise the electronic structure of elements, elements follow patterns of chemical reactivity that forms the basis of the organization of the modern periodic table.

Isotopes are different atomic versions of the same chemical element that differ only in the mass of their nucleus. As you can probably guess, the mass difference arises from the number of neutrons in the nucleus. Of the 92 naturally occurring chemical elements, only 22 are known to exist as a single nuclidic version, and so isotopes are a very common feature of the chemical elements. Isotopes can be

regarded as either “stable” or “not stable” (or “radioactive”), and the difference between the two is mostly operative. Practically speaking, radioactive isotopes are those that undergo decay to other isotopes of elements due to fundamental instabilities in the nucleus over timescales that are practical to measure. The abundances and distributions of radioactive isotopes and the products of their decay (called radiogenic isotopes) vary in nature due to this radioactive decay. These variations are a function of the age of the substance that contains the radioactive/radiogenic isotopes, and the age of the substance can be quantified by the relative abundances of these isotopes in the substance as we find them today. Stable isotopes, on the other hand, do not undergo any appreciable radioactive decay over geologic timescales and their distribution among substances in nature can vary due to physical, chemical, and biological processes. The difference in isotope composition that accompanies such a process is generally referred to as an isotope fractionation. Stable isotopes, while not being very useful for determining the age of stuff, are very useful for investigative purposes to understand how things formed. If we can understand how the physical, chemical, and biological processes that operate in nature affect the distribution of stable isotopes among naturally occurring substances, we may have a tool-kit in place with which we can understand the past by studying material in the present.

Geochemists typically study the elemental and isotopic composition of the Earth and its components in order to try to understand what it’s made of, how it formed, what it formed from, and the nature of the transformations it has undergone since its formation. Some geochemists may be interested in the chemical elemental

budget of the Earth's metallic core, while others may be interested in the composition of the Earth's rocky mantle. Others are interested in the chemical composition of the Earth's crust, since it is where we find most of the elements that make up the stuff we enjoy (like the computer I used to type this sentence!). Others may be interested in how the Earth came to have these primary layers in the first place, and the precise details of when and the dynamics of how all of that business happened. The study and application of isotopes can aid each of these investigations. Since the Earth is not isolated in space and is a component of the larger Solar System, these studies extend beyond Earth and to the study of extraterrestrial materials that come to us largely in the form of meteorites, and can form an important baseline for comparison to the Earth. Fueled by my undergraduate thesis studies (Templeton et al., 2009), I became interested in the history of life on Earth and the myriad ways in which the development and flourishment of life has shaped the Earth's surface throughout geologic time. After all, isn't that the story we're all interested in, the story of "us"?

The major players in the history of life on Earth are largely understood to be microbial. As much as we would like to think that we (*Homo sapiens sapiens*) are running the show, we are very much latecomers in the play of life on Earth. Life may have first evolved on Earth somewhere in the ballpark of 3.5-4.0 billion years ago, and modern humans have barely been around on the order of hundreds of thousands of years. If life began at the Golden Gate Bridge in San Francisco and has made it as far as the Washington Monument in Washington, D.C. to date, humans evolved as part of the journey somewhere in the vicinity of the National WWII Memorial (for those that are unfamiliar with the National Mall, these two monuments are across the

street from one another!). In this analogy, hard bodied animals that can form appreciable fossils did not appear in the record of the journey until somewhere in the vicinity of Cleveland, OH (assuming life took I-80 East most of the way!). Microorganisms are the ones that have both made the entire journey and in many ways have made various aspects of the journey possible. They fall into two of the three conventionally considered domains of life: bacteria and archaea.

The notebook that the Earth has used to record much of its surface history is what geologists and geochemists generally refer to as the "sedimentary rock record". Most of the sedimentary rocks that comprise this notebook formed in aqueous environments where life may proliferate. The scribes of this history are the processes that shaped this rock record, including its mineralogical, chemical, and isotopic composition. Microbial authors have been major contributors to this notebook, and at least one of the many languages they've written in has been isotopic. The chemical elements that encode this isotopic information are of course those that are essential for life in one way or another.

The major elements required for life as we know it are sometimes colloquially referred to as the "SPONCH" elements, a wonky acronym comprised of chemical symbols. The "S" in "SPONCH" of course refers to the element sulfur (I'll let the reader guess the rest!), and is the major focus of this dissertation. Sulfur is comprised of 4 stable isotopes (^{32}S, ^{34}S, ^{33}S, ^{36}S, in order of decreasing relative abundance in our Solar System) and has 8 available oxidation states that range from S^{2-} to S^{6+}. Oxidation state is defined as the formal charge of the atom (computed by simply taking the difference between the number of electrons and protons in the element),

and further controls the bond-forming capability and reactivity of the element. In simple terms, the more oxidation states that are available to an element, the more diverse and complex the nature of its reactivity towards other elements and compounds. The diversity of oxidation states and isotopes that make up sulfur, in addition to its biological importance, make it one of the most interesting and exciting elements to study in Earth's surface environment.

The components of the modern Earth's surface sulfur cycle that may have the greatest influence on the isotopic aspects of the rock record—and, thus, our understanding of important aspects of the history of life on Earth—are highlighted in Figure 1.1. Among the major features of the sulfur cycle featured in Figure 1.1 is microbial sulfate reduction (or MSR for short). MSR is a metabolism carried out by numerous bacteria and archaea that couples the overall oxidation of organic matter to the reduction of sulfate (SO_4^{2-}), producing sulfide (e.g., H_2S) as a waste product. Since sulfate is used as the terminal electron acceptor rather than molecular oxygen (O_2), we call this an *anaerobic* respiration process. Respiration processes in general can be thought of as the complimentary set of processes to those associated with primary production that are responsible for the generation of organic carbon (the make-up of organisms) from inorganic carbon. The balance of these two general sets of processes (primary production and respiration) is critically important to the habitability of the Earth's surface for many organisms. For example, the fundamental imbalance between the two is what allows molecular oxygen (O_2; a byproduct of oxygenic photosynthesis, a major aspect of primary production) to linger in the surface environment for us to breathe.

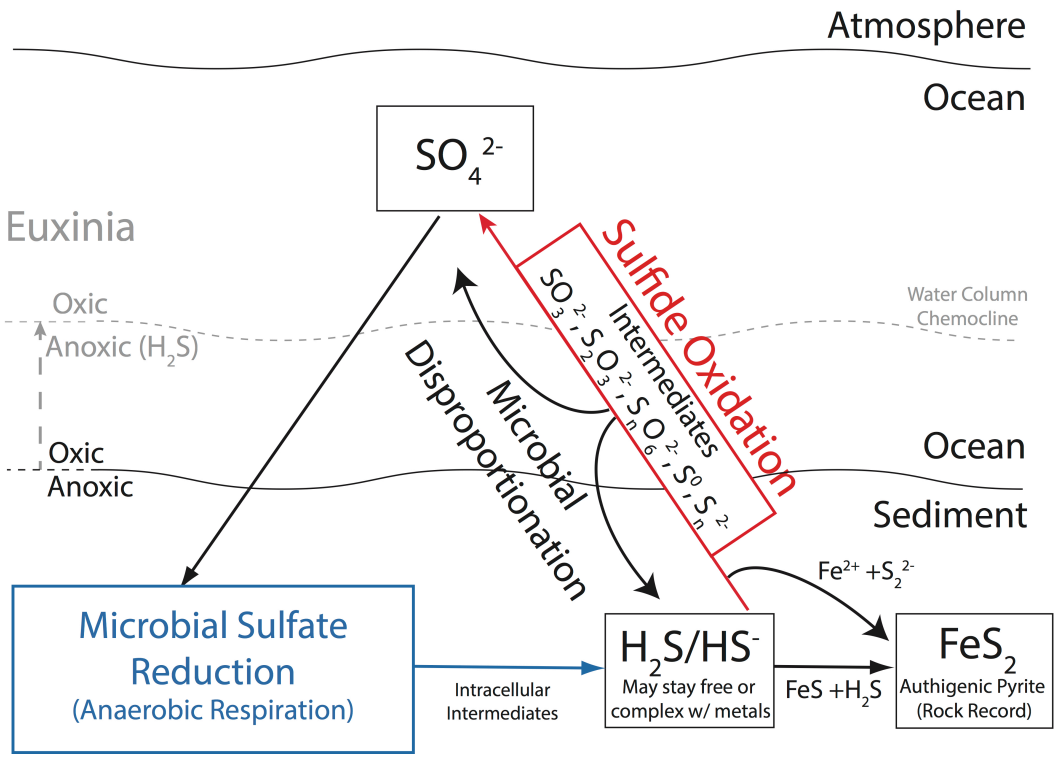

Figure 1.1: Schematic diagram illustrating some of the major features of the modern marine sulfur cycle, which is microbially dominated. Oxidation processes may be either chemical or biological.

Aerobic respiration processes seem to dominate much of the present respiration budget, but the anaerobic process of microbial sulfate reduction is second in line due to the high abundance of sulfate in the oceans. In terms of dissolved anions, sulfate is second in abundance only to chloride in seawater and is by far much more concentrated in the oceans than molecular oxygen. Recent models based on sulfate concentrations profiles in a large collection of globally distributed seafloor drill cores indicate that microbial sulfate reduction accounts for 12-29% of the respiration of the organic muck that rains out of the water column to the seafloor per year (Bowles et al., 2014). MSR is therefore not only a major feature of the global sulfur cycle, it's also a major geochemical process that is intimately tied to the global carbon cycle. Since the product of microbial sulfate reduction is hydrogen sulfide, it

is straightforward to realize that microbial sulfide production is also a global geochemical process. The generation and fate of this microbially produced sulfide is ultimately what makes the global sulfur cycle so complex, and allows us to examine the sulfur cycle as it operated in the past via its entrapment in minerals that can survive in sedimentary rocks throughout the ages.

From studies of modern coastal marine sediments, it appears that most of the sulfide produced by microbial sulfate reduction is ultimately oxidized back to sulfate (~80-95%; Jørgensen, 1977; Jørgensen, 1982; Jørgensen et al., 1990; Canfield and Teske, 1996; Jørgensen and Nelson, 2004), with very little of the sulfide being tied up (or left behind) in mineral form (~5-20%). This further straightforwardly indicates that sulfide oxidation processes may be just as major of a geochemical process as MSR itself. The primary sulfur mineral that may be left behind from the complex sulfur cycle in sediments is pyrite, which when formed *in situ* is termed "authigenic" pyrite (this qualifier distinguishes pyrite generated this way from pyrite that may have formed in a magma chamber as a rock crystallized, which would have no biological influence). The isotopic information encoded in authigenic pyrite reflects the myriad of sulfur cycling processes that are shown in Figure 1.1, including the biological and chemical aspects of this cycle. Understanding the details of what controls isotopic fractionation during these processes is critical in deciphering the isotopic pyrite record, and sulfur cycling processes in general.

The research that is presented in this dissertation provides fundamental calibrations of isotope effects that may be used to decipher the complexities of isotope fractionations among naturally occurring sulfur compounds in aqueous

environments. To illustrate this further, I show in Figure 1.2 cartoon diagrams of two examples of the two major features of the sulfur cycle that I've discussed above: the reductive sulfur cycle (represented as a sulfur-centric cellular schematic of a sulfate reducer) and the oxidative sulfur cycle (represented as a schematic chemical mechanism of sulfide oxidation by molecular oxygen). Highlighted in color shapes are the various isotopic fractionations among aqueous sulfur compounds that I've attempted to constrain in this dissertation. These constraints provide critical information that will inform models of the sulfur cycle from the cellular level up to the global level. More detailed and specific descriptions of these determinations and their motivation are provided in the remaining sections of this introductory chapter.

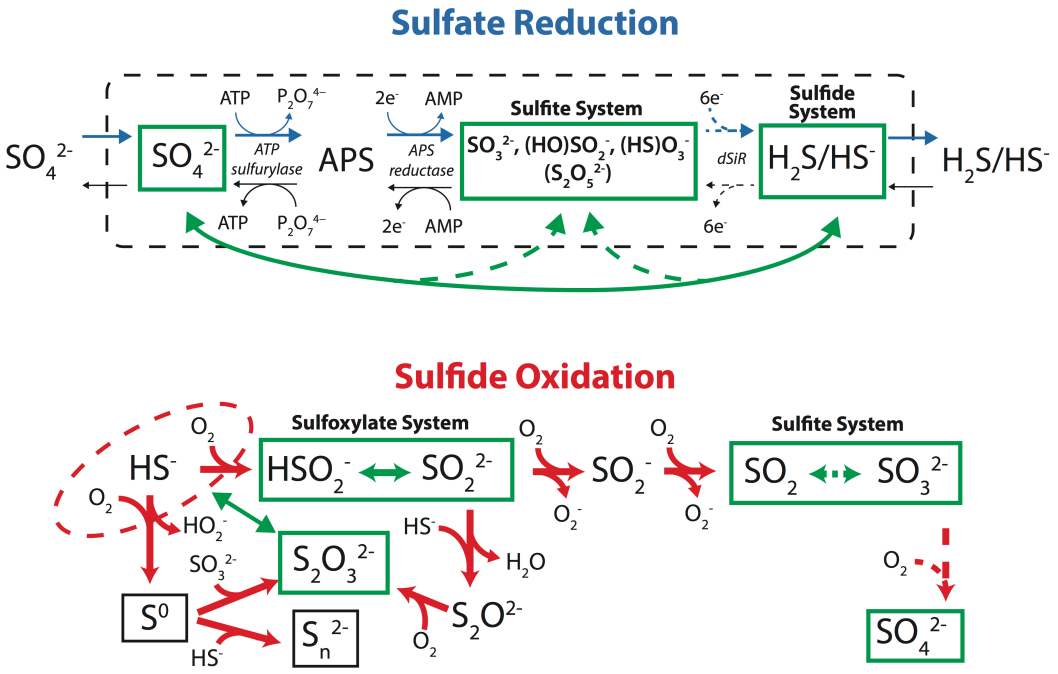

Figure 1.2: Schematic representations of processes that comprise two of the major features of the modern sulfur cycle: microbial sulfate reduction (e.g., after Wing and Halevy, 2014; dashed rounded box indicates the cellular membrane) and sulfide oxidation (the polar mechanism, drawn after Zhang and Millero, 1993). The green boxes and arrows represent equilibrium fractionation factors that have been estimated in this dissertation (Chapter 2). The dashed red ellipse represents the study of sulfide oxidation presented in Chapter 3. The fractionation factors presented in this dissertation will aid in the study of major features of the sulfur cycle past and present using sulfur isotopes.

2.0 Dissertation Overview

This dissertation contains new constraints on sulfur isotopic fractionation factors in aqueous sulfur systems for numerous applications, ranging from high temperature hydrothermal systems to the low temperature intracellular conditions of sulfur-metabolizing microorganisms. I utilized both theoretical calculations and experimental approaches to constrain isotope effects.

In Chapter 2, I present theoretical calculations rooted in the principles of quantum mechanics (Gaussian 09; Frisch et al., 2010) that allow the prediction of equilibrium isotope effects among aqueous sulfur compounds spanning the entire range of oxidation states available to sulfur. These calculations appear to be the first comprehensive study of the isotope partitioning behavior of a wide variety of aqueous sulfur compounds utilizing an explicit solvation model, where aqueous solutes are modeled in clusters of water molecules. Explicit solvation models have been demonstrated in recent theoretical studies to be essential to the modeling of aqueous compounds for the computation of theoretical equilibrium fractionation factors (e.g., Rustad et al., 2008; Li et al., 2009; Zeebe, 2009; Rustad et al., 2010; Li and Liu, 2011). Chapter 2 not only functions as a source of new constraints for fractionation factors, but also provides a review of previous experimental determinations. My theoretical calculations compare well to the available experimental constraints within a reasonable estimation of uncertainties, and highlights where future experimental research may be needed. My calculations also provide valuable constraints on minor isotope fractionations and their relationship to major isotope fractionations, and

broadly define the mass dependence of equilibrium isotope exchange in aqueous systems.

The calculations in Chapter 2 additionally provide new insights, particularly in the poorly documented sulfite ($SO_3^{2-}{}_T$) and sulfoxylate ($SO_2^{2-}{}_T$) systems where I highlight the role of isomers of protonated compounds in influencing isotope fractionations. I point out that such isomerization phenomenon may have a role to play in the overall isotope fractionations expressed during the highly influential dissimilatory sulfate reduction metabolism, where inorganic (i.e., non-chelated or non-enzymatically-bound) sulfite compounds are pivotal intracellular intermediates (*cf.* Figure 1.2). It is additionally likely that isomerization phenomenon will have influence on the isotope fractionations expressed in other redox processes involving sulfite compounds (e.g., bisulfite oxidation in atmospheric water droplets) that will need to be considered in the interpretation of future studies.

In Chapter 3, I present experimental determinations of reaction rates and sulfur isotope fractionations associated with the homogeneous oxidation of sulfide by molecular oxygen in aqueous solution, following up on the classic study of Brian Fry and colleagues (Fry et al., 1988). A major motivation for this study was to explore the mass-dependence of isotope fractionations associated with sulfide oxidation via the analysis of all three stable isotope ratios of sulfur. The need for such constraints has become apparent in recent years in the evaluation of multiple sulfur isotope systematics in many natural systems where sulfur compounds are oxidatively cycled, for example: the global oceans (e.g., Zerkle et al., 2009; Johnston, 2011), the chemoclines of sulfidic and redox stratified waters (e.g., Zerkle et al., 2010), organic-

rich sediments undergoing early diagenesis (e.g., Pellerin et al., 2015), the hydrothermal waters of hot springs (e.g., Yellowstone National Park; Kamyshny et al., 2014), and even most recently in the genetic relationships between inorganic sulfur compounds of mixed valence in solar system materials that have complex histories (e.g., CM chondrites; Labidi et al., submitted). In each of these settings, the isotope effects associated with oxidative processes may have influenced the isotopic compositions of sulfur phases that result from sulfur cycling.

For the experimental study described in Chapter 3, an attempt was additionally made to ground my sulfide oxidation experiments in the extensive sulfide oxidation kinetics literature by designing my experiments to constrain reaction rates in addition to isotopic fractionations. Poor reproducibility of sulfide oxidation rates between laboratories over the last several decades indicate that the kinetics of sulfide oxidation is not a trivial pursuit, and issues of variability likely stem from varying degrees of trace catalyst contaminations in experimental approaches (*cf.* Millero, 1986; Luther et al., 2011). Isotope fractionations and rates are both intimate expressions of the reaction mechanism and are likely to co-vary, and the meaning of measured isotopic fractionations may be ambiguous or difficult to interpret without tying the fractionations to rates (specifically, overall rate constants). I show that the rate constants and activation energy for the autoxidation of sulfide derived from my experiments are highly consistent with the extensive kinetic studies of the Frank J. Millero group (Millero et al., 1987; Zhang and Millero, 1993), and provide new rate/fractionation factor relationships for sulfide oxidation.

3.0 Context for Research Presented in this Dissertation

The analysis and consideration of all three isotope ratios of sulfur ($^{33}S/^{32}S$, $^{34}S/^{32}S$, $^{36}S/^{32}S$) has revolutionized the utility of sulfur isotopes in (bio)geochemical studies (Johnston, 2011). This revolution was gradually spurred on by the efforts of workers in the group of Mark Thiemens at UCSD in the 1990's in their examination of the multiple sulfur isotope compositions of various meteorite groups (e.g., Gao and Thiemens, 1993; Cooper et al., 1997; Farquhar et al., 2000a) and the anomalous isotope effects associated with photochemical reactions of gaseous sulfur compounds (e.g., Colman et al., 1996; Zmolek et al., 1999; Farquhar et al., 2001). Following this trajectory, a major discovery was made via the multiple sulfur isotope analysis of pyrite in Archean and younger sedimentary rocks (Farquhar et al., 2000b) that revealed so-called anomalous or "mass-independently fractionated" (or "MIF") sulfur isotope compositions uniquely associated with Archean rocks. These signals are highly likely to be the result of atmospheric photochemistry involving SO_2 and perhaps other gaseous sulfur compounds that require low atmospheric oxygen fugacity for their generation and preservation (e.g., Farquhar et al., 2001; Pavlov and Kasting, 2002). The analyses presented in Farquhar et al. (2000b) provided key constraints on the anoxic nature of the Archean atmosphere and the first glimpse of the "smoking gun" isotope signal for when the Earth's atmosphere began to accumulate molecular oxygen above an operationally defined threshold value (*cf.* Pavlov and Kasting, 2002; Farquhar and Wing, 2003; Johnston, 2011). These studies further inspired the analysis of multiple sulfur isotopes in other low temperature systems to see what other information can be provided.

Apart from the numerous follow-up studies documenting and bolstering the so-called sulfur "MIF record" to constrain the history of atmospheric oxygen (e.g., Johnston, 2011), much of the effort in the sulfur isotope community of the past 10-15 years has been concentrated on the multiple sulfur isotope fractionations associated with microbial metabolisms, particularly sulfate reducing organisms (Farquhar et al., 2003; Johnston et al., 2005; Johnston et al., 2007; Farquhar et al., 2007; Sim et al., 2011a,b; Leavitt et al., 2013; Wing and Halevy, 2014; Leavitt et al., 2015; Bradley et al., 2016). Microbial sulfate reduction is a major geochemical process responsible for ca. 12-29% of the respiration of the organic carbon flux to the seafloor per year in the modern oceans (Bowles et al., 2014) and has strongly impacted the isotopic composition of the authigenic pyrite rock record throughout geologic time (e.g., Canfield, 2001; Canfield, 2004). Additionally, microbial sulfate reduction may be among the earliest forms of metabolism for which we have putative isotopic evidence in the rock record (e.g., Shen et al., 2001; Shen and Buick, 2003; Ueno et al., 2008; Shen et al., 2009; Wacey et al., 2010; Wacey et al., 2011; see also Johnston, 2011). Recent efforts have been directed at understanding the sulfur isotope fractionations associated with the metabolism in more detail via all three isotope ratios of sulfur to further enhance and inform interpretations of the rock record.

One of the key initial insights from the early investigations (Farquhar et al., 2003) was the observation that small but resolvable $\Delta^{33}S$ and $\Delta^{36}S$ fractionations accompany microbial sulfate reduction. Values of $\Delta^{33}S$ and $\Delta^{36}S$ are defined as an exponential relationship between a measured major isotope ratio of sulfur ($^{34}R = {}^{34}S/{}^{32}S$) and minor isotope ratio of sulfur (e.g., $^{33}R = {}^{33}S/{}^{32}S$), i.e.:

$$\Delta^{33}S_{A\text{-}B} = {}^{33}R_A/{}^{33}R_B - ({}^{34}R_A/{}^{34}R_B)^{0.515} \quad (1)$$

$$\Delta^{36}S_{A\text{-}B} = {}^{36}R_A/{}^{36}R_B - ({}^{34}R_A/{}^{34}R_B)^{1.9} \quad (2)$$

A and B refer to substance "A" and substance "B" and the exponents of 0.515 and 1.9 are the reference exponents approximating the expected relationship associated with low-temperature equilibrium isotope exchange. These effects have since been documented for other sulfur metabolizing microorganisms, including sulfur disproportionating bacteria (Johnston et al., 2005) and anaerobic phototrophic sulfide oxidizing bacteria (Zerkle et al., 2009), and have largely been explained utilizing isotope fractionation network models as being the result of mixing and un-mixing of fractionated sulfur pools within the metabolism (e.g., Farquhar et al., 2003; Johnston et al., 2007). These efforts led to the intriguing observation that the multiple sulfur isotope fractionations imparted to sulfate and sulfide may be unique for these three metabolisms (considered generically), forming the basis for the possibility of metabolic-specific biosignatures based on sulfur isotopes (Johnston, 2011). Of these three major sulfur metabolisms, it is only sulfide oxidation that has a significant abiological counterpart that operates under temperature regimes that overlap with biological processes. It became clear from this context that constraints were needed for the multiple sulfur isotope effects associated with abiological sulfide oxidation that has led to the study presented in Chapter 3 of this dissertation. The data in Chapter 3 may further refine multiple sulfur isotope oxidative biosignatures and further constrain the isotope effects associated with the oxidative sulfur cycle.

Throughout the course of the experimental research presented in Chapter 3, it became apparent that the reference exponents (represented as lambda values: ${}^{33/34}\lambda_{ref}$

= 0.515, $^{36/34}\lambda_{ref}$ = 1.9) may require further examination in order to properly interpret the mass dependence associated with sulfide oxidation. Even my earliest preliminary experiments appeared to reveal that the exponents associated with sulfide oxidation did not correspond to the reference exponents within uncertainty (i.e., $^{33/34}\lambda \neq 0.515$, $\Delta^{33}S \neq 0$). This observation was not exactly anticipated, and in addition to repeating the observation I sought to further understand the quantitative meaning of the reference exponents. The reference exponents have been chosen by the community to approximate equilibrium isotope exchange at low temperature (i.e., well below the high temperature limit as $T \rightarrow \infty$), and the questions arose: how much variability in the exponent can we expect from equilibrium isotope exchange and what are its major controls? Variability in the equilibrium isotope exchange exponents relating mass dependence was understood early on to be a function of bonding environment at low temperatures (e.g., Matsuhisa et al., 1978) but had not been elaborated upon in the sulfur system. Farquhar et al. (2003) estimated that variability in the $^{33/34}\lambda$ exponent associated with equilibrium isotope exchange to be on the order of 0.514 – 0.516 based on theoretical calculations of equilibrium isotope fractionation factors among $H_2S/SO_3^{2-}/SO_4^{2-}$ using experimental vibrational spectra and force field models. The data provided in the theoretical study of Otake et al. (2008) for gas phase reactions is additionally consistent with this range. The theoretical study in Chapter 2 expands upon the analysis of Farquhar et al. (2003) and includes many more aqueous sulfur compounds utilizing vibrational spectra derived from quantum mechanical calculations. The expected variability defined in Farquhar et al. (2003) is largely unchanged by the calculations presented in Chapter 2, but my calculations provide

much more detail on the first order controls on this variability. The theoretical calculations in Chapter 2 are used as a reference frame for examining the mass dependence associated with sulfide oxidation in Chapter 3.

In addition to further constraining the mass dependence of equilibrium isotope exchange, the theoretical calculations may have applicability to microbial metabolisms. The expression of sulfur isotope fractionations for multiple sulfur isotopes associated with microbial metabolism have largely been evaluated in the context of network models, all the way from the earliest evaluations (for $^{34}S/^{32}S$: Rees, 1973; for $^{33}S/^{32}S$ and $^{34}S/^{32}S$: Farquhar et al., 2003) to the most recent (Wing and Halevy, 2014). These models describe the overall isotope fractionations associated with a process based on: (1) the network of steps that comprise the process, (2) the isotope fractionations associated with each of those steps, and (3) the relative fluxes of mass between these steps. The earliest network models to consider multiple sulfur isotopes (Farquhar et al., 2003) were based on metabolic steps for sulfate reduction proposed by early studies (Harrison and Thode, 1958; Rees, 1973) and used constraints for fractionations associated with steps using estimates of equilibrium fractionation factors among major reactant/intermediate/product pairs (i.e., $H_2S/SO_3^{2-}/SO_4^{2-}$). As this work developed, constraints from the biochemical literature were incorporated to expand the network of steps to include more complex pathways (Brünner and Bernasconi, 2005) and were subsequently adopted for multiple sulfur isotopes (e.g., Farquhar et al., 2007; Johnston et al., 2007). Later models (Bradley et al., 2011) further expanded and refined the considered network based on insights gained from sulfite interactions with enzymes via the crystal

structure studies of dissimilatory sulfite reductase (Oliviera et al., 2008; Parey et al., 2010), the key enzyme that is responsible for the step-wise reduction of the intermediate sulfite to terminal product sulfide (e.g., Figure 1.2). The overall aim of these studies was to constrain the appropriate network of intracellular steps occurring in the metabolism to adequately model the system to explain the broad range of fractionations that had been directly measured for the metabolism both in terms of $^{34}S/^{32}S$ and $^{33/34}\lambda$ (or $\Delta^{33}S$), and in many cases relied on equilibrium fractionations among key inorganic sulfur compounds as end-member constraints.

The following experimental and model studies aimed to pinpoint the key variables that contribute to the widespread variability in isotope fractionations associated with microbial sulfate reduction (Sim et al., 2011a,b; Leavitt et al., 2013; Wing and Halevy, 2014; Bradley et al., 2016). Among the most recent experimental efforts are those that have been concentrated on constraining sulfur isotope fractionations as a function of cell-specific sulfate reduction rate (csSRR) using experiments performed in continuous flow bioreactors with pure cultures (Sim et al., 2011a, b; Leavitt et al., 2013). These studies have importantly elucidated how cell specific sulfate reduction rate is a primary driver in controlling the expression of fractionations in the metabolism. For example, the maximum $^{34}S/^{32}S$ fractionations associated with MSR are associated with the lowest csSRR and may approach the magnitude of the equilibrium isotope fractionation factor between sulfate and sulfide in terms of both $^{34}S/^{32}S$ and $^{33/34}\lambda$ (Sim et al., 2011a), and decrease with increasing rate until reaching a plateau where $^{34}S/^{32}S$ fractionations and $^{33/34}\lambda$ are much lower (Sim et al., 2011a, b; Leavitt et al., 2013). Wing and Halevy (2014) built a network

model to explain these broad observations and was the first of its kind to tie the flux terms in the network model directly to enzyme kinetics and thermodynamics, where flux terms had previously been treated as free variables. Although still preliminary in its widespread application due to a paucity of key constraints, the model approach of Wing and Halevy (2014) allows for the exploration of the thermodynamic and kinetic controls on the expression of isotope fractionations (some of them strain-specific) in the experimental studies of Sim et al. (2011a,b) and Leavitt et al. (2013) as a function of the respiration rate per cell. In this sense, the field has experienced a shift from batch experiments and bulk isotope fractionation models to experiments and models that control for the overall rates of the process, and have yielded considerable insight along the way into some of the key variables that control the net isotope fractionations produced by the metabolism.

The overall arc of multiple sulfur isotope research as applied to microbial metabolism (sulfate reduction) appears to be bending towards elucidating the numerous intracellular mechanisms for isotope exchange, especially as the biochemical mechanisms for the enzymatic transformations of sulfur within sulfate reduction become increasingly more detailed (e.g., Santos et al., 2015) and their potential physiological controls undergo further investigation (e.g., Bradley et al., 2016). For example, Leavitt et al. (2015) provide information regarding the isotope fractionations associated with the reduction of bulk sulfite via dissimilatory sulfite reductase *in vitro*, and it appears ongoing studies may be aimed at isolating intermediate sulfur compounds from within cells grown under controlled conditions for their isotopic analysis. These studies seek to provide specific fractionation factors

associated with each step in the metabolism that will further elucidate controls on the expression of isotope fractionations in conjunction with network models such as Wing and Halevy (2014). In addition to the broader efforts to constrain the chemical and isotope exchange mechanisms and their influence on the expression of overall isotope fractionations within the metabolism more generically, the physiological controls on isotopic fractionations resulting from an organism's response to environmental factors (e.g., sulfate concentrations) that arise from strain-specific factors are beginning to be explored as well (Bradley et al., 2016).

The work presented in this dissertation (Chapter 2) will provide critical information that may be used in future studies to further probe the mechanism of sulfite reduction via dissimilatory sulfite reductase. I point out in Chapter 2 that an often-ignored feature of inorganic sulfite chemistry is the isomerization of bisulfite (HSO_3^-), where protons can be bound to either oxygen atoms or sulfur atoms. The implication of this isomerization is that there are three major sulfite species present in aqueous solutions at ambient temperature and circumneutral pH (depending on ionic strength) as opposed to the typically assumed singular sulfite *sensu stricto* in network models and other experimental approaches related to the sulfate reduction metabolism. The equilibrium quotients for bisulfite isomerization have been documented (Horner and Connick, 1986; Littlejohn et al., 1992; Risberg et al., 2007) but have been largely unrecognized by the sulfur isotope community, and perhaps as a result have not yet been constrained as a function of a wide range of solution conditions. I show that the relative abundances of the bisulfite isomers have consequences for isotope fractionations between bulk bisulfite and sulfite in solution,

due to the vastly different isotope partitioning behavior of the isomer that is in minor abundance at low temperature. I additionally hypothesize that the minor isomer may be sterically hindered in its reaction towards the siroheme active site in dissimilatory sulfite reductase, potentially leading to its discrimination during enzymatic sulfite reduction that may have consequences for the expression of isotope fractionations involving this enzyme. In this sense, although Chapter 2 is not a biochemical study, it may provide key constraints for the further elucidation of isotopic fractionations associated with the enzyme mediated redox reactions associated with microbial metabolism.

In the context of existing isotope fractionation network models that are applied to microbial sulfate reduction, the equilibrium isotope fractionations among sulfide species, sulfite species, and sulfate provided in Chapter 2 are likely to inform future network models constructed similarly to Wing and Halevy (2014) and those that came before. Wing and Halevy (2014) used estimates for equilibrium isotope fractionations cited from the theoretical study of Otake et al. (2008) to constrain isotope fractionations in the equilibrium limit that is postulated to prevail under certain conditions (i.e., exceedingly low cell-specific sulfate reduction rates; Wing and Halevy, 2014). These critically include equilibrium fractionations factors between SO_4^{2-}/SO_3^{2-} (approximating steps between intracellular sulfate and sulfite, bridged by the activated sulfate complex adenosine phosphosulfate, or APS) and SO_3^{2-}/H_2S (approximating the dissimilatory sulfite reductase step)[1] (see Figure 1.2).

[1] Note: Wing and Halevy (2014) appear to have incorrectly cited the study of Otake et al. (2008) as providing constraints for fractionations involving SO_3^{2-}, and they appear to have used the Otake et al. (2008) calculations of SO_3 (the trigonal planar gas phase sulfur trioxide) in its place. The isotope partitioning behavior of SO_3 and SO_3^{2-} are not expected to be similar due to differences in their

These are conceptually the same types of constraints used in the earliest multiple sulfur isotope network models of Farquhar et al. (2003) that utilized theoretical calculations based on experimental vibrational spectra. In this framework, the theoretical calculations in Chapter 2 allow for the consideration of much more complete aqueous speciation: $SO_4^{2-}/(SO_3^{2-}{}_T = SO_{2(aq)} + (HO)SO_2^- + (HS)O_3^- + SO_3^{2-})$ and similarly $(SO_3^{2-}{}_T = SO_{2(aq)} + (HO)SO_2^- + (HS)O_3^- + SO_3^{2-})/(H_2S_T = H_2S + HS^-)$, and indicate that the estimations for these fractionations will depend on speciation and therefore intra- and extra-cellular solution conditions (temperature, ionic strength, pH, and so on). The study of Chapter 2 therefore serves as a set of internally consistent constraints that can be readily applied to models of microbial metabolism, and provide a useful summary of the literature on equilibrium isotope fractionation factors among aqueous sulfur compounds.

oxidation state and molecular structure (see Chapter 2), and so it would appear that a quantitative re-evaluation of their model results might be warranted in light of this observation. This, however, does not undermine their contribution and merely represents a direction for further exploration.

Chapter 2: Theoretical estimates of equilibrium sulfur isotope effects in aqueous systems: Highlighting the role of isomers in the sulfite and sulfoxylate systems

Abstract

I present theoretical calculations of reduced partition function ratios (RPFR) for all three isotope ratios of sulfur ($^{33}S/^{32}S$, $^{34}S/^{32}S$, $^{36}S/^{32}S$) at the B3LYP/6-31+G(d,p) level of theory for aqueous sulfur compounds modeled in 30-40 H_2O clusters spanning the range of sulfur oxidation state (S^n, n = -2 to +6). Major isotope RPFRs ($^{34}S/^{32}S$; denoted $^{34}\beta$) scale to a first order with sulfur oxidation state and coordination, where higher oxidation states have higher $^{34}\beta$ and $^{34}\beta$ generally increase with increasing coordination of the sulfur atom.

Exponents defining mass dependent relationships based on RPFRs ($^{n/34}\lambda_\beta = \ln(^x\beta)/\ln(^{34}\beta)$, x = 33 or 36) conform to tight ranges over a wide range of temperature for all aqueous compounds ($^{33/34}\lambda_\beta \approx 0.5148\text{-}0.5159$, $^{36/34}\lambda_\beta \approx 1.89\text{-}1.90$ from $T \geq 0^\circ C$). The exponents converge near a singular value for all compounds at the high temperature limit ($^{33/34}\lambda_{\beta,\, T\rightarrow\infty} = 0.51587 \pm 0.00003$ and $^{36/34}\lambda_{\beta,\, T\rightarrow\infty} = 1.8905 \pm 0.0002$; 1 s.d. of all computed compounds) and typically follow trends based on oxidation state and coordination similar to those seen in $^{34}\beta$ values below the high temperature limit.

Theoretical fractionation factors are compared to experimental constraints for $HSO_3^-{}_{T(aq)}/SO_{2(g,\ aq)}$, $SO_{2(aq)}/SO_{2(g)}$, $H_2S_{(aq)}/\ H_2S_{(g)}$, $H_2S_{(aq)}/HS^-_{(aq)}$, $SO_4^{2-}{}_{(aq)}/H_2S_{T(aq)}$, $S_2O_3^{2-}{}_{(aq)}$ (intramolecular), and $S_2O_3^{2-}{}_{(aq)}/H_2S_{T(aq)}$, and generally agree within a

reasonable estimation of uncertainties. We make predictions for fractionation factors where other constraints are unavailable. Isotope partitioning of the isomers of protonated compounds in the sulfite and sulfoxylate systems depend strongly on whether protons are bound to either sulfur or oxygen atoms. The magnitude of the $HSO_3^-{}_T/SO_3^{2-}$ major isotope ($^{34}S/^{32}S$) fractionation factor is predicted to increase with temperature from 0-70˚C due to the combined effects of the large magnitude $(HS)O_3^-/SO_3^{2-}$ fractionation factor ($1000\ln{}^{34}\alpha_{(HS)bisulfite\text{-}sulfite}$ = 19.9 ‰, 25˚C) relative to the $(HO)SO_2^-/SO_3^{2-}$ fractionation factor ($1000\ln{}^{34}\alpha_{(HO)bisulfite\text{-}sulfite}$ = -2.2 ‰, 25˚C) and the increased stability of the $(HS)O_3^-$ isomer with increasing temperature. I additionally hypothesize that the complex speciation of sulfite in intracellular media could have an impact on the isotope fractionations expressed during the reduction of bulk sulfite by the enzyme dissimilatory sulfite reductase in sulfate reducing microorganisms.

1.0 Introduction

1.1 Overview

Quantum mechanical electronic structure calculations of aqueous clusters complement experimental investigations of isotope effects in aqueous systems (e.g., Rustad et al., 2008; Rustad et al., 2010; Zeebe, 2009) and have been instrumental for predicting isotope effects when experimental determinations are unavailable (e.g., Li et al., 2009; Li and Liu, 2011). Theoretical approaches are especially useful for compounds like those of the sulfite and sulfoxylate systems that contain isomers and dimers that are difficult to experimentally isolate. The aim of the present study is to: (1) provide an internally consistent set of constraints for equilibrium isotope fractionations among aqueous sulfur compounds relevant to both low and high

temperature conditions, emphasizing the poorly documented sulfite and sulfoxylate systems; (2) provide new constraints on the exponents of mass-dependence associated with equilibrium isotope fractionation in aqueous systems and their relationships to sulfur oxidation state and bonding environment; (3) compare our theoretical constraints to the available experimental datasets and make predictions where estimates are currently unavailable, assessing where future experimental work may be needed; and (4) illustrate the effects of isomerization on isotope partitioning in the sulfite system where isomerization leads to relatively large and apparently unusual effects in observable isotope fractionation behavior (e.g., influencing magnitudes, directions, and the temperature dependence of bulk fractionation factors).

1.2 Sulfite and sulfoxylate in the sulfur cycle

The sulfite (denoted $SO_3^{2-}{}_T$) and sulfoxylate systems (denoted $SO_2^{2-}{}_T$) are the series of inorganic compounds and oxyanions that contain sulfur in the +4 and +2 oxidation states, respectively. These oxidation states are intermediate between the most common end member sulfur oxidation states of -2 as the most reduced (e.g., $H_2S/HS^-/S^{2-}$) and +6 as the most oxidized (e.g., SO_4^{2-}). Sulfite is a well-documented intermediate in a variety of settings where sulfur is cycled, and sulfoxylate species, while very rarely observed, are inferred to be a 'missing-link' oxidation state in sulfur redox processes between zero-valent sulfur compounds (e.g., generically as S^0) and those of the sulfite system. Both sulfite and sulfoxylate exhibit complex speciation in solution—including numerous isomers and dimers of protonated species—that is

often ignored in (bio)geochemical applications where these compounds are key intermediates. Here I provide a brief review of their roles in the sulfur cycle.

Sulfite in the sulfur cycle

Sulfite *sensu lato* in natural environments is typically transient and does not comprise a significant fraction of the bulk sulfur in Earth's surface environment but nevertheless plays essential roles in the environmental cycling of sulfur and related elements. The hydrolysis and subsequent oxidation of sulfur dioxide in atmospheric water droplets is a major pathway of acid-rain formation (e.g., Brandt and van Eldik, 1995). Sulfite is a major intermediate in both the oxidative and reductive portions of the sulfur cycle, including the microbial production and subsequent oxidation of sulfide (HS^-/H_2S; Zhang and Millero, 1993; Zopfi et al., 2004). In marine sediments containing relatively high amounts of organic matter, sulfide is generated as a byproduct of anaerobic respiration (dissimilatory sulfate reduction) and ca. 80-95% of the sulfide produced is eventually re-oxidized through intermediates like sulfite back to sulfate (Jørgensen, 1977; Jørgensen, 1982; Jørgensen et al., 1990; Canfield and Teske, 1996; Jørgensen and Nelson, 2004). Depending on the conditions and biota present, the sulfite thus produced can support or supplement a variety of metabolisms carried out by microorganisms that oxidize, reduce, and disproportionate sulfite and other intermediate sulfur compounds for overall energy conservation and metabolic function.

At the intracellular level, sulfite (*sensu lato*) is a pivotal intermediate during dissimilatory sulfate reduction, which in general is responsible for the oxidation of much of the organic matter contained in modern marine sediments (e.g., Bowels et

al., 2014). Intracellular sulfite within a dissimilatory sulfate reducer sits between two reversible transformations: (1) its production via the reduction of activated sulfate (adenosine-5'-phosphosulfate; cleaving an S-O bond) and (2) its reaction with the siroheme active site of dissimilatory sulfite reductase (dSiR) where it is reduced to eventually form the end waste product sulfide via other enzymatically-bound intermediates like sulfoxylate (S^{2+}) and zero-valent sulfur (S^0) (Parey et al., 2010). The sulfide thus produced and its subsequent cycling in the environment places primary controls on the isotopic composition of authigenic pyrite, which in sedimentary rocks serves as a primary archive of the sulfur cycle through geologic time. Isotope network models that attempt to place constraints on the sulfur isotope fractionations that occur during the step-wise reduction of sulfate within MSR have all, thus far, greatly simplified the intracellular inorganic speciation of sulfite (assuming sulfite *sensu stricto* only) and have yet to take into consideration the potentially complex effects of sulfite speciation.

Despite the recognized importance of sulfite in the overall cycling of sulfur, the determination of the equilibrium isotope fractionations among various sulfite species has received very little attention. To my knowledge, only one set of experimental constraints has been reported (Eriksen, 1972a; Eriksen, 1972b; Eriksen, 1972c), suggesting a fractionation factor between bulk bisulfite in solution and gaseous SO_2 ($1000\ln{}^{34}\alpha_{\text{bisulfite-SO2(g)}}$) of 10.9 ± 1.4 ‰ (1 s.d., 10 experiments) at 25˚C (Eriksen, 1972a). No resolvable change in this fractionation factor was observed over the investigated temperature range of 25-45˚C. Fractionations among aqueous sulfite species (e.g., the bisulfite compounds and sulfite) are completely unconstrained.

Given that these are the dominant species under most natural conditions as well as within sulfate reducing organisms, these fractionations are key to a detailed understanding of sulfite isotope systematics in natural systems.

Sulfoxylate in the sulfur cycle

Sulfoxylate species are difficult to detect and analyze and their role in the (bio)geochemical cycling of sulfur is not well understood. Hoffmann and Lim (1979) were among the first to suggest sulfoxylate as a reaction intermediate of the sulfide oxidation mechanism in a scheme of hypothetical reactions known as the polar mechanism (*cf.* Zhang and Millero, 1993). In this scheme, sulfoxylate is postulated to be among the initial products of oxidation and a key intermediate in the formation of sulfite species (via its oxidation and/or decomposition) and thiosulfate (via a series of reactions with residual sulfide; Zhang and Millero, 1993).

Vairavamurthy and Zhou (1995) confirmed the presence of an S^{2+} oxyanion during sulfide oxidation via sulfur k-edge X-Ray Absorbance Near Edge Structure (S-XANES) spectroscopy and attributed it to the sulfoxylate (SO_2^{2-}) structure based on Fourier Transformed Infrared (FT-IR) spectroscopic analysis. Tossel (1997) later compared the spectral observations of Vairavamurthy and Zhou (1995) and their pH dependence with calculated vibrational frequencies of sulfoxylate compounds, and argued that the species identified by Vairavamurthy and Zhou (1995) is more likely a bisulfoxylate species where the proton is bound to an oxygen (denoted here as $(HO)SO^-$). The latter argument is consistent with the predicted speciation of sulfoxylate under their experimental conditions (pH = 11.5-12) according to the dissociation quotients of Makarov et al. (2010).

Sulfur in the +2 oxidation state has also been a hypothesized (but mostly undocumented) intermediate during dissimilatory sulfate reduction. In recent biochemically-informed models (Oliveira et al., 2008; Parey et al., 2010; Bradley et al., 2011; Wing and Halevy, 2014; Santos et al., 2015), the reduction of sulfite at the siroheme-[4Fe-4S] catalytic site in dissimilatory sulfite reductase occurs stepwise, first producing a bound S^{2+} intermediate, then a bound S^0-intermediate before eventually forming sulfide facilitated via a complex mechanism involving a Dsr-related protein known as DsrC (Oliveira et al., 2008; Santos et al., 2015). Reactions of these enzymatically-bound intermediate moieties (S^{2+}, S^0) via nucleophilic attack by residual non-enzymatically bound sulfite species have been hypothesized pathways for the generation of polythionates (principally trithionate, $S_3O_6^{2-}$) and thiosulfate ($S_2O_3^{2-}$) that have been observed in some MSR culture experiments (Parey et al., 2010). If the hypothesized S^{2+} intermediates detach from the catalytic site and form free aqueous species, they are likely to be included within the sulfoxylate system and their inorganic speciation and isotope partitioning behavior could play additional roles in the distribution of sulfur (and oxygen) isotopes within the MSR framework. In principle, the hydrolytic decomposition/disproportionation of sulfoxylate species and other reaction products (e.g., S_2O^{2-}) could play additional roles in distributing isotopes among different intracellular sulfur pools.

2.0 Background: Aqueous sulfur speciation

A major motivation for this study is to explore the effects of complex speciation on isotope partitioning in the sulfite and sulfoxylate systems (particularly

with respect to isomers and dimers, where applicable). Here, I provide a brief review of aqueous sulfur speciation with emphasis on sulfite and sulfoxylate.

2.1 Sulfite system chemistry

The most common species in the sulfite system (S^{4+}) include: gaseous and aqueous sulfur dioxide ($SO_{2(g)}$ and $SO_{2(aq)}$), bisulfite isomers ($(HO)SO_2^-$ and $(HS)O_3^-$; collectively $HSO_3^-{}_T$), dimers of bisulfite (such as pyrosulfite: $S_2O_5^{2-}$), and sulfite *sensu stricto* (SO_3^{2-}). The hypothetical sulfurous acid (two generic groups of isomers: $SO(OH)_2$ and $(HS)O_2OH$; collectively H_2SO_3) may be intermediary in the hydrolysis of SO_2 to form bisulfite anions, but has never been detected in solution (Gerding and Nijveld, 1936; Falk and Giguere, 1958; Zhang and Ewing, 2002; Voegele et al., 2004). Sulfurous acid (and related isomers) is therefore unlikely to be a significant component of the mass balance.

Sulfite species are distributed in solution as a continuum that depends on pH, temperature, ionic strength (μ), and total S(IV) concentration (see Figure 2.1). A summary of select dissociation, isomerization, and dimerization quotients is included in Table 2.1. At $\mu \sim 0$ *m* and 25˚C, dissolved SO_2 dominates sulfite solutions under extremely acidic conditions (pH < 1.9), bisulfite compounds dominate at 1.9 < pH < 7.2, and sulfite *sensu stricto* at pH > 7.2 (Martell and Smith, 1982; Beyad et al., 2014).

Bisulfite exists in two isomeric forms: one tetrahedral form where the proton is bound to the sulfur—denoted herein as $(HS)O_3^-$—and another that is pyramidal where the proton is bound to one of the oxygen atoms—denoted herein as $(HO)SO_2^-$ (Golding, 1960 and references therein; Connick et al., 1982; Horner and Connick,

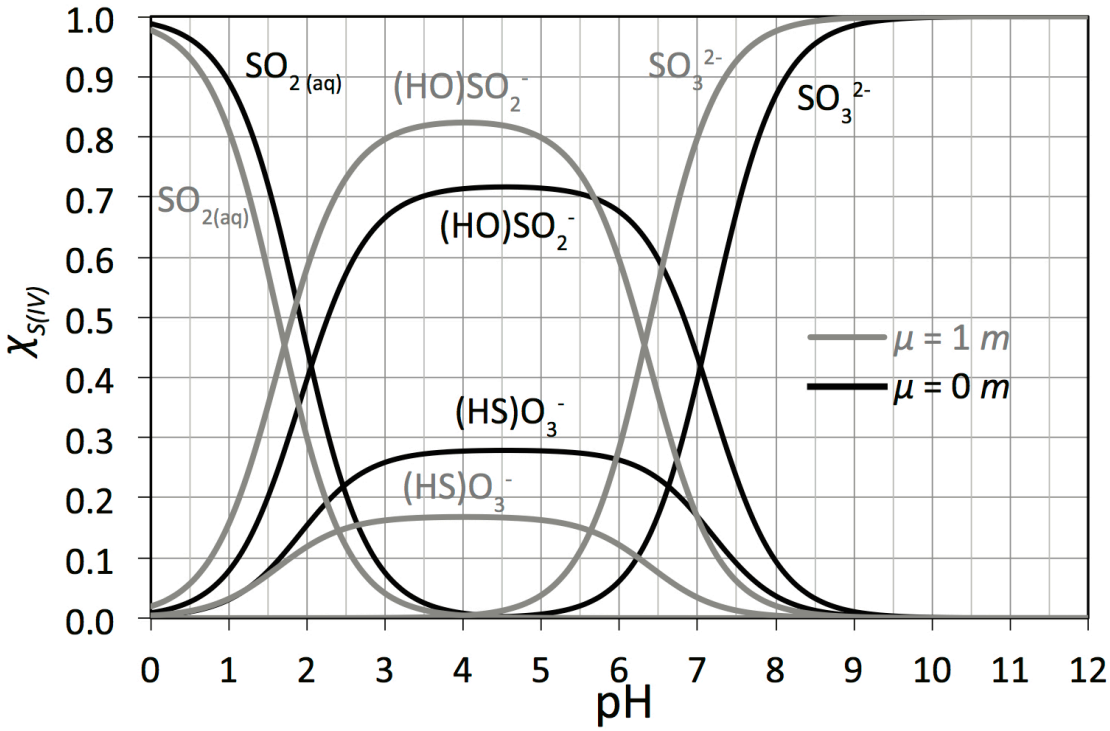

Figure 2.1: Mole fraction of sulfite species ($\chi_{S(IV)}$) as a function of pH at 25˚C, highlighting the isomers of bisulfite (not including bisulfite dimers for simplicity; [S4+]T < ~0.1 M). The solid black curves are computed using dissociation and isomerization quotients determined at an ionic strength of zero (Damian Risberg et al., 2007; Beyad et al., 2014; Martell and Smith, 1982) and the gray curves at an ionic strength of 1 m (Horner and Connick, 1986; Millero et al., 1989).

1986; Littlejohn et al., 1992; Risberg et al., 2007). The relative proportions of the bisulfite isomers in solution is given by the isomerization quotient (Q_i), defined as:

$$(HS)O_3^- \rightleftharpoons (HO)SO_2^- \quad Q_i = [(HO)SO_2^-]/[(HS)O_3^-], \quad (1)$$

where brackets "[ ]" denote concentrations. Studies utilizing ^{17}O-NMR, IR-Raman, and sulfur k-edge XANES spectroscopy have shown that the OH-bonded pyramidal isomer of bisulfite is the dominant form in solution at low temperature, comprising ~72-84% of bisulfite at 25˚C depending on ionic strength (see Figure 2.1; Horner and Connick, 1986; Littlejohn et al., 1992; Risberg et al., 2007).

The relative proportion of the bisulfite isomers is temperature-dependent and the proportion of the HS-bonded isomer increases with increasing temperature

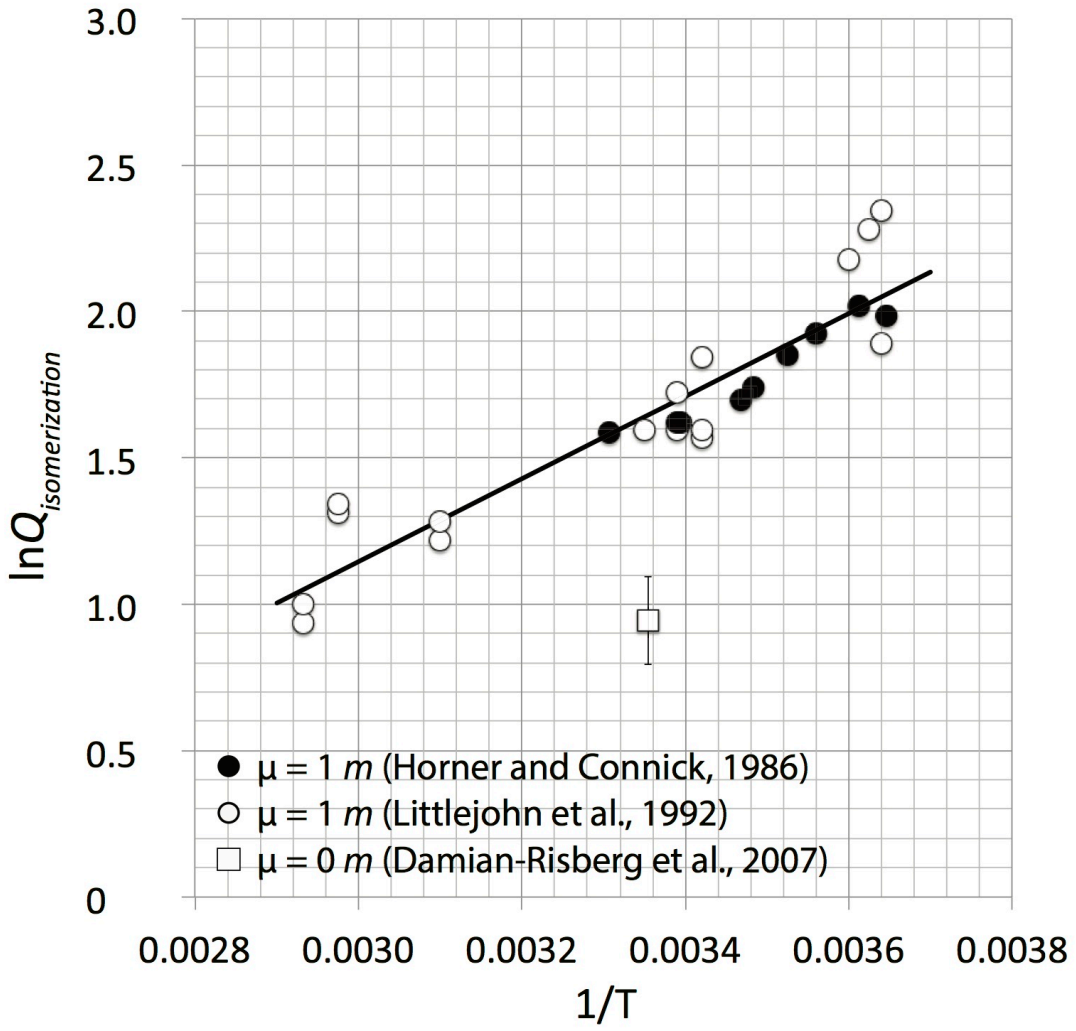

Figure 2.2: Experimental constraints on the bisulfite isomerization quotient as a function of temperature, defined as Q_i = $[(HO)SO_2^-]/[(HS)O_3^-]$. The μ = 1 *m* constraints are from Horner and Connick (1986) (black circles) and Littlejohn et al. (1992) (white circles) and the μ = 0 *m* constraint is from Risberg et al. (2007) (white square). The least-squares linear regression of the 1 *m* constraints yields: $\ln Q_i$ = 1413(±119)/T – 3.1(±0.4) (valid over ≈ 0-67˚C).

(Horner and Connick, 1986; Littlejohn et al., 1992; Risberg et al., 2007). Horner and Connick (1986) and Littlejohn et al. (1992) determined the quotient in a medium of relatively high ionic strength (μ = 1 *m*) over a total temperature range of 2-67˚C, from which the following temperature dependence is obtained (see Figure 2.2):

$$\ln Q_i = 1413(\pm 119)/T - 3.1(\pm 0.4) \qquad (T = 275\text{-}340\ K;\ \mu = 1\ m) \qquad (2)$$

The isomerization quotient may also vary significantly as a function of ionic strength as indicated by the lower Q_i more recently determined in a low-ionic strength medium at 25˚C (Risberg, 2007; see Table 2.1 and Figures 2.1 and 2.2). This suggests that application of the quotients of Horner and Connick (1986) and Littlejohn et al. (1992) to solutions of lower ionic strength may significantly underestimate the amount of $(HS)O_3^-$ present in solution. However, the exact effect of ionic strength on the isomerization quotient is yet to be quantified over a wide range of temperatures relevant to many natural systems.

Bisulfite can also form dimers in solution (*cf.* Golding, 1960). The principle dimer of bisulfite is $S_2O_5^{2-}$ known as pyrosulfite or disulfite, whose structure can be schematically illustrated as: $(O_2S\text{-}SO_3)^{2-}$ (note, however, that an aqueous form with a bridging oxygen—$(O_2S\text{-}O\text{-}SO_2)^{2-}$—remains to be ruled out in solution; Williamson and Rimstidt, 1992). The extent of dimerization varies as a function of the total bisulfite concentration and is quantified as the dimerization quotient (Q_d):

$$2HSO_3^-{}_T \rightleftharpoons S_2O_5^{2-} + H_2O \qquad Q_d = [S_2O_5^{2-}]/[HSO_3^-{}_T]^2 \; ; (M^{-1}) \qquad (3)$$

Studies directed at quantifying the dimerization quotient have produced varied results (see Table 2.1). Some of the discrepancies may have arisen from a variety of experimental errors in the earliest determinations (see discussion in Connick et al., 1982). The existing experimental datasets indicate that total bisulfite has to reach concentrations on the order of $\geq$ 0.1 M in order for significant conversion to the dimer to occur. For example, the dimer comprises ≤1% of total bisulfite at $[HSO_3^-]_T \leq 0.12$ M at μ=1 *m* and ≤ 1% of total bisulfite at $[HSO_3^-]_T \leq$ ~0.29 M at $\mu = 0$ (using the quotients of Connick et al., 1982). Recently, Beyad et al. (2014) found evidence

for a protonated dimer ($HS_2O_5^-$) via UV-spectrophotometric titrations and quantified its dissociation quotient (Table 2.1).

2.2 Sulfoxylate system chemistry

The sulfoxylate system comprises aqueous sulfur compounds and oxyanions in the 2+ oxidation state (S^{2+}): the sulfoxylate ion (SO_2^{2-}), bisulfoxylate ($(HS)O_2^-$ and/or $(HO)SO^-$), and species of the general composition H_2SO_2 (mostly including sulfoxylic and sulfinic acid). Electronic structure calculations have shown that the lowest energy configurations of H_2SO_2 in vacuum (i.e., predicted to be most stable in gas phase) are rotamers of sulfoxylic acid, where the protons are bound to each of the oxygen atoms and differ structurally in the relative orientation of the O-H bonds (Steiger and Steudel, 1992; Tossell, 1997; Napolion et al., 2008; Crabtree et al., 2013). Other isomers of H_2SO_2 of potential significance are those termed sulfinic acid, where one proton is bound to the sulfur atom and the other to one of the oxygen atoms. The relative stabilities of these isomers in solution are not constrained, nor are the isomers of the first acid dissociation products ("bisulfoxylate"): $(HS)O_2^-$ and $(HO)SO^-$. Sulfur monoxide (SO) would be the hypothetical unhydrolyzed component of the system (analogous to SO_2 in the sulfite system) but it is extremely unstable and not known to undergo hydrolysis to form H_2SO_2 (Lyons and Nickless, 1968 and references therein). Sulfur monoxide will therefore not be considered here as a component of this system.

The distribution of sulfoxylate species as a function of solution conditions is not well constrained. Makarov et al. (2010) is among the few studies to report the acid dissociation quotients of sulfoxylic acid, and their values are reproduced in Table

2.2. In general, it appears that sulfoxylic acid and bisulfoxylate are the primary species under most environmentally-relevant conditions, where sulfoxylic (or sulfinic) acid dominates at pH < 7.97, bisulfoxylate species from 7.97 < pH < 13.55, and the unprotonated sulfoxylate divalent anion at pH > 13.55 (T= 25˚C, μ = 0.1 *m*; Makarov et al., 2010).

2.3 Aqueous sulfide, thiosulfate, and sulfate

Aqueous sulfide compounds (H_2S, HS^-, and S^{2-}) and sulfate (SO_4^{2-}) represent the lowest and highest oxidation states of sulfur (-2 and +6, respectively), and are the most abundant forms of sulfur in natural systems, either in aqueous or mineral form. Thiosulfate ($S_2O_3^{2-}$) is also a relatively common mixed-valence intermediate in sulfur cycling processes (e.g., Jørgensen, 1990; Jørgensen and Nelson, 2004; Zopfi et al., 2004).

The first acid dissociation quotient (pQ_{d1}) of H_2S is very close to neutral pH at 25˚C and μ = 0 *m* ($H_2S \rightleftharpoons HS^- + H^+$, pQ_{d1} = 6.98; Hershey et al., 1988). In the range of ca. 100-350˚C, pQ_{d1} increases with increasing temperature (e.g., at 300˚C, $pQ_{d1} \approx$ 8.2; Ellis and Giggenbach, 1971; Ohmoto and Lasaga, 1982). The second acid dissociation quotient ($HS^- \rightleftharpoons S^{2-} + H^+$, pQ_{d2}) is not as well constrained, but likely to be on the order of $pQ_{d2} \approx$ 17-18 at 25˚C (Ellis and Giggenbach, 1971; Schoonen and Barnes, 1988; Migdisov et al., 2002). Thus, S^{2-} may only comprise an appreciable component of aqueous sulfide speciation in highly alkaline solutions possibly at high temperature (Ellis and Giggenbach, 1971). Under the conditions of most natural systems, aqueous sulfide is therefore predominately in the form of H_2S or HS^- (and any ion pairs, e.g., $NaSH_{(aq)}$, $FeS_{(aq)}$).

Sulfuric acid (H_2SO_4) is a very strong acid and the doubly protonated form generally does not form an appreciable component of the mass balance of sulfate solutions at low temperature, but it may become a significant species in low pH solutions at high temperature (Ohmoto and Lasaga, 1982 and references therein). The second acid dissociation quotient for sulfuric acid ($HSO_4^- \rightleftharpoons SO_4^{2-} + H^+$) is pQ_{d2} = 1.99 ± 0.01 at 25˚C and μ = 0 *m* (Martell and Smith, 1982) but has values as high as 6.4 at 350˚C (*cf.* Ohmoto and Lasaga, 1982 and references therein).

Thiosulfate ($S_2O_3^{2-}$, schematically: $S\text{-}SO_3^{2-}$) contains two sulfur atoms: one outer ("sulfanyl") sulfur in a -1 oxidation state and another inner ("sulfonate") sulfur in a +5 oxidation state that is four-fold coordinated with the sulfanyl sulfur and three oxygen atoms (Vairavamurthy et al., 1993). There are many hypothetical forms of protonated thiosulfate: isomeric forms of $HS_2O_3^-$ (e.g., $(HS)SO_3^-$, $S_2O_2OH^-$) and isomeric forms of $H_2S_2O_3$ (e.g., $(HS)SO_2(OH)$ and $S_2O(OH)_2$) (Steudel and Steudel, 2009). Anhydrous forms of $H_2S_2O_3$ have been reported in syntheses as well as solid forms of $HS_2O_3^-$ ($[NH_4][HS_2O_3]$) (Steudel and Prenzel, 1989 and references therein), but protonated forms in the aqueous phase are unstable (e.g., decomposing readily to elemental sulfur, sulfur dioxide, and water) and have never been directly detected in solution via spectroscopic techniques (e.g., Steudel and Prenzel, 1989; Steudel and Steudel, 2009). Acid dissociation quotients for $H_2S_2O_3$ have been reported: $pQ_{d1} \approx$ 0.6 and pQ_{d2} = 1.6 ± 0.1 at 25˚C and μ = 0 *m* (Martell and Smith, 1982) and these pQ_d values may increase with increasing temperature over hydrothermal ranges (Ohmoto and Lasaga, 1982 and references therein).

3.0 Methods

3.1 Overview: The Bigeleisen and Mayer equation

Theoretical calculations of equilibrium fractionation factors use the principles of quantum mechanics to calculate the ground-state vibrational frequencies of molecules for use in the Bigeleisen and Mayer equation (BM-equation; Bigeleisen and Mayer, 1947; Urey, 1947). These techniques have been widely applied since the derivation of the BM-equation and many extensive reviews cover this approach in detail (e.g., Urey, 1947; Chacko et al., 2001; Wolfsberg et al., 2010; Liu et al., 2010).

To begin, consider the isotope exchange reaction:

$$AX + B^*X \rightleftharpoons A^*X + BX, \quad (4)$$

where A, B and X are generic elements and the superscript "*" denotes the heavy isotope of element X. The equilibrium constant for this exchange reaction can be written in terms of isotope ratios:

$$K = (A^*X)(BX)/(AX)(B^*X) = (^*X/X)_{AX}/(^*X/X)_{BX} \quad (5)$$

Using the basic principles of statistical mechanics, the isotope ratios *X/X can be recast in terms of partition function ratios *Q/Q of isotopomer pairs:

$$K = (^*Q_{total}/Q_{total})_{AX}/(^*Q_{total}/Q_{total})_{BX} \quad (6)$$

where,

$$\frac{^*Q_{total}}{Q_{total}} = \frac{^*Q_{translational}\,^*Q_{rotational}\,^*Q_{vibrational}\,^*Q_{electronic}\,^*Q_{nuclear}\cdots}{Q_{translational}Q_{rotational}Q_{vibrational}Q_{electronic}Q_{nuclear}\cdots} \quad (7)$$

Writing the total partition function for a molecule as a product of the partition functions of different energy terms is equivalent to stating that the total energy of a molecule is given by the sum of its constituent types of energy (translational, rotational, vibrational, etc.). Though widely applied, this formulation is not exact and

introduces approximations including the "Rigid-Rotator-Harmonic-Oscillator" approximation that neglects any coupling between rotational and vibrational modes (e.g., McQuarry, 2000). This necessitates harmonic vibrational frequencies be used in the $Q_{vibrational}$ terms (*cf.* Liu et al., 2010).

For typical isotope exchange reactions of low-mass elements like sulfur, only the translational, rotational, and vibrational partition functions are considered at the typical desired levels of precision in the fractionation factor (order of tenths of a permil or lower). In other words, the *Q/Q terms for electronic, nuclear, etc. can be considered unity to a good approximation for isotope equilibria involving low-mass elements. The partition functions for translational, rotational, and vibrational energies are typically given by:

$$Q_{translational} = V \left(\frac{2\pi MkT}{h^2}\right)^{3/2} \quad (8)$$

$$Q_{rotational} = \frac{\pi^{1/2}(8\pi^2 kT)^{3/2}(I_A I_B I_C)^{1/2}}{s h^3} \quad (9)$$

$$Q_{vibrational} = \prod_i^{3n-6} \frac{e^{-hc\omega_i/2kT}}{1-e^{-hc\omega_i/kT}} \quad (10)$$

Where V is the molecular volume, M is the molecular mass, k is the Boltzmann constant, T is temperature, h is the Planck constant, $I_{\#}$ is the moment of inertia around axis # (A, B, and C represent the principle axes of rotation for a polyatomic molecule), s is the symmetry number, c is the speed of light, ω_i is the wave number for harmonic vibrational mode i (note vibrational frequency $\nu_i = c\omega_i$), and the product in $Q_{vibrational}$ is over all harmonic vibrational modes (number of modes equal to 3n – 6 for a non-linear molecule and 3n – 5 for a linear molecule, where n is the number of atoms in the molecule). $Q_{translational}$ and $Q_{rotational}$ are classical

formulations (often considered adequate) and $Q_{vibrational}$ is the quantum mechanical formulation in the harmonic vibrational ground state (i.e., zero-point energy state).

When considered as $^*Q_{total}/Q_{total}$, many of the terms in the above formulations cancel leaving the $^*Q_{total}/Q_{total}$ partition function ratio as a function of the isotopomer-specific quantities: symmetry number, molecular mass, moments of inertia, and harmonic vibrational frequencies (*cf.* Urey, 1947). A further formalism is applied (the Teller-Redlich spectroscopic theorem, additionally dropping a term that always cancels in fractionation factors), the overall result being the so-called Reduced Partition Function Ratio (RPFR), or Bigeleisen and Mayer equation (or Urey model), that puts $^*Q_{total}/Q_{total}$ in terms of the isotopomer-specific quantities of symmetry numbers and vibrational frequencies only:

$$\mathrm{RPFR} = \frac{s}{s^*}\prod_i^{3n-6}\frac{u_i^*\, e^{-u_i^{*}/2}(1-e^{-u_i})}{u_i\, e^{-u_i/2}(1-e^{-u_i^{*}})} \qquad (11)$$

Where $u_i=hc\omega_i/kT$. In many cases, isotopic substitution does not change the symmetry of the isotopomer and the quantity s/s^* is unity, leaving the RPFR in terms of harmonic vibrational frequencies. In all cases, symmetry numbers do not influence isotope partitioning and merely represent the relative probabilities of forming asymmetric vs. symmetric molecules (Bigeleisen and Mayer, 1947). For this reason, the s/s^* term is often factored out to the left-hand side of the equation.

RPFRs are commonly represented as β-values, where $\beta = [\mathrm{RPFR}]^{1/n}$ and n equals the number of substituted isotopes in equivalent elemental sites (Richet et al., 1977; Chacko et al., 2001). Defined this way, β-values represent RPFRs of singly-substituted isotopomers. Fractionation factors (denoted α) between two compounds are easily computed by taking the ratio of their respective β-values: e.g., $\alpha_{A\text{-}B} = \beta_A/\beta_B$.

In this formulation (single isotope exchange), the fractionation factor (α) is equivalent to the equilibrium isotope exchange constant (K).

3.2 Mass dependence of isotope effects and reduced partition function ratios

The mass dependence of an isotope effect relating a minor isotope fractionation factor and the major isotope fractionation factor is given by an exponential relationship (Craig, 1957; Matsuhisa et al., 1978; Clayton and Mayeda, 1996; Miller, 2002), which yields the following for the sulfur isotope system:

$$^{33}\alpha = (^{34}\alpha)^{33/34\lambda} \quad (12)$$

$$^{36}\alpha = (^{34}\alpha)^{36/34\lambda} \quad (13)$$

Such exponential forms were postulated early in stable isotope investigations to explain mass dependence (e.g., Craig, 1957; Swain, et al., 1958) and were recognized in the early stages of sulfur isotope geochemistry as the most accurate means to describe the generalized mass dependence among multiple sulfur isotope measurements of natural samples as the slopes of regressions of isotope data in $\ln(^{n}R/^{n}R_{ref})$ vs. $\ln(^{34}R/^{34}R_{ref})$ space (n = 33 or 36; Hulston and Thode, 1965; note: some adopt the delta prime notation as an equivalent expression, i.e., $\delta'^{n}S=1000\ln(^{n}R/^{n}R_{ref})$). The capital delta values commonly employed in multiple sulfur isotope studies ($\Delta^{33}S$ and $\Delta^{36}S$) are defined from such exponential relationships as deviations from a reference exponent ($\Delta^{33}S = {}^{33}\alpha - (^{34}\alpha)^{0.515}$ and $\Delta^{36}S = {}^{36}\alpha - (^{34}\alpha)^{1.9}$), where the reference exponents are intended to represent the approximate relationship of mass dependence for typical equilibrium isotope exchange reactions at lower temperatures (i.e., well below the high temperature limit). Similar exponential relationships can be applied to a RPFR ratio computed for single major and minor

isotope substitution relationship, e.g., $^{33}\beta = (^{34}\beta)^{33/34\lambda}$ (Matsuhisa et al., 1978). We will refer to the mass dependence exponent computed from RPFRs (represented as β values) as $^{n/34}\lambda_{\beta}$ (n = 33 or 36).

3.3 Quantum mechanical software: Gaussian 09

Harmonic vibrational frequencies can be readily obtained via quantum mechanical software for use in the BM-equation. These methods rely either on approximate solutions to the Schrödinger equation (e.g., the Hartree-Fock and Møller-Plesset approaches; HF, MP2, MP3, etc.) or solutions to approximations of the Schrödinger equation (e.g., density functional theory and related hybrid methods like B3LYP and others) with varying levels of basis sets applied to model the Hamiltonian operator and wave function (or approximations to the wave function; i.e., electron density for DFT methods) to obtain solutions containing terms related to the energy of a molecular system (e.g., Simons, 1991; Cramer, 2002). We use Gaussian 09 software (Frisch et al., 2010) at the B3LYP/6-31+G(d,p) level of theory and basis set in this study. The B3LYP method is a hybrid HF/B-LYP theoretical approach (employing the Becke and Lee, Yang, & Parr 3-parameter gradient-corrected correlational functional; Lee et al., 1988; Becke, 1993; Foresman and Frisch, 1996) that includes electron correlation. The basis set is the double-zeta Pople basis set (6-31) with diffuse functions added (+) to the non-hydrogen atoms (often required for modeling anions) and polarization functions (p functions for all atoms, d functions for all non-hydrogen atoms) for additional flexibility in the computation of molecular orbitals. Overall, it is a low/moderate approach used for computational practicality for the relatively large molecular clusters computed here.

3.4 Explicit solvation model

Optimization and frequency calculations were carried out with the sulfur molecules of interest explicitly coordinated with water molecules in clusters containing up to 30-40 H_2O. Optimizations of molecular clusters were carefully performed step-wise. First, the sulfur molecules of interest were coordinated with ca. 24-27 water molecules and optimized at relatively low levels of theory and basis set (i.e., B3LYP/6-31G(d)), after which more water molecules added until clusters reached the maximum size of 30-40 depending on the molecule and the required solvation coverage. In the building of clusters, care was taken to ensure the proper orientation of water molecules with respect to themselves and solute anions for efficient optimizations and to avoid solute migration to the edge of the cluster. The majority of the final optimization and frequency calculations were performed at the B3LYP/6-31+G(d,p) level on a desktop computer at the University of Maryland. For some of the sulfite calculations, coordinates from lower-level B3LYP/6-31G(d) optimizations (computed at the University of Maryland) were run at the B3LYP/6-31+G(d,p) level on the high performance computation cluster (Scylla) at the Woods Hole Oceanographic Institution.

3.5 Sources of uncertainty

Uncertainties in our theoretically estimated fractionation factors can derive from three main sources: (1) errors arising from the harmonic and other approximations in the derivation of the Bigeleisen and Mayer equation (requiring higher-order corrections, e.g., for anharmonicity), (2) inadequacies in the theoretical method, and (3) variability arising from the water cluster geometry. All RPFRs and

fractionation factors in this study are reported in the harmonic approximation due to the inability to apply appropriate anharmonic corrections to our cluster calculations at this time. We compute the anharmonic corrections to the ZPE (AnZPE) for a handful of gaseous sulfur molecules (H_2S, $S(OH)_2$, $(HS)O_2H$, SO_2, SO_3) at the B3LYP/6-31+G(d,p) level to gain insight into the magnitude of these corrections for more complex systems (section 5.1). We have additionally chosen not to apply any scaling factors (harmonic or otherwise) to our harmonic frequencies due to the potential issues associated with this practice (section 5.1), but we do discuss the effects of harmonic scaling derived from high level gas phase calculations (CCSD/aug-cc-pVTZ) on fractionation factors for individual systems (following the approach of Li and Liu, 2011) (section 5.4). Unless otherwise noted, all plotted and tabulated RPFRs and fractionation factors utilize un-scaled harmonic frequencies at the B3LYP/6-31+G(d,p) level. To evaluate variability associated with cluster geometry, we performed a series of at least duplicate constructions and optimizations for a select set of 30-40H_2O clusters in the sulfite system: SO_3^{2-}, $(HS)O_3^-$, $(HO)SO_2^-$, and the bisulfite dimer pyrosulfite, $S_2O_5^2$. Uncertainties derived from the above sources are discussed in more detail in section 5.1.

4.0 Results

Optimized geometries of the 30H_2O molecular clusters of compounds in the sulfite, sulfoxylate, and other systems (sulfide, thiosulfate, sulfate) are presented in Figure 2.3, Figure 2.4, and Figure 2.5, respectively.

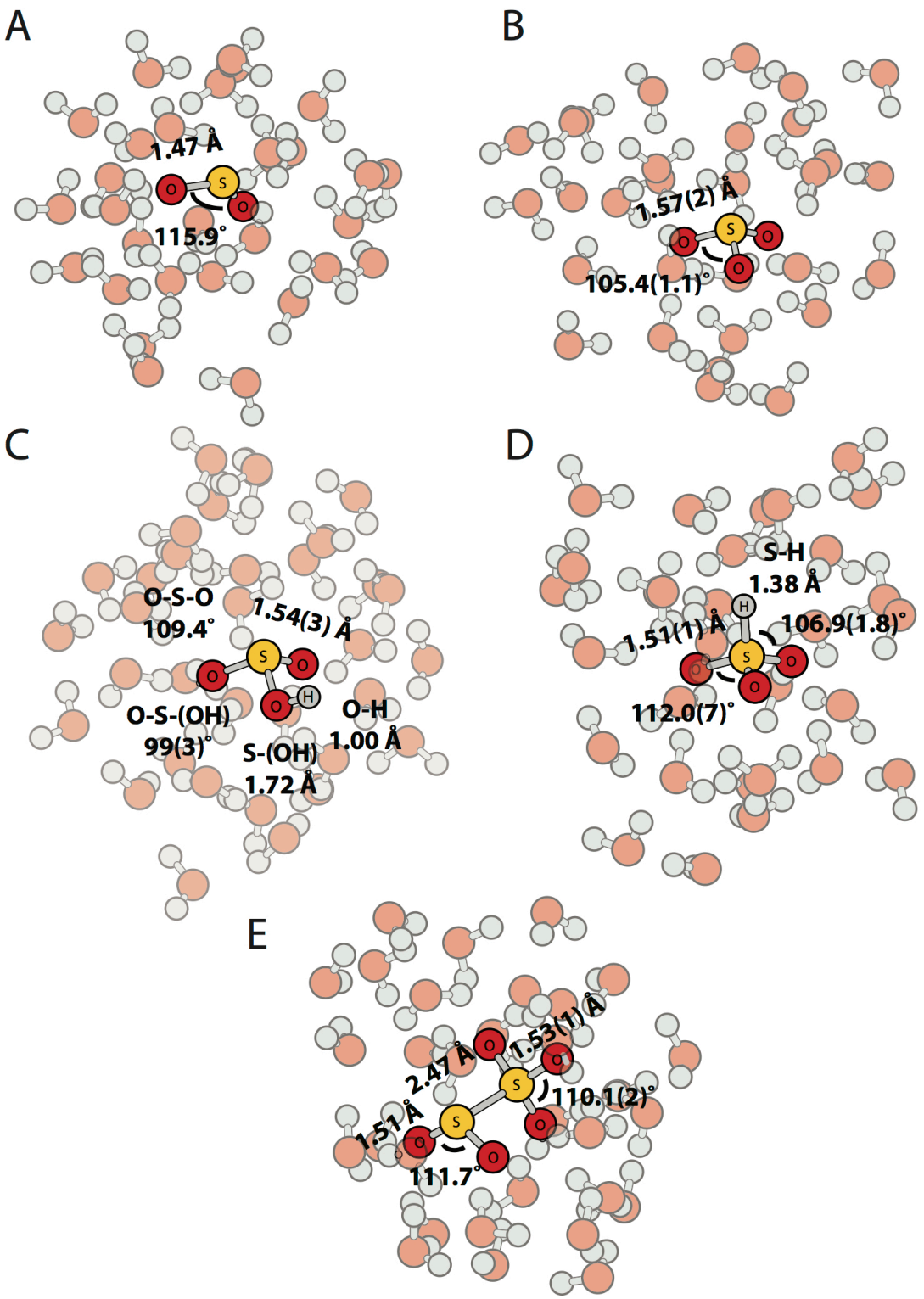

Figure 2.3: Optimized geometries of sulfite species in $30H_2O$-$34H_2O$ clusters. (A) Sulfur dioxide ($SO_{2(aq)}$•$30H_2O$), (B) sulfite *sensu stricto* (SO_3^{2-}•$30H_2O$), (C) OH isomer of bisulfite ($(HO)SO_2^-$ •$34H_2O$), (D) HS isomer of bisulfite ($(HS)O_3^-$•$30H_2O$), and (E) the bisulfite dimer, disulfite ($S_2O_5^{2-}$ •$30H_2O$) containing the shortest computed S-S bond length.

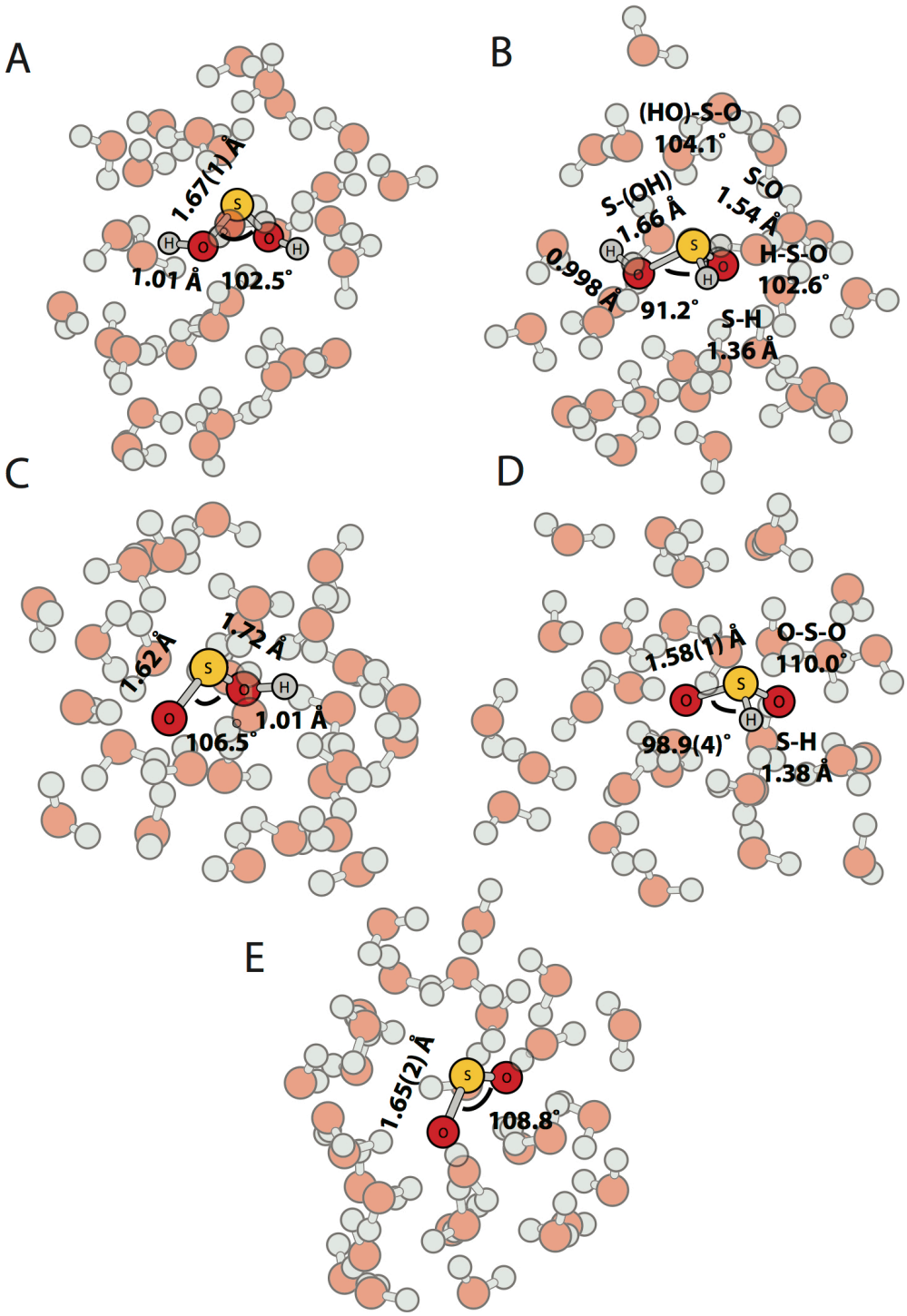

Figure 2.4: Optimized geometries of sulfoxylate species in $30H_2O$ clusters. (A) Sulfoxylic acid ($S(OH)_2$), (B) sulfinic acid ($(HS)O_2H$), (C) OH isomer of bisulfoxylate ($(HO)SO^-$), (D) SH isomer of bisulfoxylate ($(HS)O_2^-$), and (E) sulfoxylate (SO_2^{2-}).

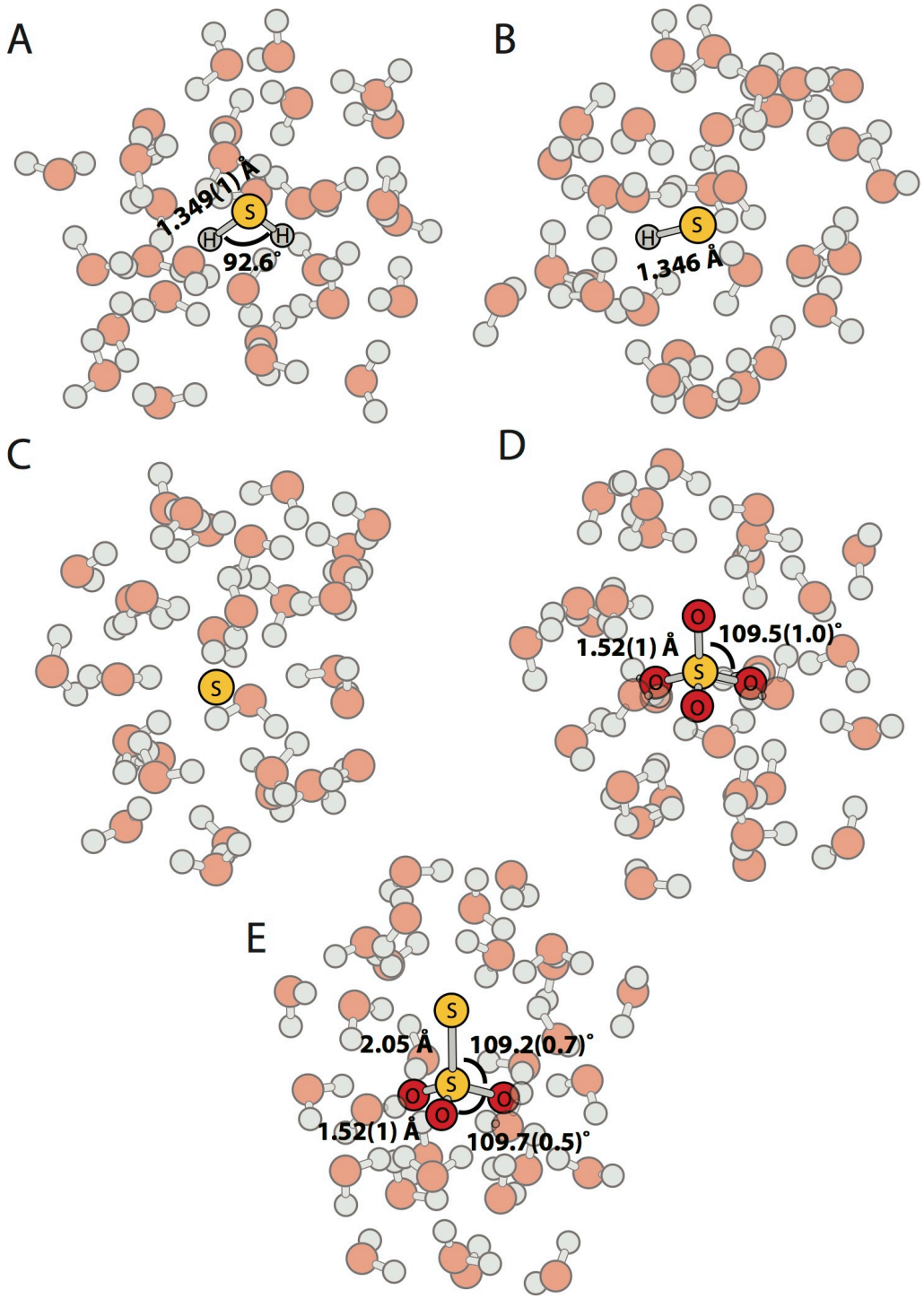

Figure 2.5: Optimized geometries of sulfide species, sulfate, and thiosulfate in $30H_2O$ clusters. (A) Hydrogen sulfide (H_2S), (B) bisulfide (HS^-), (C) sulfide anion (S^{2-}), (D) sulfate (SO_4^{2-}), and (E) thiosulfate ($S_2O_3^{2-}$).

4.1 Reduced partition function ratios

The major isotope RPFRs ($^{34}\beta$) calculated at the B3LYP/6-31+G(d,p) level are presented in Figure 2.6 as functions of inverse absolute temperature (1000/T; 273-373 K) for all aqueous cluster calculations, including the sulfite system, sulfoxylate system, sulfide system, sulfate, and thiosulfate (inner 'sulfonate' sulfur, and the outer 'sulfanyl' sulfur). A tabulation of coefficients to polynomial fits to the RPFRs over 0-2000˚C based on all three isotope ratios of sulfur is given in Table 2.3 in the form of $A/T^4 + B/T^3 + C/T^2 + D/T + E$ (T in Kelvin).

Our calculated $^{34}\beta$ values generally scale with the oxidation state of sulfur, where higher oxidation states generally have higher RPFRs than lower oxidation states, with the exception of the two sulfur atoms in thiosulfate (-1 and +5; Vairavamurthy et al., 1993). For a given temperature and oxidation state of sulfur, our calculations predict that the magnitude of the $^{34}\beta$ increases with increasing coordination of the sulfur atom. The species with the highest coordination of sulfur in each system—e.g., the 4-fold coordinated $(HS)O_3^-$ isomer of bisulfite and the 3-fold coordinated sulfinic acid and $(HS)O_2^-$ isomer of bisulfoxylate—have the highest $^{34}\beta$ of their respective systems, and species of lower coordination have lower $^{34}\beta$. For example, in the sulfite system, which contains the greatest diversity in bonding arrangements around sulfur of any system in this study—triatomic bent, pyramidal, and tetrahedral—the RPFRs scale directly with coordination where: $^{34}\beta = (HS)O_3^- > SO_3^{2-} \approx (HO)SO_2^- > SO_{2(aq)}$. Species where protonation occurs only on the oxygen atoms (i.e., $(HO)SO_2^-$, $(HO)SO^-$, and $S(OH)_2$) typically exhibit very similar RPFRs to their un-protonated counterparts.

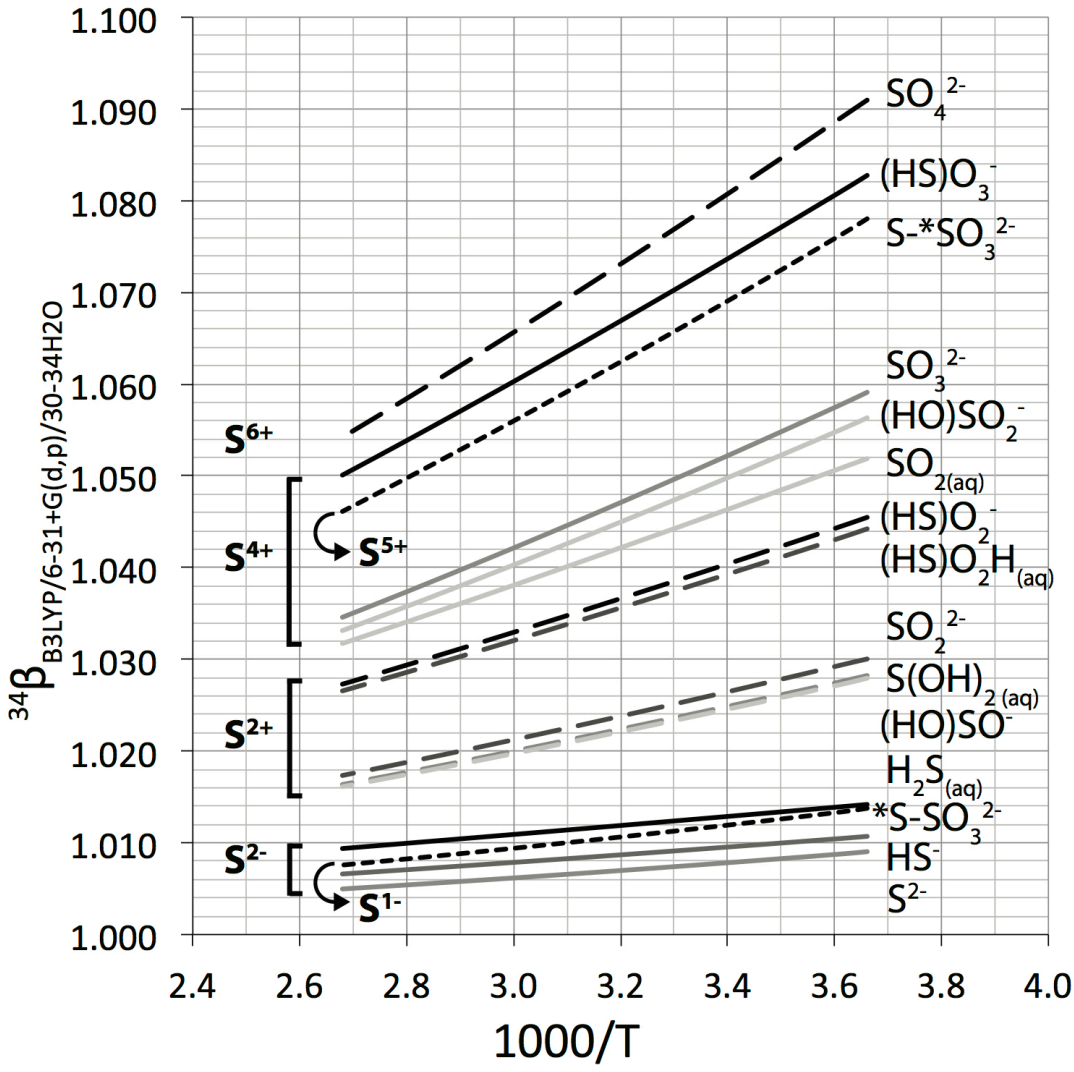

Figure 2.6: Reduced partition function ratios (noting $^{34}\beta = (RPFR)^{1/n}$, n = # of equivalent substituted sites) corresponding to the major isotope ratio of sulfur ($^{34}S/^{32}S$) for calculations in 30-34 H_2O clusters at the B3LYP/6-31+G(d,p) level of theory over T = 0-100˚C.

The isotope partitioning behavior of the bisulfite dimer, pyrosulfite ($S_2O_5^{2-}$), warrants its own separate description due to its unusual structure; it has been omitted from Figure 2.6 for simplicity of presentation and due to difficulties in constraining its structure. Disulfite contains two sulfur atoms that are coordinated differently in the molecule, where one sulfur atom (denoted "A") is 3-fold coordinated (one S and two O) and the other sulfur atom (denoted "B") is 4-fold coordinated (one S and three O).

We optimized four independently constructed $S_2O_5^{2-}$•nH_2O clusters (two n =30, one n = 31, and one n=40) and found slight variability in the 4-fold coordinated site (^{34}RPFR = 1.0609-1.0633; 25˚C) that appears to correlate with the computed structure's S-S bond length, where higher ^{34}RPFR for this site corresponded to shorter S-S bond lengths (see Figure A.1). In contrast, the 3-fold coordinated site's RPFR was found to be much more consistent between conformers (^{34}RPFR = 1.0438 ± 0.0003; 25˚C; 1 s.e., all four computed conformers) and lower than any other species in the sulfite system. In all cases, the calculated S-S bond lengths for the aqueous clusters—ranging between 2.46-2.54 Å—are significantly longer than available experimental determinations in crystalline solids (~2.2 Å; Zachariasen, 1932). For most discussions in this paper, we will be using the conformer with the shortest S-S bond length and caution that the overall RPFR for disulfite may be poorly constrained by our calculations due to a poorly constrained structure.

4.2 Mass dependence of reduced partition function ratios

In Figure 2.7, we plot the computed $^{33/34}\lambda_\beta = \ln(^{33}\beta)/\ln(^{34}\beta)$ and $^{36/34}\lambda_\beta = \ln(^{36}\beta)/\ln(^{34}\beta)$ as a function of temperature for the explicitly solvated molecular water clusters and the related gaseous species, which here only includes $SO_{2(g)}$ and $H_2S_{(g)}$. The exponents converge on or near a singular value for all compounds at the high temperature limit: i.e., $^{33/34}\lambda_{\beta,\ T\rightarrow\infty} = 0.51587 \pm 0.00003$ and $^{36/34}\lambda_{\beta,\ T\rightarrow\infty} = 1.8905 \pm 0.0002$ (1 s.e. from averaging the intercepts of the polynomial fits; Table 2.3). These calculated values are in generally good agreement with the high temperature limits that have been derived based on the atomic masses of the four sulfur isotopes (*cf.* Matsuhisa et al., 1978; Young et al., 2002):

$$^{33/34}\lambda_{T\rightarrow\infty} = (1/m_{32} - 1/m_{33})/(1/m_{32}\text{-}1/m_{34}) = 0.51588 \quad (14)$$

$$^{36/34}\lambda_{T\rightarrow\infty} = (1/m_{32} - 1/m_{36})/(1/m_{32}\text{-}1/m_{34}) = 1.8904 \quad (15)$$

The variability (or noise) in our computed exponents as the high temperature limit is approached (*cf.* Figure 2.7) is likely the result of error introduced by the cluster model and may relate specifically to the multiple vibrational modes associated with the coordinated water molecules that contribute to the overall RPFRs. Such error may be most exemplified in the calculation of the atomic sulfide ion (S^{2-} •$30H_2O$)—a sulfur species that has no vibrational modes of its own—that displays the most unusual behavior in $^{33/34}\lambda_\beta$ and $^{36/34}\lambda_\beta$ as the high temperature limit is approached.

At temperatures well-below the high temperature limit, $^{33/34}\lambda_\beta$ and $^{36/34}\lambda_\beta$ values follow trends based on coordination and oxidation state similar to those seen in $^{34}\beta$ values as a function of temperature (Figure 2.6), where the end-member oxidation states (sulfide species and sulfate) generally represent end-member values and intermediate oxidation states plot successively in between. Higher oxidation states tend to have lower $^{33/34}\lambda_\beta$ and higher $^{36/34}\lambda_\beta$ than lower oxidation states. For a given oxidation state, the more highly coordinated sulfur bonding sites generally have lower $^{33/34}\lambda_\beta$ and higher $^{36/34}\lambda_\beta$ following similar relationships to those observed in the magnitude of their RPFRs, but with some exceptions. Overall, the exponents of mass dependence for sulfur compounds spanning the entire range of available oxidation states define a narrow range that falls within $^{33/34}\lambda_\beta$ =0.5148-0.5159 and $^{36/34}\lambda_\beta$ = 1.890-1.898 over a wide range of temperature ($T \geq 0^\circ C$).

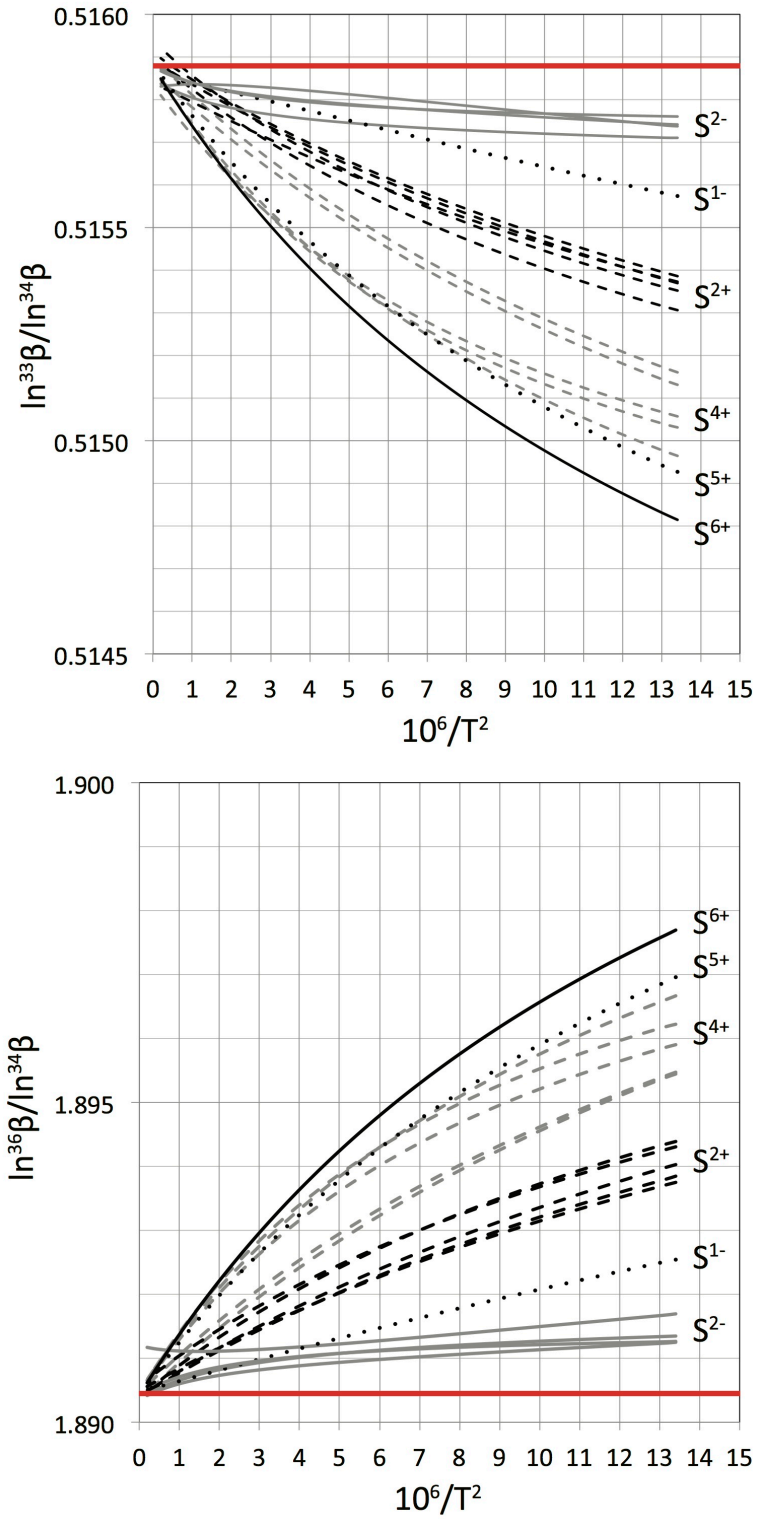

Figure 2.7: Exponents of mass dependence based on RPFRs computed from 0-2000˚C: (a; top) $^{33/34}\lambda_{\beta} \equiv \ln(^{33}\beta)/\ln(^{34}\beta)$ and (b; bottom) $^{36/34}\lambda_{\beta} \equiv \ln(^{36}\beta)/\ln(^{34}\beta)$). The horizontal red lines indicate the high temperature limits (as $T \rightarrow \infty$) based on the atomic mass of the sulfur isotopes (Matsuhisa et al., 1978).

4.3 Fractionations in the sulfite system

Triple sulfur isotope fractionations ($^{33}\alpha$ vs. $^{34}\alpha$) for aqueous species in the sulfite system ($SO_{2(aq)}$, $(HO)SO_2^-$, two conformers of $(HS)O_3^-$, $S_2O_5^{2-}$, and two conformers of SO_3^{2-}) at 25˚C are summarized in Figure 2.8. For purposes of illustration, fractionations are plotted relative to $SO_{2(aq)}$. Fractionations among the major sulfite species in solution ($SO_{2(aq)}$, $(HO)SO_2^-$, and SO_3^{2-}) are relatively small ($1000\ln^{34}\alpha < 6$ ‰). The fractionation between $(HO)SO_2^-$ and SO_3^{2-} at 25˚C is computed to be on the order of -2.2 ‰. Fractionations between the $(HS)O_3^-$ isomer and these species are much larger, where $1000\ln^{34}\alpha$ relative to $SO_{2\ (aq)}$ is on the order of 25 ‰ and between $(HS)O_3^-$ and SO_3^{2-} is 20 ‰ at 25˚C. The influence of the minor $(HS)O_3^-$ isomer on overall isotope partitioning in this system will be a major focus of the discussion (Section 5.4). Regression of the fractionation factors yields a mass dependent exponent $^{33/34}\lambda = 0.5147 \pm 0.0001$ (1 s.e.) with an $R^2 = 1$ and similar regressions of $\ln(^{36}\alpha)$ vs. $\ln(^{34}\alpha)$ (not shown) yield a mass dependent exponent $^{36/34}\lambda = 1.8983 \pm 0.0005$ (1 s.e.) with an $R^2 = 1$.

Fractionations of the bisulfite dimer disulfite ($S_2O_5^{2-}$) are also presented in Figure 2.8. The data points are colored grey to emphasize the potential preliminary nature of these determinations due to uncertainty in the S-S bond length (see section 4.1). The 3-fold coordinated site (with the most reproducible RPFR between conformers) has a slightly lower preference for heavier isotopes than $SO_{2(aq)}$, contrary to what would be expected from simple coordination relationships. The 4-fold coordinated site has a RPFR that is intermediary between the pyramidal and tetrahedral sulfite species. When site-averaged, the isotopic composition of disulfite

is only slightly elevated from sulfite according to the conformer plotted in Figure 2.8. Given the inverse correlation that we have observed between RPFR (namely that of the 4-fold coordinated site) and S-S bond length, we expect this value to represent a minimum site-averaged fractionation factor for the pyrosulfite dimer if our calculations overestimate the S-S bond length.

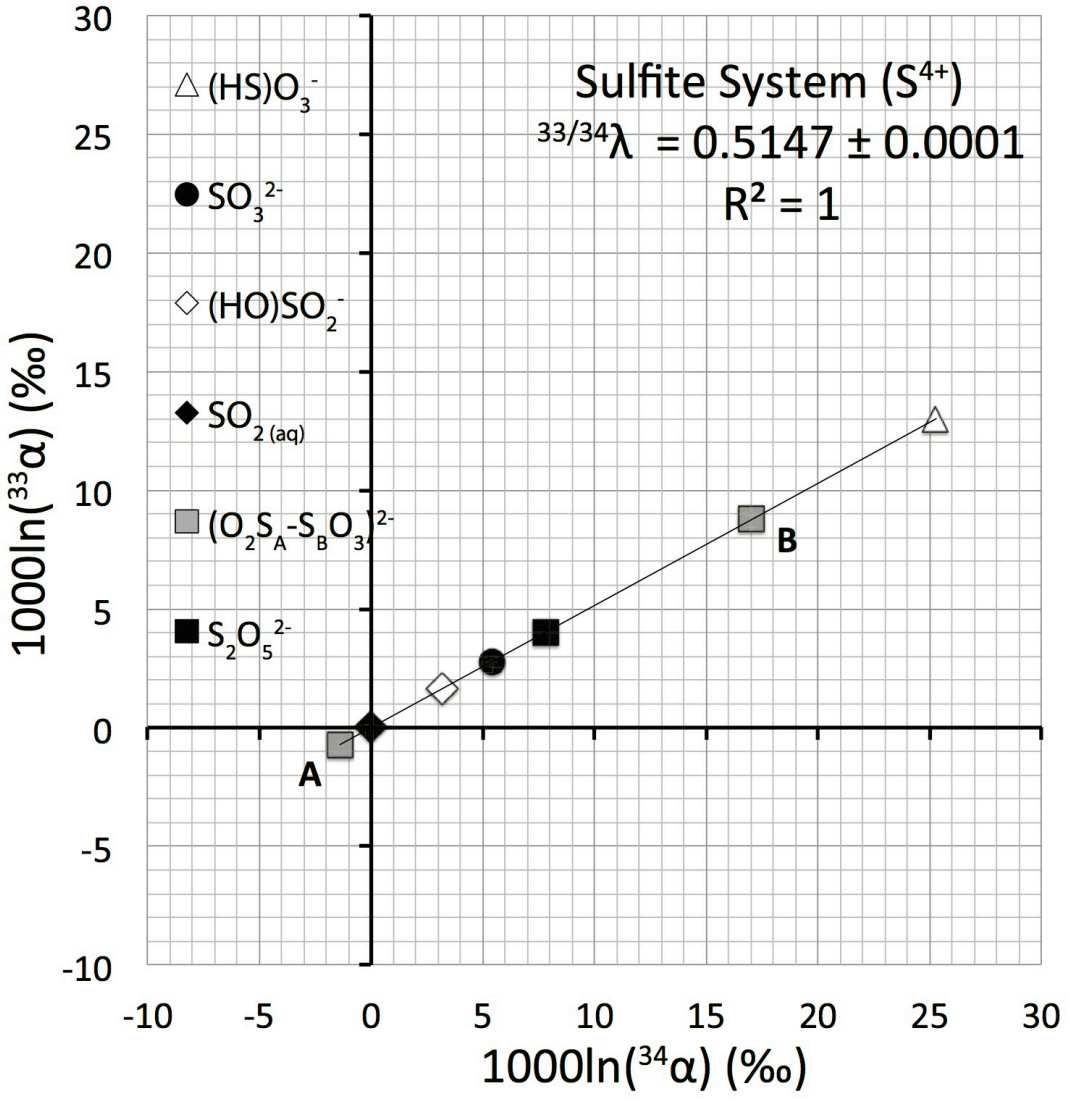

Figure 2.8: Triple isotope plot of theoretical fractionation factors for aqueous sulfite species relative to aqueous sulfur dioxide at 25˚C. The A and B subscripts for disulfite to the 3-fold and 4-fold coordinated sites within the dimer, respectively (gray squares). The $S_2O_5^{2-}{}_T$ refers to the site-averaged fractionation factor for the dimer (black square). The exponent of mass dependence ($^{33/34}\lambda = \ln(^{33}\alpha)/\ln(^{34}\alpha)$) is determined from the least squares linear regression of the fractionation factors.

4.4 Fractionations in the sulfoxylate system

Triple sulfur isotope fractionations ($^{33}\alpha$ vs. $^{34}\alpha$) for aqueous species in the sulfoxylate system (two isomers of H_2SO_2, $(HS)O_2^-$, $OS(OH)^-$, and SO_2^{2-}) at 25˚C are summarized in Figure 2.9. For purposes of illustration, fractionations are plotted relative to sulfoxylic acid, $S(OH)_2$. Similar to the sulfite system, sulfoxylate species with similar coordination around the sulfur atom ($S(OH)_2$, $(HO)SO^-$, SO_2^{2-}) are minimally fractionated with respect to one another ($1000\ln^{34}\alpha < 3$ ‰ at 25˚C) and species where protonation occurs on the sulfur atom—thus, increasing coordination around sulfur—are significantly fractionated from the other species. The $1000\ln^{34}\alpha$ between the three-fold coordinated $(HS)O_2^-$ the two-fold coordinated species is ca. 13.5-15 ‰ at 25˚C. Regression of the fractionation factors yields a mass dependent exponent $^{33/34}\lambda = 0.51530 \pm 0.00004$ (1 s.e.) with an $R^2 = 1$, and similar regressions of $\ln(^{36}\alpha)$ vs. $\ln(^{34}\alpha)$ (not shown) yield a mass dependent exponent $^{36/34}\lambda = 1.8948 \pm 0.0001$ with an $R^2 = 1$.

4.5 Fractionations in the sulfide system

Triple sulfur isotope fractionations ($^{33}\alpha$ vs. $^{34}\alpha$) for aqueous species in the sulfide system (H_2S, HS^-, and S^{2-}) at 25˚C are summarized in Figure 2.10. For purposes of illustration, fractionations are plotted relative to the divalent sulfide anion, S^{2-}. Similar to the sulfite and sulfoxylate systems, the magnitude of fractionation between sulfide species increases with coordination. In all cases, fractionations are predicted to be relatively small in the sulfide system: $1000\ln^{34}\alpha$ between H_2S and HS^- is estimated to be on the order of 3.3 ‰ and the $1000\ln^{34}\alpha$ between HS^- and S^{2-} is on the order of 1.7 ‰ at 25˚C. Regression of the fractionation

factors yields a mass dependent exponent $^{33/34}\lambda = 0.51565 \pm 0.00003$ (1 s.e.) with an $R^2 = 1$ and similar regressions of $\ln(^{36}\alpha)$ vs. $\ln(^{34}\alpha)$ (not shown) yield a mass dependent exponent $^{36/34}\lambda = 1.8910 \pm 0.0006$ with an $R^2 = 1$.

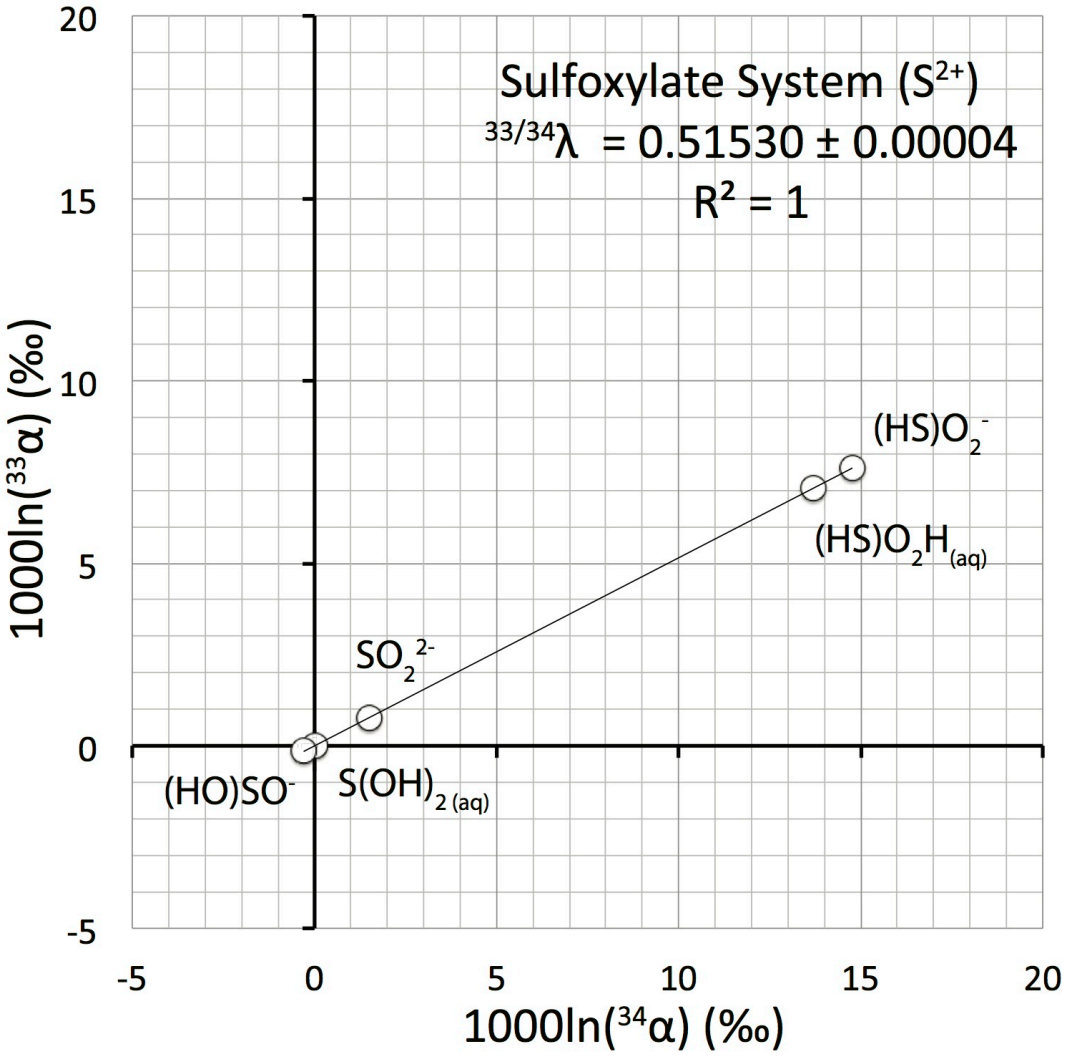

Figure 2.9: Triple isotope plot of theoretical fractionation factors for aqueous sulfoxylate species relative to sulfoxylic acid, $S(OH)_2$, at 25˚C. The exponent of mass dependence ($^{33/34}\lambda = \ln(^{33}\alpha)/\ln(^{34}\alpha)$) is determined from the least squares linear regression of the fractionation factors.

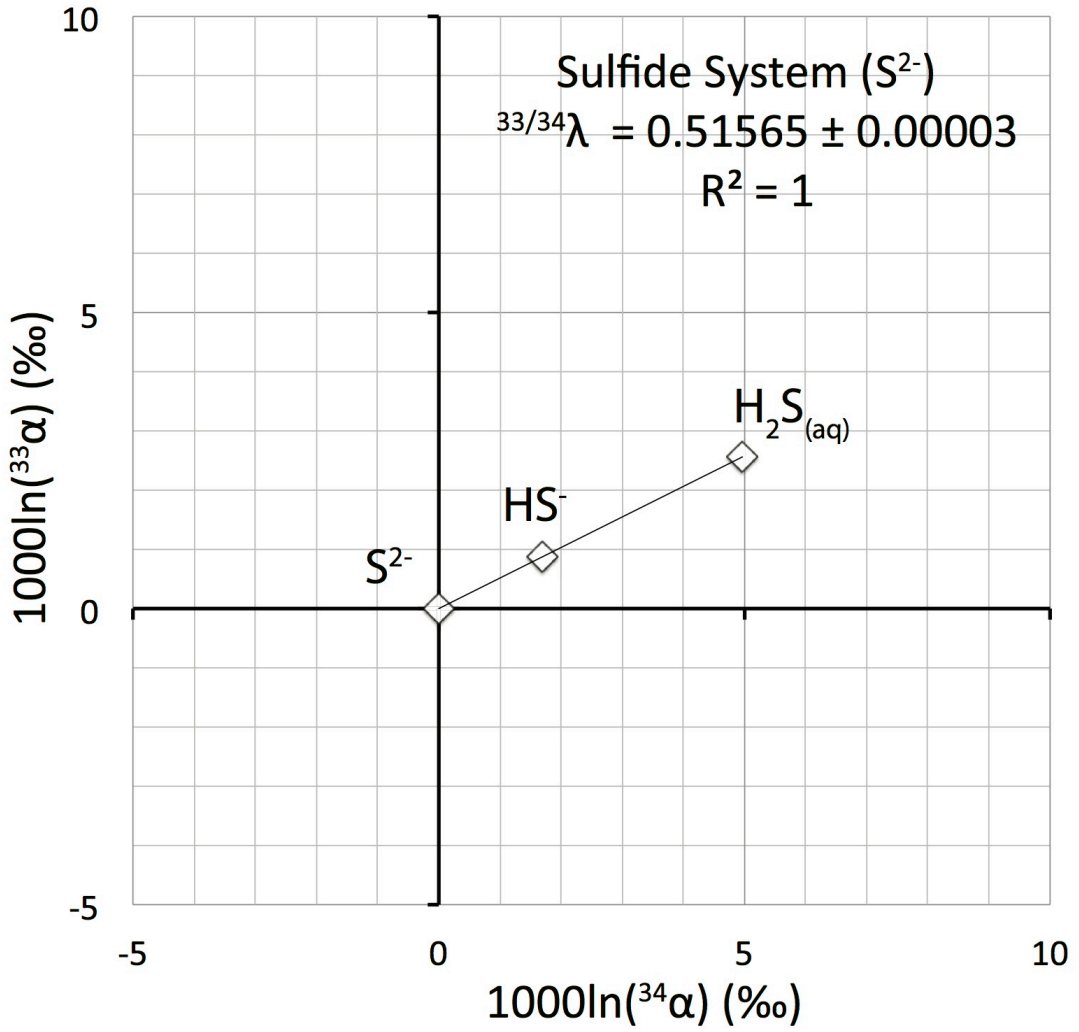

Figure 2.10: Triple isotope plot of theoretical fractionation factors for aqueous sulfide species relative to the atomic sulfide ion, S^{2-}, at 25˚C. The exponent of mass dependence ($^{33/34}\lambda = \ln(^{33}\alpha)/\ln(^{34}\alpha)$) is determined from the least squares linear regression of the fractionation factors.

4.6 Fractionations between sulfate and sulfide species

Fractionations between the two end-member oxidation states of sulfur (S^{2-} and S^{6+}) yield the largest equilibrium isotope effects in the aqueous sulfur system. The fractionation factor between SO_4^{2-} and $H_2S_{(aq)}$ is ($^{34}\alpha_{sulfate\text{-}H2S}$) is predicted to be 1.0655 with corresponding $^{33/34}\lambda$ = 0.51475 and $^{36/34}\lambda$ = 1.8981 at 25˚C. The fractionation factor between SO_4^{2-} and HS^- is ($^{34}\alpha_{sulfate\text{-}HS\text{-}}$) is predicted to be 1.0690 with corresponding $^{33/34}\lambda$ = 0.51480 and $^{36/34}\lambda$ = 1.8978 at 25˚C. Similarly, the

fractionation factor between sulfate and the atomic sulfide dianion, S^{2-}, ($^{34}\alpha_{sulfate\text{-}sulfide}$) is predicted to be 1.0708 with corresponding $^{33/34}\lambda$ = 0.51482 and $^{36/34}\lambda$ = 1.8976 at 25˚C.

4.7 Fractionations involving thiosulfate and the major sulfide species

The intramolecular fractionation factor between the outer ("sulfanyl") and inner ("sulfonate") sulfur atoms in thiosulfate ($S_2O_3^{2-}$) ($1000\ln^{34}\alpha_{outer\text{-}inner}$) is predicted to be on the order of -53.8 ‰ at 25˚C, with corresponding $^{33/34}\lambda$ = 0.51489 and $^{36/34}\lambda$ = 1.8972. The fractionation factor between the outer ("sulfanyl") sulfur atom in thiosulfate and H_2S ($1000\ln^{34}\alpha_{outer\text{-}H2S}$) is predicted to be small and on the order of –1.0 ‰ at 25˚C, where the magnitude of the major isotope fractionation factor increases with temperature (inverse temperature dependence) over the approximate temperature range of ≈ -15 to 180˚C to a maximum approaching $1000\ln^{34}\alpha_{outer\text{-}H2S} \approx$ –2 ‰ at ≈ 180˚C. This inverse temperature dependence is the consequence of a crossover in the direction of the $^{34}\alpha_{outer\text{-}H2S}$ fractionation factor at sub-0˚C temperature ($T_{34/32\text{-}crossover} \approx$ -15˚C). The fractionation factor between the outer sulfur ("sulfanyl") atom in thiosulfate and the HS^- ion ($1000\ln^{34}\alpha_{outer\text{-}HS\text{-}}$) is predicted to be 2.3 ‰ at 25˚C (opposite in direction to the similar H_2S-based fractionation factor at 25˚C) and also exhibits a crossover in proximity to ≈ 270˚C. The exponents of mass dependence ($^{33/34}\lambda$ and $^{36/34}\lambda$) associated with both $\alpha_{outer\text{-}H2S}$ and $\alpha_{outer\text{-}HS\text{-}}$ exhibit characteristic asymptotic behavior at their respective crossover temperatures (*cf.* Deines, 2003; Otake et al., 2008) (not shown) that lead to unusual exponents in proximity to the crossover temperature. For example, at 0˚C the $^{33/34}\lambda$ and $^{36/34}\lambda$ associated with $\alpha_{outer\text{-}H2S}$ are computed to be 0.5197 and 1.857, respectively. Despite

the unusual exponents associated with these crossovers, the capital delta values associated with these fractionation factors are very near zero at all relevant temperatures: e.g., at $T \geq 0^{\circ}C$, $\Delta^{33}S_{\text{outer-H2S}} \leq -0.002$ ‰ and $\Delta^{36}S_{\text{outer-H2S}} \leq -0.02$ ‰, and $\Delta^{33}S_{\text{outer-HS-}} \approx 0.000$ ‰ and $\Delta^{36}S_{\text{outer-HS-}} \leq 0.01$ ‰.

5.0 Discussion

5.1 Uncertainties in estimated fractionation factors

Uncertainties in our theoretically estimated fractionation factors can derive from three main sources: (1) errors arising from the harmonic and other approximations in the derivation of the Bigeleisen and Mayer equation (requiring higher-order corrections, e.g., for anharmonicity), (2) inadequacies in the theoretical method, and (3) variability arising from the water cluster geometry. To quantitatively evaluate these uncertainties, we adopt a similar approach to Li and Liu (2011), where a similar water cluster model was used to calculate the equilibrium isotope fractionations among aqueous selenium compounds and anions.

Harmonic approximation

The BM-equation requires that harmonic frequencies be used to justify the various approximations used in its derivation (*cf.* Rustad and Bylaska, 2007; Rustad et al., 2010; Liu et al., 2010). We therefore use the calculated harmonic frequencies to calculate RPFRs and isotope fractionation factors. An appropriate comparison of theoretically computed vibrational frequencies to those derived from experiments is not possible at this time, because the conversion of our computed harmonic frequencies to fundamental frequencies requires computation of anharmonic constants (*cf.* Liu et al., 2010). The computation of anharmonic constants for large molecular

clusters is computationally laborious and is beyond our computational resources. We therefore considered these computations beyond the scope of this study. Instead, we focus on calculations of anharmonic corrections to the BM-equation (RPFR) for simple gaseous molecules to gain insight into the magnitude of these corrections for more complex systems.

Liu et al. (2010) reviewed and applied a variety of anharmonic and higher-order corrections to the BM-equation for simple gaseous molecules at the MP2/aug-cc-pVTZ level. They show that many of these corrections are only significant when dealing with hydrogen-deuterium exchange reactions. For example, the total $^{34}S/^{32}S$-based corrected partition function ratios (CPFR) for $H_2S_{(g)}$ and $SO_{2(g)}$ are shifted by 0.3 and 0.6 ‰ at 300 K from their uncorrected RPFR counterparts, respectively, where the entirety of the correction for both compounds arises from the anharmonic contribution to the zero point energy (AnZPE; all other corrections have negligible effect; Liu et al., 2010). We have computed the anharmonic corrections to the ZPE (AnZPE) for a handful of gaseous sulfur molecules (H_2S, $S(OH)_2$, $(HS)O_2H$, SO_2, SO_3) at the B3LYP/6-31+G(d,p) level and find that they are of a similar magnitude (H_2S, $S(OH)_2$, $(HS)O_2H$, SO_2: ~ -0.5 ‰, SO_3: ~ -0.9 ‰; 25˚C) (Figure A.2). Due to the low magnitude of these corrections and the inability to apply appropriate anharmonic corrections to our cluster calculations at this time, all RPFRs and fractionation factors in this study are reported in the harmonic approximation.

Theoretical Level

The theoretical method employed can lead to significant error in the computed RPFRs and fractionation factors (*cf.* Rustad et al., 2008; Rustad et al., 2010). We

evaluated the potential error introduced by any inadequacies in our theoretical method via harmonic frequency scaling using high-level computations of simple neutral molecules modeled in the gas phase (*cf.* Li and Liu, 2011). Note that this is not the same practice as scaling theoretical harmonic frequencies to fit experimental fundamental frequencies that introduce anharmonic contributions to the theoretical frequencies.

We computed harmonic frequencies for H_2S, S_2, SO_2, and SO at the CCSD/aug-cc-pVTZ level and derived a first-order harmonic scaling factor for the B3LYP/6-31+G(d,p) level employed for our water clusters on the order of 1.01-1.02 (i.e., a uniform 1-2% positive shift in the harmonic frequencies; Figure A.3). The influence of this scaling factor on the RPFRs and the computed fractionation factors varies depending on the compound(s) and temperature considered, but is generally magnified at lower temperatures. The effect of harmonic scaling is often negligible but can be on the permil level for some computed fractionation factors that involve compounds with higher magnitude RPFRs. For example, for the $SO_4^{2-}{}_{(30H2O)}/H_2S_{(30H2O)}$ equilibrium fractionation factor (among the largest in the sulfur system at any given temperature), applying a harmonic frequency scaling factor of 1.02 yields a ~2 ‰ increase in the $^{34}\alpha$ fractionation factor at 25˚C from 1.0655 to 1.0677 but smaller shifts at higher temperatures (e.g. 1.1 and 0.6 ‰ positive shift at 200˚C and 400˚C, respectively). In some cases (but not all), the small shifts arising from harmonic frequency scaling places our theoretical fractionations factors in slightly better agreement with experimental constraints (see Section 5.4).

The practice of harmonic frequency scaling may not be ideal because different vibrational modes appear to scale slightly differently between computational methods (*cf.* Li and Liu, 2011). Furthermore, simple gaseous molecules may not capture the full range of error introduced by the level of theory employed, especially for the anions of more complex geometric and electronic structure computed in our study. From our own calculations, it appears that SO_2 may have a systematically higher scaling factor than the other compounds investigated that may be on the order of 1.065, which is why when SO_2 is included in the regression the net scaling factor increases from ~1.01 to ~1.02 (we show later that application of this higher SO_2-specific scaling factor places estimates of the $SO_{2(aq)}/SO_{2(g)}$ fractionation factor in slightly better agreement with experimental constraints, although overall the effect of the scaling is still only on the ~0.2 ‰ magnitude at 25˚C in the estimated fractionation factor). Due to these potential issues, we have chosen to not apply a harmonic scaling factor in the computations of our reported RPFRs, but we do discuss the effects of harmonic scaling on fractionation factors for individual systems (section 5.4).

Cluster Geometry

Variability in the water cluster geometry surrounding the solute of interest is another potential source of error/uncertainty in computed RPFRs and fractionation factors. From previous studies, it is generally understood that error/uncertainty arising from conformer geometries is much lower than those associated with the theoretical method (e.g., Rustad et al., 2010). Most theoretical studies of compounds in water clusters where the centrally coordinated element in the solute is undergoing isotope

substitution have found that the variability in computed RPFRs is generally at the 0.1 - 1 ‰ level (1 s.e.) from one cluster geometry to another for multiple element systems (e.g., oxy-anions and compounds of C, Se, Ge, B; Rustad et al., 2008; Rustad et al., 2010; Li et al., 2009; Li and Liu, 2011). We performed a series of at least duplicate constructions and optimizations for a select set of 30-40H_2O clusters in the sulfite system: SO_3^{2-}, $(HS)O_3^-$, $(HO)SO_2^-$, and the bisulfite dimer pyrosulfite, $S_2O_5^{2}$. Duplicate constructions and optimizations of $SO_3^{2-}\bullet 30H_2O$, $(HS)O_3^-\bullet 30H_2O$, and $(HO)SO_2^-\bullet 34H_2O$ reveal that variability due to cluster geometry may indeed be similarly small, i.e., $(HS)O_3^-\bullet 30H_2O$: $^{34}\beta$ = 1.0721±0.0001, $SO_3^{2-}\bullet 30H_2O$: $^{34}\beta$ = 1.0510±0.0003, $(HO)SO_2^-\bullet 34H_2O$: $^{34}\beta$ = 1.0487±0.0003 (all at 25˚C and 1 s.e.). The two sulfur atoms in the bisulfite dimer, labeled here as 'A' and 'B': $(O_2\text{-}^{A}S\text{-}^{B}S\text{-}O_3)^{2-}$, have similar reproducibility in their RPFRs between four separate conformers ranging from 30-40 H_2O clusters: ^{A}S: $^{34}\beta$ = 1.0438 ± 0.0003 and ^{B}S: $^{34}\beta$ = 1.0622 ± 0.0011 (25˚C, 1 s.e.), where the RPFR of the latter, higher-coordination site seems to vary systematically with the computed S-S bond-length (contributing to the slightly higher variability) and may be a special case (section 4.1).

Considering all of the uncertainties derived from the above sources, we estimate the overall uncertainties associated with our theoretically computed fractionation factors for aqueous sulfur systems to be on the order of ~0.1 to 1-2 ‰, depending on temperature and the compounds/system considered. The major source of uncertainty is believed to be from the potential inadequacy of our theoretical method (*cf.* Rustad et al., 2008; Rustad et al., 2010) and could potentially be better constrained with more sophisticated computational methods. A major aim of the

present study is to explain the available experimental constraints for equilibrium fractionations in the sulfite system in the context of the complex speciation of sulfite. Much of the uncertainty in this analysis is dominated by uncertainties in experimental determinations of equilibrium quotients (e.g. bisulfite isomerization) and experimental fractionation factors (e.g. approaching a few permil in magnitude). Much of the uncertainties in the theoretically calculated fractionation factors discussed above are either comparable to, or within this range. Therefore, we do not think the uncertainties in the calculations will affect the main conclusions of the present study.

5.2 General trends in the calculated $^{34}S/^{32}S$ RPFRs

The general relationships in the computed RPFRs for the hydrated sulfur species can be explained by the general principles of stable isotope fractionation. The two primary factors influencing the magnitude of RPFRs (Figure 2.6) are: (1) the oxidation state of sulfur, and (2) the coordination of sulfur, i.e., the number of bonds formed with other atoms. Both of these exert first order controls on the bonding environment around sulfur, particularly on the bond stiffness/strength, and are the primary factors in influencing the relative magnitudes of RPFRs that we have computed.

The oxidation state of the sulfur atom will affect the electron distribution throughout the molecule and therefore the strength and nature of the bonds with the other atoms. The force constants that describe the potential wells associated with the bonds (derived from the computation of the multidimensional electronic potential energy surface) will generally be higher for bonds associated with sulfur in higher

oxidation states, meaning simply that the bonds will be more stiff. Thus, species with higher oxidation state will generally have higher RPFRs than those with lower oxidation state in similarly coordinated structures. For example, this is reflected in the significantly lower RPFR of the sulfoxylate ion (SO_2^{2-}; S^{2+}) as compared to sulfur dioxide (SO_2; S^{4+}), which have similar bent triatomic structures and two-fold coordination of the sulfur atom with bonds to oxygen atoms.

For a given oxidation state, the coordination of the sulfur exerts another first order control on RPFRs. The BM-equation describes the relationship between isotope partitioning among molecules, zero point energies (ZPE), and molecular vibrations. The ZPE portion of the RPFR reflects the contribution from all vibrational modes and scales with the sum of the frequency shifts. Unless the bonds are weakened so much with increasing coordination that the adjusted sum of the frequency shifts decreases, the RPFR may increase with coordination. From a simple vibrational analysis of our solutes in vacuum, isotope substitution of the central sulfur atom in a bent (or linear tri-atomic), pyramidal, or tetrahedral molecular structure generally affects the asymmetric stretching and bending modes of the ground state vibrations the most and, therefore, contribute the most to the overall magnitude of the RPFR of the molecule. The number of these stretching and bending modes increases with increasing coordination of the central atom, and so all else being equal, the RPFR (and therefore, preference for the heavy isotope) may increase with increasing coordination. For example, the 2-fold coordinated $SO_{2(aq)}$ has a lower RPFR than the 3-fold coordinated SO_3^{2-} and $(HO)SO_2^-$ molecules, which have lower RPFR than the 4-fold coordinated $(HS)O_3^-$ isomer of bisulfite (all S^{4+}). Variations from these

relationships may be expected, depending on the elemental composition of the bonded atoms and, in turn, the atoms or groups they are bonded to further afield that may affect bonding environment and the manner in which frequency shifts are scaled.

Protonation of oxygen atoms has a smaller secondary effect on the sulfur isotope RPFR with respect to the centrally coordinated sulfur. These small secondary effects are due to how protonation of the oxygen atom affects its electron distribution and its bond to the sulfur atom. For example, the RPFR of the $(HO)SO_2^-$ isomer of bisulfite differs by only ~ -2 ‰ from that of the non-protonated sulfite (SO_3^{2-}) at 25˚C. The slightly higher RPFR for sulfite is likely due to the slight weakening of the S-O bond corresponding to the protonated oxygen. This is consistent with the slightly longer S-O bond length for the protonated oxygen atom (Figure 2.3). Similarly, in the sulfoxylate system, the RPFRs for $(HO)SO^-$ and $S(OH)_2$ are both lower than that for SO_2^{2-} and the corresponding S-OH bond lengths are longer than S-O bond lengths (Figure 2.4). The RPFRs for $(HO)SO^-$ and $S(OH)_2$ are nearly identical to one another (at 25˚C: $^{34}\beta$ = 1.0240 and $^{34}\beta$ = 1.0243, respectfully) and are likely within the uncertainties of the calculations. Multiple rotamers of these types yielding different orientations of the protons and OH-bonds with respect to the rest of the molecule are possible that will depend in large part on the water cluster geometry (direct coordination with water molecules) in the case of these computed structures. Such variability in structure would be expected to have small second order effects on the magnitude of sulfur RPFRs. For example, our two $34H_2O$ conformers of $(HO)SO_2^-$ do not have exactly the same structure (slightly different orientations of the

O-H bond relative to the rest of the molecule, i.e., O-S-O-H dihedral ~49-71˚) and yield highly reproducible RPFRs ($^{34}\beta$ = 1.0487±0.0003 at 25˚C, 1 s.d.).

5.3 Mass dependence of RPFRs and equilibrium fractionation factors

Using the exponential definition to describe the mass dependence of computed RPFRs and fractionation factors between the aqueous compounds investigated herein (*cf.* Craig, 1957; Hulston and Thode, 1965; Matsuhisa et al., 1978; Clayton and Mayeda, 1996; Young et al., 2002; Miller, 2002), we compute exponents of mass dependence for RPFRs ($^{33/34}\lambda_\beta$ and $^{36/34}\lambda_\beta$) over a wide range of temperature that conform to narrow ranges (0.5148-0.5159 and 1.89-1.90, respectively; Figure 2.7). The $^{33/34}\lambda_\beta$ for a given species is on a lower end of this range at low temperature and approaches the high range at high temperature, and vice-versa for $^{36/34}\lambda_\beta$. The relationships in $^{33/34}\lambda_\beta$ and $^{36/34}\lambda_\beta$ we compute as a function of temperature for the diversity of aqueous sulfur compounds investigated herein are straightforward consequences of ZPE differences among isotopomers varying as a function of the sulfur bonding environment (redox state, coordination, etc.).

From the comparison of the exponents of mass dependence obtained from the regressions of fractionation factors at 25˚C in the sulfide (S^{2-}), sulfoxylate (S^{2+}), and sulfite (S^{4+}) systems (Figures 2.8-2.10), the exponents systematically vary as a function of oxidation state in a similar manner as illustrated from their $^{33/34}\lambda_\beta$ and $^{36/34}\lambda_\beta$ in Figure 2.7:

Sulfite (S^{4+})	$^{33/34}\lambda = 0.5147 \pm 0.0001$	$^{36/34}\lambda = 1.8983 \pm 0.0005$
Sulfoxylate (S^{2+})	$^{33/34}\lambda = 0.51530 \pm 0.00004$	$^{36/34}\lambda = 1.8948 \pm 0.0001$
Sulfide (S^{2-})	$^{33/34}\lambda = 0.51565 \pm 0.00003$	$^{36/34}\lambda = 1.8910 \pm 0.0006$

Exponents based on RPFRs ($^{33/34}\lambda_{\beta}$ and $^{36/34}\lambda_{\beta}$) and those associated with fractionation factors ($^{33/34}\lambda$ and $^{36/34}\lambda$) may be shifted from one another depending on the relationships between the RPFRs of the compounds considered for the fractionation factor (*cf.* Matsuhisa et al., 1978). The exponent of mass dependence computed for a fractionation factor between two compounds (e.g., A and B; $^{33/34}\lambda_{A\text{-}B}$) generally follows:

$$^{n/34}\lambda_{A\text{-}B} = [^{n/34}\lambda_{\beta(A)}\ln(^{34}\beta_A) - {}^{n/34}\lambda_{\beta(B)}\ln(^{34}\beta_B)]/[\ln(^{34}\beta_A) - \ln(^{34}\beta_B)], \quad (16)$$

where n = 33 or 36 (we will focus on 33). Only when $^{33/34}\lambda_{\beta(A)} = {}^{33/34}\lambda_{\beta(B)}$ will $^{33/34}\lambda_{A\text{-}B}$ be identical. When $^{33/34}\lambda_{\beta(A)} \neq {}^{33/34}\lambda_{\beta(B)}$, the magnitude of $^{33/34}\lambda_{A\text{-}B}$ will be slightly shifted to either higher or lower values than either $^{33/34}\lambda_{\beta(A)}$ or $^{33/34}\lambda_{\beta(B)}$ depending on the relationships among the reduced partition function ratios (*cf.* Matsuhisa et al., 1978). In the latter case, there are two primary examples to consider: (1) When $^{34}\beta_A > {}^{34}\beta_B$ and the $^{33/34}\lambda_{\beta(A)} < {}^{33/34}\lambda_{\beta(B)}$, the computed $^{33/34}\lambda_{A\text{-}B}$ will generally be slightly lower than either $^{33/34}\lambda_{\beta(A)}$ or $^{33/34}\lambda_{\beta(B)}$; and (2) when $^{34}\beta_A > {}^{34}\beta_B$ and the $^{33/34}\lambda_{\beta(A)} > {}^{33/34}\lambda_{\beta(B)}$, the computed $^{33/34}\lambda_{A\text{-}B}$ will generally be slightly higher than either $^{33/34}\lambda_{\beta(A)}$ or $^{33/34}\lambda_{\beta(B)}$. The magnitudes of the shifts between $^{33/34}\lambda_{\beta}$ values and the $^{33/34}\lambda$ corresponding to a fractionation factor are magnified at lower temperature where differences in the magnitudes of reduced partition function ratios are largest (in the general case). The shifts are additionally magnified under hypothetical conditions where the differences between $^{33/34}\lambda_{\beta(A)}$ and $^{33/34}\lambda_{\beta(B)}$ are relatively large and differences between $^{34}\beta_A$ and $^{34}\beta_B$ are relatively small. For most fractionation factors computed among compounds of different oxidation state at low/ambient temperature, our calculations generally follow case (1). For example, at 0˚C the fractionation

factor between sulfate (SO_4^{2-}; $^{34}\beta$ = 1.0910, $^{33/34}\lambda_\beta$ = 0.5148) and sulfide (H_2S; $^{34}\beta$ = 1.0142, $^{33/34}\lambda_\beta$ = 0.5157) yields $^{33/34}\lambda$ = 0.5146, slightly lower than either compound's respective $^{33/34}\lambda_\beta$ values. Due to the narrow range in $^{33/34}\lambda_\beta$ and $^{36/34}\lambda_\beta$ that we compute over a relatively large range in $^{34}\beta$ for various aqueous sulfur compounds, it may be generally concluded (with some exceptions) that our calculations would not predict exponents of mass dependence associated with equilibrium isotope exchange significantly outside of the range of $^{33/34}\lambda \approx 0.514\text{-}0.516$ and $^{36/34}\lambda \approx 1.89 - 1.90$ over a wide range of temperature (0°C $\rightarrow\infty$).

The major exception to this generality is for equilibrium isotope exchange reactions that are predicted to have crossovers, i.e., a shift in the direction of an isotope effect where preference for heavy isotopes undergoes inversion from one compound (or bonding environment) to the other at a particular temperature. Our calculations predict crossovers in the isotope exchange reactions between the outer ("sulfanyl") sulfur atom in thiosulfate and the two principle sulfide species (H_2S, HS^-). Crossovers and their effects on the exponents of mass dependence have been described previously in gas phase reactions for the sulfur isotope system (Deines, 2003; Otake et al., 2008). Briefly, these effects relate to crossover temperatures being slightly different for exchange reactions involving isotopes of different mass, i.e., $T_{33/32\text{-crossover}} \neq T_{34/32\text{-crossover}} \neq T_{36/32\text{-crossover}}$. As a crossover temperature is approached, the exponents of mass dependence show asymptotic relationships where the exponent can take any value between $+\infty$ and $-\infty$ (Deines, 2003; Otake et al., 2008). Crossovers have been predicted in isotope exchange reactions involving H_2S and other reduced sulfur compounds containing S-S bonds (S_2/H_2S, S_8/H_2S; Deines,

2003; Otake et al., 2008) and presumably arise fundamentally from the competition between contributions from low frequency vibrational modes (like those associated with S-S bonds) and high frequency modes in H_2S (and HS^-) to the overall RPFRs as a function of temperature. Due to the small magnitude of the isotope effects in the asymptotic crossover range, these effects are not substantially expressed (i.e., $\Delta^{33}S \approx 0$, $\Delta^{36}S \approx 0$, as we have computed) without subsequent amplification via non-equilibrium isotope exchange processes (e.g., a Rayleigh distillation process; Deines, 2003; Otake et al., 2008).

In a previous study, Otake et al. (2008) emphasized computations utilizing a non-exponential formulation based on the approximation $^{33/34}\lambda \approx (^{33}\alpha - 1)/(^{34}\alpha - 1)$ to argue that their theoretical calculations of select sulfur compounds (modeled as either gas phase or in PCM solvation models) predict a range of $^{33/34}\lambda = 0.505\text{-}0.516$ (sometimes > 0.516 at low temperature) for the equilibrium fractionation factors they computed (including SO_4^{2-}-H_2S), where the reference exponent of 0.515 is approached only at high temperature. Computations of the mass dependence as $^{33/34}\lambda = \ln(^{33}\alpha)/\ln(^{34}\alpha)$ calculated from the same fractionation factors yields a much narrower range of $^{33/34}\lambda$ within 0.514-0.516 over the same temperature range (where ~0.5159 is approached at the high temperature limit, as expected), consistent with the calculations herein and the general definition of mass dependence typically employed in multiple sulfur isotope studies (and all other isotope systems involving more than two stable isotopes). In other words, the so-called 'band of mass dependence' that Otake et al. (2008) argued for as $^{33/34}\lambda \approx 0.505\text{-}0.516$ for simple equilibrium isotope exchange reactions reduces to the narrow 0.514-0.516 range when the exponential

definition of mass dependence is used. Note also that the computation of the mass dependence as $(^{33}\alpha - 1)/(^{34}\alpha - 1)$ is valid to characterize effects associated with a Rayleigh distillation process and not the condition of equilibrium isotope exchange.

5.4 Comparisons between theory and experiment (and predictions)

The validity of the theoretical fractionation factors can be assessed by comparison with available experimental constraints, with particular focus on the sulfite system. Very little is known about the behavior of sulfoxylate species in aqueous solutions (particularly the isomerization quotients for the protonated species) and so we are only able to discuss the estimated ranges of fractionations possible in this system. Calculations of the other sulfur compounds (sulfide, sulfate, and thiosulfate) can also be compared to the available experimental datasets, including: fractionations among sulfide species, fractionations between sulfate and sulfide species, the intramolecular fractionation factor for thiosulfate, and fractionations between the sulfide species and thiosulfate. We highlight potential experimental issues and include recommendations for future experimental determinations.

5.4.1 Sulfite system

Experimental constraints for the equilibrium sulfur isotope partitioning in the aqueous sulfite system are provided by Eriksen (1972a), Eriksen (1972b), and Eriksen (1972c). Eriksen (1972a) determined fractionations between bulk bisulfite and gaseous SO_2 ($HSO_3^-{}_{TOTAL}/SO_{2(g)}$) at pH =4.5 where bisulfite dominates, Eriksen (1972b) determined the fractionation between gaseous SO_2 and aqueous SO_2 ($SO_{2(aq)}/SO_{2(g)}$) in acidic solutions (pH < 0.3), and Eriksen (1972c) determined fractionations between bulk bisulfite and gaseous SO_2 as a function of the ratio of

total bisulfite: $SO_{2(aq)}$ (up to 10 M [HSO_3^-]; pH = <0.3 or 4.5), which was an attempt to study the effect of dimerization on isotope fractionations. With additional interpretation, the experiments presented in Eriksen (1972c) yield constraints on both the $SO_{2(aq)}/SO_{2(g)}$ and $HSO_3^-{}_{TOTAL}/SO_{2(g)}$ fractionation factors. Additional experimental constraints on the $SO_{2(aq)}/SO_{2(g)}$ fractionation factor are found in Chmielewski et al. (2001).

Bulk Bisulfite in Solution vs. $SO_{2(g)}$: Highlighting the role of bisulfite isomers

In Figure 2.11, we plot our calculated fractionations of bisulfite species vs $SO_{2(g)}$ and those from the experiments of Eriksen (1972a) and Eriksen(1972c) as a function of temperature. Eriksen (1972a) chose experimental conditions to minimize the presence of dimers and other sulfite species (pH = 4.5), so the experimentally determined fractionations should mostly reflect those of the two bisulfite isomers and gaseous sulfur dioxide. The $^{34}\alpha_{bisulfite(bulk)\text{-}SO2(g)}$ of Eriksen (1972a) appear to show a weak temperature dependence over the temperature range of 25-45˚C (the values are indistinguishable within the uncertainty). The constraints from Eriksen (1972c) were regressed from multiple experiments performed over a range of χ_{HSO3T}:$\chi_{SO2(aq)}$ and seem to indicate a slight normal temperature dependence (see Section 5.4.1.2).

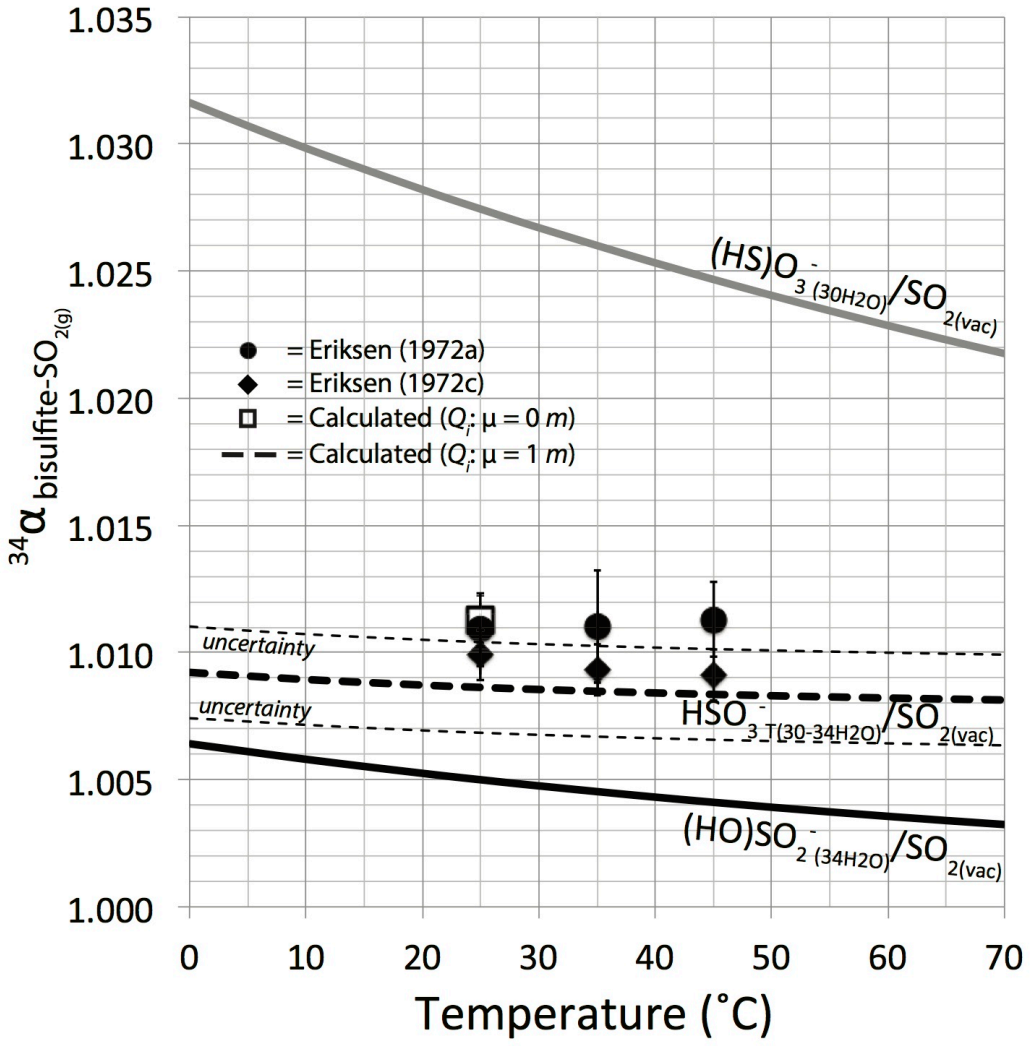

Figure 2.11: Comparison of theoretical fractionation factors to experimental constraints in the bisulfite-$SO_{2(g)}$ system as a function of temperature, highlighting the influence of bisulfite isomerization on fractionation behavior. Black data points (circles and diamonds) are from the experimental studies of Eriksen (1972a) and Eriksen (1972c). The open (white) square is our theoretical estimate for the bulk fractionation factor using the isomerization quotient at 0 *m* ionic strength from Risberg et al. (2007) following equation (17) in the text. The thick dashed curve represents our theoretical estimate (equation (17) in the text) using the isomerization quotients as a function of temperature at 1 *m* ionic strength (Horner and Connick, 1986; Littlejohn et al., 1992; Figure 2.2). The lighter dashed lines represent the uncertainty envelope derived solely from the propagation of the uncertainty of the isomerization quotient as a function of temperature that is based on the least squares linear regression in Figure 2.2.

Using our theoretical calculations, we suggest that the experimental data can be explained in terms of the isomerization of bisulfite. Using the experimental constraints for the isomerization quotient for bisulfite as a function of temperature at

1 *m* ionic strength (Horner and Connick, 1986; Littlejohn et al., 1992), we predict the $^{34}\alpha_{bisulfite(bulk)\text{-}SO2(g)}$ as the dashed curve in the figure via the following relationship:

$$^{34}\alpha_{bisulfite(bulk)\text{-}SO2(g)} = [Q_i/(1+Q_i)^{34}\beta_{(HO)bisulfite} + 1/(1+Q_i)^{34}\beta_{(HS)bisulfite}]/^{34}\beta_{SO2(g)} \quad (17)$$

Where Q_i as a function of temperature is computed via the relationship: $\ln Q_i$ = 1413(±119)/T -3.1(±0.4) (valid over ~2-67˚C, 1 *m* ionic strength; regressed from the combined datasets of Horner and Connick, 1986; Littlejohn et al., 1992). The corresponding uncertainty envelope plotted in Figure 2.11 includes only the propagated uncertainty of the temperature dependence of the isomerization quotient. The predicted $^{34}\alpha_{bisulfite(bulk)\text{-}SO2(g)}$ at μ = 1 *m* has a temperature dependence that becomes more shallow with increasing temperature, reflecting the higher proportion of the HS-isomer with increasing temperature. This relationship is roughly consistent with the weak (to non-resolvable) temperature dependence of Eriksen (1972a) and Eriksen (1972c). When we apply an isomerization quotient to our calculated fractionations performed in a low ionic strength medium (μ = 0 *m*, T = 25˚C; Risberg et al., 2007), we obtain a fractionation factor that is ~2.4 ‰ higher than that obtained from application of the μ = 1 *m* isomerization quotient (open square data point in Figure 2.11) and is indistinguishable from the experimental constraint of Eriksen (1972a) at this temperature.

The experimental data fall within the range of our calculated theoretical estimates that utilize the available experimental constraints of the relative mole fractions of bisulfite isomers present in solution in media of 0 and 1 *m* ionic strength. The experiments of Eriksen (1972a, c) were based on a distillation technique that required the solution to be constantly flushed at an unspecified “slow” rate with N_2

gas to strip SO_2 out of solution while simultaneously adding HCl to keep pH constant. Such changes in ionic strength throughout experimental runs are a plausible source of at least some of the variability in the experimental fractionations. The constant stripping of SO_2 from solution also requires that the rates of isotope exchange among the aqueous sulfite species be sufficiently rapid at all times, which may or may not be the case, and disequilibria among species and the SO_2 stripped from solution may be another source of the relatively poor reproducibility. The complete effect of ionic strength on isomerization and isotope fractionations in this system cannot be evaluated in full until the isomerization quotient is determined as a function of ionic strength over a wide range of temperatures and higher precision isotope experiments are performed (taking care in controlling ionic strength).

Despite the large uncertainties, it is clear from Figure 2.11 that (1) we are able to reproduce the general fractionation behavior in this system that has been determined experimentally, and (2) fractionation in this system is strongly influenced by the isomerization of bisulfite. Furthermore, fractionations in the sulfite system involving bisulfite may be especially dependent on ionic strength due to isomerization.

Bisulfite Dimer: Bulk Bisulfite in Solution vs. $SO_{2(g)}$ as a function of pH and $[HSO_3^-]_T$

Eriksen (1972c) measured the fractionation between gaseous SO_2 and bulk bisulfite as a function of the molar ratio of aqueous SO_2 and total bisulfite by varying $[HSO_3^-]_T$ (1.5-10 M) and pH (0.3 or 4.5). One of the primary aims of these experiments was to determine the effect of dimer formation on the observable fractionations. Assuming full isotopic equilibration throughout experimental runs,

the experiments of Eriksen (1972c) should follow the simple mass balance relationship:

$$^{34}\alpha_{S(IV)TOTAL(aq)-SO2(g)} = {}^{34}\alpha_{SO2(aq)/SO2(g)}\chi_{SO2(aq)} + {}^{34}\alpha_{HSO3\text{-}(T)/SO2(g)}\chi_{HSO3\text{-}(T)} + {}^{34}\alpha_{dimer/SO2(g)}\chi_{dimer} \quad (18)$$

Where χ and $^{34}\alpha$ refer to the mole fraction and fractionation factor (based on $^{34}S/^{32}S$) of or between the denoted species, respectively, and $HSO_3^-{}_{(T)} = (HO)SO_2^- + (HS)O_3^-$. In the absence of a dimer (or significant influence thereof), measured fractionation factors between total S(IV) species in solution and $SO_{2(g)}$ plotted against the mole fraction of total bisulfite species present should form a linear array, i.e.:

$$^{34}\alpha_{S(IV)TOTAL(aq)-SO2(g)} = {}^{34}\alpha_{SO2(aq)/SO2(g)}\chi_{SO2(aq)} + {}^{34}\alpha_{HSO3\text{-}(T)/SO2(g)}(1 - \chi_{SO2(aq)}) \quad (19)$$

Where $\chi_{HSO3(T)} = 1 - \chi_{SO2(aq)}$ due to the negligible presence of SO_3^{2-} at a pH of < 4.5. As Eriksen (1972c) originally noted, this relationship can deviate from linear due to the power of two dependence on $[HSO_3^-{}_{(T)}]$ in the dimerization quotient if the system is driven to large conversion to the dimer (i.e., high $[HSO_3^-{}_{(T)}]$) and if the fractionation between the dimer and bisulfite (total of both isomers) is relatively large.

Using the pyrosulfite conformer computed to have the lowest S-S bond length, we compute a theoretical fractionation factor at 25˚C between the site-averaged dimer and bulk bisulfite (considering both isomers) of $1000\ln^{34}\alpha_{dimer/HSO3\text{-}(T)} = -1.6$ ‰ (μ = 0 *m*; $Q_i = 2.57 \pm 0.5$; Risberg et al., 2007) and $1000\ln^{34}\alpha_{dimer/HSO3\text{-}(T)} = 0.9$ ‰ (μ = 1 *m*; $Q_i = 4.9 \pm 0.1$; Horner and Connick, 1986). This indicates that the fractionation between the dimer and bulk bisulfite may be relatively small (perhaps within the uncertainty of the theoretical calculations), and the directionality of this overall

fractionation may depend on the effects of ionic strength on the relative distribution of bisulfite isomers.

We illustrate worked examples of the relationship between the $^{34}\alpha_{S(IV)(aq)/SO2(g)}$ and $\chi_{SO2(aq)}$ using our theoretical RPFRs and equilibrium quotients from the literature (μ = 0 *m* and 1 *m*) and compare them with the experimental data of Eriksen (1972c) in Figure 2.12 under comparable conditions. The smooth curves are based on our theoretical calculations where solid curves are the linear arrays ignoring the dimer and the dashed curves are estimates with the dimer included. For the calculations including the dimer (dashed), we assumed a pH range of 0-4.5 and we additionally assumed a $[S(IV)]_T$ = 10 M (the highest of the Eriksen range) to examine the maximum possible influence of the dimer. The thinnest dashed curves represent the same calculations as the thicker dashed curves (pH = 0-4.5, $[S(IV)]_T$ = 10 M) except with an artificially increased site-averaged RPFR of the dimer (equivalent to 5 ‰) for illustrative purposes due to the possibility that our theoretical calculations are underestimating this value. Ionic strength was not held constant in the experiments of Eriksen (1972c) and so the 0 *m* and 1 *m* are shown for comparison, as these are the only conditions for which all equilibrium quotients (dissociation, isomerization, dimerization) have been experimentally determined for computing mole fractions.

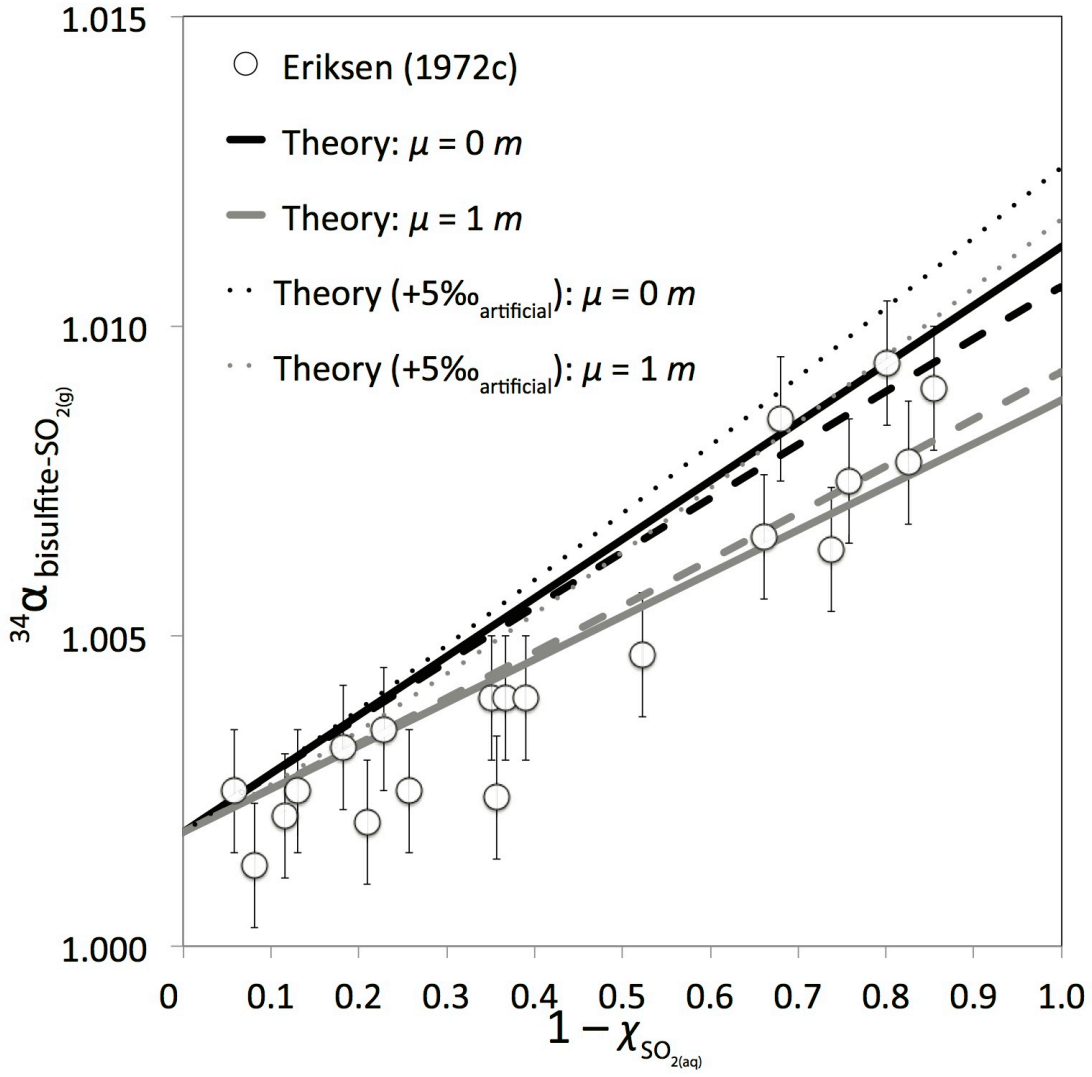

Figure 2.12: Fractionations at 25˚C in the sulfite system from Eriksen (1972c) (white circles) and a modeled system based on our theoretical fractionation factors and mass balance calculations (solid or dashed curves). Solid curves ignore the bisulfite dimer and the thick dashed curves include the dimer assuming a total bisulfite concentration of 10 M (highest in the Eriksen experimental range) and a pH range of 0.5-4.5. The lightest dashed curves are identical to the thick dashed curves but include an artificially increased RPFR for the site-averaged dimer equivalent to 5 ‰ for illustration purposes.

The calculated fractionation trends in Figure 2.12 are generally consistent with the experimental data of Eriksen (1972c), where the experimental data at relatively low $\chi_{SO2(aq)}$ appear to plot in between our estimates using equilibrium quotients performed at 0 and 1 *m* ionic strength. The presence of the dimer under conditions of $[S(IV)]_T$ = 10 M (thick dashed curves) affects the overall fractionations

between bulk bisulfite in solution and gaseous SO_2 at the sub-permil level, which is well within the uncertainty of the experimental determinations. Eriksen (1972c) originally noted that the effect of the dimer is either non-resolvable or insignificant given the linearity of the experimental dataset. Eriksen concluded that the fractionation factor between disulfite and bisulfite might not be significantly higher than non-dimer bisulfite, which is generally consistent with our theoretical calculations that take into consideration both isomers and the dimer.

Our theoretical calculations highlight the sensitivity of the fractionation trends in Figure 2.12 to the relative distributions of the bisulfite isomers. Depending on the ratio of the two isomers in solution as a function of ionic strength, the dimer is computed to either dampen or enhance fractionations between bulk aqueous S(IV) and $SO_{2(g)}$. It is important to reiterate, however, that the computed site-averaged RPFR of pyrosulfite depends on the computed S-S bond length and our shortest calculated bond length in the $30H_2O$ cluster at the B3LYP/6-31+G(d,p) level (used in this analysis) is longer (2.46 Å) than the experimentally determined value in crystalline solids (~2.2 Å; Zachariasen, 1932). Solvation could in principle affect the bond length but we are unable to find any experimental constraints in the aqueous phase. We additionally note that the precise structure of the aqueous dimer is perhaps contentious and forms with an S-O-S linkage have yet to be ruled out (*cf.* Williamson and Rimstidt, 1992). From the standpoint of our calculations, shortening the dimer S-S bond may increase the site-averaged RPFR for disulfite and change these calculated relationships depending on the magnitude of the $^{34}\alpha$ between the dimer and the pooled isomers. Our calculations based on an artificial increase in the site-averaged RPFR of

the dimer (equivalent to 5 ‰) illustrate how computed fractionation relationships may be influenced due to a potential underestimation. In this case, the fractionation factor $^{34}\alpha_{dimer/HSO3-(T)}$ is > 1 for both ionic strength conditions and the overall influence of the dimer is to enhance fractionations between aqueous S(IV) and gaseous SO_2.

Based on the seeming linearity of his dataset, Eriksen (1972c) reasoned that the dimer could be ignored and he regressed his data presented in Figure 2.12 to obtain constraints for the $^{34}\alpha_{SO2(aq)-SO2(g)}$ and $^{34}\alpha_{HSO3(T)-SO2(g)}$ fractionation factors from the end member cases of $\chi_{SO2(aq)} = 0$ and $\chi_{SO2(aq)}=1$. This yields $1000\ln^{34}\alpha_{SO2(aq)-SO2(g)} = 0.9 \pm 0.4$ ‰ and $1000\ln {}^{34}\alpha_{HSO3(T)-SO2(g)} = 9.9 \pm 1$ ‰ (1 s.e., note: the latter fractionation determined this way at 25, 35, and 45˚C are plotted in Figure 2.11), where the latter is slightly lower in magnitude (but unresolvable) from the experiments reported in Eriksen (1972a). These are highly comparable to our theoretical fractionation factors of $1000\ln^{34}\alpha_{SO2(aq)-SO2(g)} = 1.8$ ‰ and $1000\ln^{34}\alpha_{HSO3(T)-SO2(g)}$ of 11.2 and 8.8 ‰ (± 1 ‰, 1 s.e.) using isomerization quotients determined at ionic strength of 0 and 1 *m*, respectively. Although the estimates of Eriksen (1972c) are within the uncertainty of the determinations from Eriksen (1972a), the slightly lower magnitudes may reflect the slight influence of the dimer on the bulk fractionation behavior of the system, which remains to be experimentally investigated in more detail.

Solvated vs. Gaseous Sulfur Dioxide: $SO_{2(aq)}/SO_{2(g)}$

Eriksen (1972b), Eriksen (1972c), and Chmielewski et al. (2001) provide estimates of the $^{34}\alpha$ fractionation factor between gaseous and solvated sulfur dioxide. These determinations are plotted in Figure 2.13 with our computed $^{34}\alpha$ fractionation

factor based on the $SO_{2(30H2O)}$ and $SO_{2(vacuum)}$ calculations. The experiments of Eriksen (1972b) overlap with our calculated fractionation factors within experimental uncertainty but it is clear that the uncertainties in the experimental fractionation factors (reflecting experimental reproducibility) may be as large or larger than the magnitude of the fractionation factor itself and so make the comparison difficult. Estimates from the Eriksen (1972c) experiments are reported to be more precise and seem to record an inverse fractionation relationship with temperature, which is neither predicted from the theoretical calculations nor is observed in the more recent and detailed experiments of Chmielewski et al. (2001). Our calculations appear to agree with the experiments of Chmielewski et al. (2001) in terms of both temperature dependence and magnitude, where the experiments are within ca. ≤ 0.5 ‰ of the calculations. The ca. ≤ 0.5 ‰ offset between the Chmielewski et al. (2001) experiments and our calculations is systematic and could be within the uncertainties/error of both determinations. Application of the CCSD/aug-cc-pVTZ-derived harmonic scaling factor of 1.02 does not decrease the offset with the experiments substantially (~0.1 ‰ at 25˚C). Using only the SO_2 calculations in the gas phase at the CCSD/aug-cc-pVTZ and B3LYP/6-31+G(d,p) level, we can derive a scaling factor on the order of 1.065 for SO_2 alone that may be more appropriate to use in this case. When applied to our harmonic frequencies, the estimated $SO_{2(aq)}/SO_{2(g)}$ fractionation factor shifts to better agreement with the Chmielewski et al. (2001) experiments: $1000\ln(^{34}\alpha_{SO2\cdot30H2O/SO2(vacuum)}) = 2.1$ ‰ at 25˚C.

An additional consideration is the pH of the experiments of Chmielewski et al., (2001) (not reported) and whether or not any bisulfite may have been present in

the experimental solutions that may have biased the fractionation between aqueous S(IV) and gaseous SO_2 towards higher values. Even between a pH of 0.5 and 1 (Figure 2.1), bisulfite (sum of both isomers) comprises between ca. 4 and 12% of the total S(IV) in solution at low ionic strength ($\mu = 0$ *m*; Beyad et al., 2014). With ca. 4 % of bisulfite present in solution (corresponding to a pH ~ 0.5 at low ionic strength) and the remaining being $SO_{2(aq)}$, we calculate a fractionation factor between S(IV) in solution and gaseous SO_2 of ~2.2 ‰ at 25˚C based on our calculated RPFRs and assuming the isomerization quotient at low ionic strength (Q_i = 2.57± 0.5; Risberg et al., 2007), which is ~0.4 ‰ higher than our computed $SO_{2(aq)}/SO_{2(g)}$ fractionation factor and can account for much of the apparent offset between theory and experiment. We cannot uniquely attribute the offset between theory and experiment in this case to either pH/speciation or error in the theoretical calculations but our analysis nevertheless further highlights the strong role of speciation in influencing fractionation behavior in aqueous S(IV) systems.

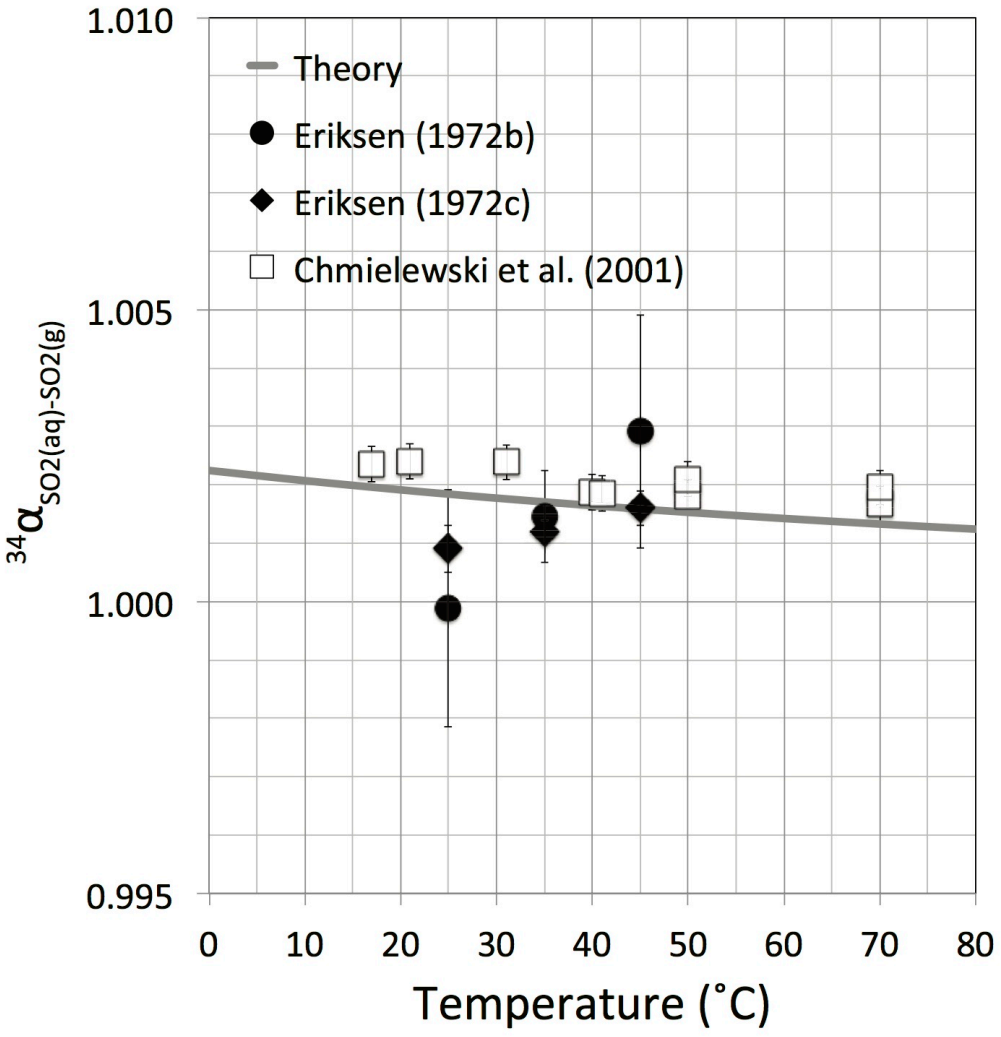

Figure 2.13: The major isotope fractionation factor between aqueous and gaseous sulfur dioxide. The curves represent our theoretical values and the data points represent experimental values from Eriksen (1972b) (black circles), Eriksen (1972c) (black diamonds), and Chmielewski et al. (2001) (white squares).

Predicted Fractionations: $[HSO_3^-]_T/[SO_3^{2-}]$

The isomerization of bisulfite appears to exert a strong influence on the observable fractionations between bulk bisulfite and sulfur dioxide in the gas phase, and there are similar consequences for fractionation behavior between bulk bisulfite and sulfite in solution. Presently, there do not appear to be any experimental

constraints for fractionations among sulfite species in solution and, thus, our theoretical estimates appear to represent the first constraints. In Figure 2.14, we plot the calculated fractionation factors between bisulfite species and sulfite as a function of temperature. Due to the very similar bonding environments around sulfur between $(HO)SO_2^-$ and SO_3^{2-} (3-fold coordination to oxygen atoms in a pyramidal structure), the $^{34}S/^{32}S$ partitioning between $(HO)SO_2^-$ and SO_3^{2-} is small, calculated to be ca. -2.2 ‰ at 25˚C. A slight preference for heavier isotopes in SO_3^{2-} is predicted, which is due to the slight weakening of the S-O bond on the protonated oxygen in $(HO)SO_2^-$. Since $(HS)O_3^-$ is four-fold coordinated (3 oxygen atoms, 1 proton) in a tetrahedral structure, it is predicted to have a much higher preference for the heavy isotopes of sulfur and is calculated to be ca. 21-16 ‰ enriched in $^{34}S/^{32}S$ relative to SO_3^{2-}.

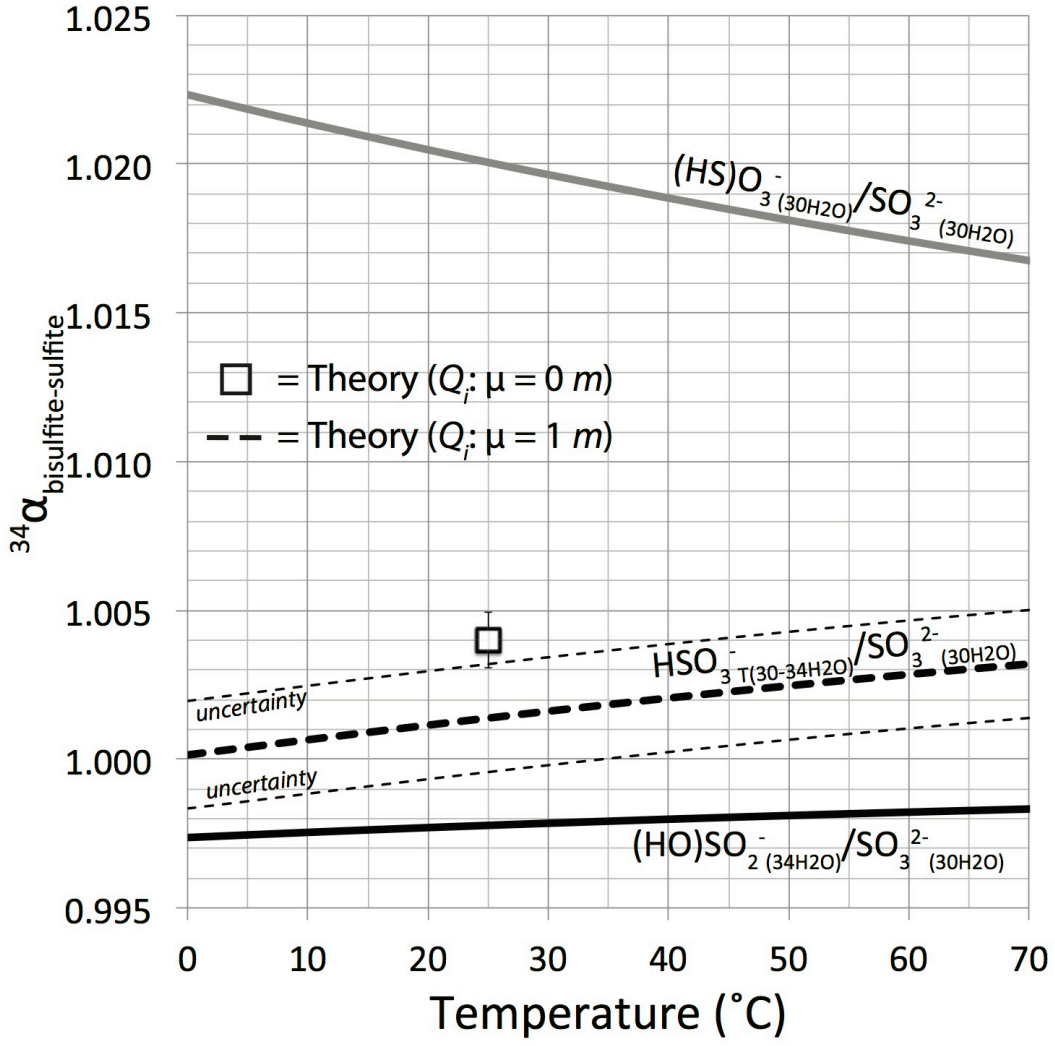

Figure 2.14: Theoretical estimates/predictions of the major isotope fractionation factors among the anions in the sulfite system: sulfite *sensu stricto* (SO_3^{2-}) and the two isomers of bisulfite. The open (white) square and the thick dashed curve are the predicted bulk fractionation factors (experimentally observable) between bulk bisulfite (both isomers) and sulfite using the isomerization quotients at ionic strengths of 0 *m* (Risberg et al., 2007) and 1 *m* (Horner and Connick, 1986; Littlejohn et al., 1992), respectively, following equation (20) in the text.

Using the isomerization quotients as a function of temperature at μ = 1 *m* (Horner and Connick, 1986; Littlejohn et al., 1992), we predict the $HSO_3^-{}_T$-SO_3^{2-} fractionation factor following a similar relationship to that of equation 10 (Section 5.4.11):

$$^{34}\alpha_{\text{bisulfite(bulk)-sulfite}} = [Q_i/(1+Q_i)\,{}^{34}\beta_{\text{(HO)bisulfite}} + 1/(1+Q_i)\,{}^{34}\beta_{\text{(HS)bisulfite}}]/{}^{34}\beta_{\text{sulfite}} \quad (20)$$

With the similarly derived uncertainty envelope estimated only from the uncertainty of the temperature dependence of the isomerization quotient. This prediction yields an apparent *increase* in the bulk bisulfite-sulfite fractionation with increasing temperature. This apparent inverse-fractionation with increasing temperature relationship is due to the combined effects of the small magnitude of the $(HO)SO_2^-$-SO_3^{2-} fractionation factor relative to that of $(HS)O_3^-$-SO_3^{2-}, and the increasing proportion of the $(HS)O_3^-$ isomer with increasing temperature. In this case, the presence of the minor $(HS)O_3^-$ isomer is controlling: (1) the magnitude and potentially the direction of the $HSO_3^-{}_T$-SO_3^{2-} fractionation factor, and (2) the apparent inverse-fractionation-temperature relationship. It is expected that similar relationships would be observed under low-ionic strength conditions, where the absolute magnitude of the fractionation may be slightly higher at any given temperature due to an increase in the proportion of the $(HS)O_3^-$ isomer at low ionic strength (see open square data point in Figure 2.14; Risberg et al., 2007). Table 2.4 contains a summary of computed theoretical fractionations vs. the experiments of Eriksen (1972c) and Chmielewski et al., (2001) at 25˚C.

5.4.2 Sulfoxylate system

As in the sulfite system, isotope partitioning in the sulfoxylate system will depend on the isomerization of sulfoxylic acid and the bisulfoxylate species (Makarov et al., 2010), which is presently not constrained in aqueous solutions. The 3-fold coordinated HS-bonded isomers in the sulfoxylate system are computed to be highly fractionated (~14-15 ‰ at 25˚C) relative to their respective two-fold

coordinated HO-bonded isomers (Figure 2.9). Depending on the relative stabilities of these isomers, equilibrium isotope partitioning in the sulfoxylate system could be as equally (or more) complex as the sulfite system. Similar effects relating to the relative stabilities of the isomers changing as a function of temperature and ionic strength could come into play, potentially leading to complex temperature-dependence of observable fractionations. Research directed at determining the distribution of these isomers in solution over a wide range of environmental conditions is needed before any detailed assessment of isotope partitioning in this system can be made. The further detection and quantification of unbound sulfoxylate species associated with chemical and enzymatic transformations (e.g., dissimilatory sulfite reductase) would also allow an assessment of the importance of these aqueous species in widespread sulfur cycling processes like dissimilatory sulfate reduction.

5.4.3 Sulfide system

The major isotope fractionation factor ($^{34}\alpha$) between aqueous and gaseous H_2S ($H_2S_{(aq)}$-$H_2S_{(g)}$) at low temperature (ca. 0-100˚C) has been previously determined experimentally (Fry et al., 1986; Geßler and von Gehlen, 1986; Szaran, 1996) and estimated theoretically by Czarnacki and Halas (2012). A summary of these determinations and our own estimate from the H_2S_{30H2O}-H_2S_{vacuum} calculations is presented in Figure 2.15. Our calculated $H_2S_{(aq)}$-$H_2S_{(g)}$ fractionation factor based on our H_2S_{30H2O}-H_2S_{vacuum} calculations at the B3LYP/6-31+G(d,p) level of theory is indistinguishable from the previous theoretical constraints based on the H_2S_{5H2O}-H_2S_{vacuum} calculations of Czarnacki and Halas (2012) at both the B3LYP/6-311++G(d,p) and MP2/6-311++G(d,p) levels of theory, which represent the highest

levels of basis set and explicit solvation (5 H_2O) applied in their study. Their calculations utilized a higher basis set (and theoretical method in the case of the MP2 calculations)—implementing the triple zeta basis set, rather than double zeta, with diffuse functions added to the hydrogen atoms—but much smaller H_2O clusters than what we have computed. Their H_2O computations coordinated the H_2S molecule in ring structures ranging from 2-5 H_2O molecules that did not approximate a complete solvation shell. Their theoretical estimates are effectively identical to our own and, taken together, broadly agree with the available experimental constraints, although the experimental constraints exhibit considerable variability from study to study.

The most detailed experimental constraints as a function of temperature come from Geßler and von Gehlen (1986) and display a very similar temperature dependence to the theoretical constraints and quantitatively agree with the theoretical estimates within about ~0.3 ‰ at all determined temperatures. The slight ~0.3 ‰ offset is systematic and may be reasonably assumed to be within the uncertainties of the respective experimental and theoretical approaches. The determinations of Szaran (1996) are typically higher in magnitude and appear to display a steeper temperature dependence than either the theoretical estimates or Geßler and von Gehlen (1986); because of this disagreement (especially with respect to the temperature dependence), it may be reasonably assumed that the experiments of Szaran (1996) do not represent true equilibrium values. The singular determination of Fry et al. (1986) at 22˚C is slightly lower than the Geßler and von Gehlen (1986), but is still within the uncertainty of their data.

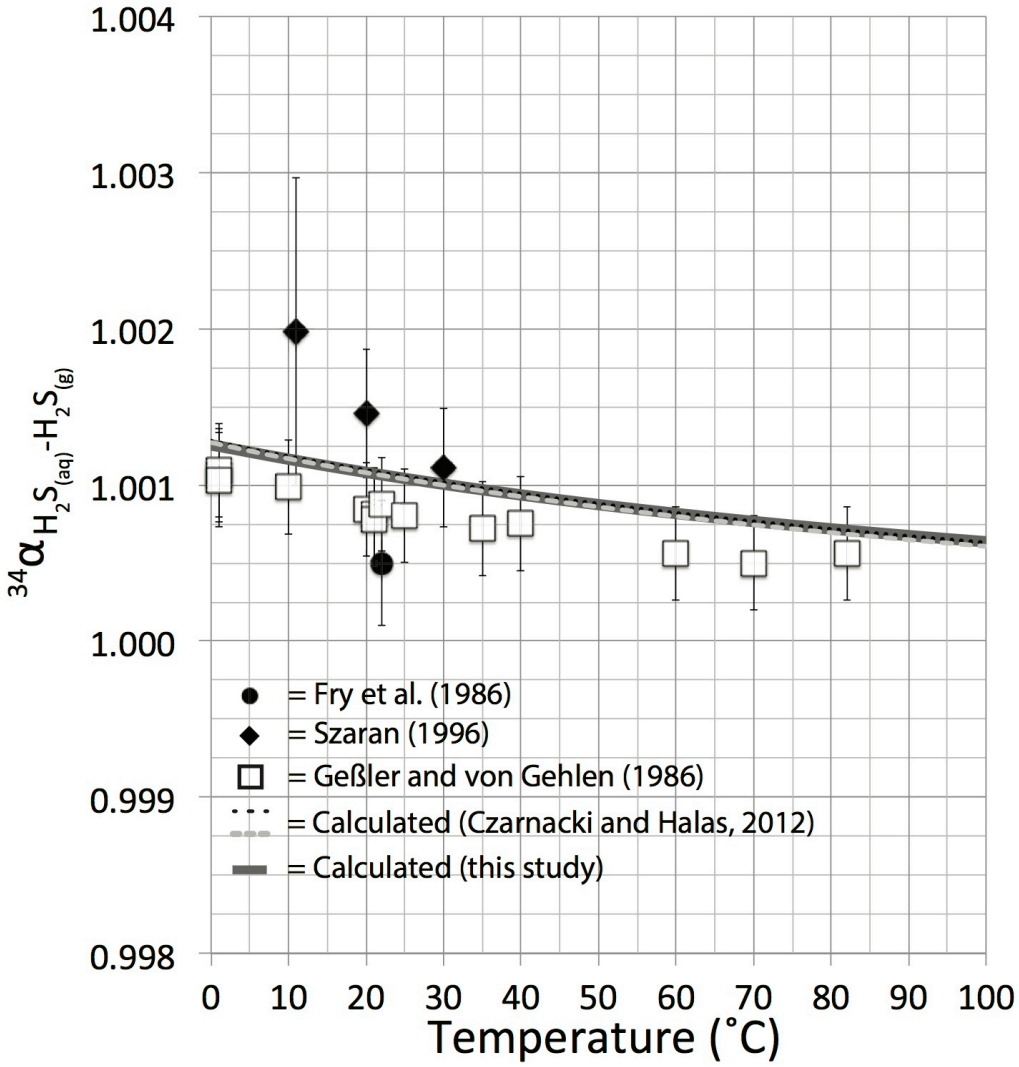

Figure 2.15: The major isotope fractionation factor between aqueous and gaseous hydrogen sulfide (H_2S). The curves represent our theoretical values and those of Czarnacki and Halas (2012) and the data points represent experimental values from the literature.

Fry et al. (1986) and Geßler and von Gehlen (1986) also provided constraints on the $H_2S_{(aq)}$-$HS^-_{(aq)}$ fractionation factor by measuring the isotopic fractionation between gaseous H_2S and dissolved sulfide in solution as a function of pH at ca. room temperature (22˚C and 20˚C, respectively). Their determinations are plotted with our theoretical estimate from our H_2S_{30H2O}-HS^-_{30H2O} calculations in Figure 2.16. In either experimental case, the fractionation factor was estimated by coupling the

determinations of the fractionation factor $H_2S_{(aq)}$-$H_2S_{(g)}$ at low pH, then measuring the same fractionation in solutions of higher pH where both $H_2S_{(aq)}$ and $HS^-_{(aq)}$ are present in solution, utilizing information about the dissociation quotient ($H_2S_{(aq)} \rightleftharpoons HS^-_{(aq)} + H^+$, estimated as $\log Q_{d1} \sim 7$ in either case) to back out an estimate for the $H_2S_{(aq)}$-$HS^-_{(aq)}$ fractionation factor by either simple mass balance calculations (Fry et al., 1986), or graphically in the case of Geßler and von Gehlen (1986). These two experimental investigations yield slightly different estimates: Fry et al. (1986) obtain a $^{34}\alpha$ for $H_2S_{(aq)}$-$HS^-_{(aq)}$ of 1.0026 ± 0.0002 (1 s.d., two experiments) at 22˚C and Geßler and von Gehlen (1986) estimate a value of ~1.0046 at 20˚C. Our theoretical value falls in between these estimates (1.0033 at 20˚C).

A primary difference between the experimental approaches of Fry et al. (1986) and Geßler and von Gehlen (1986) is in how pH was adjusted and the resulting changes in ionic strength that ensued. We hypothesize that changes in ionic strength (and the dissociation quotient) could have lead to an overestimation of the $H_2S_{(aq)}$-$HS^-_{(aq)}$ fractionation factor by Geßler and von Gehlen (1986) and may also have influenced the determination in Fry et al. (1986). These authors computed their $H_2S_{(aq)}$-$HS^-_{(aq)}$ fractionation factor using a dissociation quotient for low ionic strength media ($\log Q_{d1} = 7.04$; consistent with the thermodynamic value of 7.02 at 22˚C and $\mu = 0$ *m;* Hershey et al., 1988). From the description of the Fry et al. (1986) experiments, it is difficult to assess how ionic strength may have influenced their results, but because much more detail is provided in the Geßler and von Gehlen (1986) study, we can make quantitative reinterpretations of their data.

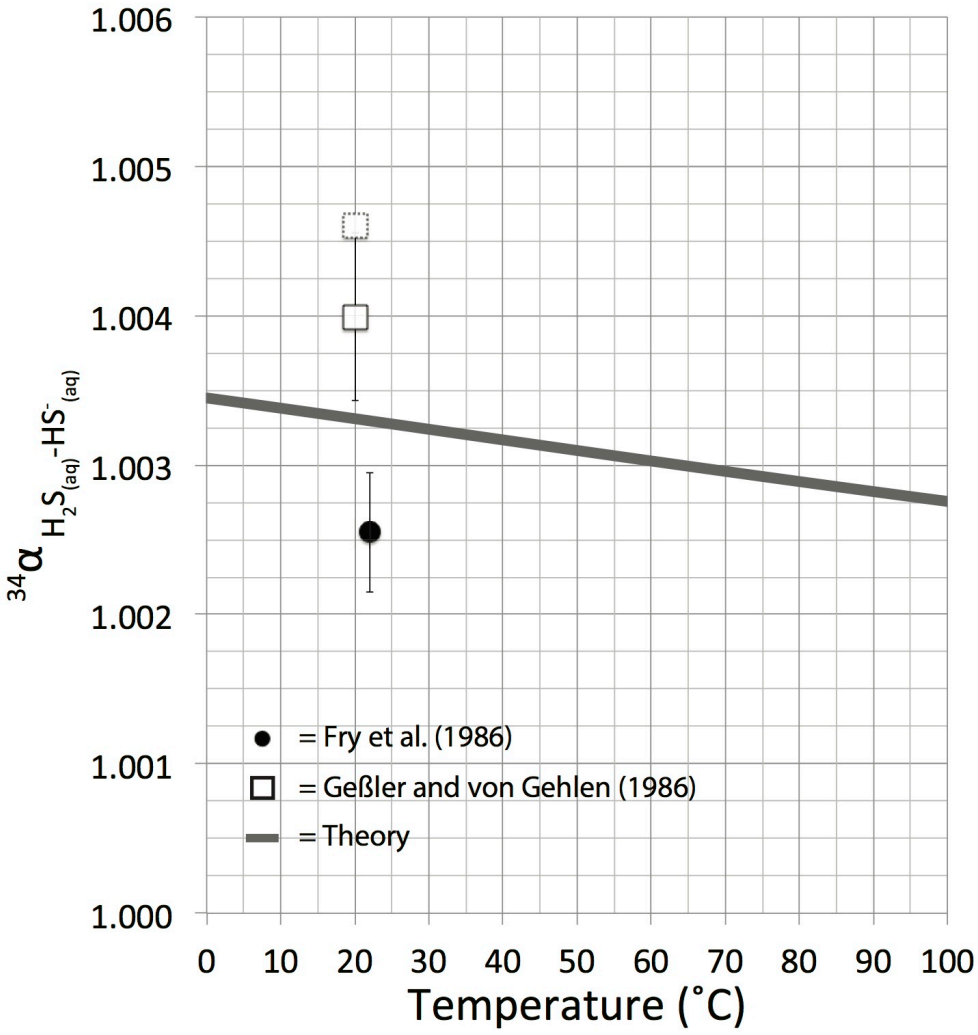

Figure 2.16: The major isotope fractionation factor between the two predominate aqueous sulfide species, $H_2S_{(aq)}$ and $HS^-_{(aq)}$, where curves represent our theoretical values and the data points are experimental constraints. The dashed white square is the estimate from Geßler and von Gehlen (1986) and the solid white square is our own re-estimate using their data and the dissociation quotients as a function of ionic strength from Hershey et al. (1988) (see section 5.4.3 for further explanation).

Geßler and von Gehlen (1986) measured fractionations between $H_2S_{(g)}$ and $H_2S_{(aq)T}$ ($H_2S_{(aq)T}$ = $H_2S_{(aq)}$ + $HS^-_{(aq)}$) at 20˚C as a function of pH utilizing different concentrations of NaOH (up to 2 M NaOH for the highest pH measurements), significantly changing ionic strength from experiment to experiment. At 20˚C, the first dissociation quotient of $H_2S_{(aq)}$ (Q_{d1}) varies as a function of ionic strength from pQ_{d1} = 7.05 at μ = 0 *m* to 6.72 at μ = 1 *m* (Hershey et al., 1988; NaCl media) and it

appears Geßler and von Gehlen (1986) assumed a constant logQ_{d1} ~ 7 for their graphical estimation of the fractionation between $H_2S_{(g)}$ and $H_2S_{(aq)T}$ as the mole fraction of $HS^-_{(aq)}$ approaches 1. We re-estimate the $H_2S_{(ag)}/HS^-_{(aq)}$ fractionation factor at 20˚C from their data using the following simple mass balance relationship (solving for $^{34}\alpha_{HS-/H2S(aq)}$):

$$^{34}\alpha_{TOTAL(aq)/H2S(g)} = {}^{34}\alpha_{H2S(aq)/H2S(g)}[\chi_{H2S(aq)} + {}^{34}\alpha_{HS-/H2S(aq)}(\chi_{HS-(aq)})] \quad (21)$$

Where $\chi_{H2S(aq)}$ and $\chi_{HS-(aq)}$ are the mole fractions of H_2S and HS^- in solution, which we estimate here by utilizing the Q_{d1} as function of ionic strength from Hershey et al. (1988) and estimating the ionic strength from the reported NaOH concentration and the reported pH. The $^{34}\alpha_{TOTAL(aq)–H2S(g)}$ is the measured fractionation between total aqueous sulfide and $H_2S_{(g)}$ at a given pH and [NaOH] and $^{34}\alpha_{H2S(aq)-H2S(g)}$= 1.0008 (approximately invariant over the ionic strength range ~0-2 M; Geßler and von Gehlen, 1986). These data are not tabulated in the original publication and, thus, the $^{34}\alpha_{TOTAL(aq)–H2S(g)}$, pH, and [NaOH] were estimated from the published figures. This procedure yields a re-estimated $^{34}\alpha$ between $H_2S_{(aq)}/HS^-_{(aq)}$ of about 1.0040 ± 0.0003 (1 s.d. of 6 experiments), slightly lower than their estimated value of 1.0046, and consistent with our interpretation that their usage of a constant Q_{d1} over an ionic strength range of ~0-2 M lead to an overestimation of the fractionation factor. This re-estimated fractionation factor is plotted Figure 2.16 in addition to their original estimate. Our theoretical estimation based on the HS^-_{30H2O} and H_2S_{30H2O} calculations plots directly in between the Fry et al. (1986) determination and our re-estimated value from Geßler and von Gehlen (1986) and is within ~0.7 ‰ of each (smaller when experimental uncertainties are taken into consideration).

5.4.4 Equilibrium isotope effect between sulfate and sulfide

Our calculations of the RPFRs of sulfide species (principally H_2S_{30H2O} and HS^-_{30H2O}) and the sulfate anion ($SO_4^{2-}{}_{30H2O}$) can be used to provide new constraints on the equilibrium isotope effect between the two end-member oxidation states of sulfur for use in both high-temperature and low-temperature applications. In Figure 2.17, we plot the computed $^{33}\alpha$ and $^{34}\alpha$ for $SO_4^{2-}{}_{30H2O}$-H_2S_{30H2O} and $SO_4^{2-}{}_{30H2O}$-HS^-_{30H2O} along with the empirical relation derived from experimental data compiled in Ohmoto and Lasaga (1982) and the recent experiments of Syverson et al. (2015), which were the first to measure $^{33}\alpha$ fractionations in this system. (Calculations of the S^{2-} ion are not included due to its likely negligible abundance over a wide range of pH and T conditions; Ellis and Giggenbach, 1971; Schoonen and Barnes, 1988; Migdisov et al., 2002). Due to the extremely low rates of isotope exchange between sulfide species and sulfate at low temperature (Ohmoto and Lasaga, 1982), the experimental constraints all fall within the 200-400˚C temperature range. Ohmoto and Lasaga (1982) reported an experiment performed at 100˚C, but it did not come close to equilibrium conditions; the measured fractionation after 240 hours of reaction only approached ~4 ‰. The reported fractionation factor for 100˚C in their paper ($^{34}\alpha_{\text{sulfate-sulfide}} \sim 1.048$) is simply the value calculated from their extrapolated empirical temperature dependence over the 200-400˚C range, from with they estimated a rate for isotopic exchange.

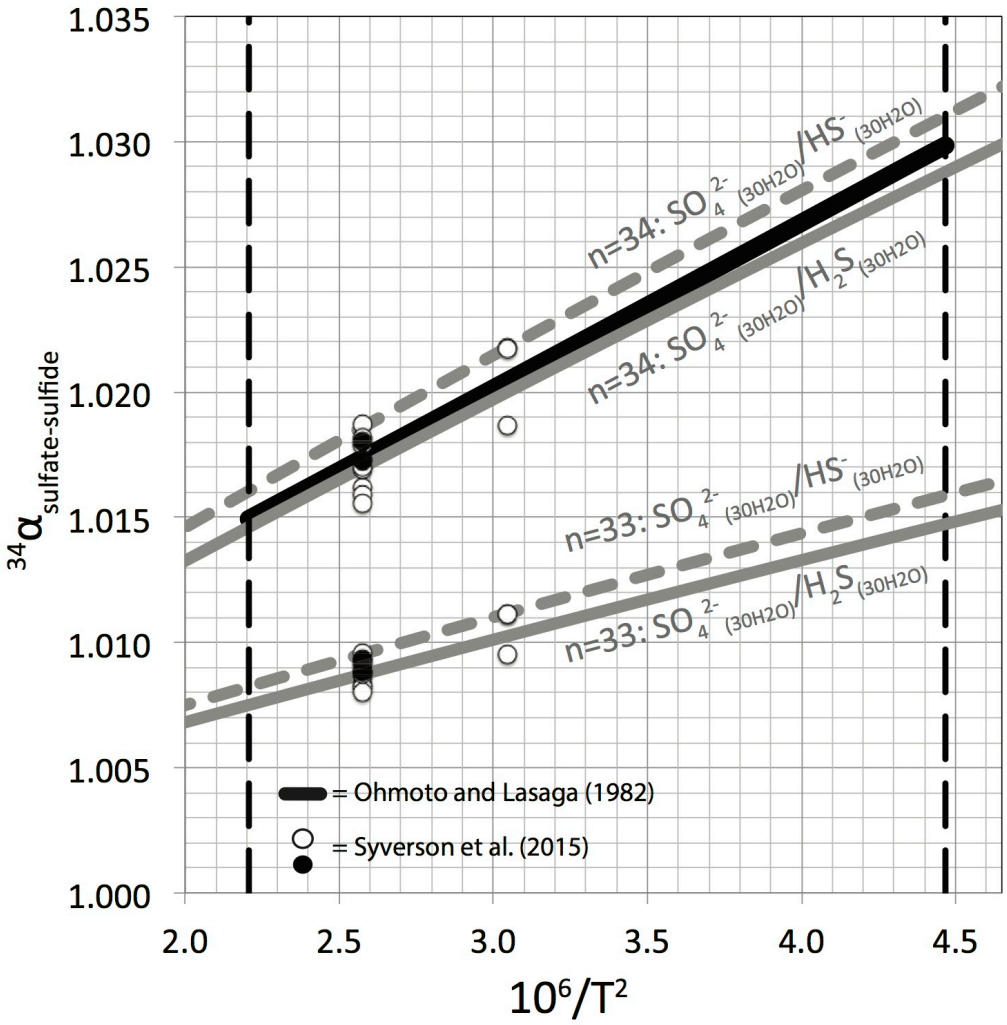

Figure 2.17: Comparison of our theoretical estimations of fractionations between sulfate and sulfide (gray curves; solid and dashed indicate H_2S and HS^-, respectively) and the available experimental constraints at high temperature (200-400˚C, range indicated by dashed vertical lines). The black curve is derived from the compilation of experimental data of Ohmoto and Lasaga (1982). The data points (circles) are the recent experimental values derived from the $FeS_{2pyrite}$-H_2S-SO_4^{2-} system (Syverson et al., 2015), where black circles indicate demonstrably equilibrated experiments via mass dependent relationships (see section 5.4.4 for further explanation).

The estimate from our $SO_4^{2-}{}_{30H2O}$-H_2S_{30H2O} calculations is consistent with the empirical relationship of Ohmoto and Lasaga (1982) over the 200-400˚C temperature range, where the maximum displacement of the two curves approaches ~1 ‰ at the lowest temperature in this range (200˚C). Additionally, the Ohmoto and Lasaga (1982) curve plots in between the computed fractionation factors for $SO_4^{2-}{}_{30H2O}$-

H_2S_{30H2O} and $SO_4^{2-}{}_{30H2O}$-$HS^-{}_{30H2O}$. As inferred from their tabulated data, the experiments from which Ohmoto and Lasaga (1982) derived this empirical relation were mostly performed at low *in situ* pH conditions (where H_2S is dominant), but some of the experiments were performed at higher pH where the HS^- ion *may* have been present in appreciable quantities; the $SO_4^{2-}{}_{30H2O}$-$HS^-{}_{30H2O}$ curves are presented mostly for reference and to illustrate the effects of simple speciation. The experiments from which this relation is derived may also have exhibited more complex *in situ* speciation than we have calculated (e.g., ion pairs of HS^- and SO_4^{2-} with Na^+ and protonated forms of sulfate, principally HSO_4^-). We would expect the differences in the SO_4^{2-}-H_2S and the HSO_4^--H_2S fractionation factor to be minimal (especially over 200-400˚C) because protonation is on one of the oxygen atoms in sulfate, and perhaps similarly small for ion pairs forming with sulfate for similar reasons. The formation of ion pairs that involve direct interactions with sulfur, such as $NaSH^0$, may have greater effects. Complications due to our relatively simplified treatment of speciation may account for some of the small displacement between the theoretical and empirical curves. Errors in the empirically derived relationship may also be present (biased high due to quenching effects, disequilibrium, etc.)—noting that Ohmoto and Lasaga (1982) had only the major isotope ratio, $^{34}S/^{32}S$, with which to judge equilibrium.

The small, apparent divergence of the Ohmoto and Lasaga (1982)-derived sulfate/sulfide fractionation factor and our own based on the $SO_4^{2-}{}_{30H2O}$-H_2S_{30H2O} calculations at the low temperature end (~200˚C) may also be within the uncertainty of the theoretical calculations. The combination of effects related to anharmonicity,

inadequacies in the theoretical method, and cluster geometry variability may contribute permil level error/uncertainty in computed fractionation factors. To explore this more quantitatively, we focus on errors arising from inadequacies in the theoretical method that may represent the major source of error in the calculations. When we apply our CCSD/aug-cc-pVTZ-derived harmonic scaling factor of 1.01-1.02 to the harmonic frequencies for the SO_4^{2-} and H_2S $30H_2O$ clusters, the resulting fractionation factors appear to come into more quantitative agreement with the Ohmoto and Lasaga (1982) curve over the entire experimental temperature range (Figure A.4), which suggests that much of the discrepancy may arise from inadequacies in the theoretical method employed in the present study. Since the discrepancy is small (sub-permil), we cannot rule out contributions from the other factors discussed above.

For comparison, we also plot in Figure A.4 other theoretical estimates based on our own calculations of $H_2S_{(vacuum)}$ and $SO_4^{2-}{}_{(vacuum)}$ using the IEF-PCM solvation model and previous theoretical calculations utilizing experimentally-derived fundamental frequencies and frequency shifts for the minor isotopes (Ono et al., 2007), both of which are several permil displaced from the experimental constraints and our $30H_2O$ cluster calculations. Comparison to our IEF-PCM calculations further emphasizes the need for explicit solvation models in placing theoretical fractionation factors more quantitatively in-line with experimental fractionation factors in aqueous systems.

Our theoretical predictions also appear to be in reasonably good agreement with the recent experimental constraints of Syverson et al. (2015) who investigated

equilibrium isotope fractionations ($^{33}\alpha$ and $^{34}\alpha$) in the H_2S-SO_4^{2-}-FeS_2 (pyrite) system at 300˚C and 350˚C. Their constraints at 350˚C are perhaps more quantitatively robust as these experiments were pursued at longer run times than the lower temperature experiments, and also in greater numbers. The starting solutions were comprised of sodium thiosulfate in acidic ferrous solutions. Upon ramping up the temperature to experimental conditions, thiosulfate undergoes quantitative hydrolytic disproportionation to sulfate and sulfide in 1:1 molar ratios (2/3 of the sulfide subsequently precipitated to form pyrite under their experimental conditions). Since the sulfate and sulfide produced tended to have resolvable $\Delta^{33}S$ values as judged from the shortest experimental runs (a mass-conservation disequilibrium effect), this approach allowed for the direct monitoring of equilibrium. Figure 2.17 shows all of their reported fractionations between sulfate and sulfide, which represent a wide range of experimental run times (ranging from < 1hr up to 4,297 hours as the longest experimental run). The lowest fractionations measured were typically those run for the shortest times and had not achieved isotopic equilibrium. The data points plotted as black circles are from end-run experimental analyses that indicated isotopic equilibrium between sulfate and sulfide by way of identical $\Delta^{33}S$ values between sulfate and sulfide within analytical uncertainty. When taken as an average for the 350˚C determination, the demonstrably equilibrated experiments yield fractionation factors of $^{33}\alpha_{\text{sulfate-sulfide}} = 1.0091 \pm 0.0003$ and $^{34}\alpha_{\text{sulfate-sulfide}} = 1.0176 \pm 0.0006$ (1 s.d.), which agree well with our estimated $^{33}\alpha_{\text{sulfate-sulfide}} = 1.0087$ and $^{34}\alpha_{\text{sulfate-sulfide}} = 1.0170$ from the $SO_4^{2-}{}_{30H2O}$-H_2S_{30H2O} calculations. We note that application of the CCSD/aug-cc-pVTZ-derived 1.01-1.02 harmonic scaling factors puts the theoretical

fractionation factors at $^{33}\alpha_{sulfate\text{-}sulfide}$ = 1.0089-1.0091 and $^{34}\alpha_{sulfate\text{-}sulfide}$ = 1.0173-1.0177 from the $SO_4^{2-}{}_{30H2O}$-H_2S_{30H2O} calculations at 350˚C.

The apparent agreement with high temperature experiments suggest that our calculations may yield reasonable estimations of these fractionations at low-temperature conditions as well (*cf.* Schauble, 2004), although it is important to note that any systematic errors in the calculations will scale inversely with temperature. Due to the extremely low rates of isotope exchange between sulfate and sulfide at low temperature, the only other low temperature constraints have relied either on BM calculations utilizing experimental vibrational spectra (fundamental frequencies) and frequency shifts for the minor isotopes via force field models (e.g., Sakai, 1968; Farquhar et al., 2003; Ono et al., 2007), or extrapolating the empirical temperature dependence of high-temperature constraints to low temperatures (Ohmoto and Lasaga, 1982). Neither approach is strictly valid—for example, computing RPFRs from experimental fundamental frequencies via the BM-equation violates the harmonic oscillator approximations used in its derivation (*cf.* Liu et al., 2010)—and so our calculations may provide some of the most reliable estimates to date at low-temperature within the harmonic approximation. The low temperature fractionations computed via our calculations will likely have the most applicability to network models of isotope partitioning for sulfate reducing organisms (*cf.* Wing and Halevy, 2014), as well as the estimation of sulfate-sulfide equilibration rates from non-equilibrated low-temperature experiments (*cf.* approach of Ohmoto and Lasaga, 1982).

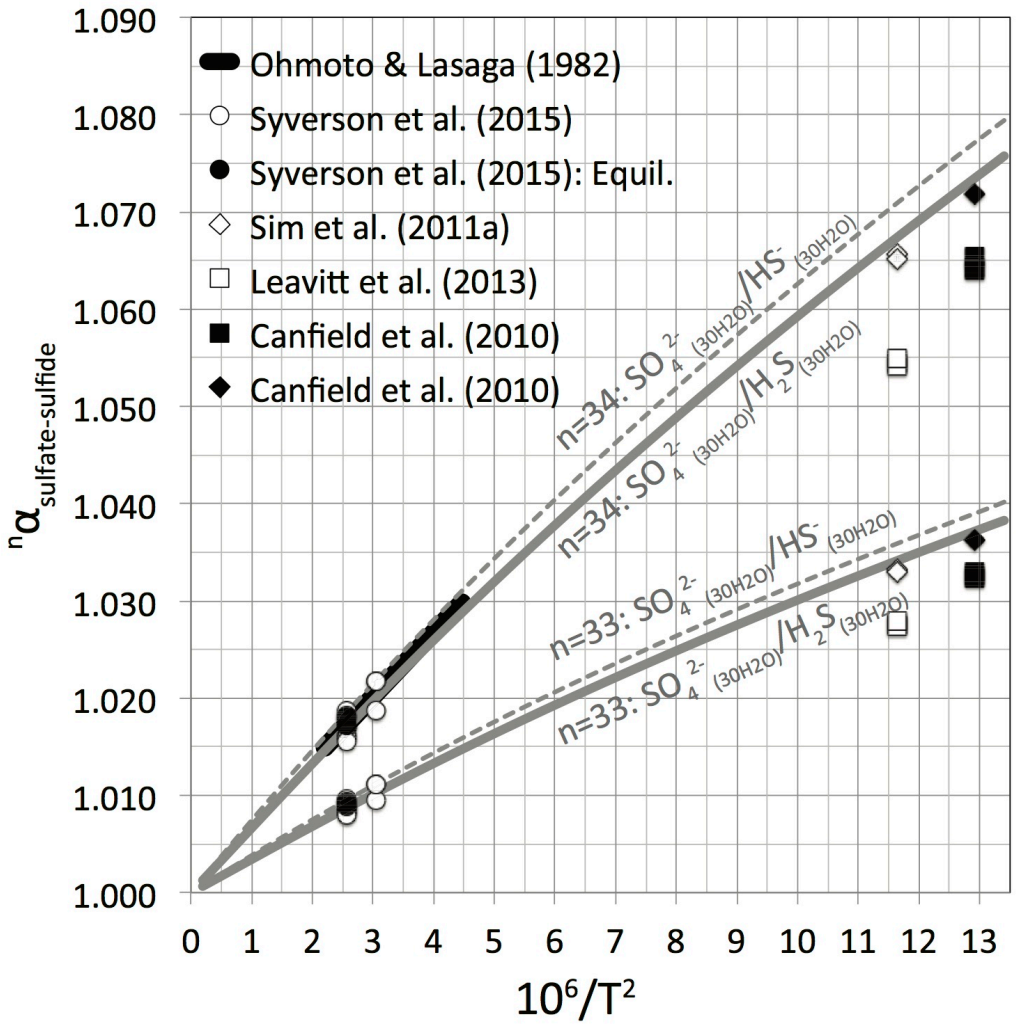

Figure 2.18: Comparison of our theoretical estimations of fractionations between sulfate and sulfide (gray curves; solid and dashed indicate H_2S and HS^-, respectively) and the available experimental constraints plotted from ambient to high temperature (0-2000˚C). Labeling is same as in Figure 2.17. Also included for reference are the largest fractionations reported in microbial sulfate reduction experiments at ambient T: (1) Pure culture experiments: white squares (Leavitt et al., 2013) and white diamonds (Sim et al., 2011a) and (2) experiments with natural populations (Canfield et al., 2010): water incubations = black squares and sediment incubations = black diamonds.

Figure 2.18 presents the data of Figure 2.17 with an expanded temperature range (down to the equivalent of 0˚C) and includes data from recent experiments from sulfate reducing organisms that have produced the largest reported fractionations (Canfield et al., 2010; Sim et al., 2011a). In recent years, it has been postulated that the maximum isotope fractionations possible in a sulfate reducing

organism approach the equilibrium fractionation factor between sulfate and sulfide species at the given growth temperature (*cf.*, Sim et al., 2011a; Wing and Halevy, 2014), which is an assertion based on the consistency between some of the largest fractionations observed in certain cultures of sulfate reducers and the available constraints on equilibrium fractionations. Using the Sim et al. (2011a) and Sim et al. (2011b) pure culture (*Desulfovibrio* sp., DMSS-1) datasets (also, see Leavitt et al., 2013 and Wing and Halevy, 2014), as cell specific sulfate reduction rates approach extremely low values (ca. < 1 fmol H_2S/day/cell), the magnitude of both the $^{34}\alpha_{sulfate\text{-}sulfide}$ fractionation and the exponent of mass dependence $^{33/34}\lambda_{sulfate\text{-}sulfide}$ appear to approach their expected equilibrium values (see Figure A.5). It is hypothesized that at these conditions the organisms are essentially facilitating near-equilibrium isotope exchange between internal reservoirs of sulfate and sulfide via their biochemical and enzymatic machinery and barely growing as a result. The largest fractionation reported between sulfate and sulfide from the Sim et al. dataset is $^{34}\alpha_{sulfate\text{-}sulfide}$ ~1.0656 ± 0.0003 and corresponding $^{33/34}\lambda_{sulfate\text{-}sulfide}$ of 0.5142 ± 0.0002 (~20˚C; Sim et al., 2011a). From this perspective, at 20˚C our calculations would predict a $^{34}\alpha_{sulfate\text{-}sulfide}$ for $SO_4^{2-}{}_{30H2O}$-H_2S_{30H2O} of 1.0674 and a $SO_4^{2-}{}_{30H2O}$-$HS^-{}_{30H2O}$ 1.0709, with corresponding $^{33/34}\lambda_{sulfate\text{-}sulfide}$ of 0.5147 and 0.5148, respectively. We note that applying our harmonic scaling factors of 1.01-1.02 will increase the $^{34}S/^{32}S$-based fractionation factor estimates slightly: for $SO_4^{2-}{}_{30H2O}$-H_2S_{30H2O} = 1.0685-1.0696 and $SO_4^{2-}{}_{30H2O}$-$HS^-{}_{30H2O}$ = 1.0720-1.0732 at 20˚C, which may be appropriate in this case due to the enhanced agreement with Ohmoto and Lasaga (1982) at high temperature. Also plotted in Figure 2.18 are the largest fractionations reported in experiments done

with natural populations isolated from sulfidic water column and sediments of the euxinic alpine Lago Cadagno (Canfield et al., 2010; both sediment and water column incubations at 5˚C). Based on the high sulfide concentrations present in the sampled portions of the system, these experiments were reasoned to largely reflect the processes of sulfate reduction with minor (perhaps negligible) influence of an oxidative/disproportionation cycle (see also Figure A.5). Our calculations do not confirm or sufficiently test any hypotheses regarding the controls on fractionation magnitudes in sulfate reducing organisms, but may provide end-member constraints for isotope fractionation network models that use equilibrium fractionation factors to approximate more complex, multi-step enzymatic redox fractionations (e.g., Wing and Halevy, 2014).

5.4.5 Fractionations involving thiosulfate and sulfide species

The isotope fractionations associated with isotope exchange between the "outer" (**S**-SO_3^{2-}; "sulfane") and "inner" (S-**S**O_3^{2-}; "sulfonate") sulfur atoms in thiosulfate ($S_2O_3^{2-}$), as well as those between these two sites and aqueous sulfide (i.e., $H_2S_{(aq)}/HS^-_{(aq)}$) have been studied experimentally (Uyama et al., 1985), and reinterpreted in terms of exchange rates and slightly revised equilibrium fractionation factors in follow up studies (Chu and Ohmoto, 1991; Chu et al., 2004). Figure 2.19 plots the experimentally derived fractionation factors ($^{34}\alpha$) for S-**S**O_3^{2-}/**S**-SO_3^{2-}, S-**S**O_3^{2-}/H_2S, and **S**-SO_3^{2-}/H_2S (100-170˚C, as compiled/evaluated in Chu et al., 2004) along with the same fractionation factors computed from our $S_2O_3^{2-}{}_{(30H2O)}$ and $H_2S_{(30H2O)}$ cluster calculations. In terms of fractionation magnitude, the fractionation between the intramolecular sites of thiosulfate appear to be in the most agreement

between the experimental dataset and our own calculations, where a slightly steeper temperature dependence is predicted from our calculations than appears to be represented in the experimental dataset.

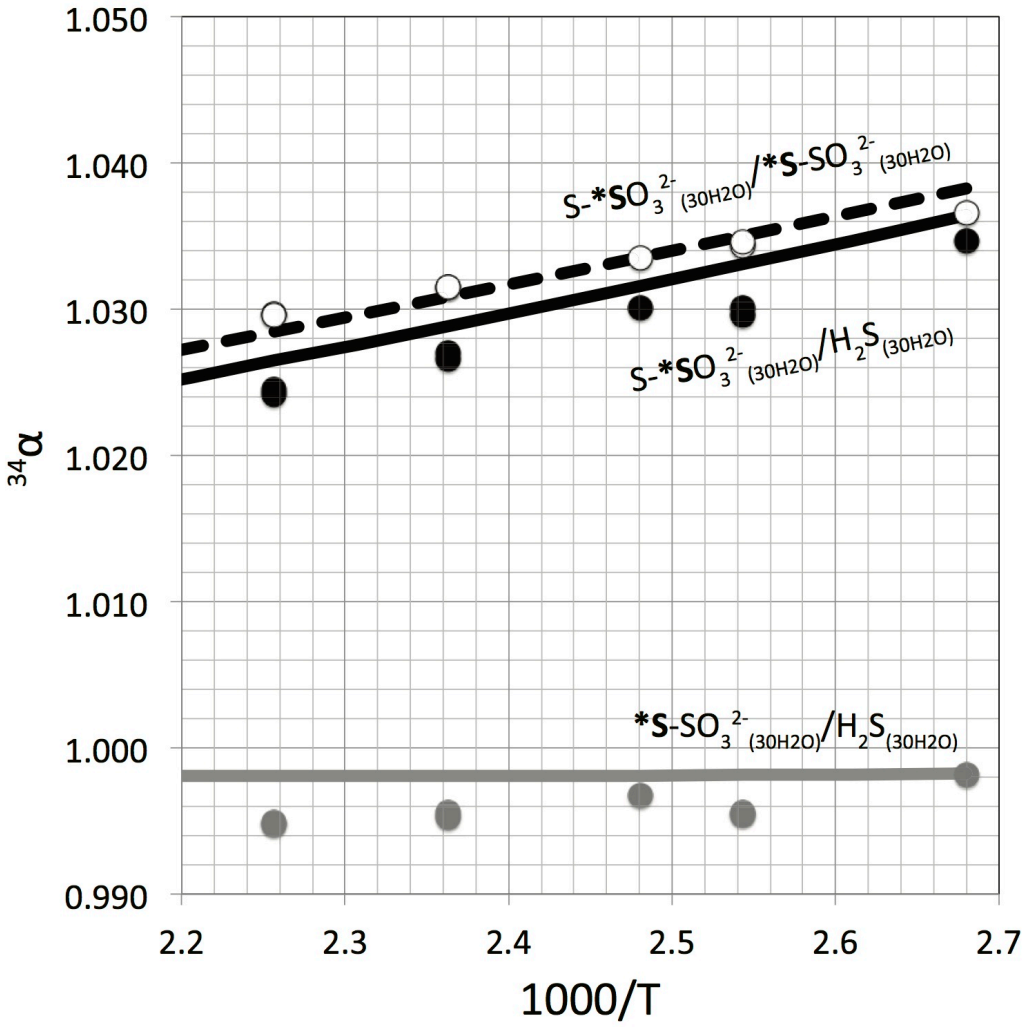

Figure 2.19: The major isotope fractionation factor for the intramolecular isotope fractionation in thiosulfate (experimental: white circles, our theoretical: dashed black curve), fractionations between the outer ("sulfanyl") sulfur in thiosulfate and $H_2S_{(aq)}$ (experimental: gray circles, our theoretical: gray curve), and the inner ("sulfonate") sulfur in thiosulfate and $H_2S_{(aq)}$ (experimental: black circles, our theoretical: black curve). Experimental data are derived by Chu et al. (2004) from the experiments of Uyama et al. (1985).

The fractionations predicted from our calculations and the experiments between the two sulfur sites in thiosulfate and H_2S appear to be systematically shifted

by a few permil, but generally agree in their temperature dependence. The experimental dataset of Uyama et al. (1985) seems to indicate that the **S**-SO_3^{2-}/H_2S fractionation factor increases in magnitude with increasing temperature over the 100-170˚C range, which the calculations also predict, and we find to be related to a crossover at sub-0˚C temperature. These offsets in the magnitude of the fractionation factors between theory and experiment appear to be the largest we have observed in our overall study and may be on the high end of the estimated uncertainties in the calculations.

The relatively large offset between theory and experiment in the thiosulfate/sulfide system may reflect speciation. The experiments were done under *in situ* pH conditions that were circumneutral (ca. 5.4-7.2) where HS^- may be present at appreciable levels at the experimental temperatures (*cf.* Ellis and Giggenbach, 1971; Hershey et al., 1988). However, the computed fractionations between the two sulfur sites in thiosulfate and HS^- do not bring the calculated fractionation factors in better agreement with the experiments. Due to the HS^- ion having a lower RPFR than H_2S, predicted fractionations between S-**S**O_3^{2-}/HS^-, and **S**-SO_3^{2-}/HS^- are shifted upward relative to the H_2S counterparts in Figure 2.19. The formation of $NaSH^0$ ion pairs could, in principle, explain some of the offset due to having a two-fold coordination around the sulfur atom. Although we have not computed this species, it would be predicted to have a higher RPFR than HS^-, perhaps comparable to H_2S. In order for the $NaSH^0$ ion pair to account for the several permil offset alone, it would need to be a major species under the experimental conditions and/or have an even higher RPFR than H_2S.

Applying the harmonic frequency scaling factor of 1.01-1.02 to the frequencies of the sulfide and thiosulfate $30H_2O$ clusters also shifts the predicted fractionation factors in the opposite direction of the experimental constraints on the order of 1-2 ‰ for the S-$\underline{\mathbf{S}}O_3^{2-}$/$H_2S$ and S-$\underline{\mathbf{S}}O_3^{2-}$/$\underline{\mathbf{S}}$-$SO_3^{2-}$ fractionation factors, and has negligible effect on the smaller $\underline{\mathbf{S}}$-SO_3^{2-}/H_2S fractionation factor. Based on our simple treatment, error arising from the employed theoretical method alone may not be able to explain the systematic offset between theory and experiment. Based on the present constraints, we cannot rule out contributions from experimental error, complex speciation effects, and other errors arising from the calculations in describing the apparent offset between our theory and experiment. The offset is somewhat puzzling given the relatively good agreement between our theoretical calculations and the experiments of the intramolecular fractionation factor for thiosulfate, as well as the H_2S/HS^- fractionation factor, and may warrant further experimental investigation.

5.5 Implications of Isomerization: Reactivity of $(HO)SO_2^-$ and $(HS)O_3^-$

On the molecular and mechanistic level, the two isomers of bisulfite have been hypothesized to have different reactivity towards oxidants due to the absence of the lone pair of electrons on sulfur in the tetrahedral $(HS)O_3^-$ form, where the pyramidal $(HO)SO_2^-$ containing the lone electron pair on the sulfur atom might be expected to be more reactive (e.g., Yiin et al., 1987; Brandt and van Eldik, 1995). In other words, the $(HS)O_3^-$ isomer is hypothesized to be sterically hindered in terms of reactions requiring access to the sulfur atom, which could be relevant for many redox reactions involving sulfite and bisulfite species. This hypothesis could be extended to

the relative reactivity of the isomers towards the active binding sites of intracellular enzymes in biological redox processes (e.g., the heme sites in reductases like dissimilatory sulfite reductase and MccA where binding occurs directly to the sulfur atom; Parey et al., 2010; Hermann et al., 2015) as the lone pair of electrons would be necessary for bond formation to the Fe in the heme groups.

To our knowledge, this hypothesis has yet to be tested rigorously and would be expected to depend on the energetics and rates of tautomerization (i.e., the intramolecular transfer of the proton from the sulfur atom to the oxygen atom):

$$(HS)O_3^- \rightarrow (HO)SO_2^- \; k_{tautomerization} \qquad (22)$$

Where $k_{tautomerization}$ represents the rate constant in the direction as indicated. If tautomerization occurs readily (i.e., had a low activation energy), perhaps the $(HS)O_3^-$ isomer could tautomerize prior to (or during) a bimolecular (or similar) reaction to expose the sulfur atom and its lone pair of electrons for binding or electron transfer in a way that led to minimal discrimination between $(HS)O_3^-$ and $(HO)SO_2^-$ during chemical reactions. Alternatively, if tautomerization was inhibited (i.e., had a high activation energy), the rates of tautomerization might be sufficiently slow to inhibit reactions involving $(HS)O_3^-$, and lead to a overall discrimination between $(HS)O_3^-$ and $(HO)SO_2^-$.

There are several consequences of the hypothesis that relatively slow tautomerization could lead to a discrimination between the bisulfite isomers during chemical reactions and, in particular, a more sluggish reactivity for the $(HS)O_3^-$ isomer. From the standpoint of isotope mass balance, assuming that the bisulfite pool is at isotopic equilibrium prior to reaction, a preference for the $(HO)SO_2^-$ isomer (or

SO_3^{2-}) upon reaction would mean that the chemical reaction preferentially samples a fractionated portion of the total sulfite pool, which our calculations predict to be due almost exclusively to the presence of the $(HS)O_3^-$ isomer that has a high RPFR and shifts the other sulfite species towards isotopically lighter values relative to the total S^{4+} composition. If the isotope effect associated with the chemical reaction is a so-called *normal* kinetic isotope effect (i.e., the typical case in which the light isotopomers react more readily than heavy isotopomers due to the predominating influence of weakly bound transition state(s)), sluggish tautomerization could lead to an apparent boost in the magnitude of the instantaneous fractionation between the bulk bisulfite pool and the pooled product. However, should the reaction be associated with a so-called *inverse* isotope effect (i.e., the atypical case of the heavy isotopomer reacting more readily than the light isotopomer), the effect of sluggish tautomerization would be less-straightforward: it could either lead to a dampening of magnitude of the apparent fractionation, or could possibly even lead to an apparent reversal in the direction of the fractionation (from inverse to normal) depending on the relative magnitudes of the fractionation associated with the kinetic isotope effect vs. that associated with the equilibrium isotope effects among the sulfite species. The complex speciation of sulfite species in solution may contribute to considerable ambiguity in the meaning of measured isotope effects associated with unidirectional reactions involving sulfite under solution conditions of mixed-species, potentially obscuring any observation of primary kinetic isotope effects.

We consider a simple qualitative example to illustrate hypothetical effects associated with bisulfite isomerization within the basic framework of sulfate

reduction. We first assume that equilibration rates between the sulfite and bisulfite isomers are sufficiently fast that they are in chemical and isotopic equilibrium at all times over all respiration rates and residence times of sulfite species within the cell. We consider a pool of sulfite species being generated via the reduction of APS. Upon the cleavage of the S-O bonds, the sulfite species would enter solution as inorganic anions and immediately undergo hydrolysis reactions to form the different bisulfite isomers, the relative equilibrium distribution of which would depend on the pH, temperature, and ionic strength conditions of the intracellular aqueous environment. Once equilibrated chemically and isotopically, this pool would be characterized by an isotopically depleted pool of sulfite *sensu stricto* and $(HO)SO_2^-$ and a relatively isotopically enriched pool of $(HS)O_3^-$. The magnitude of the bulk fractionation would depend on the relative distribution of these species and therefore depend on the temperature, ionic strength, and pH of the intracellular environment. If the active siroheme site of dSiR discriminated between the aqueous sulfite species and showed a preference for sulfite *sensu stricto* and/or $(HO)SO_2^-$, the unidirectional reduction of this sulfite could introduce an apparent amplification in the instantaneous fractionation that eventually forms sulfide, which considering mass balance could amount to an amplification on the level of several permil depending on conditions. In this simple case of hypothetical species discrimination, the $(HS)O_3^-$ isomer would effectively be acting as a relative dynamic 'sink' for heavy isotopes within the metabolism. An effect of this kind would be amplified with increasing temperature due to the increasing proportion of the $(HS)O_3^-$ isomer with increasing temperature, which would be significant for sulfate reducers that grow at higher temperatures.

Even given little to no species discrimination with respect to enzymatic redox transformations involving the sulfite species, the presence of the $(HS)O_3^-$ isomer would be predicted to cause shifts in the isotopic mass balance between the bulk intracellular sulfite pool and other downstream and upstream pools in the metabolism depending on relative reversibility. In this case, the magnitudes of these effects would likely depend on the rates of isotopic equilibrium among the sulfite species, especially in how these rates compare to the residence time of total sulfite in the cell. Since the residence time of sulfite species will vary as a function of cell specific reduction rate (which, in turn, is controlled by a wide variety of extra- and intra-cellular environmental and metabolic conditions; *cf.* Wing and Halevy, 2014), the magnitudes of any of the hypothetical effects associated with the $(HS)O_3^-$ isomer could vary considerably over wide ranges of growth conditions.

6.0 Conclusion

The calculations presented here provide detailed constraints on sulfur isotope partitioning in the sulfite system, and provide new constraints on fractionation factors involving many of the major aqueous sulfur compounds relevant to hydrothermal and (bio)geochemical cycles. From the analysis of the general consistency between our calculations and the experimental datasets (Eriksen, 1972a; Eriksen, 1972b; Eriksen, 1972c), the calculations reveal that the isomerization of bisulfite is a major control on isotope partitioning in the sulfite system. However, much uncertainty still exists in the isomerization quotient as a function of temperature over a wide range of ionic strength. Future research should be directed at constraining this quotient over a wide range of environmental conditions (temperature and ionic strength) to more precisely

determine its potential influence in the sulfur cycle. The experimental constraints on isotope partitioning among sulfite species also warrants further investigation and, subsequently, higher level calculations as needed as the precision of empirical constraints improves. Due to the complexity of sulfite solutions, precise and species-specific determinations of isotope partitioning in the sulfite system will be reliant upon the combination of experimental and theoretical techniques.

The pH and ionic strength dependency of sulfur isotope partitioning in the sulfite system is significant due to the complex speciation of sulfite. Treating the sulfite system in isotope partitioning models strictly as the pyramidal sulfite anion (SO_3^{2-}) (e.g., network models of sulfate reducing metabolisms) is clearly invalid for most conditions relevant to natural systems, particularly intracellular conditions where pH is typically circum-neutral. Future treatment and applications should include all relevant species. Assumptions about similarity in structure between sulfite species and their isotope partitioning behavior are demonstrably invalid and should be avoided in any future experimental approaches. It remains to be shown whether or not the two structural isomers of bisulfite behave differently during chemical reactions, but if they do, there could be consequences in isotope fractionations associated with chemical reactions in sulfite media where both isomers are present.

Calculations of the isotope partitioning behavior of the sulfoxylate species have been included here in the hopes of igniting research towards their further characterization in aqueous solutions. As in the sulfite system, isotope partitioning among sulfoxylate species will strongly depend on the isomerization of the protonated species, principally H_2SO_2 and bisulfoxylate species. Techniques exist for

producing these compounds via the decomposition of organic precursors (e.g., thiourea dioxide; Svarovsky et al., 2000; Makarov et al., 2002; Makarov et al., 2010) and so their characterization in aqueous solutions should be possible. If such species do exist within the microbial sulfate reduction framework, their characterization could allow for an even more elaborate understanding of sulfate reduction metabolisms. The role these compounds play in other redox processes (e.g., sulfide oxidation) could further be illuminated through these studies, and allow for detailed understandings of their mechanisms as well.

Table 2.1: Select sulfite system equilibrium quotients as reported in the literature.

Temperature (°C)	μ (M or *m*)	Q	Reference
SO_2 Dissolution (Henry's Law): $SO_{2\,(g)} \rightleftharpoons SO_{2\,(aq)}$; $Q_H = [SO_2]_{aq}/pSO_2$ (*m*/atm)			
25	0	1.23 ± 0.05	1
25	0.01 *m*	1.13 ± 0.05	2
25	1 *m*	1.04 ± 0.05	2
Overall Acid Dissociation 1: $SO_{2(aq)} + H_2O \rightleftharpoons HSO_3^-{}_T + H^+$; $Q_1 = [HSO_3^-{}_T][H^+]/[SO_{2(aq)}]$ (M or *m*)			
25	0	$10^{-1.91\ (\pm 0.02)}$	3
25	0	$10^{-1.88\ (\pm 0.06)}$	4
25	0.01 *m*	$10^{-1.88\ (\pm 0.02)}$	2
25	1 *m*	$10^{-1.63\ (\pm 0.02)}$	2
25	1 *m*	$10^{-1.37}$	3, 5
Acid Dissociation 2: $HSO_3^-{}_T \rightleftharpoons SO_3^{2-} + H^+$; $Q_2 = [SO_3^{2-}][H^+]/[HSO_3^-{}_T]$			
25	0	$10^{-7.18\ (\pm 0.03)}$	3
25	0.1 *m*	$10^{-6.90\ (\pm 0.05)}$	2
25	1 *m*	$10^{-6.40\ (\pm 0.05)}$	2
25	1 *m*	$10^{-6.34}$	3, 5
Bisulfite Isomerization: $(HS)O_3^- \rightleftharpoons SO_2(OH)^-$; $Q_i = [SO_2(OH)^-]/[(HS)O_3^-]$			
25	1.0 *m*	4.9 (± 0.1)	6
25	1.0 *m*	~4.8	7
25	~0	2.6 (± 0.5)	8
Bisulfite Dimerization: $2HSO_3^-{}_T \rightleftharpoons S_2O_5^{2-} + H_2O$; $Q_d = [S_2O_5^{2-}]/[HSO_3^-{}_T]^2$			
20	—	0.07	9
25	—	0.07	10
25	0 M	0.076	11
	2 M	0.34	
25	0 *m*	0.033	12
	1 *m*	0.088	
20	1 *m*	0.062	7
	5 *m*	0.25	
25	0	0.045	13
25	0	0.045 (±0.008)	4
Acid Dissociation of the Dimer: $HS_2O_5^- \rightleftharpoons S_2O_5^{2-} + H^+$; $Q_{dH} = [S_2O_5^{2-}][H^+]/[HS_2O_5^-]$			
25	0	$10^{-2.9\ (\pm 0.2)}$	4

[1] Goldberg and Parker (1985); [2]Millero et al. (1989); [3]Martell and Smith (1982); [4]Beyad et al. (2014); [5]Horner and Connick (2003); [6]Horner and Connick (1986); [7]Littlejohn et al. (1992); [8]Risberg et al. (2007); [9]Golding (1960); [10]Eriksen and Lind (1972);[11]Bourne et al. (1974) [12]Connick et al. (1982); [13]Ermatchkov et al. (2005)

Table 2.2: Sulfoxylate system equilibrium quotients as reported in the literature.

Temperature (°C)	μ	Q	Reference
Acid Dissociation 1: $H_2SO_{2(aq)} \rightleftharpoons HSO_2^-{}_T + H^+$; $Q_1 = [HSO_2^-{}_T][H^+]/[H_2SO_{2(aq)}]$			
25	0.1 *m*	$10^{-7.97}$	Makarov et al. (2010)
Acid Dissociation 2: $HSO_2^-{}_T \rightleftharpoons SO_2^{2-} + H^+$; $Q_2 = [SO_2^{2-}][H^+]/[HSO_2^-{}_T]$			
25	0.1 *m*	$10^{-13.55}$	Makarov et al. (2010)

Table 2.3: Coefficients from polynomial fits to RPFRs computed at the B3LYP/6-31+G(d,p) level of theory in 30-40 H_2O clusters over 273.15-2273.15 K (0-2000˚C). Values are computed using the coefficients via: $^{34}\beta$ or $^{33/34}\lambda_\beta$ or $^{36/34}\lambda_\beta = A/T^4 + B/T^3 + C/T^2 + D/T + E$, where T is in Kelvin. Extra significant figures are given to minimize rounding errors. Values for $^{33}\beta$ and $^{36}\beta$ are computed from the $^{33/34}\lambda_\beta$ and $^{36/34}\lambda_\beta$ exponents, respectively, using: $^{33}\beta = (^{34}\beta)^{33/34\lambda\_\beta}$ and $^{36}\beta = (^{34}\beta)^{36/34\lambda\_\beta}$ at a given temperature. For the bisulfite dimer ($S_2O_5^{2-}$), the S-S bond length is noted in Å and A and B refer to: $(O_2S_A\text{-}S_BO_3)^{2-}$. Note: The values of E are intercepts at the high temperature limit ($T\rightarrow\infty$) and should theoretically converge on: $^{34}\beta_{[E]} = 1$, $^{33/34}\lambda_{\beta\,[E]} = 0.51588$, and $^{36/34}\lambda_{\beta\,[E]} = 1.8904$.

		$^{34}\beta$					$^{33/34}\lambda_\beta$					$^{36/34}\lambda_\beta$				
Compound	**nH_2O**	**A×10^5**	**B×10^4**	**C×10^2**	**D×10^{-2}**	**E**	**A×10^5**	**B×10^3**	**C×10^{-1}**	**D×10^{-3}**	**E**	**A×10^6**	**B×10^4**	**C×10^{-2}**	**D×10^{-2}**	**E**
SO_4^{2-}	30	590.371	-126.799	109.869	-137.516	1.000347	-30.8690	46.1900	-2194.08	48.4610	0.515866	20.0957	-30.5253	146926	-30.9584	1.89050
$(HS)O_3^-$ [1]	30	905.705	-147.268	105.824	-92.3176	1.000195	-36.0529	47.5396	-2038.76	40.6206	0.515848	24.2746	-31.9304	136605	-20.3357	1.89051
$(HS)O_3^-$ [2]	30	914.750	-148.129	106.124	-93.3723	1.000198	-37.0901	48.3512	-2051.71	35.6621	0.515861	24.4825	-32.1287	137230	-20.8157	1.89051
S-SO_3^{2-} (inner)	30	411.460	-96.9863	90.9001	-108.003	1.000274	-24.5634	37.7929	-1869.03	39.3817	0.515874	16.0257	-24.9975	125212	-25.2475	1.89048
SO_3^{2-} [1]	30	147.138	-57.1113	64.8862	-66.7662	1.000174	-12.1588	22.3335	-1256.77	5.84049	0.515915	6.59541	-13.9300	84468.4	-15.4418	1.89047
SO_3^{2-} [2]	30	131.638	-55.2533	64.0120	-65.9924	1.000172	-10.6590	21.1779	-1242.26	13.2399	0.515915	5.78271	-13.2584	83392.1	-19.5475	1.89062
$(HO)SO_2^-$ [1]	34	227.691	-62.3345	63.6829	-69.8409	1.000178	-16.2693	26.2215	-1364.47	27.2021	0.515871	10.5895	-17.2801	90887.8	-16.5777	1.89044
$(HO)SO_2^-$ [2]	34	243.446	-64.2295	63.9099	-72.0204	1.000184	-16.7025	26.7737	-1377.83	30.2698	0.515850	11.1722	-18.0159	93369.1	-20.3001	1.89056
$SO_{2(aq)}$	30	692.521	-108.509	71.7931	-103.029	1.000245	-48.0459	57.0980	-2177.40	55.0250	0.515831	32.5900	-38.5370	145870	-29.0384	1.89048
$SO_{2(g)}$	0	754.026	-114.672	71.5395	-105.747	1.000248	-55.2114	63.5980	-2337.13	44.8960	0.515869	36.7913	-42.6517	157869	-30.8486	1.89052
$(HS)O_2^-$	30	360.997	-67.0840	54.3488	-27.5149	1.000048	-10.6136	18.2893	-982.056	3.89045	0.515901	6.79767	-12.0675	66138.9	-4.23454	1.89038
$(HS)O_2H$	30	380.899	-66.3215	52.4857	-12.5409	1.000006	-12.2554	18.5304	-918.537	-13.8604	0.515944	6.69872	-11.4303	61927.7	-4.45807	1.89057
SO_2^{2-}	30	11.8836	-20.4170	30.3733	-24.9619	1.000066	-2.56730	9.61814	-733.960	10.4911	0.515889	2.31680	-7.04182	51228.2	-5.66457	1.89041
$S(OH)_2$	30	32.5192	-21.8550	29.2787	-26.1670	1.000068	-3.24888	10.4655	-768.717	32.7233	0.515828	1.90679	-6.37994	47247.3	-8.35974	1.89051
$(HO)SO^-$	30	19.4614	-20.0430	28.5160	-24.7943	1.000065	-3.49639	9.82567	-688.628	-6.14640	0.515912	2.82153	-7.35610	50838.2	-7.70786	1.89041
$H_2S_{(aq)}$	30	462.536	-48.3382	20.1638	77.2695	0.999749	-11.2082	8.59125	-133.040	-53.7633	0.515864	7.70591	-6.05029	10354.0	35.4036	1.89025
S-SO_3^{2-} (outer)	30	-24.5550	-2.01175	11.3562	-2.64754	1.000007	2.58474	1.26805	-386.465	41.8080	0.515830	-0.678068	-1.09468	21870.8	-6.10872	1.89050
HS^-	30	213.257	-22.4384	12.2701	42.8805	0.999864	-5.47337	3.11818	-6.41346	-53.7300	0.515891	3.91822	-2.18380	-4.79300	37.4599	1.89025
$H_2S_{(g)}$	0	470.075	-48.9645	19.2083	82.5595	0.999735	-10.7593	8.05933	-103.577	-55.2088	0.515898	7.44511	-5.61973	7534.45	37.2276	1.89031
S^{2-}	30	2.46274	-2.30464	7.54757	-0.688045	1.000001	3.46783	-1.51862	-140.010	32.1639	0.515819	-2.33264	1.06520	9415.48	-25.8717	1.89127
$S_2O_5^{2-}$ [1A] (2.468 Å)	30	364.444	-73.0226	61.6230	-79.4550	1.000199	-26.4546	35.9415	-1591.09	34.2723	0.515880	17.4385	-24.0306	107998	-26.5683	1.89057
$S_2O_5^{2-}$ [1B]		380.966	-91.5445	85.5763	-103.665	1.000264	-22.1841	34.9103	-1750.48	41.3451	0.515873	14.3817	-22.9546	116418	-24.3994	1.89050
$S_2O_5^{2-}$ [2A] (2.505 Å)	30	397.137	-76.6766	62.5608	-82.4519	1.000205	-28.2450	38.4494	-1704.01	56.0947	0.515839	19.1298	-25.6490	111886	-25.5825	1.89052
$S_2O_5^{2-}$ [2B]		336.782	-85.7470	82.5440	-98.3850	1.000252	-19.6417	32.2172	-1663.53	38.7957	0.515853	13.1699	-21.6553	112295	-23.4324	1.89050
$S_2O_5^{2-}$ [3A] (2.482 Å)	31	349.189	-71.2235	60.5973	-78.5580	1.000197	-25.7908	35.3032	-1571.94	34.7375	0.515861	17.4691	-23.8774	106250	-20.6730	1.89044
$S_2O_5^{2-}$ [3B]		369.152	-89.9354	84.7548	-102.548	1.000262	-22.2684	34.7752	-1734.75	35.7416	0.515877	14.0824	-22.6706	115791	-25.4411	1.89052
$S_2O_5^{2-}$ [4A] (2.542 Å)	40	433.004	-80.4687	63.5931	-85.0203	1.000210	-30.6365	40.2622	-1719.62	44.8114	0.515845	20.8286	-27.2845	116158	-25.8011	1.89054
$S_2O_5^{2-}$ [4B]		316.881	-82.9536	81.0520	-95.5356	1.000245	-19.0720	31.5150	-1638.88	37.0809	0.515868	12.3525	-20.7774	109538	-23.1387	1.89047
Intercept (E) Average						*1.0001*					*0.51587*					*1.8905*
Intercept (E) 1 s.d.						*0.0002*					*0.00003*					*0.0002*

Table 2.4: Summary of $^{34}S/^{32}S$ based fractionation factors in the sulfite system from experiments and theoretical calculations at 25˚C.

$1000\ln{}^{34}\alpha$	**Experiment (‰)**	**Theoretical* (‰)**
$SO_{2(aq)}$-$SO_{2(g)}$	0.9 ± 0.4 [a] ~2.2 [b]	1.8
$HSO_3^-{}_T$-$SO_{2(aq)}$	9 ± 1 [a]	9.4 ± 0.9 (μ = 0 *m*) 6.9 ± 0.1 (μ = 1 *m*)
$HSO_3^-{}_T$-SO_3^{2-}	N/A	4.0 ± 0.9 (μ = 0 *m*) 1.5 ± 0.1 (μ = 1 *m*)

[a]Eriksen (1972c); [b]Chmielewski et al. (2001); *Computed at the B3LYP/6-31+G(d,p) level in aqueous 30-34H_2O clusters. The calculated values involving bisulfite were computed using isomer proportions from quotients determined at ionic strength of 0 *m* (Risberg et al., 2007) and 1 *m* ionic strength (Horner and Connick, 1986). Uncertainties on the calculated values solely represent the propagated uncertainties on the isomerization quotients reported at 25˚C in the references.

Chapter 3: Rates and multiple sulfur isotope fractionations associated with the oxidation of sulfide by oxygen in aqueous solution

Abstract

We present experimental determinations of the reaction rates and sulfur isotope fractionations associated with the oxidation of aqueous sulfide (principally HS^-) via molecular oxygen in high pH, low ionic strength carbonate/bicarbonate buffered solutions as a function of temperature (5-45˚C) and trace metal catalysis (ferrous iron, Fe^{2+}, ~50-150 nM). Rates and fractionation factors are quantified via the analysis of sulfide as a function of reaction progress. We find that the oxidation of sulfide at pH = 9.8 and 25˚C without any catalyst added is associated with a computed second order rate constant (k) of $\ln k = 3.49 \pm 0.19$ (k in $M^{-1}hr^{-1}$; 1 s.d., quadruple experiments) and the fractionation factors: $^{34}\varepsilon_{P\text{-}R} = -5.85 \pm 0.15$ ‰ and $^{33/34}\lambda = 0.5094 \pm 0.0016$ that translates to a $\Delta^{33}S_{products\text{-}sulfide} = 0.033 \pm 0.009$ ‰ (1 s.d., duplicate experiments), indicating a mass dependence that appears to be resolvable from the expectations of typical equilibrium isotope exchange ($^{33/34}\lambda_{equilibrium} \approx 0.514 – 0.516$). Fractionation factor magnitudes ($^{34}\varepsilon_{P\text{-}R}$) appear to increase slightly with rate due to increasing temperature over 5-45˚C from -5.00±0.14 ‰ to -6.34±0.24 ‰, indicating inverse fractionation temperature dependence, and may decrease slightly in magnitude with increasing rate due to ferrous iron catalysis at 25˚C (-4.90±0.11 ‰, $[Fe^{2+}]_{added} \approx 150$ nM, $\ln k = 4.22 \pm 0.04$). We do not appear to resolve any relationships between rate and $^{33/34}\lambda$ due to either temperature or ferrous iron

catalysis. We review our experiments in the context of previous studies and find that kinetic parameters derived from our experiments compare well to the extensive experiments of the Frank J. Millero group, but indicate that much variability is found in the kinetics literature that may be indicative of varying degrees of unintended trace catalysts present in experimental media or approaches. We interpret our results in the context of the two hypothetical mechanisms that have been proposed for sulfide oxidation, and suggest that the isotope fractionation relationships we observe may be indicative of reversible isotope exchange between sulfur intermediates and residual sulfide occurring as part of the mechanism, although more primary effects cannot be ruled out at present. A comparison of our fractionations to the available biological constraints (anoxygenic phototrophic bacteria) do not indicate a robust biosignature for oxidative processes based on $^{34}\varepsilon/\Delta^{33}S$ relationships, however, the two general processes may cause residual sulfide undergoing oxidation to evolve along different trajectories in $\delta^{34}S/\Delta^{33}S$ composition space under certain circumstances. Overall, the observation that the autoxidation of aqueous sulfide in high pH media is associated with a non-zero $\Delta^{33}S_{products\text{-}sulfide}$ will influence how oxidation processes are treated in environmental and global scale models of the sulfur cycle based on multiple sulfur isotopes.

1.0 Introduction

1.1 General overview: Motivation and natural settings

The oxidation of sulfide compounds is the complement of the major geochemical process of microbial sulfate reduction (MSR; or dissimilatory sulfate reduction) that intimately ties the global sulfur and carbon cycles. In coastal marine

and shelf environments, high organic carbon fluxes to the seafloor combined with high porewater sulfate and low oxygen concentrations drive the anaerobic respiration process of MSR. MSR accounts for ~12-29% of the total respiration of the organic carbon flux to the seafloor per year (Bowles et al., 2014) and can account for upwards of 50% of the total organic matter respired in localized shelf sediments (e.g., Jørgensen, 1982). MSR additionally has the potential to impart some of the largest isotope fractionations ($\delta^{34}S$) that can be expressed in natural environments between sulfate and the metabolic waste product sulfide (H_2S/HS^-) (e.g., Canfield et al., 2010; Sim et al., 2011a; Sim et al., 2011b; Leavitt et al., 2013; Wing and Halevy, 2014). The aqueous sulfide (H_2S/HS^-) generated by MSR may subsequently undergo a complex sulfur cycle that includes oxidation (chemical and microbial) and mineral formation (e.g., authigenic pyrite, $FeS_{2(authigenic)}$; Rickard and Morse, 2005). From studies of modern coastal marine sediments, it has been estimated that ca. 80-95% of MSR-produced sulfide is re-oxidized back to sulfate with the small remainder existing in mineral phases (Jørgensen, 1977; Jørgensen, 1982; Jørgensen et al., 1990; Canfield and Teske, 1996; Jørgensen and Nelson, 2004), indicating that sulfide oxidation processes are major features of the global geochemical cycle.

The environmental pathways of chemical and biological oxidation of sulfide generate sulfur compounds of intermediate oxidation state such as polysulfides, elemental sulfur, thiosulfate, polythionates, sulfite, and others that can stimulate complex cycling including microbial disproportionation (e.g., Canfield and Thamdrup, 1994; Canfield, 2001; Jørgensen and Nelson, 2004; Zopfi et al., 2004; Johnston, 2011). The microbial processes of sulfate reduction, sulfide oxidation, and

intermediate compound disproportionation can individually impart their own unique isotope signatures to coexisting sulfate and sulfide phases when $\delta^{34}S/\Delta^{33}S$ relationships are considered (e.g., Johnston, 2011). When multiple transformations such as these operate together, large additive $\delta^{34}S$ fractionations between coexisting sulfate and sulfide phases in natural systems can be generated that can surpass the magnitude of any one single process (Canfield and Thamdrup, 1994; Canfield, 2001), and $\delta^{34}S/\Delta^{33}S$ relationships can allow at least some disentangling of such compounded effects (Johnston, 2011; Pellerin et al., 2015). Despite the relatively small isotope effects ($\delta^{34}S/\Delta^{33}S$) that have been documented for bacterial sulfide oxidation (anaerobic phototrophs; Zerkle et al., 2009), these effects combined with substantial oxidative cycling can dampen the larger $\Delta^{33}S$ effects associated with MSR and disproportionation at the environmental scale, potentially masking any isotopic signatures that may allow the two metabolisms to be distinguished (Zerkle et al., 2009). Sulfide oxidation processes therefore may be influential in (or detrimental to) the preservation of certain isotopic signals in natural systems.

The environments and conditions of sulfide oxidation are diverse and extend well-beyond early diagenetic processes in marine sediments. In most surface environments, sulfide is sourced biologically or from hydrothermal vents and other volcanic sources. Other environments where the oxidation of sulfide compounds occurs include (but are not limited to): the chemocline in redox-stratified euxinic basins (e.g., Jørgensen et al., 1991; Millero, 1991a; Millero, 1991b; Millero, 1991c; Zerkle et al., 2009), the atmosphere (e.g., volcanogenic sulfur gases), terrestrial sulfide deposits (e.g., Schippers, 2004), sulfidic hot springs (e.g., Yellowstone NP,

Wyoming, USA; Xu et al., 1998; Xu et al., 2000), seafloor hydrothermal vent environments (e.g., Edwards, 2004), sulfidic caves (e.g., Frasassi cave system, Italy; Macalady et al., 2006), arctic sulfur springs (Borup Fjord Pass; Gleeson et al., 2012), and during seafloor basalt weathering, potentially playing a role in sustaining a chemolithotrophic "deep biosphere" (e.g., Bach and Edwards, 2003; Orcutt et al., 2011).

Despite the ubiquity of oxidative sulfur cycling in natural environments, the isotope effects associated with sulfide oxidation processes have received relatively little attention. Constraints on multiple sulfur isotope fractionations ($\delta^{34}S/\Delta^{33}S/\Delta^{36}S$) accompanying sulfide oxidation are presently limited to the effects associated with the anaerobic phototrophic bacterium, C*hlorobium tepidum* (Zerkle et al., 2009). The existing calibrations of chemical sulfide (H_2S/HS^-) oxidation via molecular oxygen (Fry et al., 1988) pre-date the more recent emphasis on the analysis of minor sulfur isotopes and require a re-examination for future environmental applications. Substantial oxidation of sulfide occurs via abiotic chemical pathways in natural environments that are the result of mechanisms that are entirely different than intracellular metabolic pathways that can lead to different isotope fractionations. The calibration of isotope fractionations associated with chemical oxidation is therefore required for a more complete treatment of oxidation pathways in the study of sulfur isotopes in natural systems. Additionally, the development of oxidative biosignatures may be possible via the elucidation of oxidation mechanisms aided by multiple sulfur isotope analysis, potentially allowing for the relative proportions of

these oxidative pathways to be quantified under some circumstances in natural environments.

1.2 The present study

We present experimental determinations of the reaction rates and sulfur isotope fractionations associated with the chemical oxidation of aqueous sulfide (principally HS^-) via molecular oxygen in high pH, low ionic strength carbonate/bicarbonate buffered solutions as a function of temperature (5-45˚C) and trace metal catalysis (ferrous iron, Fe^{2+}, ~50-150 nM). Ferrous iron is chosen to explore catalytic effects because it is one of the most sensitive, impactful, and environmentally relevant catalysts for aqueous sulfide oxidation in relatively high pH solutions (Vazquez et al., 1989: Millero, 1991a; Millero, 1991b; Millero, 1991c; Zhang and Millero, 1993). We analyze isotopic fractionations associated with all three stable isotope ratios of sulfur ($^{33}S/^{32}S$, $^{34}S/^{32}S$, $^{36}S/^{32}S$) to explore mass dependent relationships. The approach of measuring reaction rates in addition to isotopic fractionations allows us to place our experiments in the context of the extensive experimental kinetics literature (e.g., Ostlund and Alexander, 1963; Avrahami and Golding, 1968; Cline and Richards, 1969; Chen and Morris, 1972a; Chen and Morris, 1972b; Almgren and Hagstrom, 1974; O'Brien and Birkner, 1977; Millero et al., 1987a; Zhang and Millero, 1993; Luther et al., 2011), in addition to allowing us to explore rate/fractionation relationships.

The rates and isotope effects accompanying a predominately unidirectional process like the oxidation of sulfide are intimately linked expressions of the reaction mechanism. The isotope fractionations associated with sulfide oxidation are

putatively the expression of kinetic isotope effects, where multiple reaction pathways are possible due to a complex mechanism. By combining the analysis of both reaction rates and isotope fractionations, we may yield new insights into the understanding of the complex mechanism of sulfide oxidation as well as provide critical constraints for environmental and global mass balance models of the sulfur cycle based on all four sulfur isotopes that require consideration of oxidative pathways.

1.3 Additional background: Kinetic experiments of HS^- oxidation via O_2

The isotope fractionations associated with sulfide oxidation via molecular oxygen are expressions of the reaction mechanism and are likely to co-vary with reaction rate. Numerous experimental studies have investigated the rates of chemical sulfide (H_2S/HS^-) oxidation via molecular oxygen (O_2) in relatively low-ionic strength experimental buffer solutions (Avrahami and Golding, 1968; Chen and Morris, 1972a; Luther et al., 2011; Millero et al., 1987a; O'Brien and Birkner, 1977) and seawater (Almgren and Hagstrom, 1974; Cline and Richards, 1969; Millero et al., 1987a; Ostlund and Alexander, 1963; Zhang and Millero, 1993). The reaction has also been studied as a function of various catalysts including trace metals (e.g., Chen and Morris, 1972b; Hoffman and Lim, 1979; Vazquez et al., 1989; Zhang and Millero, 1993) and organic compounds (Chen and Morris, 1972b).

The rate of sulfide oxidation is understood to follow a general rate law:

$$-d[(H_2S)_T]/dt = k[(H_2S)_T]^a[O_2]^b \qquad (1)$$

Where $(H_2S)_T$ refers to the sum of all aqueous sulfide species (H_2S, HS^-, S^{2-}), brackets denote concentrations, k is the overall rate constant, and a and b denote the reaction order with respect to sulfide and oxygen, respectively. The overall rate constant is a

function of temperature, pH, and ionic strength (Millero et al., 1987a). The reaction orders with respect to sulfide and oxygen are interpreted in terms of the stoichiometry of the rate determining step(s) in the reaction and are quantified experimentally.

Rate law parameters (*k*, a, and b) are often determined by monitoring sulfide concentrations with time during oxidation under controlled conditions, which has been done mostly using spectrophotometric and colorimetric techniques (Avrahami and Golding, 1968; Cline and Richards, 1969; Chen and Morris, 1972a,b; Luther et al., 2011; Millero et al., 1987a; O'Brien and Birkner, 1977; Zhang and Millero, 1993) or electromotive force (emf) techniques (Ostlund and Alexander, 1963; Almgren and Hagstrom, 1974). Experimental studies often yield inconsistent results when compared between laboratories (*cf.* reviews in Millero, 1986; Millero et al., 1987a; Zhang and Millero, 1993). We compile in Table 3.1 the kinetic parameters calculated from experiments performed under pH conditions where HS^- dominates the speciation. Millero et al. (1987a) provide evidence that the rates of oxidation are uniform (within reasonable experimental uncertainty) over pH ranges where a singular sulfide species (i.e., HS^- or H_2S) is present, thus, differences in rate law parameters above a pH of ~8 may not be expected to be major. Most studies have found the reaction to be first order with respect to sulfide (a = 1) and likely also first order with respect to oxygen (b = 1) (*cf.* Zhang and Millero, 1993), although some investigations yield non-integer values (e.g., Chen and Morris, 1972a,b). Computed second order rate constants derived from the experiments presented in Table 3.1 vary considerably. Millero et al. (1987a) demonstrated that the emf approach utilized by some workers (Ostlund and Alexander, 1963; Almgren and Hagstrom, 1974) yields

erroneously high rates that are artifacts of the detection method. For experiments performed under comparable conditions using comparably reliable chemical assays for sulfide, the disagreement persists in rate constants and in some cases reaction orders.

The reaction rate of aqueous sulfide oxidation is highly sensitive to the presence of trace metals in solution, where the apparent second order rate constant may vary as a result of trace metal catalysis by several orders of magnitude under otherwise equivalent solution conditions (Vazquez et al., 1989; Zhang and Millero, 1993). The results from recent experiments performed under trace metal clean conditions (Luther et al., 2011) indicate that varying amounts of unintended catalysis may have impacted most experimental studies of sulfide oxidation to date. To our knowledge, the experimental analysis of a full rate law for the catalyzed reaction constraining the role of catalysts on all kinetic parameters has yet to be performed in detail, and may be necessary for a coherent interpretation of the available experimental literature. The issue of contaminating trace catalysts may complicate the calibration of rates and isotope fractionations in the laboratory. These issues informed our experimental design and led to our emphasis on measuring reaction rates and comparing them to those of previous studies, and led to our study of the direct effect of an exemplary trace metal catalyst (ferrous iron) on rates and isotope fractionations.

Table 3.1: Conditions and rate law parameters from experimental studies of sulfide oxidation via molecular oxygen, where $-d[(H_2S)_T]/dt = k[(H_2S)_T]^a[O_2]^b$. The value of b has not been determined by most experimental studies and parentheses indicate the values assumed by the original authors. The column ln*k* represent the second order (a = 1, b = 1) rate constant either as reported in the reference or computed here (units: $M^{-1}hr^{-1}$). The half-time of sulfide disappearance ($t_{1/2}$) is computed for 25°C experiments assuming $[O_2]$ = 250 μM, and is reported in units of hours. Medium key: w = water (low ionic strength buffer solution), sw = seawater (with reported salinity, when available).

Reference	Medium	T (°C)	pH	a	b	ln*k*	$t_{1/2}$
Avrahami and Golding (1968)	w	25	12	1	n.d.	5.3	14
	w	25	14	1	n.d.	6.2	6
Chen and Morris (1972a)	w	25		1.34	0.56	N/A	N/A
O'Brien and Birkner (1977)	w	25	10	1	0.80 ±0.25 (1)	4.9	21
Millero et al. (1987a)	w	25	8.0	1	n.d. (1)	4.3 ± 0.6	44 ± 30
Zhang and Millero (1993)	w	25	8.2	1	1	3.75	65
Luther et al. (2011)	w	25	12	1	n.d. (1)	1.94 ± 0.05	397
This study	w	25	9.8	1	n.d. (1)	3.5 ± 0.2	86 ± 16
Ostlund and Alexander (1963)	sw	25	8.2	1	n.d.	9.4*	0.23*
Almgren and Hagstrom (1974)	sw	24	8	1	n.d.	7.4 ± 0.6*	2 ± 1*
Millero et al. (1987a)	sw (S=35)	25	8.0	1	n.d. (1)	5.2 ± 0.6	16 ± 9
Zhang and Millero (1993)	sw (S=35)	25	8.2	1	1	4.81 ± 0.02	23
Cline and Richards (1969)	sw	9.8	7.5-7.8	1	1	~6.9	N/A

*Demonstrably erroneous due to electromotive force sulfide detection method (Millero et al., 1987a).

2.0 Methods

2.1 Reaction vessel

The reaction vessel consists of all plastic and/or Teflon components: a polypropylene bottle (2 L, Nalgene) fitted with a 2-3 port Teflon-seal and gasket cap (Vaplock), Teflon magnetic stir bar, and 1/8“ OD PEEK tubing submerged in the reaction solution for aliquot time series sampling for concentration and isotopic analyses (Figure A.6). Aliquot sampling is performed via peristaltic pump. All components are acid-soaked (6 M HCl) for several weeks followed by a Milli-Q soak

of comparable duration, and subsequently rinsed several times with Milli-Q prior to loading of reaction solution. The use of plastics/Teflon and extensive acid cleaning is employed to minimize trace metal contamination that could affect the rates and observed isotopic fractionations (*cf.* Vazquez et al., 1989; Luther et al., 2011). An extensive set of preliminary kinetic experiments performed mostly in custom-made glass reaction vessels revealed poor reproducibility of rates that likely stemmed in part from varying levels of trace metal catalysis from the glassware. We also avoided submerging any probes (e.g., pH, DO) in the primary reaction solution during experimental runs to avoid any potential catalytic effects; pH measurements were made on aliquots removed from the reaction vessel. Roughly half the volume of the reaction vessel is air-headspace by design to enhance air-solution gas exchange. Temperature control is achieved by the submersion of reaction vessels in a circulated VWR temperature bath (Model 1186D; stable to 0.01˚C).

2.2 Reaction solution

Reaction solutions are comprised of 1 L Milli-Q buffered with $NaHCO_3/Na_2CO_3$ (0.002-0.02 M) to a pH of ~ 9.8. Buffer solutions were prepared using acid-cleaned volumetric flasks (Nalgene, polypropylene, 1 L) following the cleaning protocol for the reaction vessel (Section 2.1) and using reagent grade Na_2CO_3 and $NaHCO_3$ (Sigma Aldrich: ≥99.5% Na_2CO_3 and 99.7-100.3% $NaHCO_3$). Simple bicarbonate/carbonate buffers were chosen due to their relevance in buffering many natural systems. Under these conditions, the speciation of sulfide is overwhelmingly in the singly protonated anionic form of HS^- (~100% HS^-; Hershey et al., 1988). $H_2S_{(aq)}$ in solution was avoided to prevent sulfide loss via degassing,

which could confound the rate and isotope effect determination. Prior to sulfide injection, reaction solutions are allowed to thermally equilibrate in the temperature bath overnight. The following morning, reaction solutions are bubbled for one hour with ambient air immediately prior to sulfide injection in an attempt to guarantee reaction solutions are saturated with respect to O_2 (*cf.* Millero et al., 1987a).

Stock sulfide solutions were prepared from sodium sulfide nonahydrate crystals ($Na_2S•9H_2O$; J.T. Baker, 101.3%) stored at -20˚C and rinsed in N_2-purged Milli-Q and patted dry with Kimwipes prior to weighing. Fresh stocks of sodium sulfide were prepared for every experiment by dissolving rinsed and dried crystals in small concentrated batches (~5 ml, ~0.2 M) in acid cleaned polypropylene VWR centrifuge tubes under an anoxic N_2:H_2 atmosphere (95:5) within 30 min of injection into experimental solutions. Aliquots of these stock sulfide solutions (1 ml; ~0.2 M) were injected into experimental solutions using a graduated pipette (Neptune, natural polypropylene). Blanks of thiosulfate and sulfite in these stock solutions were typically below the detection limits at the level of dilution in reaction solutions as determined by HPLC (≤0.1 μM) following Zopfi et al. (2004). For the Fe^{2+}-catalyzed experiments, stock solutions of $FeSO_4$ (~50-150 μM; Sigma Aldrich, ferrous sulfate heptahydrate) freshly prepared under N_2:H_2 (95:5) atmosphere within 10 min of the beginning of experiments were added (1 ml aliquot) immediately following the injection of sulfide (note: these procedures lead to negligible sulfate blanks in the final reaction solution of < 0.15 μM). No observed precipitate was observed by eye upon the addition of ferrous iron to experimental sulfide solutions at these low levels.

2.3 Concentration analyses

Concentration analyses of aqueous sulfide were performed via the methylene blue spectrophotometric technique of Cline (1969) and were performed in either duplicate or triplicate for each sampling (reproducibility was typically ≤ 5%, 2 s.d.). Oxygen concentrations were estimated under experimental conditions as a function of temperature and ionic strength (Benson and Krause, 1980; Benson and Krause, 1984) as implemented in the USGS DOTABLES online software utility (http://water.usgs.gov/software/DOTABLES/).

2.4 Kinetics

The experiments are designed after a standard rate law for sulfide oxidation via molecular oxygen (Equation 1: *cf.* Millero et al., 1987a; Zhang and Millero, 1993). Following the majority of previous studies and taking the reaction order with respect to sulfide to be unity (Table 1), we took steps to keep O_2 constant for at least the early portions of the experiments such that the overall rate law can be simplified to a pseudo-first order rate law:

$$d[(H_2S)_T]/dt = k'[(H_2S)_T] \qquad (2)$$

Where $k' = k[O_2]^b$ and is referred to as the pseudo-first order reaction constant and can be determined from monitoring sulfide concentration with time via the time-integrated and linearized form of the pseudo-first order rate law:

$$\ln[(H_2S)_T]_t = \ln[(H_2S)_T]_{t=0} + k't \qquad (3)$$

Where t is time and the subscript t=0 denotes the initial concentration of sulfide. The value of k' can be determined via the least squares linear regression of sulfide concentration data following Equation 3. Measured k' can then be computed into the

overall rate constant *k* using knowledge of the oxygen concentration (and reaction order, b) in the experiment.

We did not determine the reaction order with respect to oxygen in our experiments and therefore rely on determinations from previous experiments to compute overall rate constants. In general, the value of b is not well constrained and poor agreement exists among the available experimental studies (Table 1): Chen and Morris (1972a, b) derive b = 0.56 ± 0.03, O'Brien and Birkner (1977) derive 0.80 ± 0.25 (interpreted by the original authors to be unity), and Zhang and Millero (1993) derive b =1 from experiments in seawater. In principle, the experimentally observed reaction orders in a complex mechanism may vary depending on solution conditions if the changes to conditions influence the relative pathways of the reaction that influence the rate determining step(s) of the reaction, but ultimately it is unclear where the variability in reaction orders may arise in the published experimental datasets. We note that variability in apparent rate parameters may accompany the presence of unintended trace catalysts (e.g., trace metals) and detailed experiments investigating the role of catalysts on reaction orders have yet to be performed. We adopt the reaction order with respect to oxygen from the experiments of Zhang and Millero (1993). The reaction is therefore taken to be second order overall (a + b = 1 + 1 = 2) and *k* will be computed and reported in units of $M^{-1}hr^{-1}$ in our study.

Most experiments were performed with an initial sulfide concentration of around $2.2x10^{-4}$ M (220 μM) and O_2 from air equilibrated with the reaction solution. The initial sulfide concentration was chosen as a near-optimal compromise between (1) having sufficient sulfide for isotopic measurement throughout experimental runs

(SF_6 GS-IRMS requires about 10-12 μmoles of sulfur for high precision $^{33}S/^{32}S$, $^{34}S/^{32}S$, and $^{36}S/^{32}S$ analysis) and (2) not being so high as to overwhelm the available oxygen supply and, therefore, interfere substantially with the kinetic analysis. Some difficulties arose in keeping O_2 constant throughout experimental runs because oxygen from air in equilibrium with our solutions had a concentration on par or only slightly in excess (~1.2-1.3x molar) of our sulfide concentrations at 25˚C and even lower (~ 0.8x) for experiments performed at 45˚C. However, reliable rate information can be obtained from concentration data prior to obvious oxygen limitation.

2.5 Isotopic analyses: SF_6 GS-IRMS

Aliquots of experimental solution were extracted throughout experimental runs (totally 5-6 samplings) in total volumes corresponding to ~10-12μmoles of sulfide (typically, 60-110 ml of experimental solution) and immediately fixed in an equivalent volume of 200 g/L zinc acetate trapping solution as ZnS and frozen for later processing. The initial processing of sequestered ZnS involves thawing and immediate filtration (0.2 μm, Whatman or Millipore). The filters containing ZnS precipitate are then immediately added to 100 ml round bottom flasks with syringe side arms for routine acid volatile sulfide (AVS) extraction that allows quantitative re-precipitation of sulfide as Ag_2S. Briefly, this involves injection of 20 ml of 5 N HCl into the round bottom flask containing the filter + precipitate under flow of N_2 through a condenser, water trap, and capture solution (0.02 M $AgNO_3$, 0.2 M HNO_3) that quantitatively sequesters the acid-liberated sulfide as Ag_2S. Samples of Ag_2S were then allowed to settle overnight, after which time they were rinsed in a sequence

of Milli-Q, 1 M NH_4OH, and Milli-Q (3x each, with centrifugation and vortex mixing) and dried for later fluorinations. Multiple blanks were run on acidified filters following the protocol above and no detectable Ag_2S was obtained, indicating that the filter (and reagents) contribute no significant AVS.

Silver sulfide samples were weighed in small aluminum foil envelopes, added to nickel reaction tubes, and reacted in the presence of 100-fold molar excess F_2 gas at ~250˚C overnight (12+ hours) to quantitatively convert to SF_6 gas. The SF_6 gas is cryogenically separated from HF and other non-sulfur condensable fluorination byproducts by utilizing a chilled ethanol slurry (-115˚C) before further purification via Gas Chromatography. The yields of this fluorination, extraction, and SF_6 purification were 100% (± 5%) for all experimental samples reported herein. The SF_6 gas is analyzed for isotope ratios as ion current beams of $^{32}SF_5^+$, $^{33}SF_5^+$, $^{34}SF_5^+$, and $^{36}SF_5^+$ at 127, 128, 129, and 131 mass numbers, respectively, on a ThermoFinnigan MAT 253 at the University of Maryland, College Park.

Since these experiments involve the evaluation of the small isotope effects and the mass dependence of sulfide oxidation utilizing samples that are minimally fractionated from one another (i.e., 5-6 samples per experiment spanning a $^{34}S/^{32}S$ range typically of ≤ 3-4 ‰), a rigorous protocol of cleaning of the fluorination line was enacted for many experiments to avoid any contamination from any residual Ag_2S from previous user's fluorinations. Prior to any loading of Ag_2S samples from sulfide oxidation experiments, the nickel bombs were emptied of all previous residual aluminum foil packets, reattached and baked for 12-24 hours under vacuum (to remove most of the trace adsorbed H_2O) and then blank fluorinated overnight 2-3

times. This protocol was sufficient to ensure clean, high quality fluorinations for high precision analyses.

2.6 Isotope effect determination

The isotope effect of sulfide oxidation was determined by measuring the isotopic composition of the residual reactant sulfide as a function of reaction progress in a closed system following the Rayleigh equation:

$$\ln({}^{n}R_{R,}/{}^{n}R_{R\_0}) = ({}^{n}\alpha_{P\text{-}R} - 1)\ln f_R \qquad (4)$$

Where ${}^{n}R$ refers to the isotopic ratio (n=33, 34, or 36), subscript *R* refers to residual reactant (0 refers to initial), $\alpha_{P\text{-}R}$ is the fractionation factor (in terms of products, *P*, relative to reactants, *R*), f_R is the fraction of reactant remaining (i.e., $[(H_2S)_T]/[(H_2S)_T]_0$), and the trace abundance approximation has been applied (i.e., $f_R = ({}^{32}S_R + {}^{33}S_R + {}^{34}S_R + {}^{36}S_R)/({}^{32}S_{R\_0} + {}^{33}S_{R\_0} + {}^{34}S_{R\_0} + {}^{36}S_{R\_0}) \approx {}^{32}S_R/{}^{32}S_{R\_0}$; Mariotti et al., 1981). This approach has been derived and reviewed in detail elsewhere (e.g., Bigeleisen and Wolfsberg, 1958; Mariotti et al.,1981; Scott et al., 2004) and implemented in previous sulfide oxidation experiments in Fry et al. (1988). For the extraction of a primary kinetic isotope effect, this approach assumes that sulfide does not undergo any other isotope exchange reactions throughout experimental runs other than its unidirectional reaction to products. Isotope effects determined this way can be influenced by other isotope exchange reactions involving sulfide that may occur as part of, or result of, the reaction mechanism.

2.7 Mass dependence of sulfide oxidation

Mass dependent relationships among fractionation factors involving three isotopes are defined as exponential relationships (*cf.* Craig, 1957; Matsuhisa et al., 1978; Clayton and Mayeda, 1996; Miller, 2002), such as:

$$^{33}\alpha_{P\text{-}R} = (^{34}\alpha_{P\text{-}R})^{33/34\lambda} \qquad (5)$$

$$^{36}\alpha_{P\text{-}R} = (^{34}\alpha_{P\text{-}R})^{36/34\lambda} \qquad (6)$$

Where the $^{33/34}\lambda$ and $^{36/34}\lambda$ values are the exponents relating mass dependence. The exponential definitions of the $\Delta^{33}S_{P\text{-}R}$ and $\Delta^{36}S_{P\text{-}R}$ values follow directly from these relationships as deviations from a reference exponent:

$$\Delta^{33}S_{P\text{-}R} = {}^{33}\alpha_{P\text{-}R} - (^{34}\alpha_{P\text{-}R})^{0.515} \qquad (7)$$

$$\Delta^{36}S_{P\text{-}R} = {}^{36}\alpha_{P\text{-}R} - (^{34}\alpha_{P\text{-}R})^{1.9} \qquad (8)$$

The values of 0.515 and 1.9 are the chosen reference exponents that approximate the mass-dependence of most common equilibrium isotope exchange reactions at low temperature (i.e., well below the high temperature limit). Exponents associated with sulfide oxidation in this study are computed from experimentally determined fractionation factors via the equivalent relations:

$$^{33/34}\lambda = \ln(^{33}\alpha_{P\text{-}R})/\ln(^{34}\alpha_{P\text{-}R}) \qquad (9)$$

$$^{36/34}\lambda = \ln(^{36}\alpha_{P\text{-}R})/\ln(^{34}\alpha_{P\text{-}R}) \qquad (10)$$

The uncertainty of the experimentally derived exponents can be straightforwardly estimated solely from the isotopic data collected throughout an experiment via the least squares linear regression of $\ln(^{n}R_{R,t}/^{n}R_{R,t=0})$ vs. $\ln(^{34}R_{R,t}/^{34}R_{R,t=0})$ (where n = 33 or 36) that computes the mass-dependence of a Rayleigh process as $(^{n}\alpha_{P\text{-}R} - 1)/(^{34}\alpha_{P\text{-}R} - 1)$, where n = 33 or 36, i.e.:

$$\ln({}^{n}R_{R,t}/{}^{n}R_{R,t=0}) = [({}^{n}\alpha_{P\text{-}R} - 1)/({}^{34}\alpha_{P\text{-}R} - 1)]\ln({}^{34}R_{R,t}/{}^{34}R_{R,t=0}) \quad (11)$$

We make the assumption that the uncertainty estimate for the value of $({}^{n}\alpha_{P\text{-}R} - 1)/({}^{34}\alpha_{P\text{-}R} - 1)$ from the least squares linear regression is comparable to the uncertainty on the exponent that applies to the primary reaction ($^{n/34}\lambda$).

3.0 Results

3.1 Concentration profiles at 25˚C

Plotted in Figure 3.1 are representative sulfide concentration profiles of experiments performed at 25˚C as a function of time in terms of fraction of sulfide remaining (f = $[HS^-]/[HS^-]_{initial}$, brackets denoting concentrations) for experiments with and without an added ferrous iron catalyst. The data points are the measured concentrations and the smooth curves are modeled based on a pseudo first order rate law using the pseudo first order rate constant derived from the sulfide concentrations (Section 3.2; Table 3.2). Each experiment appears to exhibit an induction period where sulfide concentrations do not change appreciably (within the uncertainty of the measurements) that ranges between ~8-13 hours for the experiments where no ferrous iron was added to a few hours for experiments where ferrous iron was added (Table 3.2). A pronounced induction period of 36-48 hours was also observed in the experiments where no ferrous iron was added performed at 5˚C (Table 3.2). The precision of the duration of the induction period is limited by the chosen sampling interval. For the extraction of the pseudo first order rate constants, concentrations during the induction period are not taken into consideration and in most cases the average of sulfide concentrations during the induction period is taken to be the initial concentration as reported in Table 3.2. The two sets of explicitly catalyzed

experiments where ferrous iron was added exhibit a distinct break in rate near the 30 hour mark. For these experiments, two individual pseudo first order rate constants were extracted from the experimental data: one prior to the break in rate (denoted "catalyzed"), and one following the break in rate (denoted "uncatalyzed) (Table 3.2).

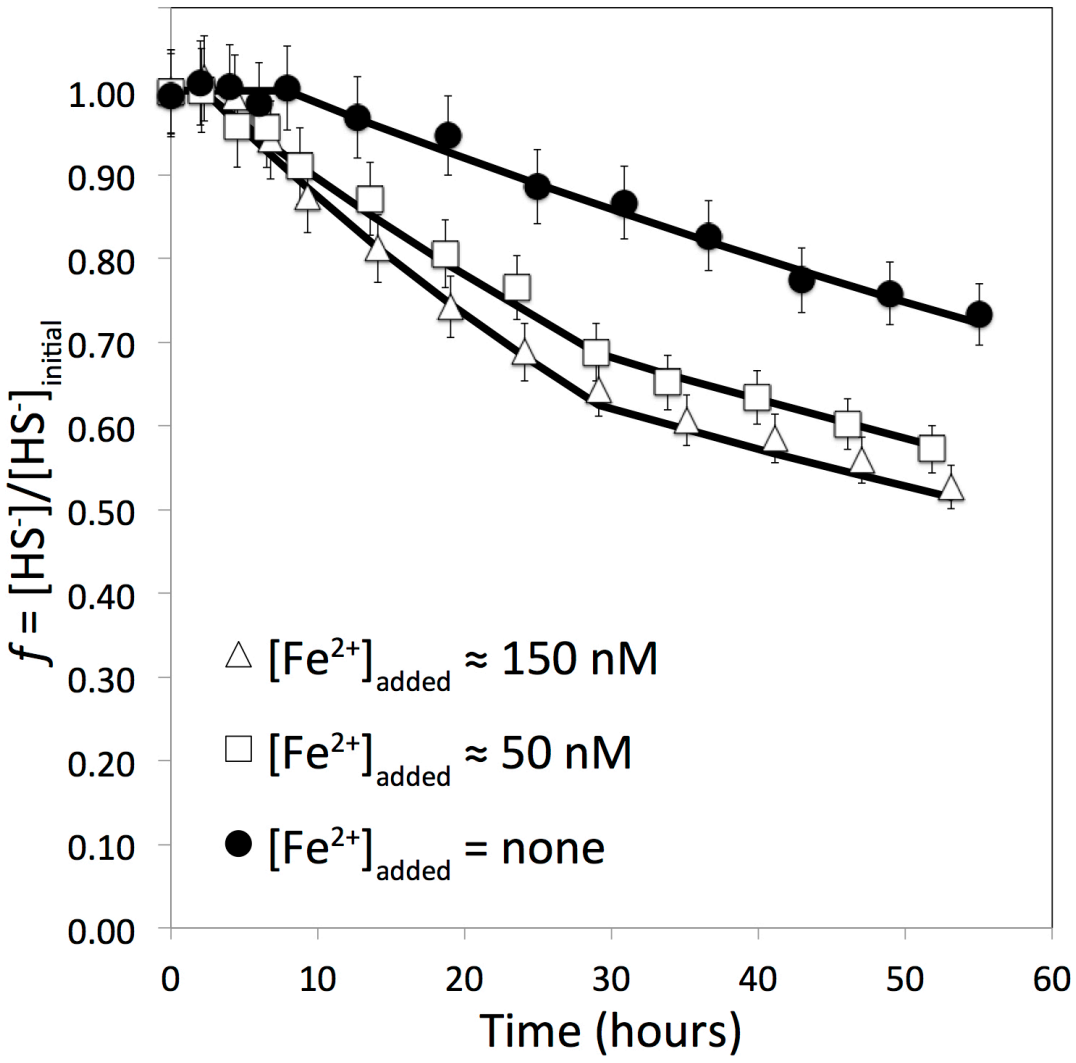

Figure 3.1: Representative concentration profiles plotted in terms of fraction of sulfide remaining for oxidation experiments performed at 25˚C (monitored continuously for ~50-55 hours), with and without an added ferrous iron catalyst. Uncertainties for individual concentration analyses were typically ≤ 5 % based on either duplicate or triplicate analyses (2 s.d.) (a uniform 5% uncertainty is plotted).

3.2 Rate constants

The computed second order rate constants derived from our experiments (Table 3.2) are plotted in Figure 3.2 as a function of inverse temperature in a classic Arrhenius plot. Rate constants from the comparable experiments of Millero et al. (1987a) and Luther et al. (2011) are shown for reference and discussion (Section 4.2). The least squares linear regression of the second order rate constants (experiments without added ferrous iron catalyst) yields an apparent activation energy of E_a = 60 ± 3 kJ/mol. The second order rate constants from the explicitly catalyzed ferrous iron experiments (denoted "catalyzed" in Table 3.2) are a factor of ~1.5-2 times higher than those where no ferrous iron was added. The second order rate constants from ferrous iron catalyzed experiments following the pronounced break in rate (denoted "uncatalyzed" in Table 3.2; not plotted) are indistinguishable from those extracted from experiments without added ferrous iron. Our calculated second order rate constants might be viewed as minimum values due to the assumption that our experimental solutions were in equilibrium with ambient air at the experimental temperatures.

3.3 Fractionation factors

Table 3.3 summarizes the isotopic composition of sulfide (relative to the initial composition of sulfide in a given experiment) as a function of sulfide remaining in our oxidation experiments ($f_{sulfide}$ = $[HS^-]/[HS^-]_{initial}$). For all experiments, the isotopic composition of sulfide increases in magnitude as a function of reaction progress—indicating a normal isotope effect where products are isotopically depleted relative to reactants—and changes by only ~2.4 – 3.7 ‰ based

on $^{34}S/^{32}S$ over the entirety of experimental runs for all experiments, which span a range of reaction completion (1-$f_{sulfide}$) of ca. 33-47%.

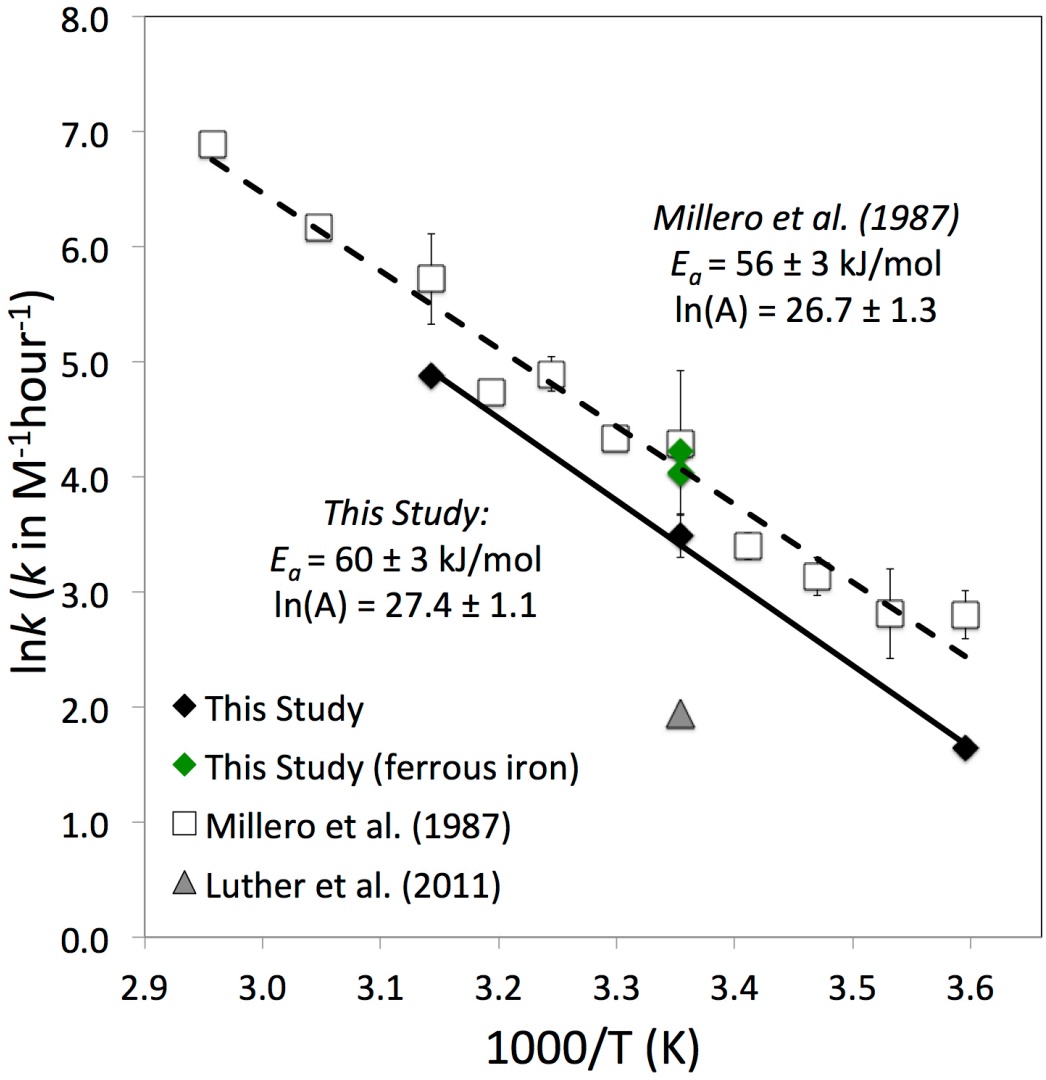

Figure 3.2: Overall second order rate constants derived from our experimental data plotted as a function of inverse temperature in a classic Arrhenius plot. The apparent activation energy (E_a) is derived from the slope of the relationship and is based on a least squares linear regression. Our experiments with ferrous iron added are shown for reference. Also plotted for reference are data from Millero et al. (1987a) and Luther et al. (2011) (discussion: Section 4.2).

Figure 3.3 is a representative plot illustrating how fractionation factors are extracted by the least squares linear regressions for all three sulfur isotope ratios as a function of reaction progress via the Rayleigh equation (Equation 4). Table 3.3

contains a summary of fractionation factors derived this way from all experiments. Major isotope fractionation factors derived from the isotopic data are plotted in Figure 3.4 and appear to exhibit slight but systematic relationships between fractionation magnitude and rate as a function of both temperature (Figure 3.4a) and explicit ferrous iron catalysis (Figure 3.4b). These variations are relatively small and very near the precision/reproducibility of the experiments. Fractionation factors appear to generally decrease in magnitude with increasing rate due to ferrous iron catalysis, and appear to generally increase in magnitude with increasing rate due to increasing temperature.

The exponents of mass dependence ($^{33/34}\lambda$ and $^{36/34}\lambda$; Table 3.3) extracted from the experimental data are plotted in Figure 3.5 as a function of temperature (Figure 3.5a-b) and ferrous iron catalysis (Figure 3.5c-d). The exponents associated with equilibrium isotope exchange among aqueous sulfur compounds (Eldridge et al., in review; Chapter 2) are also plotted for reference. The $^{33/34}\lambda$ appear to be resolvably lower in magnitude than exponents expected from equilibrium isotope exchange. Any relationships between $^{33/34}\lambda$ and rate as functions of both ferrous iron catalysis and temperature do not appear to be resolvable. The $^{36/34}\lambda$ may also exhibit deviations from equilibrium isotope exchange exponents but are not as well resolved by the experimental data and, similarly, do not appear to exhibit any resolvable relationships with reaction rate due to explicit catalysis or temperature.

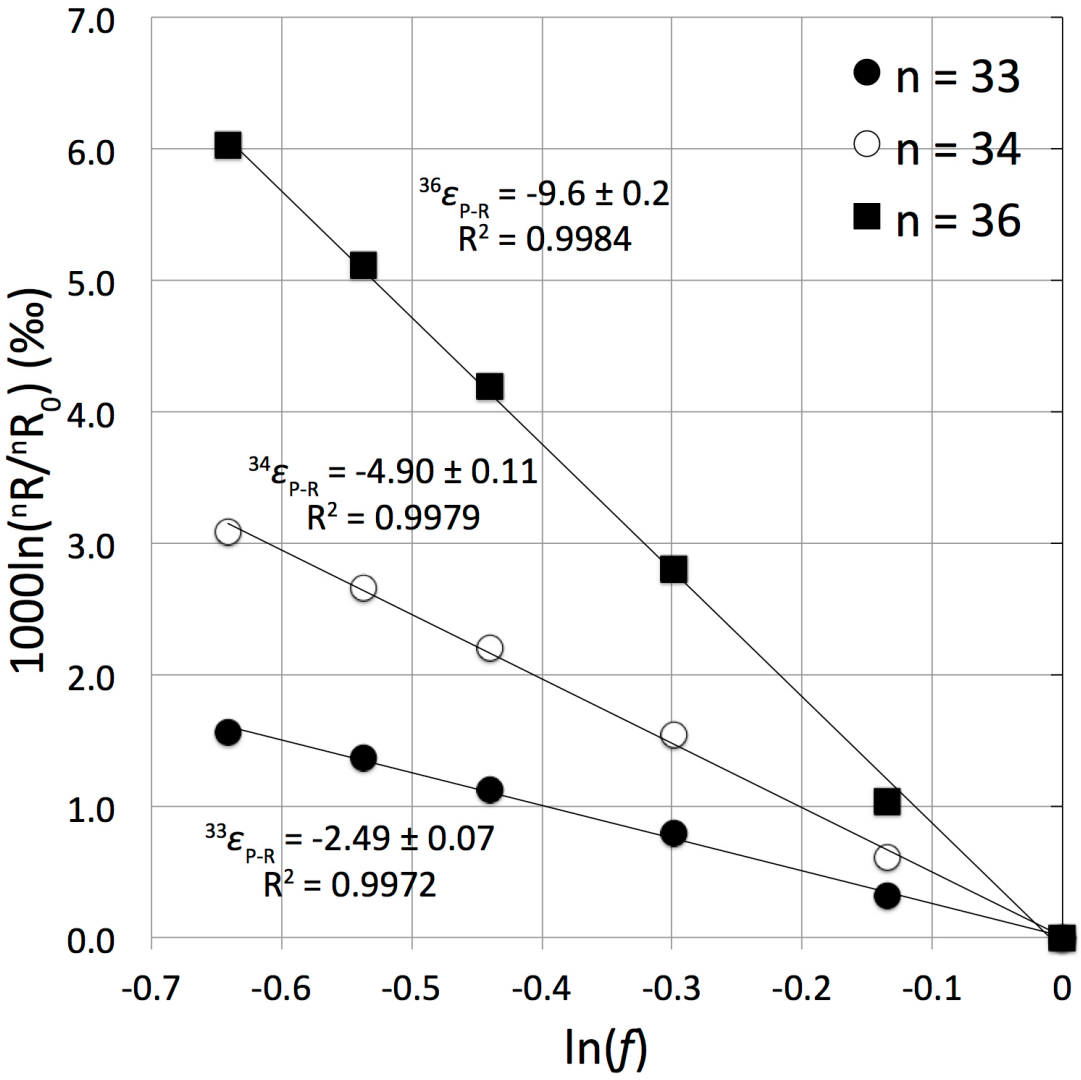

Figure 3.3: Example plot illustrating how fractionation factors (${}^{n}\varepsilon_{P\text{-}R} = ({}^{n}\alpha_{P\text{-}R} - 1)\text{x}1000$, P = products, R = reactant) are derived from experimental data via the Rayleigh equation (Equation 4) in this study. Data are from the ferrous iron catalyzed ($[Fe^{2+}]_{added} \approx 146$ nM) experiment at 25˚C denoted "SOX-Fe150" (see Table 3.3). ${}^{n}R = {}^{n}S/{}^{32}S$ (n = 33, 34, 36) and refer to the isotopic composition of residual sulfide relative to its initial composition (${}^{n}R_0$). Uncertainties on fractionation factors are 1 s.d. and are based on the least squares linear regressions.

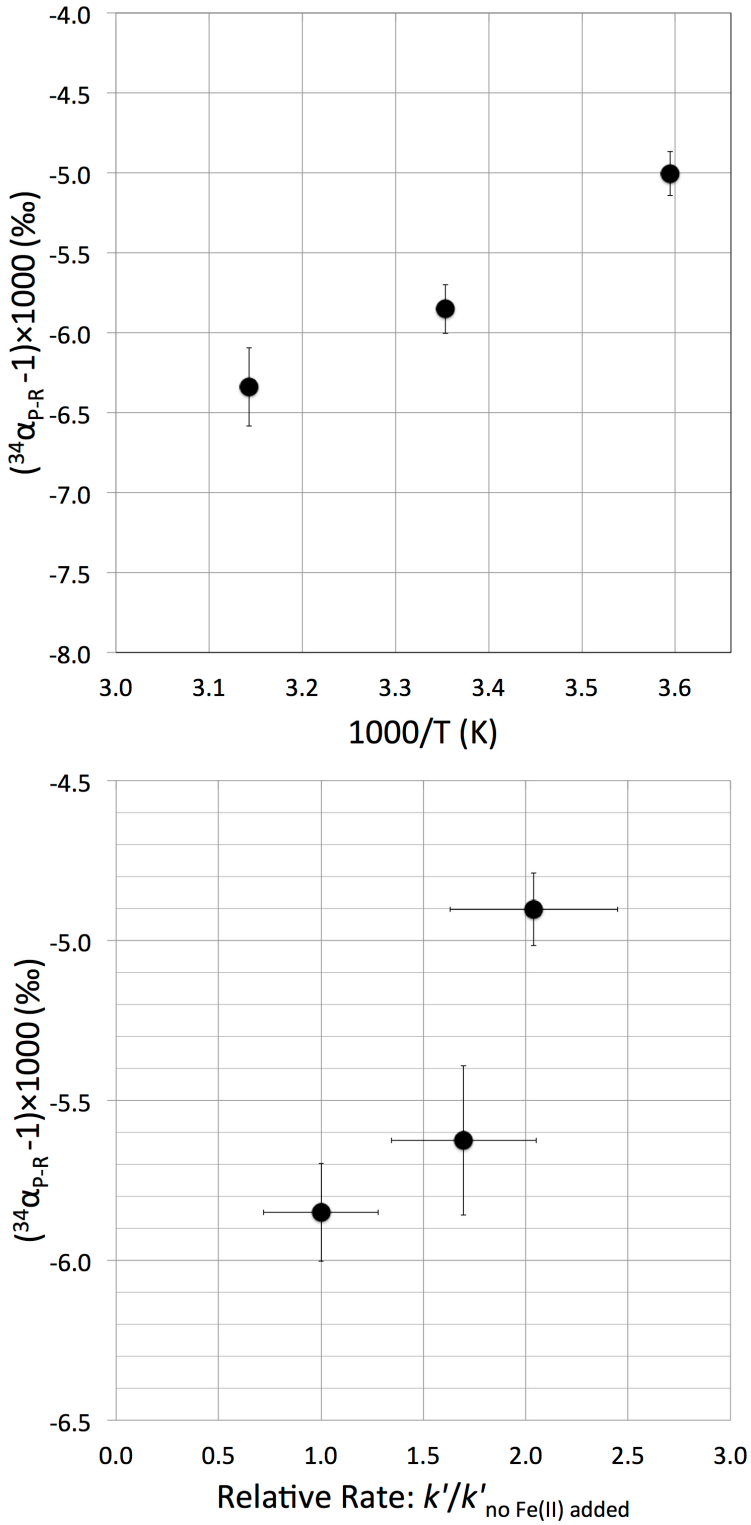

Figure 3.4: Major isotope fractionation factors plotted as a function of inverse temperature (a; top) and ferrous iron catalysis (b; bottom), where the latter are plotted as a function of relative rate and correspond to the ratio of the pseudo first order rate constants (*k'*) derived from "catalyzed" portions of each experiment to the pseudo first order rate constants from experiments at 25˚C where no ferrous iron was added (see Table 3.2).

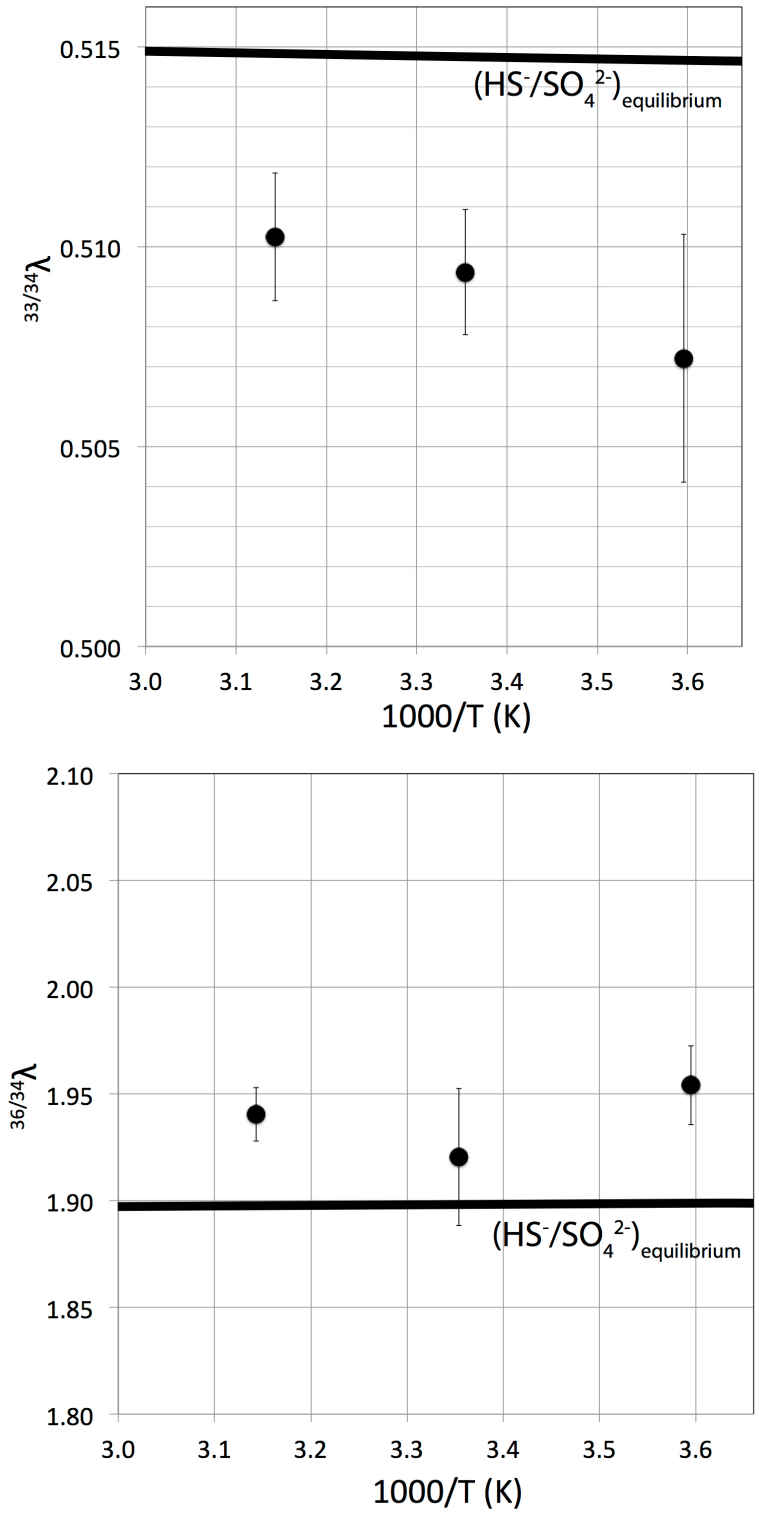

Figure 3.5 (a-b): Exponents of mass dependence derived from experimental data as a function of inverse temperature: (a; top) $^{33/34}\lambda$ and (b; bottom) $^{36/34}\lambda$. The exponents for the equilibrium isotope exchange between HS^- and SO_4^{2-} from Eldridge et al. (in review) (Chapter 2) are shown for reference.

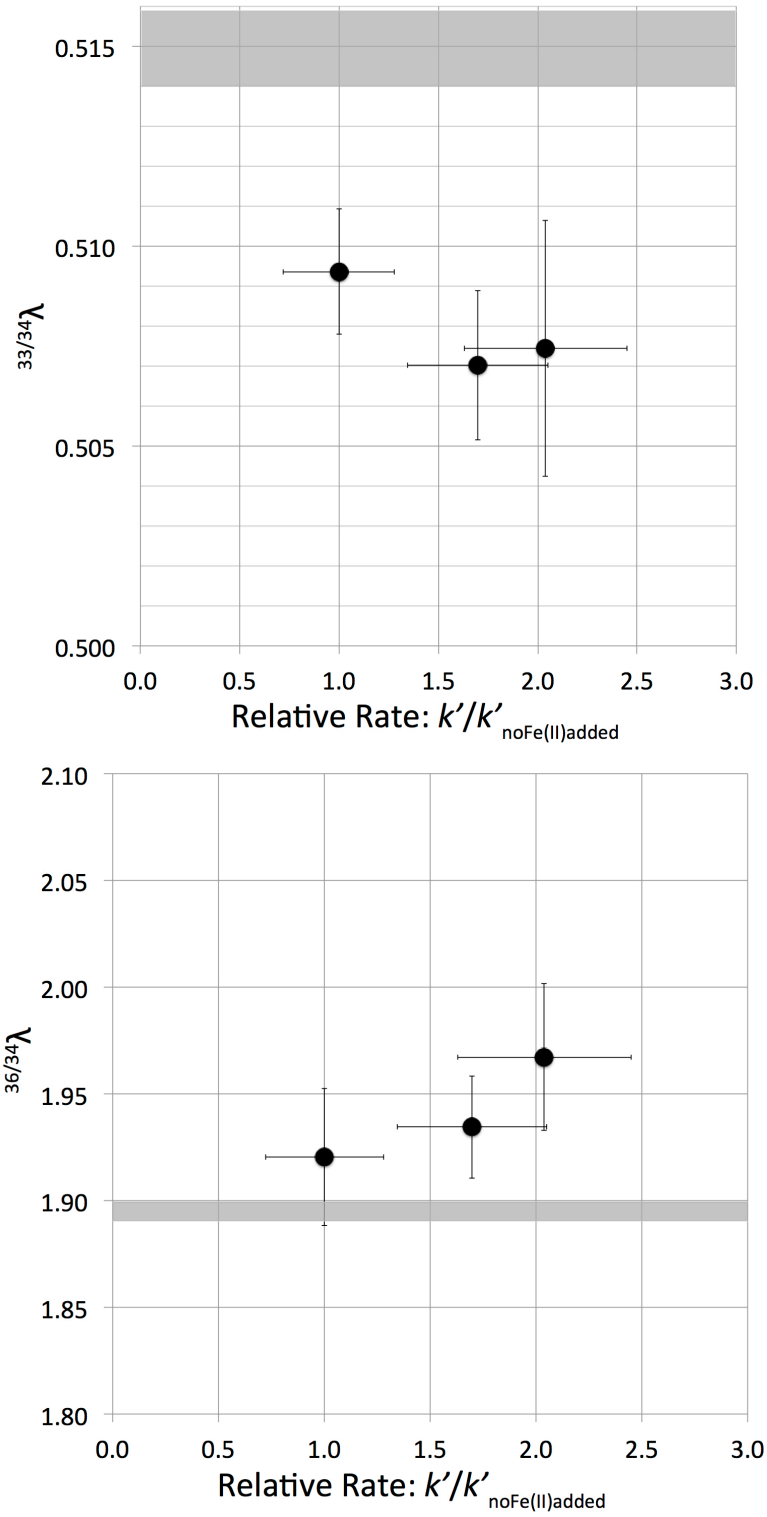

Figure 3.5 (c-d): Exponents of mass dependence derived from experimental data as a function of ferrous iron catalysis at 25˚C: (c; top) $^{33/34}\lambda$ and (d; bottom) $^{36/34}\lambda$. The gray fields are the estimated ranges for equilibrium isotope exchange among a wide variety of aqueous sulfur compounds ($T \geq 0$˚C) and are based on the recent calculations of Eldridge et al. (in review) (Chapter 2).

4.0 Discussion

4.1 Overview of sulfide oxidation mechanisms

Two mechanisms have been proposed for the autoxidation of aqueous sulfide (*cf.* Zhang and Millero, 1993): the polar mechanism (Hoffman and Lim, 1979) and the free radical chain mechanism (e.g., Chen and Morris, 1972a; Zhang and Millero, 1993). Schematic representations of the two mechanisms are presented in Figure 3.6 (after Zhang and Millero, 1993). Neither of these mechanisms has been satisfactorily ruled-out and the process of autoxidation could draw on aspects of each.

The free-radical mechanism for sulfide oxidation (Figure 3.6a) includes many free radicals in a complex chain network that accounts for many of the major products observed in sulfide oxidation experiments (Chen and Morris, 1972a; Zhang and Millero, 1993). The free-radical mechanism initiates via the reaction of sulfide and molecular oxygen to produce the sulfanyl radical ($HS^{\bullet}$) and superoxide (O_2^-). The sulfanyl radical may then oxidize to form S^0 or step-wise via sulfoxy-radicals to ultimately to form sulfite. Sulfite may further oxidize to sulfate via a complex free radical chain mechanism of its own (*cf.* Connick et al., 1995; Connick and Zhang, 1996), and S^0 may react with residual sulfide to produce polysulfides (*cf.* Chen and Morris, 1972a). Further reactions of the sulfanyl radical with intermediate product sulfite may lead to disulfur sulfoxy-radicals that eventually autoxidize to form thiosulfate. We are not aware of any experiments that have directly detected the hypothesized free radicals and so such a mechanism may be much more complex than postulated (*cf.* the complex free radical chain mechanism of bisulfite oxidation; Connick et al., 1995; Connick and Zhang, 1996).

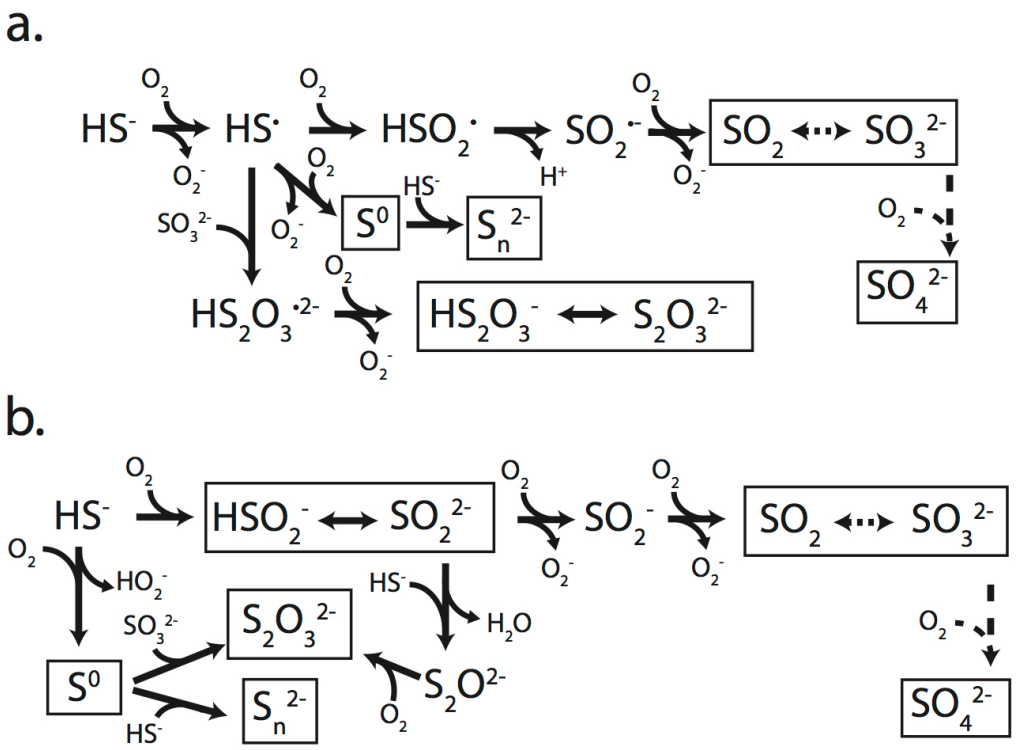

Figure 3.6: Schematic representations of the two major mechanisms that have been proposed for sulfide oxidation via molecular oxygen (drawn after Zhang and Millero, 1993). (a) The free radical mechanism (Chen and Morris, 1972a), and (b) the polar mechanism (Hoffman and Lim, 1979; Zhang and Millero, 1993). The boxes indicate intermediate or product compounds that have been detected in sulfide oxidation experiments: sulfite (SO_3^{2-}), thiosulfate ($S_2O_3^{2-}$), and sulfate (SO_4^{2-}) are commonly observed (e.g., Zhang and Millero, 1993); polysulfides (S_n^{2-}) were detected in the circum-neutral pH experiments of Chen and Morris (1972a); and sulfoxylate (SO_2^{2-}) was detected via XANES spectroscopy by Vairavamurthy and Zhou (1995). Mechanisms for the subsequent oxidation of most intermediates are omitted for simplicity. The dashed arrow representing the oxidation of sulfite to sulfate via O_2 represents an overall reaction (non-stoichiometric) that proceeds through a highly complex free radical chain mechanism of its own (Connick et al., 1995; Connick and Zhang, 1996). The oxygen species O_2^- (superoxide) and HO_2^-/O_2^{2-} (peroxide) generated by numerous reactions in each mechanism are referred to as reactive oxygen species (ROS) throughout the text and may also serve as oxidants for sulfur compounds.

The polar mechanism also accounts for the major products observed in sulfide oxidation experiments (e.g., polysulfides, elemental sulfur, sulfoxylate, sulfite, thiosulfate, sulfate; *cf.* Cline and Richards, 1969; Chen and Morris, 1972a; Zhang and Millero, 1993; Vairavamurthy and Zhou, 1995) without invoking many of the free-radical sulfur compounds called for by the radical mechanism (Figure 3.6b).

Reactions of sulfide with molecular oxygen are postulated to be among the initial steps, generating either a zero-valent sulfur atom (S^0) or sulfoxylate compounds (SO_2^{2-} and pH-dependent protonated varieties); the former is postulated to yield reactive oxygen species (ROS), such as peroxide (O_2^{2-}), that react with sulfide more rapidly than dissolved molecular oxygen. Sulfide can react with first formed zero-valent sulfur atoms (S^0) or sulfoxylate compounds to yield the polysulfides and thiosulfate, respectively. The oxidation of sulfoxylate compounds ultimately may yield sulfite compounds, generating further ROS. The subsequent oxidation of sulfite to sulfate (potentially via a highly complex free radical chain mechanism; *cf.* Connick et al., 1995; Connick and Zhang, 1996) may be the major pathway of sulfate formation in most sulfide oxidation experiments (*cf.* Chen and Morris, 1972a; Zhang and Millero, 1993). In all cases, the ROS produced as part of this reaction scheme can also react with sulfide or other sulfur intermediates.

The hypothesized effect of trace Fe^{2+} as a catalyst in sulfide oxidation in the presence of molecular oxygen begins with its own oxidation by O_2 (Vazquez et al., 1989; Zhang and Millero, 1993), generating ferric iron and superoxide (*cf.* Millero et al., 1987b) (note: pH-dependent speciation/complexation/hydrolysis omitted in many of the following reactions for simplicity):

$$Fe^{2+} + O_2 \rightarrow Fe^{3+} + O_2^{-}. \qquad (12)$$

Reactions of this kind are thermodynamically favorable at high pH for singlet or triplet O_2 (Luther, 2010) and proceed rapidly at high pH (Millero et al., 1987b). The produced superoxide can further react with ferrous iron to produce peroxide, which is also thermodynamically favorable at high pH (Luther, 2010):

$$Fe^{2+} + O_2^- \rightarrow Fe^{3+} + O_2^{2-}. \qquad (13)$$

Ferrous iron can be regenerated via the reaction of ferric iron with sulfide to form the sulfanyl radical (Vazquez et al., 1989; Zhang and Millero, 1993), e.g.:

$$HS^- + Fe^{3+} \rightarrow HS^{\bullet} + Fe^{2+}. \qquad (14)$$

In this conceptual model, the Fe facilitates the transfer of electrons from sulfide to O_2, generating the highly reactive sulfanyl radical that can readily oxidize to S^0 (Luther, 2010) and/or other sulfur intermediates by O_2 or ROS in solution. The ROS (e.g., O_2^- and O_2^{2-}) produced by the oxidation of ferrous iron may also serve as oxidants for sulfide. The more precise mechanism of the reaction of sulfide with ferric iron is more complex than represented here (*cf.* Yao and Millero, 1996) and may involve ion-pair formation between iron and sulfide and surface-dependent processes if the ferric iron forms particulates or nano-particulates in solution.

In our study, we quantified the rate constants and isotope effects associated with sulfide oxidation by tracking the concentration and isotopic composition of sulfide as a function of time. Several reactions involving sulfide could hypothetically take place during oxidation when molecular oxygen (O_2) is the ultimate oxidant due to the potential for ROS to form as part of the mechanism (with or without trace metal catalysts), each with their own unique reaction coordinates, transition states, rate constants (k), activation energies (E_a), and primary kinetic isotope effects (e.g., ${}^{34}k/{}^{32}k$), e.g.:

$HS^- + O_2 \rightarrow$ Products $\qquad k_{\text{oxygen}}, E_{a\_\text{oxygen}}, {}^{34}k/{}^{32}k_{\text{oxygen}} \qquad (15)$

$HS^- + O_2^- \rightarrow$ Products $\qquad k_{\text{superoxide}}, E_{a\_\text{superoxide}}, {}^{34}k/{}^{32}k_{\text{superoxide}} \qquad (16)$

$HS^- + O_2^{2-} \rightarrow$ Products $\qquad k_{\text{peroxide}}, E_{a\_\text{peroxide}}, {}^{34}k/{}^{32}k_{\text{peroxide}} \qquad (17)$

$HS^- + M^{n+} \rightarrow$ Products $\quad k_{trace\_metal}, E_{a\_trace\_metal}, {}^{34}k/{}^{32}k_{trace\_metal}$ (18)

$HS^- + S_{int} \rightarrow$ Products (e.g., $S_2O_3^{2-}$) $\quad k_{S\text{-}int}, E_{a\_S\text{-}int}, {}^{34}k/{}^{32}k_{S\text{-}int}$ (19)

$HS^- + Fe^{3+} \rightarrow$ Products $\quad k_{ferric\_iron}, E_{a\_ferric\_iron}, {}^{34}k/{}^{32}k_{ferric\_iron}$ (20)

The latter potentially being relevant in our Fe^{2+} explicitly catalyzed experiments. This listing is not exhaustive and other reactions involving sulfide may be possible. The rates and isotope fractionations that we have measured may be expressions of varying contributions of the reactions above, and these sets of reactions will be used as framework for interpreting our experimental results.

4.2 Rate constants and Arrhenius parameters: Comparison to previous experiments

Select second order rate constants derived from previous experiments performed in low ionic strength buffer solutions (Avrahami and Golding, 1968; O'Brien and Birkner, 1977; Millero et al., 1987a; Zhang and Millero, 1993; Luther et al., 2011) are plotted in Figure 3.7a as a function of pH along with our own for comparison. We focus primarily on experiments performed at high pH where HS^- dominates the speciation (the pK_a for $H_2S = HS^- + H^+$ at 25˚C is additionally plotted for $\mu = 0$ and 0.1 *m* from Hershey et al., 1988). From experiments performed at 55˚C, Millero et al. (1987a) found that the rates of sulfide oxidation as a function of pH largely reflect the speciation of sulfide, where the second order rate constant appears to have a near constant value under pH conditions where either HS^- or H_2S individually dominate the speciation (where $k_{H2S} < k_{HS\text{-}}$), and intermediary values under circumneutral pH conditions where both are present in appreciable amounts. Similar experiments of Zhang and Millero (1993) performed at 45˚C in similarly low ionic strength solutions show similar relationships with pH. For illustrative context,

we plot the experiments of Millero et al. (1987a) as a function of pH originally performed at 55˚C corrected for temperature using their 25˚C determinations and roughly corrected for any pH shifts that may occur due to temperature using the dissociation quotients of Hershey et al. (1988). We performed a similar exercise using the data of Zhang and Millero (1993) as a function of pH for a handful of experiments performed in low ionic strength solutions at 45˚C (solution conditions: 0.02 M carbonate/bicarbonate buffers). Our temperature corrections are based on the respective Millero group experiments performed at high pH and therefore largely reflect the activation energy of HS^- oxidation (vs. that of H_2S oxidation). Experiments performed at low pH are omitted from this exercise due to the introduction of spurious errors into any similarly T-corrected low pH rate constants that would require specific knowledge of the activation energy for H_2S oxidation.

Taken altogether, the experimental determinations in Figure 3.7a (including our own) define a range in the second order rate constant that spans well over an order of magnitude under pH conditions above 8, far outside the range of what might be expected from the broad observations of pH dependence from the Frank Millero group studies (Millero et al., 1987a; Zhang and Millero, 1993). The experiments of Avrahami and Golding (1968) yield among the highest rate constants and increase with increasing pH in the pH = 12-14 region. The rate constants at pH ~ 8 derived from Zhang and Millero (1993) at 25˚C are on the low end of the determinations of Millero et al. (1987a) and taken together span a range on the order of a factor of three. The experiments of O'Brien and Birkner (1977) are near the upper end of the Millero

group range. Our own experiments are on the lower end of the Millero group range and are perhaps most consistent with Zhang and Millero (1993).

A direct comparison to the experimental dataset of Chen and Morris (1972a) is more difficult due to the different rate law parameters derived from their experimental data than most other studies (they obtained a = 1.34 and b = 0.56 with a rate constant in units of $M^{-0.9}hr^{-1}$; Table 3.1). Chen and Morris (1972a) also observed complex patterns in the rate of oxidation at 25˚C as a function of pH (6 – 12.5) where maximum rates were found at a pH of ~8 and ~11 with a local minimum at a pH of ~9 (difference between max/min is on the order of ~3.3x), which are trends not reproduced by Millero et al. (1987a) at 55˚C. To make rough comparisons to our experiments, we will focus on experiments from Chen and Morris (1972a) performed under the most comparable conditions to our own: $[H_2S_T]_{initial}$ = 200 μM under relatively low initial $[O_2]_{initial}$:$[H_2S_T]_{initial}$ ratios (i.e., $[O_2]_{initial}$ = 160-480μM) over pH = 8.34-11.75. We use their reported data to re-derive the initial rates of sulfide oxidation determined from their experiments and then assume a = 1 and b = 1 and the given initial sulfide and oxygen concentrations to compute a hypothetical second order rate constant to put on more comparative grounds to our own. These are plotted in Figure 3.7b as a function of the $[O_2]_{initial}$:$[H_2S_T]_{initial}$ ratio of the experiment (along with other experiments performed under comparable $[O_2]_{initial}$:$[H_2S_T]_{initial}$; Avrahami and Golding, 1968; Luther et al., 2011). Computed this way, our rates are similar to the Chen and Morris (1972a) experiments, where the second order rate constants computed from our repeat experiments span a similar range as those computed from Chen and Morris (1972a) as a function of pH under otherwise similar conditions.

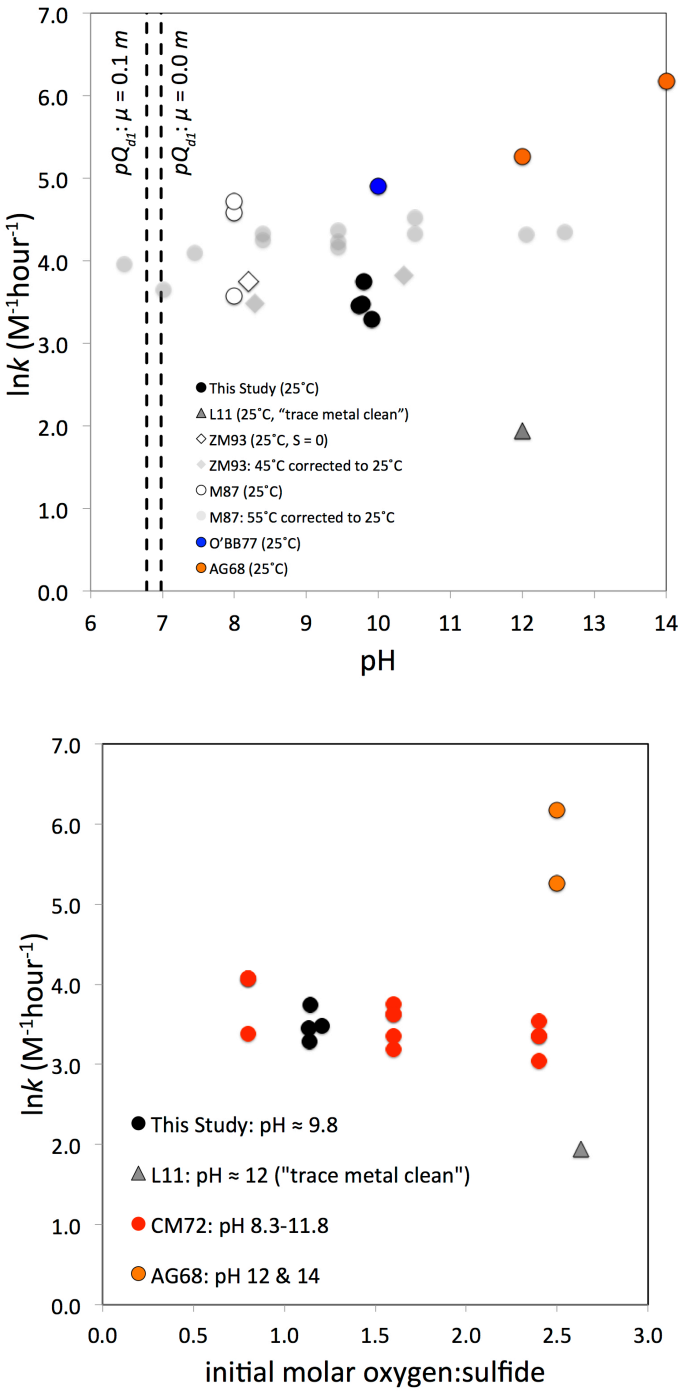

Figure 3.7: (a; top) Second order rate constants derived from experiments in low ionic strength buffer solutions (i.e., not seawater) as a function of pH. The first dissociation quotient for H_2S (pQ_{d1}) is shown for reference as a function of ionic strength (μ = 0 – 0.1 *m*) from Hershey et al. (1988). (b; bottom) Computed second order rate constants derived from the rate data of Chen and Morris (1972a) from experiments comparable to the present study as a function of the initial molar oxygen to sulfide ratio, with a handful of other experimental studies shown for reference. References: AG68 = Avrahami and Golding (1968), CM72 = Chen and Morris (1972a), O'BB77 = O'Brien and Birkner (1977), M87 = Millero et al. (1987a), ZM93 = Zhang and Millero (1993), and L11 = Luther et al. (2011).

Luther et al. (2011) report the lowest second order rate constant observed to date from experiments performed under trace metal clean conditions. Assuming that the broad observations regarding the pH dependence from the Millero group are valid at 25˚C (Millero et al., 1987a; Zhang and Millero, 1993) and the reaction remains second order overall (a = 1, b = 1), the data of Luther et al. (2011) suggest that much of the variability seen in Figure 3.7a-b at high pH is due to varying levels of unintended trace metal catalysts impacting the experimental determination of rates. The experiments of Luther et al. (2011) performed in Mg^{2+}-scrubbed NaOH (25˚C, pH ~ 12) in a class 100 clean bench utilizing triple acid-washed plastic tubes (trace metal clean HCl) yield an overall rate constant that is ca. 10x lower than those of Millero et al. (1987a) (on average) and ca. 5x lower than our experiments (Table 3.1, Figure 3.2, and Figure 3.7). Trace metal catalysts are documented to cause several order of magnitude changes in the apparent overall second order rate constants associated with sulfide oxidation under otherwise equivalent conditions even at relatively low (nM) levels depending on the metal (Vazquez et al., 1989). Trace metal (or perhaps other catalytic) contaminants in the reagents (e.g., buffer salts), the reaction vessel and its components, and/or atmosphere in the laboratory environment seem to be among the likely causes.

The activation energy that we derive from our experiments (60 ± 3 kJ/mol: Figure 3.2) is indistinguishable from Millero et al. (1987a) (56 ± 3 kJ/mol) (0.02 M borate buffer, pH = 8.0, T = 5-65˚C) despite our computed overall rate constants being on the lower end of their range. It is possible that our estimates of the second order rate constants are biased slightly low due to the assumption that our

experiments were saturated with respect to oxygen from air. If this is the case, any bias must be systematic as a function of temperature in order to obtain a similar activation energy to Millero et al. (1987a). We took a similar approach to Millero et al. (1987a) to saturate our experiments with air (bubbling buffer solutions with ambient air for 1 hour before and after allowing the experimental buffer to thermally equilibrate overnight in the temperature bath prior to the injection of sulfide). The apparent offset may be reasonably assumed to be either within the error of the determinations (e.g., due to variations, systematic or otherwise, in the initial oxygen concentrations in our experiments that were not directly determined) or the result of slightly different impacts of trace catalysts that do not substantially affect the derivation of the apparent activation energy.

In summary, the second order rate constants and apparent activation energy calculated from our experiments compare relatively well to the experiments of the Frank Millero group (Millero et al., 1987a; Zhang and Millero, 1993) and reasonably well to experiments performed under comparable conditions from Chen and Morris (1972a), although considerable variability between experimental studies is generally observed in the literature. Trace metal clean experiments (Luther et al., 2011) may indicate that most experimental studies of sulfide oxidation are impacted by unintentional trace metal catalysis. The sources and compositions of these catalysts are ultimately unknown and a detailed investigation is warranted, but is beyond the scope of the present study.

4.3 Induction period

Most of our sulfide oxidation experiments exhibit a resolvable induction period before any obvious reaction proceeds (Table 3.2; Figure 3.1). The duration of the induction period appears to be a function of temperature (e.g., decreases from ~36-48 hours at 5˚C to ~8-12 hours at 25˚C to undetectable at 45˚C) and explicit ferrous iron catalysis. The presence of an induction period suggests that the reaction is autocatalytic and requires the build-up of a key intermediate (or intermediates) to effective concentrations to catalyze the reaction (Chen and Morris, 1972a). An induction period may additionally imply a chain mechanism (Chen and Morris, 1972a; Millero, 1986) whereby these autocatalytic intermediates are continuously generated as the reaction proceeds at sufficient levels to sustain the reaction once it has begun. The autocatalytic intermediates (or chain carriers) are likely to be either highly reactive sulfur or oxygen species (RSS or ROS). The presence of an induction period also implies that the direct reaction of HS^- with O_2 is kinetically inhibited and proceeds slowly, consistent with many elementary (1 to 2 electron transfer) reactions between H_2S/HS^- and O_2 being thermodynamically unfavorable (Luther, 2010; Luther et al., 2011).

Induction periods have been observed in some previous sulfide oxidation experiments (Chen and Morris, 1972a) but do not appear to be a consistently observed feature of the reaction (none reported in the Millero group experiments; Millero et al., 1987a; Vazquez et al., 1989; Zhang and Millero, 1993; or many earlier experiments, including those in seawater at 10˚C; Cline and Richards, 1969). Chen and Morris (1972a) report induction periods over a wide range of experimental

conditions (25˚C, pH = 6.0 – 11.75, $[H_2S_T]_{initial}$ = 50-200μM, $[O_2]_{initial}$ = 160-800μM) between 0.2 – 6 hours that may roughly correlate inversely with the overall rate constant, which is generally consistent with our observations (Table 3.2). It is noteworthy that experiments performed at lower temperatures in previous studies (as low as 5-10˚C; Cline and Richards, 1969; Millero et al., 1987a; Zhang and Millero, 1993) were not reported to exhibit induction periods, as our experiments exhibited an induction period on the order of 1.5-2 days at 5˚C (Table 3.2).

The addition of trace levels of ferrous iron appears to decrease the induction period in our experiments (e.g., Figure 3.1). As noted above, the catalytic cycle of ferrous iron likely involves the production of ROS and ferric iron, each of which are likely to be more effective oxidants towards sulfide than O_2 that may decrease the duration of an induction period. Trace metal catalysts such as ferrous iron have also been observed to decrease induction periods in sulfite (S^{4+}) oxidation experiments (e.g., Brandt and van Eldik, 1995). We put forth the hypothesis that induction periods may become undetectable upon sufficient levels of catalysis (intentional or unintentional) (*cf.* Chen and Morris, 1972b). We propose that the lack of consistency in the observation of induction periods between experimental studies may be yet another feature of varying trace catalyst (metal or other) contaminations between laboratories and experimental approaches. Other than trace metals, reactive intermediate sulfur compounds (such as sulfite, elemental sulfur, or others) present in sulfide stock solutions may also influence the detection of induction periods by serving at autocatalysts, either via their reaction with sulfide or their own oxidation that may produce reactive oxygen species or other compounds that may serve as

autocatylsts for sulfide oxidation. Our approach of preparing fresh stock sulfide solutions under anoxic conditions immediately before each experiment may have inhibited the production of reactive sulfur intermediates that could serve as autocatalysts at a sufficient enough level to allow the detection of induction periods.

4.4 Fe^{2+} addition: Explicitly catalyzed experiments

Following a shortened induction period, our experiments where we added Fe^{2+} (~50-150 nM) to starting experimental solutions indicate that the reaction rate is increased (relative to our experiments where Fe^{2+} was not added) for a period of ca. 20-25 hours before the reaction rate shifts to a value that is indistinguishable from our experiments where no Fe^{2+} was added (Figure 3.1; Table 3.2). These observations suggest that the Fe^{2+} catalytic effect might be relatively short-lived and the overall oxidation of ferrous iron to ferric iron via oxygen or ROS at the levels we studied may eventually go to completion or far enough to completion such that neither form(s) of iron influence the observed oxidation rates at a certain time-point in the experiments. Zhang and Millero (1993) observed similar behavior in sulfide oxidation experiments catalyzed by trace levels of Fe^{3+} (rather than Fe^{2+}) in seawater, finding that apparent rates returned to "background" levels from obviously catalyzed levels after only 30 minutes of reaction under their experimental conditions. They attributed this behavior to the formation of non-reactive colloidal forms of Fe^{3+} that can form over such short time scales. They argue that only dissolved forms of Fe^{3+} at trace-levels influence the rates of sulfide oxidation and colloidal ferric oxides may be ineffective as catalysts. Zhang and Millero (1991) also observed similar effects using both Fe^{2+} and Fe^{3+} as catalysts for sulfite (SO_3^{2-}) oxidation. Thus, our hypothesis is

the oxidation of Fe^{2+} in our experiments may have generated trace-levels of colloidal Fe^{3+} that built up over time such that ferric iron eventually could not effectively complete the catalytic cycle. It is not clear why similar effects were not reported in Fe^{2+}-catalyzed sulfide oxidation experiments of the Milllero group under high pH (Vazquez et al., 1989; Zhang and Millero, 1993) but this may be due to the fact that the Millero group experiments went to completion in a matter of hours due to the ~10x lower initial concentrations of sulfide used, and may have finished before this effect could be observed.

If this reasoning is correct, an alternative end-member case may be considered for the effect of ferrous iron on the enhancement of rates of sulfide oxidation. If we consider a hypothetical situation where the oxidation of ferrous iron under the relatively high pH conditions of our experiments yields a phase of ferric iron that is completely unable to react with sulfide to participate in a true catalytic cycle, the relatively short-lived enhancement of oxidation rates with increasing ferrous iron added would primarily be the result of the enhanced generation of reactive oxygen species (ROS) via the oxidation of ferrous iron. In this case, ferrous iron is not acting as a catalyst in sulfide oxidation in the classic sense but rather providing a "jump-start" for the reaction by providing a source of ROS via a parallel oxidation reaction. If this were solely the case, this would imply that the oxidation of ferrous iron at trace levels is severely inhibited in the presence of sulfide where an estimated half-time of ferrous iron oxidation would be on the order of hours instead of seconds/minutes as has been observed in sulfide-free experiments at high pH (Millero et al., 1987b). This would additionally imply that the reaction rates between sulfide and ROS are

extremely high due to the very low concentrations of ROS produced by the oxidation of trace levels of ferrous iron. We cannot rule out a ferrous/ferric catalytic cycle as described previously under high pH conditions (Vazquez et al., 1989; Zhang and Millero, 1993) using our experimental data and it is probable that both ferric iron phases and ROS as produced via the oxidation of ferrous iron are contributing to the enhanced rates of sulfide oxidation in addition to reducing the duration of the induction period.

4.5 Isotope fractionations: Comparison to previous studies

Fry et al. (1988) report $^{34}S/^{32}S$-based fractionation factors for the oxidation of sulfide via molecular oxygen in distilled water (pH = 11) and artificial seawater (pH = 8.2) at 22-25˚C that were determined by tracking the isotopic composition of sulfide as a function of reaction progress as undertaken in the present study (Equation 4). Fry et al. (1988) obtain $1000\ln^{34}\alpha_{products\text{-}sulfide} = -4.8 \pm 0.5$ ‰ in distilled water (average of three experimental sets, 1 s.d.) and $1000\ln^{34}\alpha_{products\text{-}sulfide} = -5.8 \pm 2.4$ ‰ in artificial seawater (average of two experimental sets, 1 s.d.). Any difference in the isotope effect as a function of pH and ionic strength over this range was not resolved and their recommended value of $1000\ln^{34}\alpha_{products\text{-}sulfide} = -5.2 \pm 1.4$ ‰ (1 s.d.) is the average of all 5 experimental sets. These values compare well with our own values derived from experiments performed at pH ≈ 9.8 and 25˚C, where we obtain $1000\ln^{34}\alpha_{products\text{-}sulfide} = -5.85 \pm 0.15$‰ (duplicate experiments, 1 s.d.).

4.6 Major isotope discrimination as a function of explicit catalysis and temperature

A primary kinetic isotope effect associated with a unidirectional reaction is a direct expression of the reaction mechanism, i.e., isotope discrimination occurring as reactants (one comprised of the isotopic species of interest) form a reaction coordinate and transition state along the saddle of the activation energy barrier and transmit to form products. For an elementary bimolecular reaction, the magnitude and direction of the isotope effect depends on the relative vibrational and translational energies of the reactant isotopomers, their respective transition states formed with the other reactant, and transmitted products as they pass through the potential energy landscape defined by the electronic structure of the system, where other effects such as quantum tunneling through the energy barrier to reaction may play additional roles. In the case of a complex, multi-step mechanism, the measured isotope effect would presumably be the expression of the effects of multiple reaction coordinates and transition states being formed from multiple intermediates, where the measured fractionation may represent a "bulk" fractionation that might largely reflect a hypothetical rate-determining step (or set of rate-determining steps) in the reaction.

In the case of complex mechanisms like sulfide oxidation, the information about isotope fractionation obtained from an experiment may depend on the manner in which the effect is measured. For example, when multiple pathways and intermediates are involved, measuring the fractionation by tracking the isotopic composition of the reactant (i.e., sulfide) as a function of reaction progress may yield different information than measuring the final product isotopic composition (i.e., sulfate) as a function of reaction progress, as both may be influenced by different

reactions involving different intermediates. Since we measured the isotopic composition of sulfide as a function of reaction progress, we will focus on reactions involving sulfide directly.

Several reactions involving the reactant sulfide are outlined above (Equations15-20) that could hypothetically take place during oxidation when molecular oxygen (O_2) is the ultimate oxidant, due to: (1) the potential for ROS to form as part of the mechanism (with or without added catalysts), (2) the high likelihood of reactions involving added (or contaminating) trace metals and other catalysts (e.g., organics), and (3) other reactions involving sulfur intermediates. Each of these reactions has a unique reaction coordinate, transition state, rate constant, activation energy, and primary kinetic isotope effect. The isotope effect measured by tracking the isotopic composition of sulfide with time ($^{34}k/^{32}k_{\text{measured}}$) likely represents some composite (or "bulk") fractionation caused by many reactions occurring in tandem, e.g.:

$$^{34}k/^{32}k_{\text{measured}} = f_{\text{oxygen}}(^{34}k/^{32}k_{\text{oxygen}}) + f_{\text{superoxide}}(^{34}k/^{32}k_{\text{superoxide}}) + f_{\text{peroxide}}(^{34}k/^{32}k_{\text{peroxide}}) + f_{\text{trace\_metal}}(^{34}k/^{32}k_{\text{trace\_metal}}) + f_{\text{S-intermediate}}(^{34}k/^{32}k_{\text{S-intermediate}}) + \ldots \quad (21)$$

Where the f terms represent the relative fractional contribution of each pathway to the overall oxidation rate, which are not constrained by the data and are ultimately unknown. This makes the interpretation of experimentally measured kinetic isotope effects associated with sulfide oxidation complex and perhaps ambiguous as to their mechanistic meaning.

Our explicitly Fe^{2+}-catalyzed experiments appear to show trends of decreasing magnitude in the $^{34}S/^{32}S$-based fractionation factor with increasing reaction rate and

catalysis (Figure 3.4b). By adding a ferrous iron catalyst, we are likely inducing a shift in the relative contributions of the reactions above (Equations 15-20, 21) to the overall rates and isotope fractionations, particularly towards a greater influence for those involving ROS and ferric iron. In the classic view, catalysts increase reaction rates by providing an alternative pathway for the reaction that has lower activation energy. The decrease in the magnitude of the fractionation factor with increasing rate/catalysis is consistent with the simple hypothesis that pathways of lower activation energy have associated with them a smaller discrimination between isotopomers of sulfide (i.e., smaller magnitude isotope effects). In the simple case where lower E_a leads to lower $^{34}k/^{32}k$, catalysis may always lead to lower magnitude isotopic fractionations. Alternatively, it may be fortuitous that the pathways of oxidation that are provided by explicit ferrous iron catalysis have smaller isotope effects associated with them. Other forms of catalysis may have different consequences for the observed isotopic fractionations, since isotopic fractionations will ultimately depend on the mechanism involved and the properties of transition states. Experiments investigating the role of other catalysts for sulfide oxidation, such as organic compounds or other trace metals that may have different mechanisms than ferrous iron, and their effects on reaction rates and isotope fractionations will allow these relationships to be explored in further detail.

The major isotope fractionation factors derived from our non-explicitly catalyzed experiments performed as a function of temperature appear to exhibit a temperature dependence that is inverse to expectation: fractionation magnitudes appear to increase with increasing temperature and increasing rate (Figure 3.4a). This

relationship between rate and isotope fractionation as a function of temperature is additionally contrary to the rate/fractionation relationships observed as a function of Fe^{2+}-catalysis. Single-step, elementary reactions are expected to generate normal temperature dependences except when there are competing contributions from high and low frequency modes to the partition function ratios between the reactants and transition state. The key transition states involved with oxidation reactions involving HS^- and their vibrational properties are presently unknown. Such a hypothesis may be directly testable for sulfide oxidation reactions using advanced quantum mechanical calculations utilizing a form of transition state theory or RRKM theory that probe a wide range of transition states for elementary electron exchange reactions between HS^- and O_2, ROS, and other oxidants in simulated explicitly solvated environments.

An inverse fractionation temperature dependence may alternatively suggest a mechanism with more than one "rate-determining" reactions, where more than one reaction pathway for sulfide oxidation exert similar magnitude contributions to the overall reaction rate and isotope fractionation. The inverse temperature dependence may thus be interpreted to be the result of a shift in the relative contributions of the reactions that are contributing to the bulk effect as a function of temperature, where reactions that have slightly larger isotope effects are being expressed more with increasing temperature. The relative shift in the contribution(s) of these reactions would apparently be large enough over the studied temperature range to combat the decrease in the fractionation magnitude with increasing temperature that would be expected to occur for each individual contributing reaction. Within the context of the

extant sulfide oxidation mechanisms, the two sets of competing reactions may be related to overall reactions involving sulfide and oxygen species (O_2 and ROS) and sulfide and reactive sulfur intermediates. Both the polar and free radical mechanisms call for the reaction of residual sulfide with a sulfur intermediate to ultimately produce thiosulfate, which comprises a significant proportion of the mass balance in our (and previous) experiments. The apparent inverse magnitude temperature dependence that we observe may be providing evidence that a highly reactive sulfur intermediate may be undergoing reversible isotope exchange with sulfide along a pathway such as this, where the rates and influence of this exchange become greater with increasing temperature (see also Section 4.7).

4.7 Mass dependence of sulfide oxidation

The exponent of mass-dependence describing $^{32}S/^{33}S/^{34}S$ fractionation relationships ($^{33/34}\lambda$) associated with sulfide oxidation appears to be lower (at a resolvable level) than the exponents generally associated with equilibrium isotope exchange among aqueous sulfur compounds (Figure 3.5a-d; *cf.* Eldridge et al., in review; Chapter 2). Such exponents lead to small positive shifts in computed $\Delta^{33}S_{P\text{-}R}$ associated with sulfide oxidation. For example, for experiments at 25˚C and no ferrous iron added, our measured $^{33/34}\lambda = 0.5094 \pm 0.0016$ associated with $^{34}\varepsilon_{P\text{-}R} = -5.85 \pm 0.15$ ‰ translates to a $\Delta^{33}S_{products\text{-}sulfide} = 0.033 \pm 0.009$ ‰ (1 s.d., duplicate experiments). Similar effects may also be exhibited in $^{36/34}\lambda$ and $\Delta^{36}S$, where $^{36/34}\lambda$ may be higher than exponents associated equilibrium isotope exchange and may translate to small negative shifts in $\Delta^{36}S_{P\text{-}R}$ associated with sulfide oxidation.

Hypotheses to explain this apparent deviation from "canonical" or "typical" mass-dependence may be: (1) the mass-dependent fractionation law in operation here is akin to those associated with unidirectional processes like evaporation and diffusion where terms related to translations along the reaction coordinate influence the mass-dependence differently than vibrational energies between reactants and products (Young et al., 2002); or (2) the exponent is the result of so-called "mass-conservation" effects, i.e., the reversible exchange of isotopes among fractionated reservoirs within a complex (multi-pool) network (*cf.* Farquhar et al., 2003), which could conceivably arise from the complex sulfide oxidation mechanism.

The mass dependence associated with equilibrium isotope exchange among solutes in aqueous systems follow relatively simple rules that are generally understood. In the high temperature limit, the exponent of mass dependence for equilibrium isotope exchange reactions approaches a singular value for all compounds in a given isotope system that depends solely on the atomic masses (m) of the isotopes (Matsuhisa et al., 1978), e.g., for $^{32}S/^{33}S/^{34}S$:

$$^{33/34}\lambda_{T\rightarrow\infty} = (1/m_{32} - 1/m_{33})/(1/m_{32}\text{-}1/m_{34}) = 0.51588 \quad (22)$$

At the low temperature limit, the exponent will vary depending on differences in the zero point energies of the isotopologues (Matsuhisa et al., 1978) and these differences influence the temperature dependence of the exponent and its value under the conditions relevant to aqueous systems. These variations have been theoretically estimated using quantum mechanical calculations for a variety of aqueous sulfur compounds and have been shown to follow systematic relationships that depend to a first order on the oxidation state of sulfur and its coordination (Eldridge et al., in

review) (Chapter 2). For temperatures greater than 0˚C, the $^{32}S/^{33}S/^{34}S$-based exponents derived from our theoretical reduced partition function ratios (RPFRs, or β) of aqueous sulfur compounds (i.e., computed as $\ln(^{33}\beta)/\ln(^{34}\beta)$) conform to a relatively tight range of ca. 0.5148-0.5159 (Eldridge et al., in review) (Chapter 2). Slight shifts in the exponents may accompany the transformations of RPFRs into fractionation factors (*cf.* Eldridge et al., in review; Matsuhisa et al., 1978) but do not exceed ~0.514-0.516 for equilibrium isotope exchange in aqueous systems except where there are crossovers (*cf.* Deines, 2003), but these effects may not translate to substantial $\Delta^{33}S$ effects due to the very small isotope fractionations in proximity to crossover temperature.

Young et al. (2002) argue that mass-dependent fractionation laws associated with equilibrium isotope exchange reactions and some simple irreversible processes may be different. Utilizing considerations from both classical transition state theory (e.g., Bigeleisen, 1949) and Rice-Ramsperger-Kassel-Marcus (RRKM) theory (e.g., Marcus and Rice, 1951), Young et al. (2002) argue that certain simple unidirectional processes like evaporation and unimolecular dissociation reactions can be shown to good approximation to follow mass fractionation laws where:

$$^{33/34}\lambda \approx \ln(^{32}m/^{33}m)/\ln(^{32}m/^{34}m) \qquad (23)$$

Where the 'm' can refer to atomic, molecular, or reduced masses of isotopic molecules depending on the process considered. They suggest that this relationship can lead to exponents that are lower than those expected from equilibrium isotope exchange, the magnitude of which depends on the isotopologues considered and whether molecular/atomic or reduced masses are used. For example, if one derives

an exponent from this relation using the reduced masses of isotopologues of HS^-, the exponent is 0.51565 and well within the range of equilibrium isotope exchange, but if molecular masses are used (perhaps more relevant in the classical sense), the exponent shrinks to 0.50809 (similarly, if one uses the atomic masses, the exponent is 0.50831). The simple form of this relation may hold true only if several approximations can be reasonably assumed to hold that may not be applicable to more complex unidirectional reactions like electron transfer redox reactions in aqueous media and the complex autocatalyitc chain mechanisms that might be associated with sulfide oxidation, but the general argument that the theory of unidirectional reactions (i.e., transition state theory and RRKM theory) might predict different mass fractionation laws is something to consider in evaluating the mass dependence of sulfide oxidation. This is another hypothesis that may be directly testable for sulfide oxidation reactions using advanced quantum mechanical calculations utilizing a form of transition state theory or RRKM theory that probe a wide range of activated complexes for elementary electron exchange reactions between HS^- and O_2, ROS, and other oxidants in simulated explicitly solvated environments.

Apart from arising from varying contributions from the terms in the partition function ratios that describe translational and vibrational energies (e.g., Young et al., 2002), the other possibility for the experimentally observed sub-canonical exponent is that it arises from a mass-conservation effect. Effects of this kind are well documented in other complex reaction networks like those associated with sulfur redox metabolism that are the basis for multiple sulfur isotope biosignatures (e.g.,

phototrophic sulfide oxidation: Zerkle et al., 2009; dissimilatory sulfate reduction and disproportionation: e.g., Farquhar et al., 2003; Johnston et al., 2005; Johnston et al., 2007; Farquhar et al., 2007; Johnston, 2011). A mass conservation effect requires reversibility in the reaction network associated with the oxidation mechanism such that an isotopically fractionated sulfur intermediate undergoes reversible non-equilibrium exchange with the residual sulfide. Both mechanisms that have been proposed for sulfide oxidation (polar and free radical) may allow for reversible isotope exchange and may occur in at least the following ways: (1) reversible exchange between sulfide and zero-valent sulfur species and polysulfides, (2) reversible exchange between sulfide and the outer, "sulfanyl" sulfur in thiosulfate (*cf.* Uyama et al., 1985; Chu et al., 2004), and (3) hydrolytic disproportionation reactions of other hypothetical intermediates such as S_2O^{2-} that yield sulfide as a product.

The magnitudes of the $^{34}S/^{32}S$ fractionations associated with the plausible exchange reactions in the HS^--S_n^{2-}-S^0 and HS^--$S_2O_3^{2-}$ systems are likely to be small and the effects in the apparent exponent relations among these pools may not be large enough to explain our measured effects. For example, from theoretical computations of aqueous sulfur compounds in water clusters (Eldridge et al., in review; Chapter 2), the equilibrium isotope effect between the outer "sulfanyl" sulfur in thiosulfate and HS^- at 25˚C is predicted to be on the order of $1000\ln(^{34}\alpha_{sulfanyl/HS^-}) \approx 2$ ‰ with a corresponding $^{33/34}\lambda = 0.5151$. Although not well constrained in the published literature, fractionations among sulfide compounds and the polysulfides would also be expected to be similarly small (*cf.* Amrani et al., 2006). Additionally, polysulfides thus far have not been demonstrated to comprise a significant portion of the sulfur

balance in sulfide oxidation experiments performed at high pH (*cf.* Chen and Morris, 1972a; Zhang and Millero, 1993) and may not be likely candidates. In order for these exchange reactions to produce significant mass conservation effects, the non-equilibrium $^{34}S/^{32}S$ fractionation magnitudes among these compounds would need to be substantially higher than their equilibrium counterparts, which from the available constraints seems unlikely. In the only other study to measure isotope fractionations associated with sulfide oxidation, Fry et al. (1988) measured the isotopic compositions of pooled-products (sulfate + sulfite, thiosulfate + polythionate) and found the fractionations between these pools and residual sulfide to be less than or equal to the overall ~ -5 ‰ effect. Compound- and site-specific isotope analyses of key reaction intermediates may allow the further testing of such hypotheses.

Reactions that may be able to produce a mass conservation effect in the sulfide oxidation mechanism beyond these simple isotope exchange reactions may relate to the hydrolytic disproportionation of highly-reactive intermediates, producing sulfide and another sulfur compound of higher valence. One potential example of this kind of reaction may occur along the hypothesized pathway to thiosulfate formation. In the polar mechanism, one of the initial products of sulfide oxidation is a member of the sulfoxylate system (*cf.* Hoffmann and Lim, 1979; Zhang and Millero, 1993):

$$HS^- + O_2 \rightarrow HSO_2^- \qquad (24)$$

Where sulfoxylate is represented here generically as a bisulfoxylate species, noting that sulfoxylate is a documented intermediate of sulfide oxidation (Vairavamurthy and Zhou, 1995; Tossel, 1997). Sulfoxylate is postulated to undergo either further

oxidation to form sulfite species or the following series of reactions involving residual sulfide to form thiosulfate (*cf.* Zhang and Millero, 1993):

$$HSO_2^- + HS^- \rightarrow S_2O^{2-} + H_2O \quad (25)$$

$$S_2O^{2-} + O_2 \rightarrow S_2O_3^{2-} \quad (26)$$

We note that Equation 25 is a reverse hydrolysis reaction and, if it occurs and is additionally reversible under experimental conditions, might lead to the transferal of fractionated sulfide back to the residual sulfide pool via the hydrolytic disproportionation of S_2O^{2-}. Just how fractionated this returned sulfide is relative to the residual sulfide will depend on the magnitude of the isotope effects associated with the formation and disproportionation of S_2O^{2-}. The influence of this return flow of sulfide on the bulk isotopic composition of the residual sulfide pool will further depend on the magnitude of the flux of this produced sulfide. Although highly speculative, if hydrolytic disproportionation reactions of this kind involving S_2O^{2-} or other presently undocumented intermediates comprise a substantial pathway for sulfur isotope exchange within the overall sulfide oxidation mechanism, they may be responsible for a mass conservation effect that is recordable in residual sulfide. Such reactions may additionally play roles in the major isotope fractionation ($^{34}S/^{32}S$) behavior that we observe as a function of temperature.

4.8 Implications: Environmental sulfur cycle

Our observation that the overall oxidation of sulfide via molecular oxygen is accompanied by exponents of mass dependence that may be different at a resolvable level from ranges consistent with equilibrium isotope exchange will change how chemical oxidation processes are treated in future models of the sulfur cycle based on

multiple sulfur isotopes (such as Zerkle et al., 2009; Zerkle et al., 2010; Pellerin et al., 2015). Due to the similarity in the direction and magnitude of the $\Delta^{33}S_{products\text{-}sulfide}$ effect associated with chemical oxidation (this study) to that documented for phototrophic oxidation (Zerkle et al., 2009), chemical sulfide oxidation may have similar obscuring impacts on the expression of larger $\Delta^{33}S$ signals associated with other metabolic transformations such as disproportionation in the presence of a substantive oxidative sulfur cycle that have been illustrated previously in environmental-scale models (Zerkle et al., 2009). Our new constraints on minor isotope fractionations do not indicate an obviously robust biosignature for oxidative pathways based on $\delta^{34}S/\Delta^{33}S/\Delta^{36}S$ relationships. However, due to the inversion in the major isotope ratio ($^{34}S/^{32}S$) fractionation factor associated with sulfide oxidation between chemical oxidation ($HS^- \rightarrow$ products, normal $^{34}S/^{32}S$ isotope effect; this study; Fry et al., 1988) and phototrophic oxidation ($H_2S/HS^- \rightarrow S^0$, inverse $^{34}S/^{32}S$ isotope effect; e.g., Fry et al., 1984; Zerkle et al., 2009) that was first noted by Brian Fry and colleagues (Fry et al., 1988), the differentiation of these two general pathways may still be possible under certain circumstances. For example, the isotopic composition of residual sulfide undergoing oxidation would be expected to evolve along different trajectories in $\delta^{34}S/\Delta^{33}S$ (and potentially $\delta^{34}S/\Delta^{36}S$) space depending on whether chemical or phototrophic oxidation dominates in a given environment. These relationships may provide interpretive power in the elucidation of sulfur isotope systematics in chemoclines of euxinic water bodies that may vary due to seasonal fluctuations that could affect oxidation pathways (e.g., Lago di Cadagno; Canfield et al., 2010). Additionally, future experiments investigating the isotope

effects and mass dependence associated with sulfide oxidation via other oxidants important in natural systems (e.g., heterogeneous reactions between H_2S/HS^- and solid FeOOH or MnO_2 phases) are warranted and can test whether the $\Delta^{33}S_{P\text{-}R}$ that we have observed for O_2-oxidation is unique or common to sulfide oxidation mechanisms, and furthermore, if uncommon could potentially lead to the development of resolvable signatures associated with chemical oxidation pathways.

5.0 Conclusions

We present rates and multiple sulfur isotope fractionations associated with the oxidation of sulfide with molecular oxygen. Our rates and activation energy that we derive from our experiments compare well to the extensive experimental work of the Frank J. Millero group (Millero et al., 1987a; Zhang and Millero, 1993), but kinetic parameters derived from experiments in the literature are generally variable. Such variability may be the result of unintended trace metal catalysis that may have additionally impacted the experimental results of the present study based on the much lower oxidation rates obtained by Luther et al. (2011) under trace metal clean conditions. Our experiments reproduce induction periods that have been observed in some previous studies (Chen and Morris, 1972a) that furthermore indicate that the reaction of HS^- with O_2 proceeds slowly and likely via an autocatalytic mechanism that is not well understood in detail. We appear to observe that induction periods are shortened upon ferrous iron catalysis, and further note that inconsistencies in the observation of induction periods in the literature may be another impact of unintended trace catalysis, either via trace metals or reactive intermediate sulfur compounds (e.g., the latter present as blanks in sulfide stock solutions). The effect of the ferrous iron

catalyst on oxidation rates at the levels in our experiments appears to be short-lived, where rates indistinguishable from experiments where no ferrous iron catalyst resume after ca. 20-25 hours of catalyzed reaction. This behavior may reflect the formation of unreactive colloidal phases of ferric iron that are unable to complete a catalytic cycle that have been described previously (e.g., Zhang and Millero, 1993).

The major isotope fractionation factors ($^{34}S/^{32}S$) that we derive from our experiments are similar to previous experimental determinations under comparable conditions by Fry et al. (1988). We observe small but resolvable relationships between $^{34}S/^{32}S$ fractionation factor and rate associated with ferrous iron catalysis, where increased catalysis appears to decrease the magnitude of the isotope fractionation at the levels we have studied. This may be the result of smaller magnitude isotope effects associated with pathways of lower activation energy that are provided by the catalytic cycle associated with ferrous iron. Additionally, we observe that sulfide oxidation is associated with a temperature dependence that is inverse to expectation, where $^{34}S/^{32}S$-based fractionation magnitudes appear to increase with increasing rate due to increased temperature. The origin of this inverse effect is ultimately unclear, and may either be due to the competition of low and high frequency modes between sulfide and any number of key transition states it may form with reactants as part of the mechanism (e.g., reactive oxygen species or even reactive sulfur intermediates) or the result of more than one "rate-determining" reaction with different isotope effects having a substantive influence on overall rates and isotopic fractionations. This observation may also be providing evidence for reversible

isotope exchange between residual sulfide and a reactive sulfur intermediate (e.g., along the pathway to thiosulfate formation).

All fractionations in this study appear to exhibit a mass dependence with respect to $^{33}S/^{32}S$ and $^{34}S/^{32}S$ relationships that is distinguishable at a resolvable level from the range expected for equilibrium isotope exchange, and may also be present for $^{36}S/^{32}S$ and $^{34}S/^{32}S$ relationships. We do not appear to resolve any differences in these relationships as a function of sulfide oxidation rate associated with either ferrous iron catalysis or temperature. This observation will change how chemical oxidation processes are treated in future models of the sulfur cycle. Similar impacts to phototrophic oxidation are expected for chemical oxidation on the $\Delta^{33}S$ of major phases in natural environments that have been described previously (Zerkle et al., 2009) that have been influenced by the compounded effects of sulfate reduction, sulfide oxidation, and disproportionation of intermediates. The isotope effects related to chemical and phototrophic sulfide oxidation may cause residual sulfide undergoing oxidation to follow different trajectories in $\delta^{34}S/\Delta^{33}S$ space, potentially allowing these two pathways to be isotopically resolved under some circumstances.

The extraction of a primary kinetic isotope effect associated with the unidirectional oxidation of sulfide to products via O_2 is probably not possible due to the plethora of hypothetical reactions that sulfide may undergo as part of the overall mechanism. Intermediate sulfur compounds that may be produced as part of the mechanism can undergo side reactions with residual sulfide, providing mechanisms for additional isotope exchange that convolute the expression of any primary isotope effects. For example, the inverse magnitude $^{34}S/^{32}S$-based fractionation behavior that

we observe as a function of temperature might indicate that the isotope fractionations we have measured are not the result of any singular primary kinetic isotope effect. The apparent mass dependence of sulfide oxidation that we observe and the resulting effect on $\Delta^{33}S$ is additionally consistent with mass conservation principles that require exchange reactions occurring between sulfide and reactive sulfur intermediates. However, more primary mechanisms for the observed fractionation behavior cannot be ruled out at present. Future studies directed at the detection of hitherto unobserved and hypothetical reaction intermediates (e.g., free radical species) may further pin-down the reaction mechanism. The isolation and compound-specific isotope analysis of key reaction intermediates and products under kinetically controlled conditions may further elucidate some of the isotope exchange reactions responsible for the measured effects. Finally, sophisticated quantum mechanical calculations rooted in the theory of unidirectional reactions (e.g., transition state theory, RRKM theory) probing the transition states associated with elementary electron exchange reactions between HS^-/H_2S and O_2, reactive oxygen species, and relevant sulfur intermediates, may elucidate some of the primary kinetic isotope effects associated with oxidation that may provide further interpretive power of the more complex series of reactions occurring in oxygenated sulfide solutions that we have investigated here.

Table 3.2: Experimental conditions and rate parameters from sulfide oxidation experiments. The reported pH values are averages of measurements performed on 5-6 aliquots taken throughout experimental runs. Subscripts on concentration values indicate: T = total dissolved species in solution (e.g., $[(CO_3^{2-})_T] = [CO_3^{2-}] + [HCO_3^-]$), i = initial concentrations (*italics* indicate estimated values), and added = amount added. I.P. is the estimated induction period (N/A = not clearly resolved). *k'* is the pseudo first order rate constant (Equation 3) and *k* is the computed second order (overall) rate constant using the estimated $[O_2]_i$ and assuming b = 1 (Zhang and Millero, 1993). The two sets of rate constants derived from the ferrous iron explicitly catalyzed experiments indicate values before the pronounced break in rate ("Catalyzed") and after ("Uncatalyzed") (see Figure 3.1). Uncertainties are 1 s.d.

I.D.	T (°C)	pH	$[(CO_3^{2-})_T]$ (M)	$[(H_2S)_T]_i$ (µM)	$[O_2]_i$ (µM)*	$[Fe^{2+}]_{added}$ (nM)	I.P. (hr)	k' (hr^{-1})	k ($M^{-1}hr^{-1}$)	ln$k$
SOX-5	5	9.77 ±0.07	0.002	224	*399*	0	~36-48	0.0021 ±0.0001	5.15 ±0.21	1.64 ±0.04
SOX-25(A)	25	9.80 ±0.01	0.02	226	*258*	0	~6-8	0.0109 ±0.0008	42.4 ±3.0	3.75 ±0.07
SOX-25(B)	25	9.78 ±0.05	0.02	214	*258*	0	N/A	0.0084 ±0.0006	32.4 ±2.5	3.48 ±0.08
SOX-25(C)	25	9.91 ±0.05	0.002	226	*258*	0	~8-13	0.0069 ±0.0003	26.8 ±1.0	3.29 ±0.04
SOX-25(D)	25	9.73 ±0.04	0.002	227	*258*	0	~8-13	0.0082 ±0.0004	31.6 ±1.6	3.45 ±0.05
Average (SOX-25)		**9.81 ±0.04**						**0.0086 ±0.0017**	**33.3 ±6.6**	**3.49 ±0.19**
SOX-45	45	9.94 ±0.02	0.002	221	*186*	0	N/A	0.0243 ±0.0012	131 ±7	4.87 ±0.05
Experiments with ferrous iron added									"Catalyzed"	
SOX-Fe50(A)	25	9.82 ±0.01	0.02	220	*258*	46	~6-8	0.0153 ±0.0008	59.1 ±3.2	4.08 ±0.05
SOX-Fe50(B)	25	9.78 ±0.04	0.02	225	*258*	46	~4-6	0.0139 ±0.0007	53.9 ±2.8	3.99 ±0.05
Average (SOX-Fe50)		**9.80 ±0.02**						**0.0146 ±0.0009**	**56.5 ±3.7**	**4.03 ±0.07**
SOX-Fe150	25	9.81 ±0.03	0.02	226	*258*	153	~2	0.0175 ±0.0007	67.9 ±2.5	4.22 ±0.04
									"Uncatalyzed"	
SOX-Fe50(A)	"	"	"	"	"	"	"	0.0077 ±0.0008	29.8 ±3.1	3.39 ±0.10
SOX-Fe50(B)	"	"	"	"	"	"	"	0.0077 ±0.0005	29.8 ±1.8	3.39 ±0.06
SOX-Fe150	"	"	"	"	"	"	"	0.0081 ±0.0004	31.3 ±1.4	3.44 ±0.05

*Estimated under experimental conditions after Benson and Krause (1980; 1984) (http://water.usgs.gov/software/DOTABLES/).

Table 3.3: Isotopic analyses of sulfide from oxidation experiments. $f = [(H_2S)_T]/[(H_2S)_T]_{initial}$. $\delta^nS' = 1000\ln(^nR/^nR_{initial})$, where n = 33, 34, 36 and $^nR = {}^nS/{}^{32}S$. Extra significant figures for δ^nS' are reported to minimize rounding errors. Fractionation factors are computed via the Rayleigh equation (Equation 4) and are reported as: $^n\varepsilon_{P-R} = (^n\alpha_{P-R} - 1)x1000$, P = products, R = reactant. The reported uncertainties for fractionation factors and exponents are 1 s.d., and are based on least square linear regressions.

Identifier	T (°C)	$[Fe^{2+}]_{added}$	f	$\delta^{33}S'$	$\delta^{34}S'$	$\delta^{36}S'$	$^{33}\varepsilon_{P-R}$	$^{34}\varepsilon_{P-R}$	$^{36}\varepsilon_{P-R}$	$^{33}\lambda$	$^{36}\lambda$
SOX-5	5	0	1.006	0.000	0.000	0.000	-2.54	-5.00	-9.75	0.5072	1.95
			0.894	0.216	0.449	0.801	*±0.08*	*±0.14*	*±0.34*	*±0.0031*	*±0.02*
			0.712	0.864	1.725	3.362					
			0.619	1.210	2.381	4.573					
			0.574	1.387	2.745	5.348					
SOX-25(A)	25	0	0.990	0.000	0.000	0.000	-3.00	-5.90	-11.03	0.5089	1.88
			0.904	0.318	0.619	1.029	*±0.09*	*±0.14*	*±0.50*	*±0.0027*	*±0.06*
			0.795	0.635	1.265	2.094					
			0.701	1.062	2.080	3.773					
			0.642	1.315	2.580	4.824					
SOX-25(B)	25	0	1.000	0.000	0.000	0.000	-2.96	-5.81	-11.38	0.5098	1.96
			0.976	0.032	0.073	0.232	*±0.14*	*±0.27*	*±0.49*	*±0.0016*	*±0.02*
			0.826	0.610	1.209	2.389					
			0.721	0.904	1.779	3.525					
			0.666	1.215	2.382	4.708					
SOX-45	45	0	1.000	0.000	0.000	0.000	-3.24	-6.34	-12.27	0.5103	1.94
			0.817	0.643	1.269	2.517	*±0.12*	*±0.24*	*±0.43*	*±0.0016*	*±0.01*
			0.724	1.025	1.999	3.920					
			0.635	1.389	2.713	5.294					
			0.569	1.871	3.670	7.097					
SOX-Fe50 (A)	25	~50	1.000	0.000	0.000	0.000	-2.88	-5.66	-10.94	0.5081	1.94
			0.970	0.094	0.178	0.402	*±0.12*	*±0.21*	*±0.33*	*±0.0028*	*±0.02*
			0.930	0.210	0.397	0.738					
			0.751	0.952	1.835	3.461					
			0.654	1.248	2.454	4.734					
			0.574	1.564	3.068	5.971					
SOX-Fe50 (B)	25	~50	1.000	0.000	0.000	0.000	-2.83	-5.59	-10.77	0.5059	1.93
			0.958	0.044	0.115	0.365	*±0.21*	*±0.41*	*±0.77*	*±0.0025*	*±0.04*
			0.911	0.170	0.359	1.018					
			0.766	0.916	1.827	3.653					
			0.653	1.174	2.319	4.675					
			0.573	1.496	2.977	5.816					
SOX-Fe150	25	~150	1.000	0.000	0.000	0.000	-2.49	-4.90	-9.62	0.5074	1.97
			0.874	0.316	0.604	1.033	*±0.07*	*±0.11*	*±0.19*	*±0.0032*	*±0.03*
			0.742	0.789	1.543	2.804					
			0.644	1.126	2.198	4.188					
			0.585	1.367	2.661	5.112					
			0.527	1.561	3.084	6.027					

Chapter 4: Conclusions and Future Directions

This dissertation contains the results of efforts directed at the determination of isotope effects in inorganic aqueous sulfur systems. The motivation for these determinations is largely articulated in the context of constraining isotope fractionations that can occur as part of the much broader sulfur cycle. This chapter will review some of the primary highlights from the results of this dissertation and give an overview of future directions of my research into isotope partitioning among aqueous sulfur compounds.

1.0 Highlights

Chapter 2

1) My theoretical calculations of equilibrium fractionation factors generally compare reasonably well to the available experimental constraints, indicating that explicit solvation models applied to aqueous sulfur compounds and computed at low/moderate levels of theory (B3LYP/6-31+G(d,p)) without any form of frequency scaling can reproduce experimental data within a reasonable estimation of uncertainty.
2) My calculations highlight the fundamental first order controls on the isotope fractionation behavior of aqueous sulfur compounds in the sulfide, thiosulfate, sulfoxylate, sulfite, and sulfate systems, and define the broad ranges in fractionation factors based on the traditional $^{34}S/^{32}S$ measurements as well as those of the minor isotopes. These calculations will have value especially in

the present implementation of network models of microbial metabolisms such as sulfate reduction (e.g., Wing and Halevy, 2014).

3) My theoretical calculations further refine the exponents defining mass-dependent relationships associated with equilibrium isotope exchange in aqueous systems, which are presently the basis of the widely applied reference exponents in sulfur isotope studies of $^{33}\lambda_{ref}$ = 0.515 and $^{36}\lambda_{ref}$ = 1.9. My calculations allow for the quantification of the range of exponents associated with equilibrium isotope exchange, which rarely vary outside the range of ca. $^{33}\lambda \approx$ 0.514-0.516 and $^{36}\lambda \approx$ 1.89-1.90 over temperatures relevant to most aqueous systems. The exceptions to these rules appear to be in systems where crossovers exist (e.g., thiosulfate/sulfide), but these would be restricted to specific temperature conditions and would not produce any substantial $\Delta^{33}S$ or $\Delta^{36}S$ effects at any temperature, and would require subsequent amplification for their expression (e.g., Deines, 2003).

4) Utilizing my calculations for aqueous sulfite compounds and the available isomerization quotients, I am able to reproduce the experimental $^{34}S/^{32}S$ fractionations determined in the $SO_{2(g)}/HSO_3^-{}_T$ system by Eriksen (1972a,b,c). These calculations indicate that the isomerization of bisulfite exerts a primary control on isotope fractionations involving sulfite compounds, due to the high magnitude RPFR of the bisulfite isomer present in minor abundance at low temperature: $(HS)O_3^-$. I point out that the isomerization quotient defining the relative abundances of $(HO)SO_2^-$ and $(HS)O_3^-$ has yet to be quantified over a wide range of temperatures as a function of ionic strength, and indicate that

such constraints will be necessary for the further evaluation of the full effect of bisulfite isomerization on isotope partitioning in (bio)geochemical systems. I further speculate that bisulfite isomerization may have implications for the mechanism of the interactions between sulfite compounds and the active siroheme sites of enzymes that are responsible for the stepwise reduction/oxidation of sulfite/sulfide in microbial metabolism (e.g., dissimilatory sulfite reductase), which may have influence on the overall magnitudes of fractionations expressed during these transformations.

Chapter 3

1) The rates and activation energy that I derive from my aqueous sulfide oxidation experiments compare well to the extensive experimental work of the Frank J. Millero group (Millero et al., 1987a; Zhang and Millero, 1993), but kinetic parameters derived from experiments in the literature are generally variable. Such variability may be the result of unintended trace metal catalysis that may have additionally impacted the experimental results of the present study based on the much lower oxidation rates obtained by Luther et al. (2011) under trace metal clean conditions.
2) My experiments reproduce induction periods that have been observed in some previous studies (Chen and Morris, 1972a) that furthermore indicate that the reaction of HS^- with O_2 proceeds slowly and likely via an autocatalytic mechanism that is not well understood in detail. We appear to observe that induction periods are shortened upon ferrous iron catalysis, and further note

that inconsistencies in the observation of induction periods in the literature may be another impact of unintended trace catalysis.

3) The major isotope fractionation factors ($^{34}S/^{32}S$) that I derive from my experiments are consistent with the previous experiments under comparable conditions by Fry et al. (1988).

4) Small but resolvable relationships between $^{34}S/^{32}S$ fractionation factor and rate associated with ferrous iron catalysis appear to be observed, where increased catalysis appears to decrease the magnitude of the isotope fractionation factor at the levels we have studied. This may be the result of smaller magnitude isotope effects associated with pathways of lower activation energy that are provided by the catalytic cycle associated with ferrous iron.

5) The measured $^{34}S/^{32}S$-based fractionation magnitudes appear to increase with increasing rate due to increased temperature, indicating apparent inverse fractionation temperature dependence associated with sulfide oxidation. The origin of this inverse effect is ultimately unclear, and may either be due to the competition of low and high frequency modes between sulfide and any number of key transition states it may form with reactants as part of the mechanism (e.g., reactive oxygen species or even reactive sulfur intermediates) or the result of more than one "rate-determining" reaction with different isotope effects having a substantive influence on overall rates and isotopic fractionations. This observation may also be providing evidence for

reversible isotope exchange between residual sulfide and reactive sulfur intermediates (e.g., along the pathway to thiosulfate formation).

6) All fractionation factors derived from my experiments appear to exhibit a mass dependence with respect to $^{33}S/^{32}S$ and $^{34}S/^{32}S$ relationships that is distinguishable at a resolvable level from the range expected for equilibrium isotope exchange, and may also be present for $^{36}S/^{32}S$ and $^{34}S/^{32}S$ relationships. We do not appear to resolve any differences in these relationships as a function of sulfide oxidation rate associated with either ferrous iron catalysis or temperature. This observation will change how chemical oxidation processes are treated in future models of the sulfur cycle that are based on all three isotope ratios of sulfur.
7) Based on a comparison to available biological constraints (Zerkle et al., 2009), my data do not seem to indicate a robust biosignature for sulfide oxidation processes based on multiple sulfur isotope relationships. However, the isotope effects related to chemical and phototrophic sulfide oxidation may cause residual sulfide undergoing oxidation to follow different trajectories in $\delta^{34}S/\Delta^{33}S$ space, potentially allowing these two pathways to be isotopically resolved under some circumstances.

2.0 Future directions

High temperature fractionations between SO_2/H_2S: A role for S_3^-?

One obvious fractionation factor that can be computed from the theoretical data presented in Chapter 2 that was omitted from my analysis is that between sulfur dioxide and hydrogen sulfide (SO_2/H_2S), which may play a role in isotope

partitioning in high temperature magmatic and hydrothermal systems and can influence the isotopic composition of volcanogenic sulfur gases in certain geologic environments (e.g., Thode et al., 1971 and references therein). The studies of Thode's group (i.e., Grinenko and Thode, 1970; Thode et al., 1971) appear to be the only experimental investigations of these fractionation factors that are available. The experiments of Thode et al. (1971) were performed in the temperature range of ca. 500-1000˚C and were based on the equilibration of $SO_{2(g)}$ and $H_2S_{(g)}$ (derived from elemental sulfur via hydrolytic disproportionation, i.e.: $3S^0 + 2H_2O = 2H_2S + SO_2$) and their rapid quenching via a liquid nitrogen trap, from which the two gases were cryogenically separated in a series of cold traps of varying temperature for their respective isotopic analysis. The experiments of Grinenko and Thode (1970) performed at lower temperature (ca. 350-500˚C) were slightly more complex, where pairs of SO_2/S^0 and H_2S/S^0 were isolated and isotopically analyzed from experiments performed at the same temperature and the fractionation factor derived by taking the quotient of the two. The results from these two approaches are plotted in Figure 4.1 and appear to form a fairly consistent array as a function of temperature over ca. 350-1000˚C.

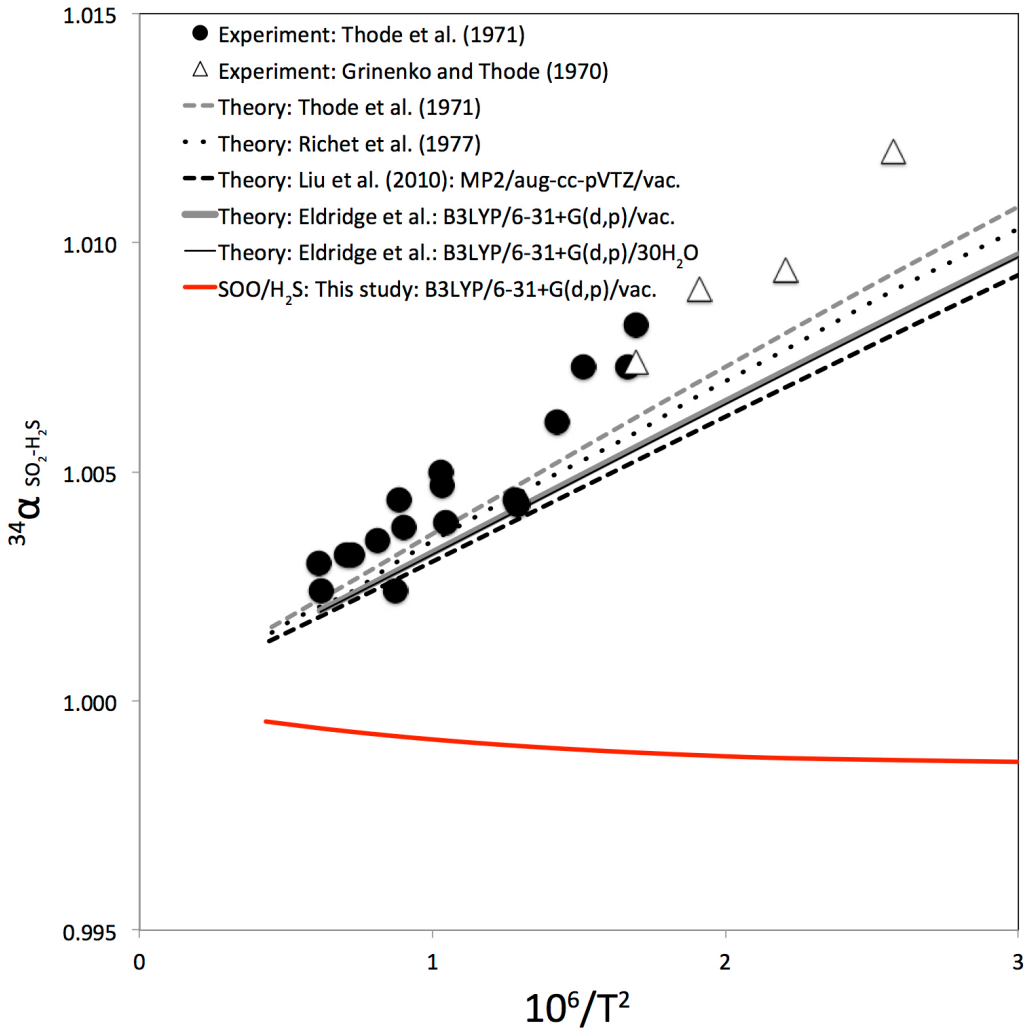

Figure 4.1: Comparison between the experimental determinations (data points) and theoretical estimations (curves) of the equilibrium isotope fractionation factor between SO_2 and H_2S.

Thode et al. (1971) originally noted a disagreement between their experimental determinations and theoretical fractionations that they calculated using the vibrational spectra for SO_2 and H_2S available at the time. This disagreement is highlighted in Figure 4.1 and includes additional theoretical estimates including my own based on RPFRs presented in Chapter 2 and others in the literature (Thode et al., 1971; Richet et al., 1977; Liu et al., 2010). The two general approaches indicate substantially different trajectories for the fractionation factor as a function of

temperature, where the offset ranges from 2.5 – 4 ‰ at the lowest temperature (~ 350 ˚C; Grinenko and Thode, 1970) depending on the theoretical approach. The theoretical constraints all agree within about 1 ‰ over the plotted temperature range and the calculations based on recent quantum mechanical calculations (Chapter 2; Liu et al., 2010) agree with each other at the level of ≤ 0.5 ‰. The broad agreement among the theoretical calculations relative to the experimental constraints would seem to suggest that the offset arises either from issues with the experimental determinations or a mismatch in the consideration of the sulfur mass balance between the two approaches, both of which Thode et al. (1971) originally suggested.

The presence of another sulfur compound under experimental conditions that is either a component of SO_2 or H_2S, or is rapidly converted to either SO_2 or H_2S upon the quenching of SO_2 and H_2S, could have influenced the experimental determinations. Thode et al. (1971) intriguingly suggested that isomerization of SO_2 could be responsible for the offset between theory and experiment, citing the photolysis experiments of Norrish and Oldenshaw (1959) that postulated the existence of SO_2 isomers and the early theoretical study of Hayes and Pfeiffer (1968) that suggested that SO_2 isomerization may be the result of double minima present in the SO_2 electronic potential energy surface (PES). Later computations of the electronic PES of SO_2 revealed the possibility of an asymmetric form containing schematic bonding as SOO (Farantos et al., 1977). The most recent computations of the electronic PES in the ground state SO_2 system confirm that an SOO bonded form is a metastable local minimum in the PES for SO_2, and is separated from the global minimum SO_2 (OSO) by two transition states and another local minimum

corresponding to a metastable isomer in the symmetric OSO form (Rodrigues et al., 2002). I am not aware of any experiments that have directly detected any of these hypothetical isomers, and the relative proportions of these isomers in SO_2 gases as a function of temperature do not appear to be known. To at least partially investigate the possibility of SO_2 isomers influencing fractionations in the SO_2/H_2S system, I have computed in Figure 4.1 the fractionation factor between the asymmetric SOO isomer of SO_2 and H_2S (B3LYP/6-31+G(d,p)/vacuum; computed to be bent triatomic with S-O-O bond angle of ~122˚) and interestingly find that the fractionation is predicted to be in the opposite direction from the common symmetrical OSO form, indicating that the SOO form present in any amount cannot be responsible for the offset. The usage of higher levels of theory in this analysis (e.g., MP2/aug-cc-pVTZ or CCSD/aug-cc-pVTZ) would not affect this overall conclusion.

Recent discoveries of the stability of the S_3^- radical at elevated temperatures and pressures might provide clues to the offset in the SO_2/H_2S system that I am actively investigating with theoretical calculations. Solutions containing S_3^- were studied and known early (e.g., Giggenbach, 1970; Chivers, 1974) and S_3^- has long been known to be responsible for the blue coloring of sodalite minerals (e.g., McLaughlan and Marshall, 1970; Chivers, 1974), but S_3^- was only recently experimentally demonstrated to be a stable component in aqueous sulfur systems under equilibrium conditions at elevated temperatures and pressures relevant to geological environments (Pokrovski and Dubrovinsky, 2011; Pokrovski and Dubessy, 2015; see also the recent review of Chivers and Elder, 2013). From the recent study and analysis of Pokrovski and Dubessy (2015), it is generally understood that S_3^-

stability is enhanced by: (1) T ≥ 250˚C, (2) high sulfur contents (>5000 ppm S_{total}), (3) acidic to neutral pH conditions, and (4) oxygen fugacity (f_{O2}) conditions that favor the stability of coexisting mixed valence sulfur species. The maximum concentrations of S_3^- approach ~10% of sulfur compounds (~30% in terms of moles of the total sulfur in the system if comprised of mostly $H_2S/S_3^-/SO_4^{2-}$) in experiments performed at 500˚C, P = 750-1400 bars, with starting solutions of either $S_2O_3^{2-}$ or SO_4^{2-}/H_2S ([S_{total}] ≈ 0.3-1 *m*) (Pokrovski and Dubessy, 2015). At present, much uncertainty still exists in the relative abundance of S_3^- under conditions ≥ 500˚C where many of the experiments of Thode and colleagues (i.e., Thode et al., 1971) were performed.

Any role that S_3^- may have played in the experimental determinations of the SO_2/H_2S fractionation factor by Thode and colleagues will depend on several factors. First, S_3^- must be a major component of the sulfur mass balance under the experiments of Thode and colleagues and must contribute significant sulfur to H_2S and/or SO_2 upon the cryogenic quenching of H_2S and SO_2 such that it modifies the isotopic composition of either (with respect to each other) relative to their equilibrium values. The latter will largely depend on: (1) the relative proportions of $H_2S/SO_2/S_3^-$ under the experimental conditions, (2) the RPFRs of the S_3^- ion relative to SO_2 and H_2S, and (3) the stoichiometry, products, and any further isotope effects associated with the decomposition reactions of S_3^- that might occur upon cryogenic quenching.

Preliminary calculations that I have performed of the S_3^- ion in water clusters seem to indicate that at elevated temperatures, the RPFRs associated with all sulfur atoms in S_3^- are lower than that for H_2S. This means that S_3^- in equilibrium with SO_2

and H_2S is predicted to be isotopically depleted relative to both SO_2 and H_2S. If for the moment we assume that the inclusion of sulfur from S_3^- into SO_2 or H_2S upon cryogenic quenching does not have an associated isotope effect, the inclusion of any significant amounts of sulfur from S_3^- into either SO_2 or H_2S would be predicted to have the effect of driving their compositions towards more isotopically depleted values relative to their equilibrium compositions. In order for such a process to lead to an apparent enhancement in the fractionation factor between SO_2 and H_2S, the mass balance would likely have to favor the inclusion of most of the sulfur from S_3^- into H_2S.

The conversion of S_3^- upon cryogenic quenching of SO_2 and H_2S (e.g., approach of Thode et al., 1971) may involve the decomposition of S_3^- to H_2S and SO_2, possibly following an overall hydrolytic decomposition reaction:

$$6S_3^- + 10H_2O + 6\ H^+ = 5SO_2 + 13H_2S \qquad (6)$$

The stoichiometry of Equation 6 roughly coincides with two moles of sulfur from S_3^- going to H_2S per mole of S_3^-, and roughly one mole going to SO_2. If this is the dominant decomposition pathway, it could hypothetically lead to an apparent enhancement of the SO_2/H_2S fractionation factor measured by Thode et al. (1971) by shifting the composition of H_2S to more isotopically depleted values, the magnitude of the shift depending on the magnitudes of the fractionations involved and the mass balance of the system.

Alternatively, the conversion of S_3^- to SO_2 and H_2S upon quenching may follow an oxidation reaction considering that S_3^- stability is a strong function of f_{O2} (*cf.* Pokrovski and Dubessy, 2015), i.e.:

$$2S_3^- + 5O_2 + 2H^+ = 5SO_2 + H_2S \qquad (7)$$

Such a reaction would be predicted to include much more sulfur from S_3^- into SO_2, and if it were isotopically depleted as my preliminary calculations seem to suggest, this decomposition pathway would likely have the opposite effect to enhancing the apparent SO_2/H_2S fractionation factor. I will be able to investigate these possibilities in more quantitative detail when computations are completed of the solvated S_3^- $\bullet 36H_2O$ at the B3LYP/6-31+G(d,p) level that are presently ongoing utilizing the computation resources of the Scylla computer cluster at WHOI in collaboration with Weifu Guo. A detailed evaluation of the mass balance of the experimental systems of Thode's group will also be required, which may be at least partially possible under some of the experimental conditions using the thermodynamic data for the S_3^- ion presented in Pokrovski and Dubessy (2015).

The offset may also of course be due to experimental issues that Thode and colleagues originally discussed (*cf.* Thode et al., 1971). The source gas used for isotopic analysis was SO_2, and numerous corrections to the raw isotopic data had to be applied. These importantly include corrections related to the oxygen isotope compositions of source gases between SO_2 isolated directly from experiments and SO_2 derived from the combustion of Ag_2S that corresponded to H_2S isolated from experimental systems; the former critically relied on estimations of the oxygen isotope fractionation factor between SO_2 and H_2O under the elevated temperatures of experimental conditions and the assumption had to be made that this equilibrium was not reset or altered upon quenching or subsequent processing. Other corrections had to be applied for non-equilibrium conversion to elemental sulfur in some experiments

upon quenching, which was assumed to be independent of temperature. Thode et al. (1971) noted potential limitations in their ability to adequately quantify these corrections and indicated that they may also be responsible for the offset between theory and experiment, in lieu of more complicated arguments involving the hypothetical influence of other sulfur compounds. Updated constraints on these fractionation factors utilizing modern SF_6 techniques may circumvent at least some of the issues encountered by Thode and colleagues. However, the intriguing possibility that S_3^- may comprise a significant proportion of the mass balance of such experiments (Pokrovsky and Dubessy, 2015) and may be the primary species through which isotope exchange occurs between SO_2 and H_2S (*cf.* Truche et al., 2014; Pokrovsky and Dubessy, 2015) will likely require a new and detailed experimental evaluation that may be aided by theoretical calculations such as my own.

Appendices

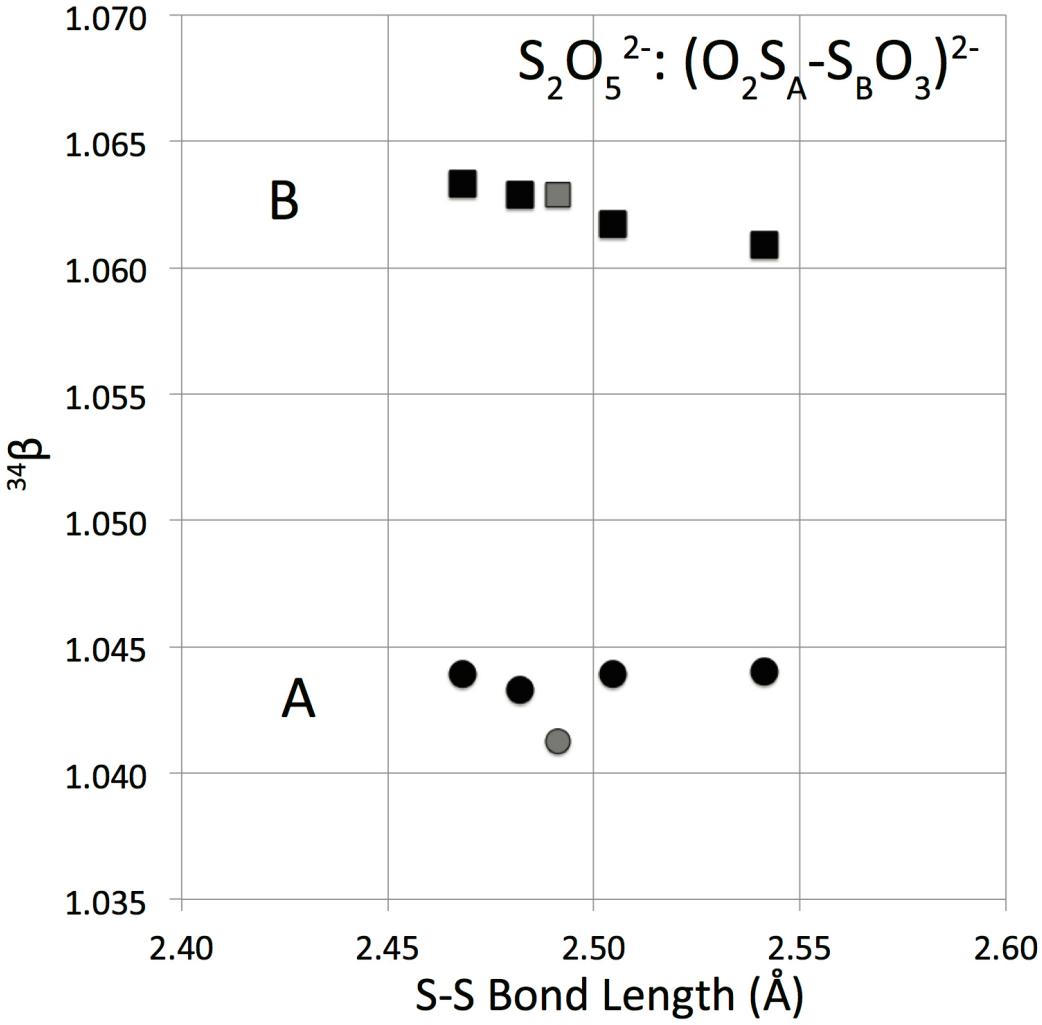

Figure A.1: RPFRs of the two sulfur sites in pyrosulfite ($S_2O_5^{2-}$•30-40H_2O) at the B3LYP/6-31+G(d,p) level as a function of S-S bond length (note: there is no correlation between RPFR magnitudes and solvation coverage or water cluster size over this range). The black squares indicate the four-fold-coordinated site 'B' and the white circles indicate the three-fold-coordinated site 'A'. The gray data points are the same calculations but in vacuum (i.e., $S_2O_5^{2-}{}_{vacuum}$) and are included for reference.

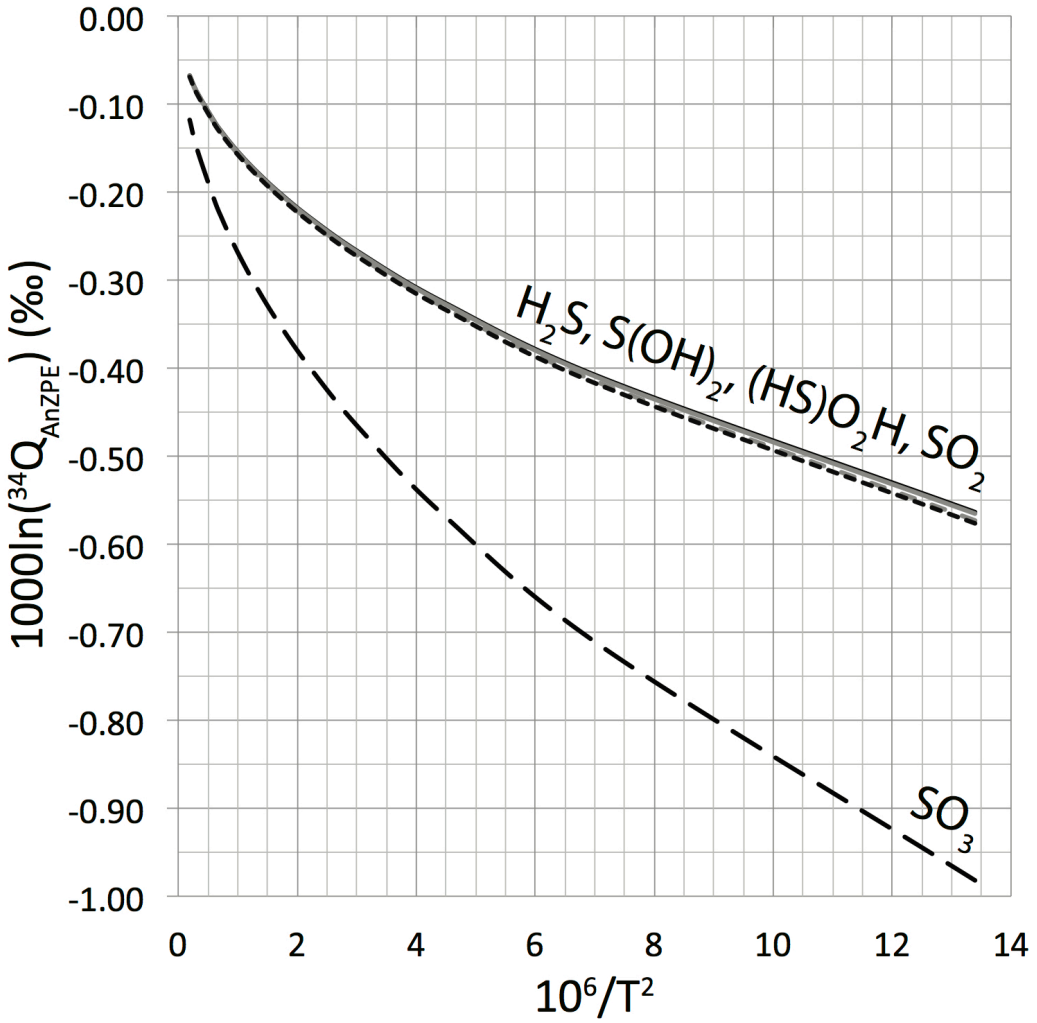

Figure A.2: Anharmonic correction to the zero point energy (AnZPE) (*cf.* Liu et al., 2010) for RPFRs presented as permil values (‰) over T = 0-2000˚C at the B3LYP/6-31+G(d,p) level for gaseous sulfur molecules spanning a range of oxidation state (S^n): $H_2S_{(g)}$ (n = -2), $S(OH)_{2(g)}$ and $(HS)O_2H_{(g)}$ (n = +2), $SO_{2(g)}$ (n = +4), and $SO_{3(g)}$ (n = +6).

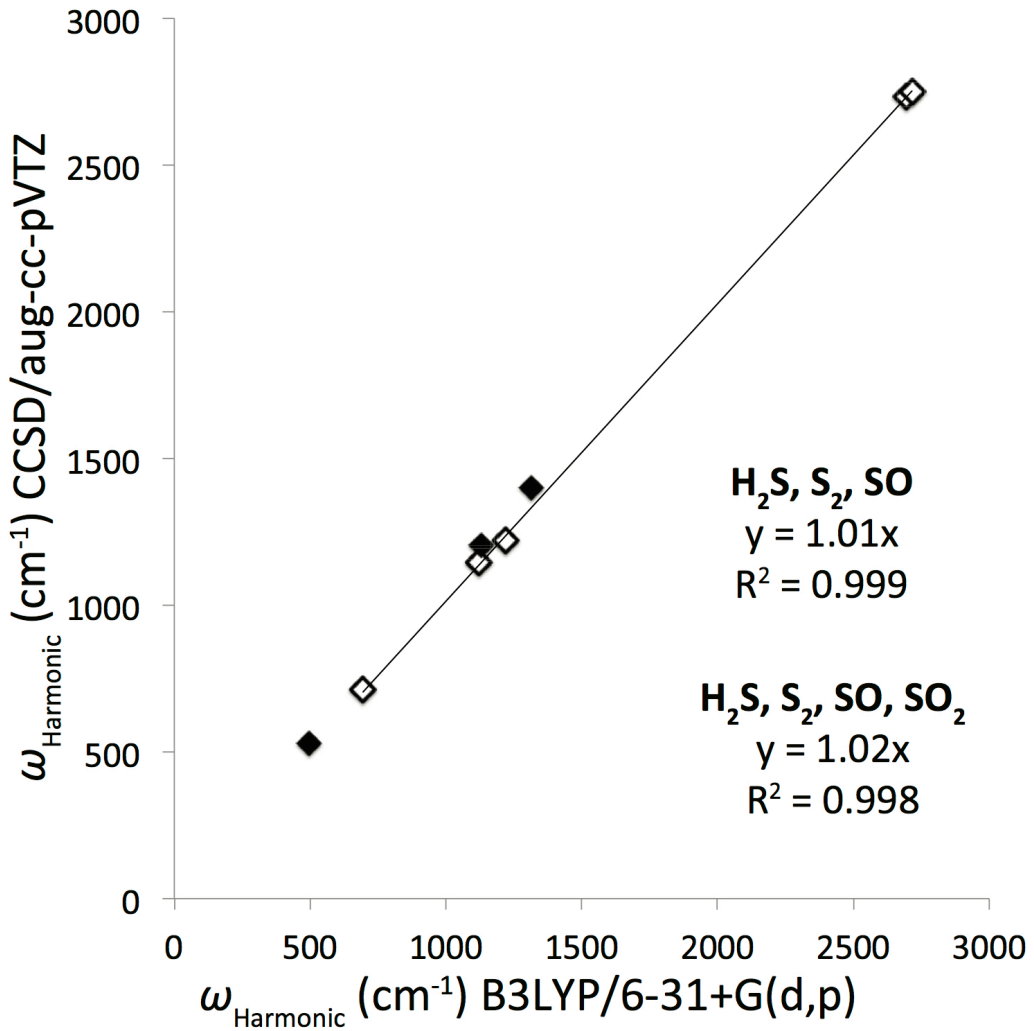

Figure A.3: Harmonic frequency scaling factors (based on harmonic wave numbers, $\omega_{Harmonic}$) for the B3LYP/6-31+G(d,p) level derived from CCSD/aug-cc-pVTZ calculations of gaseous sulfur molecules (*cf.* Li and Liu, 2011) and based on least squares linear regressions. The black diamonds correspond to $SO_{2(g)}$ (individual scaling factor of ≈ 1.065) and the white diamonds correspond to $H_2S_{(g)}$, $S_{2(g)}$, and $SO_{(g)}$ (scaling factor of ≈ 1.01). The scaling factor of ≈ 1.02 is derived from consideration of all gaseous molecules in the figure.

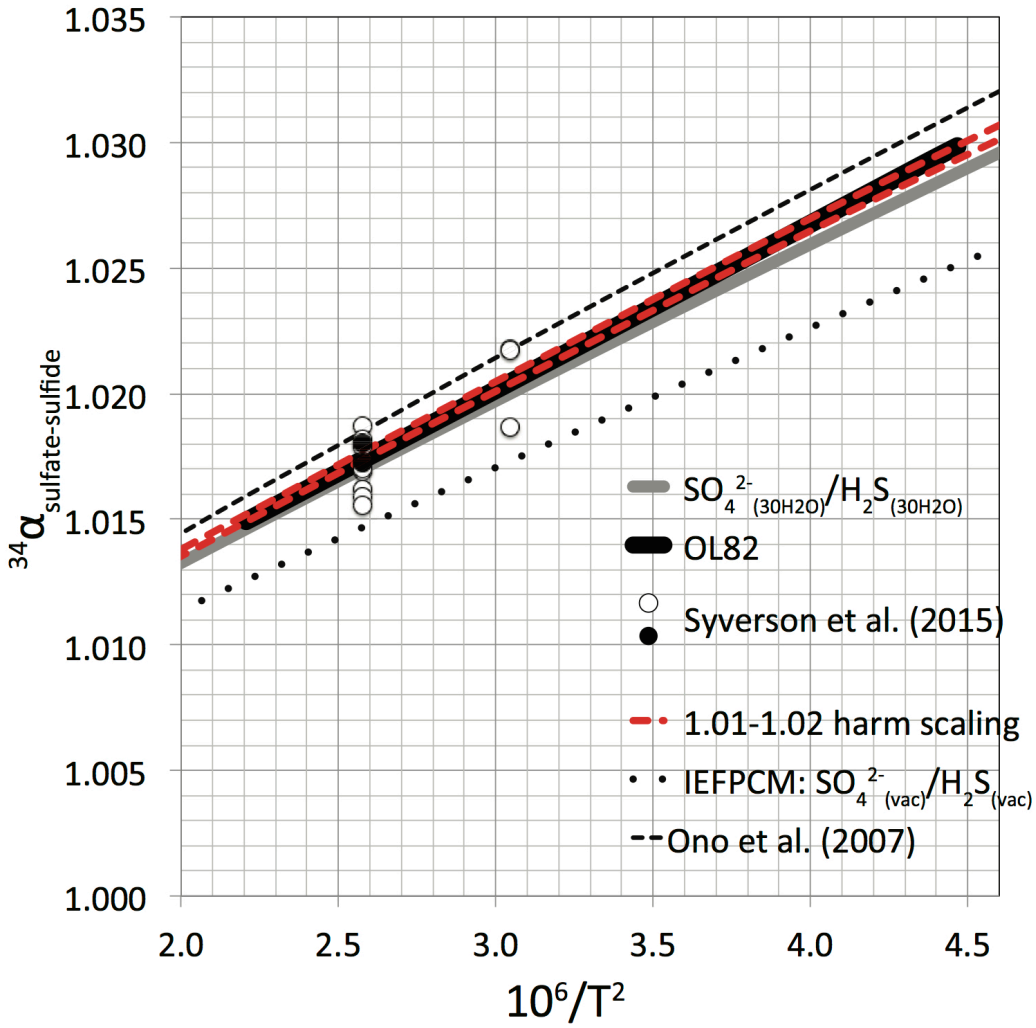

Figure A.4: Major isotope fractionation factor in the sulfate(SO_4^{2-})-sulfide(H_2S) system focusing on the effect of harmonic frequency scaling on our estimated theoretical fractionation factors. Applying harmonic scaling factors of 1.01-1.02 (derived from CCSD/aug-cc-pVTZ calculations in gas phase; red dashed curves) appears to place our theoretical constraints (unscaled: gray solid curve) in better agreement with the experimental constraints of Ohmoto and Lasaga (1982) (black curve) and Syverson et al. (2015) (black circles = demonstrably equilibrated) over the temperature range of 200-400˚C. Also presented for reference are our own calculations in the gas phase with the IEF-PCM implicit solvation model applied (dashed dots) and previous vibrational spectroscopy-based estimates (based on experimental fundamental frequencies with computed frequency shifts) from Ono et al. (2007). In all cases, our calculations that apply the explicit solvation model appear to match the experimental data far better than any other approach.

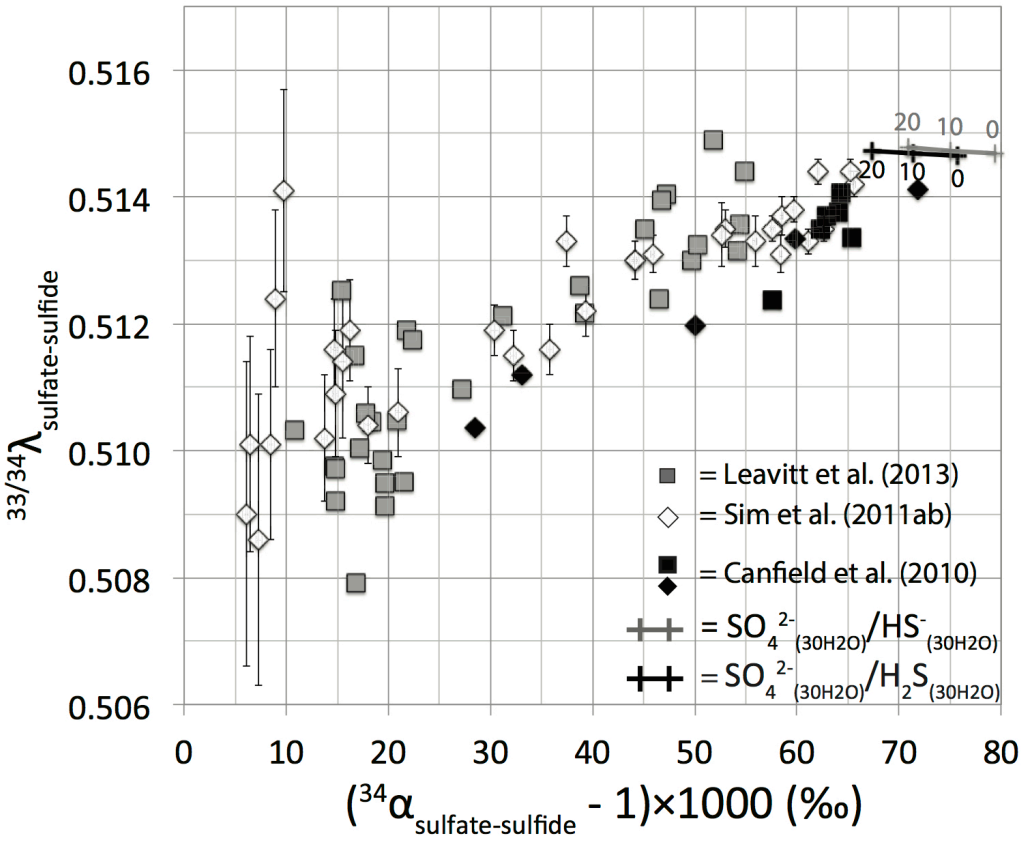

Figure A.5: The exponent of mass dependence ($^{33/34}\lambda$) and major isotope ratio fractionation factor ($^{34}\alpha_{sulfate\text{-}sulfide}$) reported from recent pure culture experiments (~20˚C; Leavitt et al., 2013; Sim et al., 2011a; Sim et al., 2011b) and natural populations (5˚C; Canfield et al., 2010). For the pure culture experiments, cell specific sulfate reduction rates (csSRR) generally decrease from left to right in the plot, where the largest $^{34}\alpha_{sulfate\text{-}sulfide}$ correspond to the lowest csSRRs and appear to approach equilibrium values (our theoretical calculations from 0-20˚C shown for reference; see also Wing and Halevy, 2014 for model-based discussions of these relationships). csSRRs were not measured in the natural population experiments of Canfield et al. (2010) but fractionations appear to follow broadly similar fractionation trends in this composition space to the pure culture experiments.

Synopsis of Lessons Learned: Experimental Design of Sulfide Oxidation

A schematic diagram of the apparatus used in the experiments presented in Chapter 3 is shown in Figure A.6. The design that was finally chosen to carry out the experiments to collect the data presented in Chapter 3 ended up being the simplest, and also perhaps not the most optimal for a diverse range of measurements. For example, the design of Chapter 3 did not allow for the determination of the isotopic compositions of the products and intermediates of sulfide oxidation, which would further constrain the isotopic mass balance of the reaction and also perhaps elucidate some of the strange isotope fractionation behavior observed in residual sulfide. Included in this appendix section will be a summary of the experimental designs that led up to the design in Chapter 3, and a series of brief notes to the experimenter wishing to improve upon the design for further exploration of the rates and isotopic fractionations associated with sulfide oxidation.

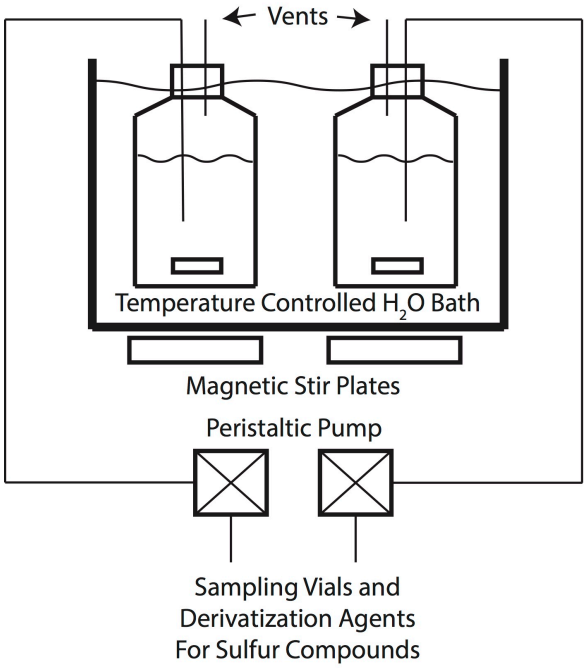

Figure A.6: Schematic of apparatus used in sulfide oxidation experiments presented in Chapter 3.

The first set of experiments that I carried out that served the basis for generating preliminary data for grant proposals (not presented in this dissertation) were performed very closely to the design of Fry et al. (1988). I used a 1 L glass septum bottle that I filled with a 1 L phosphate buffer solution. This bottle was purged with ultra high purity molecular oxygen from a tank for about an hour before I transferred the bottle into an anoxic chamber under N_2 atmosphere (temperature control ~ 25˚C). Sulfide was injected into these bottles from stock solutions prepared as described in Chapter 3, but in this case using a metal syringe to pierce the septum ($[HS^-]_{initial}$ = 0.001-0.01 M). Aliquots for concentration and isotopic analysis were collected using a metal syringe as the reaction took place, and ambient atmosphere (N_2) was drawn into the vessel upon sampling to maintain pressure within the vessel. These experiments were the first to show small shifts in the $\Delta^{33}S_{P\text{-}R}$ associated with sulfide oxidation (consistent with the results presented in Chapter 3), although revealed a major isotope fractionation factor that was on the low end of the range measured by Fry et al. (1988) that was on the order of $^{34}\varepsilon_{P\text{-}R}$ ~ -3-4‰, and lower than any fractionation factors that were later measured as part of the dataset in Chapter 3. Rate information could in principle be extracted from these experiments but was complicated by ambiguity in the oxygen concentration of the experiment, including its starting concentration and the ambiguity related to changes in its partial pressure as aliquot sampling commenced. Numerous elements of the design of these first experiments were not ideal, including the usage of glass bottles (cleaned with detergent), metal syringes for injection and sampling, and poor oxygen control, that undoubtedly contributed trace catalysts for the reaction in addition to making the

measurement of rates difficult. Designs of this kind are not recommended for relatively clean and detailed studies of sulfide oxidation.

After collecting a round of preliminary data for grant proposals following this design, it became apparent to me that the experiments really needed to be designed with quantifying rates in mind. The earliest conceptions of these experiments also ambitiously included the measurement of the isotopic compositions of the intermediates and products (e.g., sulfite, thiosulfate, sulfate), and so were conceived to have relatively high initial sulfide concentrations (as in the preliminary experiments, $[HS^-]_{initial}$ = 0.001-0.01 M). Because dissolved oxygen in aqueous solution in equilibrium with air only has a concentration on the order of 250 μM, oxygen was also conceived to be scaled-up in these experiments so that it would not become limiting and complicate the measurements of rates. I was generally aware of the issue of trace metal catalysis at this point but did not appreciate the full magnitude of the problem, and so was still using glass apparatuses (mostly detergent cleaned) for reaction vessels at this time.

These basic considerations led to a design of the experiments where the headspace of the reaction vessel was connected to an ultra high purity oxygen tank with pressure control via a series of regulators that I had scavenged from an old gas chromatography system (*cf.* Figure A.7). The reaction vessels were still glass, and included custom made rubber stoppers that included glass tubes for both aliquot sampling and connection of the headspace to the O_2 tank and regulator system. Numerous experiments were carried out with this design with the help of undergraduate student Noah Bowman for his senior thesis project. For this series of

experiments, we focused only on constraining the kinetics of the reaction and did not collect aliquots for isotopic analysis. We were also performing these experiments utilizing the temperature baths described in Chapter 3 for more refined temperature control.

Generally speaking, experiments with this design did not yield very reproducible kinetic data. Plots of $\ln[HS^-]$ vs. time did not generally yield linear trends conforming to pseudo first order kinetics and instead yielded trends with broad sinusoidal behavior in many cases. I interpreted this behavior as likely being the result of poor control of oxygen partial pressure in the experimental systems via the regulators since the extraction of the pseudo first order rate constant is a function of oxygen concentration, but did not systematically test this hypothesis much further. Additionally, quantification of the oxygen concentrations in the experiments proved difficult for numerous reasons. To this end, I went as far as making a custom-made flow-through glass reactor designed to fit a DO probe for direct measurements of oxygen in the reaction solution extracted from the pressurized vessel via peristaltic pump, but this did not prove viable. It was also during this time that we became fully appreciative of the severity of the issue of trace metal catalysis via the detailed reading of Luther et al. (2011). These considerations led to a complete re-design of the experiments, including the usage of entirely plastic components (to undergo extensive acid cleaning prior to loading with reaction solutions) and also a much simpler manner in which oxygen is supplied to the vessel that would allow its quantification for the estimation of overall rate constants. Hence, the design described in Chapter 3 that yielded the dataset that is the basis for the chapter (Figure A.6).

In retrospect, there are numerous elements of the experimental design that could be improved for follow-up experiments to those presented in Chapter 3. Future experiments should be concentrated at least on measuring the isotopic compositions of products and intermediates as I had originally conceived, in addition to the rates and isotope effects based on sulfide analyses. These will likely require a design that can be thought of as a combination of the approaches of Chapter 3 and the experiments utilizing oxygen supply and control via an O_2 tank connected to the headspace that Noah and I had attempted prior. Below I list some simple considerations for such experiments:

(1) All reaction vessel components will need to be plastic, as in Chapter 3, to minimize the introduction of trace catalysts. These may either be prepared as described in Chapter 3, which reproduce the rates of the Frank Millero group, or prepared in the manner of Luther et al. (2011) to study increasingly "less catalyzed" systems.

(2) Oxygen partial pressure control should be possible in principle utilizing more modern and precise regulators than we employed. Additional considerations for these systems would be to make them relatively trace metal clean. It is conceivable that particulates containing metals could be introduced into the reaction vessel via the tanks and regulator systems. Components on these lines may thus need to be equipped with filtration measures to remove particulates, particularly in immediate vicinity to the headspace of reaction vessels. These might include a series of filters of increasingly fine mesh size. It is

conceivable that components of these gas delivery systems may also need to be acid-washed plastic, but this may be a secondary consideration.

(3) Magnetic stir bars were implemented in our design with stir rates on the order of 400-600 revolutions per minute. More vigorous stirring and mixing systems may improve air/solution O_2 exchange. Their implementation will need to involve consideration of trace metal contamination.

(4) An additional issue that was not discussed in Chapter 3 is the catalytic effect of light (direct or indirect) on reaction rates. Reactions between light and oxygen compounds in aqueous solution may produce the reactive oxygen species that might serve as autocatalysis for sulfide oxidation as part of the overall mechanism. The photo-oxidation of ferrous iron, used as an explicit catalyst in a set of experiments in Chapter 3, could also influence results when such catalysts are employed. The experiments presented in Chapter 3 were continuously monitored over timescales of days and performed under varying light conditions. Light contributions were solely from fluorescent lights in the laboratory (no windows are present in the labs). The plastic bottles used were not fully transparent to light but also not fully opaque either, and opaque plastic bottles may be ideal for future experimentation to avoid any potential effects associated with light. It should be noted that there is no systematic relationship between when lights were on or off and the major features of the kinetic behavior seen in concentration profiles (e.g., induction periods and breaks in rate attributed to the exhaustion of the ferrous iron catalysts), and it

is not expected to be a major influence on the results of Chapter 3. This, however, does not preclude its consideration in future experimental designs.

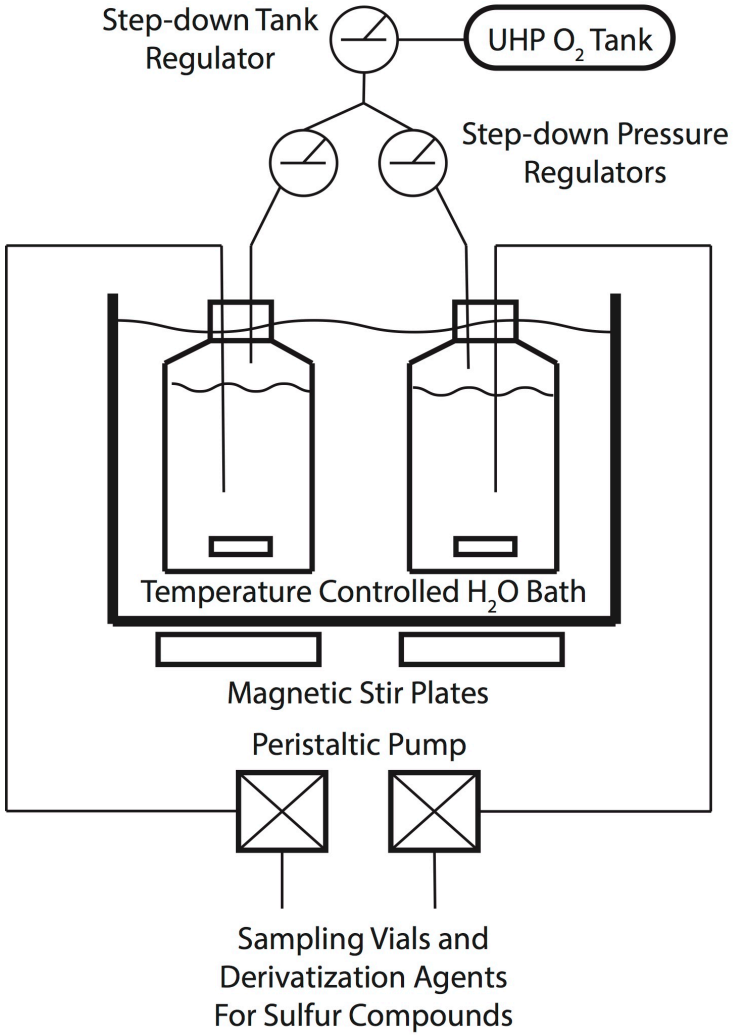

Figure A.7: Schematic of experimental apparatus that may allow the isotopic analysis of oxidation products in addition to the isotopic analysis and rates based on reactant sulfide via scaling up both oxygen and sulfide concentrations in the experiment.

Bibliography

Almgren T. O. M. and Hagstrom I. (1974) The Oxidation Rate of Sulphide in Sea Water. *Water Research* **8**, 395-400.

Amrani A., Kamyshny A., Lev O. and Aizenshtat Z. (2006) Sulfur Stable Isotope Distribution of Polysulfide Anions in an (NH4)2Sn Aqueous Solution. *Inorg. Chem.* **45**, 1427–1429.

Avrahami M. and Golding R. M. (1968) The oxidation of the sulphide ion at very low concentrations in aqueous solutions. *J. Chem. Soc. A Inorganic, Phys. Theor.* **68**, 647-651.

Bach W. and Edwards K. J. (2003) Iron and sulfide oxidation within basalt ocean crust: Implications for chemolithoautotrophic microbial biomass production. *Geochim. Cosmochim. Acta* **67**, 3871–3887.

Becke A. D. (1993) Density functional thermochemistry: the role of exact exchange. *J. Chem. Phys.* **98**, 5648–5652.

Benson B. B. and Krause Jr. D. (1980) The concentration and isotopic fractionation of gases dissolved in freshwater in equilibrium with the atmosphere. 1. Oxygen. *Limnol. Oceanogr*, **25**, 662-671.

Benson B. B. and Krause D. (1984) The concentration and isotopic fractionation of oxygen dissolved in freshwater and seawater in equilibrium with the atmosphere. *Limnol. Oceanogr.* **29**, 620–632.

Beyad Y., Burns R., Puxty G. and Maeder M. (2014) A speciation study of sulfur(iv) in aqueous solution. *Dalton Trans.* **43**, 2147–52.

Bigeleisen J. (1949) The Relative Reaction Velocities of Isotopic Molecules. *J. Chem. Phys.* **17**, 675–678.

Bigeleisen J. and Mayer M.G. (1947) Calculation of equilibrium constants for isotopic exchange reactions. *J. Chem. Phys.* **15**, 261-267.

Bigeleisen J. and Wolfsberg M. (1958) Theoretical and Experimental Aspects of Isotope Effects in Chemical Kinetics. *Adv. Chem. Phys.* **1**, 15–76.

Bourne D.W.A., Higuchi T. and Pitman I.H. (1974) Chemical equilibria in solutions of bisulfite salts. *J. Pharm. Sci.* **63**, 865-868.

Bowles M. W., Mogollón J. M., Kasten S., Zabel M. and Hinrichs K.-U. (2014) Global rates of marine sulfate reduction and implications for sub-sea-floor metabolic activities. *Science* **344**, 889–91.

Bradley A. S., Leavitt W. D. and Johnston D. T. (2011) Revisiting the dissimilatory sulfate reduction pathway. *Geobiology* **9**, 446–457.

Bradley A. S., Leavitt W. D., Schmidt M., Knoll A. H., Girguis P. R. and Johnston D. T. (2016) Patterns of sulfur isotope fractionation during microbial sulfate reduction. *Geobiology* **14**, 91–101.

Brandt C. and van Eldik R. (1995) Transition Metal-Catalyzed Oxidation of Sulfur(IV) Oxides. Atmospheric-Relevant Processes and Mechanisms. *Chem. Rev.* **95**, 119–190.

Brunner B. and Bernasconi S. M. (2005) A revised isotope fractionation model for dissimilatory sulfate reduction in sulfate reducing bacteria. *Geochim. Cosmochim. Acta* **69**, 4759–4771.

Canfield D. E. (2001) Biogeochemistry of Sulfur Isotopes. *Rev. Mineral. Geochemistry* **43**, 607–636.

Canfield D. E. (2004) The evolution of the Earth surface sulfur reservoir. *Am. J. Sci.* **304**, 839–861.

Canfield D. E. and Teske a (1996) Late Proterozoic rise in atmospheric oxygen concentration inferred from phylogenetic and sulphur-isotope studies. *Nature* **382**, 127–132.

Canfield D. E. and Thamdrup B. (1994) The production of 34S-depleted sulfide during bacterial disproportionation of elemental sulfur. *Science* **266**, 1973–1975.

Canfield D. E., Farquhar J. and Zerkle A. L. (2010) High isotope fractionations during sulfate reduction in a low-sulfate euxinic ocean analog. *Geology* **38**, 415–418.

Chacko T., Cole D. R. and Horita J. (2001) Equilibrium Oxygen, Hydrogen and Carbon Isotope Fractionation Factors Applicable to Geologic Systems. *Rev. Mineral. Geochemistry* **43**, 1–81.

Chen K.Y. and Morris J.C. (1972a) Kinetics of Oxidation of Aqueous Sulfide by O2. *Environ. Sci. Technol.* **6**, 529–537.

Chen K.Y. and Morris J.C. (1972b) Oxidation of Sulfide by O2: Catalysis and Inhibition. *J. Sanit. Eng. Div.* **98**, 215–227.

Chivers T. (1974) Ubiquitous trisulphur radical ion S3-. *Nature* **252**, 32–33.

Chivers T. and Elder P. J. W. (2013) Ubiquitous trisulfur radical anion: fundamentals and applications in materials science, electrochemistry, analytical chemistry and geochemistry. *Chem. Soc. Rev.* **42**, 5996.

Chmielewski A. G., Derda M., Wierzchnicki R. and Mikolajczuk A. (2002) Sulfur isotope effects for the {SO2(g)-SO2(aq)} system. *Nukleonika* **47**, S69–S70.

Chu X-L. and Ohmoto H. (1991) Kinetics of isotope exchange reactions involving intra- and intermolecular reactions: I. Rate law for a system with two chemical compounds and three exchangeable atoms. *Geochim. Cosmochim. Acta* **55**, 1953–1961.

Chu X-L., Ohmoto H. and Cole D. R. (2004) Kinetics of sulfur isotope exchange between aqueous sulfide and thiosulfate involving intra- and intermolecular reactions at hydrothermal conditions. *Chem. Geol.* **211**, 217–235.

Clayton R. N. and Mayeda T. K. (1996) Oxygen isotope studies of achondrites. *Geochim. Cosmochim. Acta* **60**, 1999–2017.

Cline J.D. and Richards F. (1969) Oxygenation of hydrogen sulfide in seawater at constant salinity, temperature and pH. *Environ. Sci. Technol.* **3**, 838–843.

Cline J.D. (1969) Spectrophotometric Determination of Hydrogen Sulfide in Natural Waters. *Limnol. Oceanogr.* **14**, 454–458.

Colman J. J., Xu X., Thiemens M. H. and Trogler W. C. (1996) Photopolymerization and Mass-Independent Sulfur Isotope Fractionations in Carbon Disulfide, *Science*, **273**, 774–776.

Connick R.E. and Zhang Y.-X. (1996) Kinetics and Mechanism of the Oxidation of HSO3- by O2. 2. The Manganese(II)-Catalyzed Reaction. *Inorg Chem* **35**, 4613–4621.

Connick R.E., Tam T. M. and Von Deuster E. (1982) Equilibrium constant for the dimerization of bisulfite ion to form disulfite(2-) ion. *Inorg. Chem.* **21**, 103–107.

Connick R.E., Zhang Y.-X., Lee S., Adamic R. and Chieng P. (1995) Kinetics and Mechanism of the Oxidation of HSO3- by O2. 1. The Uncatalyzed Reaction. *Inorg. Chem.* **34**, 4543–4553.

Cooper G.W., Thiemens M. H. and Jackson T. L. (1997) Sulfur and Hydrogen Isotope Anomalies in Meteorite Sulfonic Acids, *Science.* **277**, 1072–1074.

Crabtree K. N., Martinez O., Barreau L., Thorwirth S. and McCarthy M. C. (2013) Microwave detection of sulfoxylic acid (HOSOH). *J. Phys. Chem. A* **117**, 3608–3613.

Craig H. (1957) Isotopic standards for carbon and oxygen and correction factors for mass-spectrometric analysis of carbon dioxide. *Geochim. Cosmochim. Acta* **12**, 133–149.

Cramer C.J. (2002) *Essentials of Computational Chemistry: Theories and Models*. Jon Wiley & Sons, New York.

Czarnacki M. and Hałas S. (2012) Ab initio calculations of sulfur isotope fractionation factor for H2S in aqua–gas system. *Chem. Geol.* **318–319**, 1–5.

Deines P. (2003) A note on intra-elemental isotope effects and the interpretation of non-mass-dependent isotope variations. *Chem. Geol.* **199**, 179–182.

Edwards K.J. (2004) Formation and degradation of seafloor hydrothermal sulfide deposits. In Sulfur Biogeochemistry – Past and Present (eds. J.P. Amend, K.J. Edwards, T.W. Lyons). GSA Special Papers 379, pp. 83-96.

Eldridge D.L., Guo W., and Farquhar J. Theoretical estimates of equilibrium sulfur isotope effects in aqueous sulfur systems: Highlighting the role of isomers in the sulfite and sulfoxylate systems. *Geochim. Cosmochim. Acta* (submitted)

Ellis A.J. and Giggenbach W. (1971) Hydrogen sulphide ionization and sulphur hydrolysis in high temperature solution. *Geochim. Cosmochim. Acta* **35**, 247-260.

Eriksen T.E. (1972a) Sulfur Isotope Effects. I. The Isotopic Exchange Coefficient for the Sulfur Isotopes 34S-32S in the System SO2g-HSO3-aq at 25, 35, and 45 degrees C. *Acta Chem. Scand.* **26**, 573–580.

Eriksen T.E. (1972b) Sulfur Isotope Effects. II. The Isotopic Exchange Coefficient for the Sulfur Isotopes 34S-32S in the System SO2g-Aqueous Solutions of SO2. *Acta Chem. Scand.* **26**, 581–584.

Eriksen T.E. (1972c) Sulfur Isotope Effects. III. Enrichment of 34S by Chemical Exchange Between SO2g and Aqueous Solutions of SO2. *Acta Chem. Scand.* **26**, 975–979.

Eriksen T.E. and Lind J. (1972) Spectrophotometric determination of sulfur-dioxide and thiosulfate in aqueous-solutions of hydrogen sulfite. *Acta Chem. Scand.* **26**, 3325-3332.

Ermatchkov V., Kamps Á. P. S. and Maurer G. (2005) The chemical reaction equilibrium constant and standard molar enthalpy change for the reaction {2HSO3(aq) ⇌ S2O 2-5 (aq) + H2O(1)}: A spectroscopic and calorimetric investigation. *J. Chem. Thermodyn.* **37**, 187–199.

Falk M. and Guguere P.A. (1958) On the nature of sulphurous acid. *Can. J. Chem.* **36**, 1121-1125.

Farantos S., Leisegang E. C., Murrell J. N. and Sorbie K. (1977) Analytical potentials for triatomic molecules from spectroscopic data III. Application to A2B molecules whose surfaces have more than one minimum. *Mol. Phys.* **34**, 947–962.

Farquhar J., Savarino J., Jackson T. L. and Thiemens M. H. (2000a) Evidence of atmospheric sulphur in the martian regolith from sulphur isotopes in meteorites. *Nature* **404**, 50–52.

Farquhar J., Bao H., and Thiemens, M.H. (2000b) Atmospheric Influence of Earth's Earliest Sulfur Cycle. *Science.* **289**, 756–758.

Farquhar J., Savarino J., Airieau S. and Thiemens M. H. (2001) Sulfur isotope effects during SO2 photolysis : Implications for the early atmosphere *J. Geophys. Res.* **106**, 32829–32839.

Farquhar J. and Wing B. A. (2003) Multiple sulfur isotopes and the evolution of the atmosphere. *Earth Planet. Sci. Lett.* **213**, 1–13.

Farquhar J., Johnston D. T., Wing B.A., Habicht K.S., Canfield D. E., Airieau S. and Thiemens M.H. (2003) Multiple sulphur isotopic interpretations of biosynthetic pathways: implications for biological signatures in the sulphur isotope record. *Geobiology* **1**, 27–36.

Farquhar J., Johnston D. T. and Wing B.A. (2007) Implications of conservation of mass effects on mass-dependent isotope fractionations: Influence of network structure on sulfur isotope phase space of dissimilatory sulfate reduction. *Geochim. Cosmochim. Acta* **71**, 5862–5875.

Foresman J.B. and Frisch Æ. (1996) *Exploring Chemistry with Electronic Structure Methods, 2nd Ed.* Gaussian, Inc., Wallingford, CT.

Frisch M. J., Trucks G. W., Schlegel H. B., Scuseria G. E., Robb M. A., Cheeseman J. R., Scalmani G., Barone V., Mennucci B., Petersson G. A., Nakatsuji H., Caricato M., Li X., Hratchian H. P., Izmaylov A. F., Bloino J., Zheng G., Sonnenberg J. L., Hada M., Ehara M., Toyota K., Fukuda R., Hasegawa J., Ishida M., Nakajima T., Honda Y., Kitao O., Nakai H., Vreven T., Montgomery J. A. Jr., Peralta J. E., Ogliaro F., Bearpark M., Heyd J.J., Brothers E., Kudin K. N., Staroverov V. N., Keith T.,Kobayashi R., Normand J., Raghavachari K., Rendell A., Burant J. C., Iyengar S. S., Tomasi J., Cossi M., Rega N., Millam J. M., Klene M., Knox J. E., Cross J. B., Bakken V., Adamo C., Jaramillo J., Gomperts R., Stratmann R. E., Yazyev O., Austin A. J., Cammi R., Pomelli C., Ochterski J. W., Martin R. L., Morokuma K., Zakrzewski V. G., Voth G. A., Salvador P., Dannenberg J.J., Dapprich S., Daniels A. D., Farkas Ö., Foresman J.B., Ortiz J. V., Cioslowski J., Fox D. J. (2010) Gaussian 09, Revision B.01**.** Gaussian, Inc., Wallingford CT.

Fry B., Gest H. and Hayes J.M. (1984) Isotope effects associated with the anaerobic oxidation of sulfide by the purple photosynthetic bacterium, Chromatium vinosum. *FEMS Microbio. Letters*. **22**, 283-287.

Fry B., Gest H. and Hayes J. M. (1986) Sulfur isotope effects associated with protonation of HS- and volatilization of H2S. *Chem. Geol. Isot. Geosci. Sect.* **58**, 253–258.

Fry B., Ruf W., Gest H. and Hayes J. M. (1988) Sulfur isotope effects associated with oxidation of sulfide by O2 in aqueous solution. *Chem. Geol.* **73**, 205–210.

Gao X. and Thiemens M. H. (1993) Isotopic composition and concentration of sulfur in enstatite and ordinary chondrite. *Geochim. Cosmochim. Acta* **57**, 3171–3176.

Gerding H. and Nijveld W.J. (1936) Raman Spectrum of Gaseous and Liquid Sulphur Dioxide and its Solutions in Water. *Nature* **137**, 1070-1070.

Geßler R. and Gehlen K.V. (1986) Investigation of sulfur isotope fractionation between H2S gas and aqueous solutions. *Fresenius' Zeitschrift für Anal. Chemie* **324**, 130–136.

Gleeson D. F., Pappalardo R. T., Anderson M. S., Grasby S. E., Mielke R. E., Wright K. E. and Templeton A.S. (2012) Biosignature Detection at an Arctic Analog to Europa. *Astrobiology* **12**, 135–150.

Goldberg R.N. and Parker V.B. (1985) Thermodynamics of solution of SO2(g) in water and of aqueous sulfur-dioxide solutions. *J. Res. Nat. B. Stand.* **90**, 341-358.

Golding R.M. (1960) 741. Ultraviolet Absorption Studies of the Bisulphite-Pyrosulphite Equilibrium. *J. Chem. Soc.* 3711–3716.

Grinenko V. A. and Thode H. G. (1970) Sulfur isotope effects in volcanic gas mixtures. *Can. J. Earth Sci.* **7**, 1402–1409.

Harrison A.G. and Thode H. G. (1958) Mechanism of the bacterial reduction of sulphate from isotope fractionation studies. *Trans. Faraday Soc.* **54**, 84.

Hayes E. F. and Pfeiffer G. V. (1968) On the Possible Existence of Double Minima in Potential Energy Surfaces of AB,-Type Molecules'". *J. Am. Chem. Soc.* **90**, 4773–4777.

Hermann B., Kern M., La Pietra L., Simon J. and Einsle O. (2015) The octahaem MccA is a haem c-copper sulfite reductase. *Nature* **520**, 706-709.

Hershey J. P., Plese T. and Millero F. J. (1988) The pK_1* for the dissociation of H_2S in various ionic media. *Geochim. Cosmochim. Acta* **52**, 2047–2051.

Hoffmann M. R. and Lim B. C. (1979) Kinetics and mechanism of the oxidation of sulfide by oxygen: catalysis by homogeneous metal-phthalocyanine complexes. *Environ. Sci. Technol.* **13**, 1406–1414.

Horner D. A. and Connick R. E. (1986) Equilibrium quotient for the isomerization of bisulfite ion from HSO3- to SO3H-. *Inorg. Chem.* **25**, 2414–2417.

Horner D. A. and Connick R. E. (2003) Kinetics of oxygen exchange between the two isomers of bisulfite ion, disulfite ion (S2O52-), and water as studied by oxygen-17 nuclear magnetic resonance spectroscopy. *Inorg. Chem.* **42**, 1884–1894.

Hulston J. R. and Thode H. G. (1965) Variations in the S33, S34, and S36 Contets of Meteorites and Their Relation to Chemical and Nuclear Effects. *J. Geophys. Res.* **70**, 3475–3484.

Johnston D. T. (2011) Multiple sulfur isotopes and the evolution of Earth' s surface sulfur cycle. *Earth Sci. Rev.* **106**, 161–183.

Johnston D. T., Farquhar J. and Canfield D. E. (2007) Sulfur isotope insights into microbial sulfate reduction : When microbes meet models. *Geochim. Cosmochim. Acta.* **71**, 3929–3947.

Johnston D. T., Farquhar J., Wing B. A., Kaufman A. J., Canfield D. E. and Habicht K. S. (2005) Multiple sulfur isotope fractionations in biological systems: A case study with sulfate reducers and sulfur disproportionators. *Amer. J. Sci.* **305**, 645–660.

Jørgensen B.B. (1977) The sulfur cycle of a coastal marine sediment (Limfjorden, Denmark). *Limn. Oceanog.* **22**, 814–832.

Jørgensen B.B. (1982) Mineralization of organic matter in the sea bed – the role of sulphate reduction. *Nature* **296**, 643–645.

Jørgensen B.B. (1982) Mineralization of organic matter in the sea bed – the role of sulphate reduction. *Nature* **296**, 643–645.

Jørgensen B.B. (1990) A thiosulfate shunt in the sulfur cycle of marine sediments. *Science* **249**, 152–154.

Jørgensen B.B. and Nelson D.C. (2004) Sulfide oxidation in marine sediments: Geochemistry meets microbiology. In *Sulfur Biogeochemistry – Past and Present* (eds. J.P. Amend, K.J. Edwards, T.W. Lyons). GSA Special Papers **379**, pp. 63-81.

Jørgensen B.B., Bang M. and Blackburn T. H. (1990) Anaerobic Mineralization in Marine-Sediments From the Baltic-Sea-North-Sea Transition. *Mar. Ecol. Ser.* **59**, 39–54.

Jørgensen B.B., Fossing H., Wirsen C. O. and Jannasch H. W. (1991) Sulfide oxidation in the anoxic Black Sea chemocline. *Deep Sea Res. Part A. Oceanogr. Res. Pap.* **38**, S1083–S1103.

Jørgensen B.B., and Nelson D.C. (2004) Sulfide oxidation in marine sediments: Geochemistry meets microbiology. In Sulfur Biogeochemistry – Past and Present (eds. J.P. Amend, K.J. Edwards, T.W. Lyons). GSA Special Papers **379**, pp. 63-82

Kamyshny A., Druschel G., Mansaray Z. F. and Farquhar J. (2014) Multiple sulfur isotopes fractionations associated with abiotic sulfur transformations in Yellowstone National Park geothermal springs. *Geochem. Trans.* **15**, 7.

Kamyshny A., Goifman A., Gun J., Rizkov D. and Lev O. (2004) Equilibrium distribution of polysulfide ions in aqueous solutions at 25 degrees C: a new approach for the study of polysulfides' equilibria. *Environ. Sci. Technol.* **38**, 6633–6644.

Labidi J., Farquhar J., Alexander C. M. O., Eldridge D. L. and Oduro H., Mass independent sulfur isotope signatures in CMs: Implications for the sulfur chemistry in the early solar system. *Geochim. Cosmochim. Acta*. (submitted)

Leavitt W. D., Bradley A. S., Santos A. A., Pereira I. A. C. and Johnston D. T. (2015) Sulfur isotope effects of dissimilatory sulfite reductase. *Front. Microbiol.* **6**, 1–20.

Leavitt W. D., Halevy I., Bradley A. S. and Johnston D. T. (2013) Influence of sulfate reduction rates on the Phanerozoic sulfur isotope record. *Proc. Natl. Acad. Sci. U. S. A.* **110**, 11244–9.

Lee C., Yang W. and Parr R. G. (1988) Development of the Colle– Salvetti correlation-energy formula into a functional of the electron-density. *Phys. Rev. B* **37**, 785–789.

Li X. and Liu Y. (2011) Equilibrium Se isotope fractionation parameters: A first-principles study. *Earth Planet. Sci. Lett.* **304**, 113–120.

Li X., Zhao H., Tang M. and Liu Y. (2009) Theoretical prediction for several important equilibrium Ge isotope fractionation factors and geological implications. *Earth Planet. Sci. Lett.* **287**, 1–11.

Littlejohn D., Walton S. A. and Chang S.-G. (1992) A Raman Study of the Isomers and Dimer of Hydrogen Sulfite Ion. *Appl. Spec.* **46**, 848–851.

Liu Q., Tossell J.A. and Liu Y. (2010) On the proper use of the Bigeleisen-Mayer equation and corrections to it in the calculation of isotopic fractionation equilibrium constants. *Geochim. Cosmochim. Acta* **74**, 6965–6983.

Luther G. W. (1991) Pyrite synthesis via polysulfide compounds. *Geochim. Cosmochim. Acta* **55**, 2839–2849.

Luther G. W. (2010) The role of one- and two-electron transfer reactions in forming thermodynamically unstable intermediates as barriers in multi-electron redox reactions. *Aquat. Geochemistry* **16**, 395–420.

Luther G. W., Findlay A. J., MacDonald D. J., Owings S. M., Hanson T. E., Beinart R. A. and Girguis P. R. (2011) Thermodynamics and kinetics of sulfide oxidation by oxygen: A look at inorganically controlled reactions and biologically mediated processes in the environment. *Front. Microbiol.* **2**, 1–9.

Lyons D. and Nickless G. (1968) The lower oxy-acids of sulphur. In *Inorganic Sulfur Chemistry* (ed. G. Nickless), pp. 509-534. Elsevier, New York.

Macalady J. L., Lyon E. H., Koffman B., Albertson L. K., Meyer K., Galdenzi S. and Mariani S. (2006) Dominant microbial populations in limestone-corroding stream biofilms, Frasassi cave system, Italy. *Appl. Environ. Microbiol.* **72**, 5596–5609.

Makarov S. V., Kudrik E. V., van Eldik R. and Naidenko E. V. (2002) Reactions of methyl viologen and nitrite with thiourea dioxide. New opportunities for an old reductant. *J. Chem. Soc. Dalt. Trans.*, 4074–4076.

Makarov S. V., Sal'nikov D. S. and Pogorelova A. S. (2010) Acid-base properties and stability of sulfoxylic acid in aqueous solutions. *Russ. J. Inorg. Chem.* **55**, 301–304.

Marcus R. A. and Rice O. K. (1951) The kinetics of the recombination of methyl radicals and iodine atoms. *J. Phys. Colloid Chem* **55**, 894–908.

Mariotti A., Germon J. C., Hubert P., Kaiser P., Letolle R., Tardieux a. and Tardieux P. (1981) Experimental determination of nitrogen kinetic isotope fractionation: Some principles; illustration for the denitrification and nitrification processes. *Plant Soil* **62**, 413–430.

Martell A.E. and Smith R.M. (1982) *Critical Stability Constants, Volume 5: First Supplement*. Springer Science+Business Media, New York.

Matsuhisa Y., Goldsmith J. R. and Clayton R. N. (1978) Mechanisms of hydrothermal crystallization of quartz at 250°C and 15 kbar. *Geochim. Cosmochim. Acta* **42**, 173–182.

McLaughlan S. D. and Marshall D. J. (1970) Paramagnetic Resonance of Sulfur Radicals in Synthetic Sodalites. *J. Phys. Chem.* **74**, 1359–1363.

McQuarrie D.A. (2000) *Statistical Mechanics*. University Science Books, Sausalito, California.

Migdisov A. A., Williams-Jones A. E., Lakshtanov L. Z. and Alekhin Y. V. (2002) Estimates of the second dissociation constant of H2S from the surface sulfidation of crystalline sulfur. *Geochim. Cosmochim. Acta* **66**, 1713–1725.

Miller M. F. (2002) Isotopic fractionation and the quantification of 17O anomalies in the oxygen three-isotope system: An appraisal and geochemical significance. *Geochim. Cosmochim. Acta* **66**, 1881–1889.

Millero F. J., Hubinger S., Fernandez M., and Garnett S. (1987a) Oxidation of H2S in seawater as a function of temperature, pH, and ionic strength. *Environ. Sci. Tech.* **21**, 439-443.

Millero F. J., Sotolongo S. and Izaguirre M. (1987b) The oxidation kinetics of Fe(II) in seawater. *Geochim. Cosmochim. Acta* **51**, 793–801.

Millero F. J., Hershey J. P., Johnson G. and Zhang J.-Z. (1989) The Solubility of SO2 and the Dissociation of H2S03 in NaC1 Solutions. *J. Atmos. Chem.* **8**, 377–389.

Millero F. J. (1991a) The oxidation of H2S in the Chesapeake Bay. *Estuar. Coast. Shelf Sci.* **33**, 521–527.

Millero F. J. (1991b) The oxidation of H2S in Black Sea waters. *Dee-Sea Res.* **38**, S1139-S1150.

Millero F. J. (1991c) The oxidation of H2S in Framvaren Fjord. *Limnol. Oceanogr.* **36**, 1007–1014.

Napolion B., Huang M. J. and Watts J. D. (2008) Coupled-cluster study of isomers of H2SO2. *J. Phys. Chem. A* **112**, 4158–4164.

Norrish, R.G.W. and Oldershaw, G.A. (1959) The Absorption Spectrum of SO and the Flash Photolysis of Sulphur Dioxide and Sulphur Trioxide, *Proc. Royal Soc. Lond. Series A-Math. and Phys. Sci.*, **249**,1364-5021.

O'Brien D. J. and Birkner F. B. (1977) Kinetics of oxygenation of reduced sulfur species in aqueous solution. *Environ. Sci. Technol.* **11**, 1114–1120.

Oduro H., Kamyshny A., Guo W. and Farquhar J. (2011) Multiple sulfur isotope analysis of volatile organic sulfur compounds and their sulfonium precursors in coastal marine environments. *Mar. Chem.* **124**, 78–89.

Ohmoto H. and Lasaga A. C. (1982) Kinetics of reactions between aqueous sulfates and sulfides in hydrothermal systems. *Geochim. Cosmochim. Acta* **46**, 1727–1745.

Oliveira T. F., Vonrhein C., Matias P. M., Venceslau S. S., Pereira I. a C. and Archer M. (2008) The crystal structure of Desulfovibrio vulgaris dissimilatory sulfite reductase bound to DsrC provides novel insights into the mechanism of sulfate respiration. *J. Biol. Chem.* **283**, 34141–34149.

Ono S., Shanks III W.C., Rouxel O.J., and Rumble D. (2007) S-33 constraints on the seawater sulfate contribution in modern seafloor hydrothermal vent sulfides. *Geochim. Cosmochim. Acta* **71**, 1170–1182.

Orcutt B. N., Sylvan J. B., Knab N. J. and Edwards K. J. (2011) Microbial Ecology of the Dark Ocean above, at, and below the Seafloor. *Microbiol. Mol. Biol. Rev.* **75**, 361–422.

Ostlund H. G. and Alexander J. (1963) Oxidation Rate of Sulfide in Sea Water, A Preliminary Study. *J. Geophys. Res.* **68**, 3995–3997.

Otake T., Lasaga A. C. and Ohmoto H. (2008) Ab initio calculations for equilibrium fractionations in multiple sulfur isotope systems. *Chem. Geol.* **249**, 357–376.

Parey K., Warkentin E., Kroneck P. M. H. and Ermler U. (2010) Reaction cycle of the dissimilatory sulfite reductase from archaeoglobus fulgidus. *Biochemistry* **49**, 8912–8921.

Paris G., Sessions A. L., Subhas A. V. and Adkins J. F. (2013) MC-ICP-MS measurement of 34S and 33S in small amounts of dissolved sulfate. *Chem. Geol.* **345**, 50–61.

Pavlov A. A. and Kasting J. F. (2002) Mass-independent fractionation of sulfur isotopes in Archean sediments: strong evidence for an anoxic Archean atmosphere. *Astrobiology* **2**, 27–41.

Pellerin A., Bui T. H., Rough M., Mucci A., Canfield D. E. and Wing B. A. (2015) Mass-dependent sulfur isotope fractionation during reoxidative sulfur cycling: A case study from Mangrove Lake, Bermuda. *Geochim. Cosmochim. Acta* **149**, 152–164.

Pokrovski G. S. and Dubrovinsky L. S. (2011) The S3- Ion Is Stable in Geological Fluids at Elevated Temperatures and Pressures. *Science.* **331**, 1052–1054.

Pokrovski G. S. and Dubessy J. (2015) Stability and abundance of the trisulfur radical ion S3 - in hydrothermal fluids. *Earth Planet. Sci. Lett.* **411**, 298–309.

Rees C. E. (1973) A steady-state model for sulphur isotope fractionation in bacterial reduction processes. *Geochim. Cosmochim. Acta* **37**, 1141–1162.

Richet P., Bottinga Y. and Javoy M. (1977) A review of hydrogen, carbon, nitrogen, oxygen, sulphur, and chlorine stable isotope fractionation among gaseous molecules. *Ann. Rev. Earth Planet. Sci.* **5**, 65-110.

Rickard D. and Luther G.W. (2007) Chemistry of iron sulfides. *Chem. Rev.* **107**, 514-562.

Rickard D. and Morse J. W. (2005) Acid volatile sulfide (AVS). *Marine Chem.* **97**, 141-197.

Risberg E. D., Eriksson L., Mink J., Pettersson L. G. M., Skripkin M. Y. and Sandström M. (2007) Sulfur X-ray absorption and vibrational spectroscopic study of sulfur dioxide, sulfite, and sulfonate solutions and of the substituted sulfonate ions X3CSO3- (X = H, Cl, F). *Inorg. Chem.* **46**, 8332–48.

Rodrigues S. P. J., Sabín J. a and Varandas a J. C. (2001) Single-Valued Double Many-Body Expansion Potential Energy Surface of Ground-State SO2. *J. Phys. Chem. A* **106**, 556–562.

Rustad J. R. and Bylaska E. J. (2007) Ab initio calculation of isotopic fractionation in B(OH)3(aq) and BOH4-(aq). *J. Am. Chem. Soc.* **129**, 2222–2223.

Rustad J. R., Bylaska E. J., Jackson V. E. and Dixon D. A. (2010) Calculation of boron-isotope fractionation between B(OH)3(aq) and B(OH)4 -(aq). *Geochim. Cosmochim. Acta* **74**, 2843–2850.

Rustad J. R., Nelmes S. L., Jackson V. E. and Dixon D. A. (2008) Quantum-Chemical Calculations of Carbon-Isotope Fractionation in CO 2 (g), Aqueous Carbonate Species, and Carbonate Minerals. **2**, 542–555.

Sakai H. (1968) Isotopic properties of sulfur compounds in hydrothermal processes. *Geochem. J.* **2**, 29–49.

Santos A. A., Venceslau S. S., Grein F., Leavitt W. D., Dahl C., Johnston D. T. and Pereira I. A. C. (2015) A protein trisulfide couples dissimilatory sulfate reduction to energy conservation. *Science (80-.).* **350**, 1541–1545.

Schauble E.A. (2004) Applying Stable Isotope Fractionation Theory to New Systems. *Rev. Mineral. Geochemistry* **55**, 65–111.

Schippers A. (2004) Sulfide oxidation in marine sediments: Geochemistry meets microbiology. In Sulfur Biogeochemistry – Past and Present (eds. J.P. Amend, K.J. Edwards, T.W. Lyons). GSA Special Papers 379, pp. 49-62

Schoonen M. A. A. and Barnes H. L. (1988) An approximation of the second dissociation constant for hydrogen sulfide. *Geochim. Cosmochim. Acta* **52**, 649–654.

Scott K. M., Lu X., Cavanaugh C. M. and Liu J. S. (2004) Optimal methods for estimating kinetic isotope effects from different forms of the Rayleigh distillation equation. *Geochim. Cosmochim. Acta* **68**, 433–442.

Shen Y. and Buick R. (2004) The antiquity of microbial sulfate reduction. *Earth-Science Rev.* **64**, 243–272.

Shen Y., Buick R. and Canfield D. E. (2001) Isotopic evidence for microbial sulphate reduction in the early Archaean era. *Nature* **410**, 77–81.

Shen Y., Farquhar J., Masterson A., Kaufman A. J. and Buick R. (2009) Evaluating the role of microbial sulfate reduction in the early Archean using quadruple isotope systematics. *Earth Planet. Sci. Lett.* **279**, 383–391.

Sim M. S., Bosak T. and Ono S. (2011a) Large Sulfur Isotope Fractionation Does Not Require Disproportionation. *Science* **333**, 74–77.

Sim M. S., Ono S., Donovan K., Templer S. P. and Bosak T. (2011b) Effect of electron donors on the fractionation of sulfur isotopes by a marine Desulfovibrio sp. *Geochim. Cosmochim. Acta* **75**, 4244–4259.

Simons J. (1991) An experimental chemist's guide to ab initio quantum chemistry. *J. Phys. Chem.* **95**, 1017–1029.

Steiger T. and Steudel R. (1992) Sulfur-Compounds. 149. Structures, relative stabilities and vibrational-spectra of several isomeric forms of sulphoxylic acid (H2SO2) and its anion (HSO2-)- An ab initio study. *J. Molec. Struct. (THERMOCHEM.)* **257**, 313-323.

Steudel R. and Prenzel A. (1989) Raman Spectroscopic Discovery of the Hydrogenthiosulphate Anion, HSSO3-, in Solid NH4HS2O3 [1]. *Z. Naturforsch., B: Chem. Sci.* **44**, 1499-1502.

Steudel R. and Steudel Y. (2009) Microsolvation of thiosulfuric acid and its tautomeric anions [HSSO 3]- and [SSO2(OH)]- studied by B3LYP-PCM and G3X(MP2) calculations. *J. Phys. Chem. A* **113**, 9920–9933.

Svarovsky S. A., Simoyi R. H. and Makarov S. V. (2001) A possible mechanism for thiourea-based toxicities: Kinetics and mechanism of decomposition of thiourea dioxides in alkaline solutions. *J. Phys. Chem. B* **105**, 12634–12643.

Swain C. G., Stivers E. C., Reuwer Jr. J. F. and Schaad L. J. (1958) Use of hydrogen isotope effects to identify the attacking nucleophile in the enolization of ketones catalyzed by acetic acid. *J. Am. Chem. Soc.* **80**, 5885–5893.

Syverson D. D., Ono S., Shanks W. C. and Seyfried W. E. (2015) Multiple sulfur isotope fractionation and mass transfer processes during pyrite precipitation and recrystallization: An experimental study at 300 and 350°C. *Geochim. Cosmochim. Acta* **165**, 418–434.

Szaran J. (1996) Experimental investigation of sulphur isotopic fractionation between dissolved and gaseous H2S. *Chem. Geol.* **127**, 223–228.

Templeton A.S., Knowles E.J., Eldridge D.L., Arey B.W., Dohnalkova A.C., Webb S.M., Bailey B.E., Tebo B.M., and Staudigel H. (2009) A seafloor microbial biome hosted within incipient ferromanganese crusts. *Nature Geoscience* **2**, 872-876.

Thode H. G., Cragg C. B., Hulston J. R. and Rees C. E. (1971) Sulphur isotope exchange between sulphur dioxide and hydrogen sulphide. *Geochim. Cosmochim. Acta* **35**, 35–45.

Tossell J. A. (1997) Theoretical studies on possible sulfur oxides with +2 oxidation states in aqueous solution. *Chem. Geol.* **141**, 93–103.

Ueno Y., Ono S., Rumble D. and Maruyama S. (2008) Quadruple sulfur isotope analysis of ca. 3.5Ga Dresser Formation: New evidence for microbial sulfate reduction in the early Archean. *Geochim. Cosmochim. Acta* **72**, 5675–5691.

Urey H.C. (1947) The thermodynamic properties of isotopic substances. *J. Chem. Soc. (Lond.)*, 562-581.

Uyama F., Chiba H., Kusakabe M., and Sakai H. (1985) Sulfur isotope exchange reactions in the aqueous system: thiosulfate-sulfide-sulfate at hydrothermal temperature. *Geochem. J.* **19**, 301-315.

Vairavamurthy A., Manowitz B., Luther G. W. and Jeon Y. (1993) Oxidation-State of Sulfur in Thiosulfate and Implications for Anaerobic Energy-Metabolism. *Geochim. Cosmochim. Acta* **57**, 1619–1623.

Vairavamurthy M.A. and Zhou W. (1995) Characterization of a transient +2 sulfur oxidation state intermediate from the oxidation of aqueous sulfide. In *Geochemical Transformations of Sedimentary Sulfur* (eds. M.A. Vairavamurthy and M.A.A. Schoonen). American Chemical Society, Washington, D.C. pp. 280-292.

Vazquez F., Zhang J.-Z. and Millero F. J. (1989) Effect of Metals on the Rate of the Oxidation of H2S in Seawater. *Geophys. Res. Lett.* **16**, 1363–1366.

Voegele A. F., Tautermann C. S., Loerting T. and Liedl K. R. (2003) On the Formation of the Sulfonate Ion from Aqueous SO2 Solution. **3**, 1–9.

W. F. Giggenbach (1970) The blue solutions of sulphur in oleum, *J. Chem. Soc. D-Chem. Comm*., **14**, 0577-6171.

Wacey D., Kilburn M. R., Saunders M., Cliff J. and Brasier M. D. (2011) Microfossils of sulphur-metabolizing cells in 3.4-billion-year-old rocks of Western Australia. *Nat. Geosci.* **4**, 698–702.

Wacey D., McLoughlin N., Whitehouse M. J. and Kilburn M. R. (2010) Two coexisting sulfur metabolisms in a ca. 3400 Ma sandstone. *Geology* **38**, 1115–1118.

Williamson M.A. and Rimstidt J. D. (1992) Correlation between structure and thermodynamic properties of aqueous sulfur species. *Geochim. Cosmochim. Acta* **56**, 3867–3880.

Wing B. A. and Halevy I. (2014) Intracellular metabolite levels shape sulfur isotope fractionation during microbial sulfate respiration. *Proc. Natl. Acad. Sci.* **111**, 18116–18125.

Wolfsberg M., Van Hook W.A., Paneth P., Rebelo L.P.N. (2010) *Isotope Effects in the Chemical, Geological, and Bio Sciences*. Springer, New York.

Xu Y., Schoonen M.A.A., Nordstrom D. K., Cunningham K. M. and Ball J. W. (2000) Sulfur geochemistry of hydrothermal waters in Yellowstone National Park, Wyoming, USA. II. Formation and decomposition of thiosulfate and polythionate in Cinder Pool. *J. Volcanol. Geotherm. Res.* **97**, 407–423.

Xu Y., Schoonen M. A. A., Nordstrom D. K., Cunningham K. M. and Ball J. W. (1998) Sulfur geochemistry of hydrothermal waters in Yellowstone National Park: I. The origin of thiosulfate in hot spring waters. *Geochim. Cosmochim. Acta* **62**, 3729–3743.

Yao W. and Millero F. J. (1996) Oxidation of hydrogen sulfide by hydrous Fe(III) oxides in seawater. *Mar. Chem.* **52**, 1–16.

Yiin B.S., Walker D.M., and Margerum D.W. (1987) Non-Metal Redox Kinetics General-Acid-Assisted Reactions of Chloramine with Sulfite and Hydrogen Sulfite. *Inorg. Chem.* **26**, 3435-3441.

Young E. D., Galy A. and Nagahara H. (2002) Kinetic and equilibrium mass-dependent isotope fractionation laws in nature and their geochemical and cosmochemical significance. *Geochim. Cosmochim. Acta* **66**, 1095–1104.

Zachariasen W.H. (1932) The crystal lattice of potassium pyrosulphite, K2S2O5, and the structure of the pyrosulphite group. *Phys. Rev.* **40**, 923.

Zeebe R. E. (2009) Hydration in solution is critical for stable oxygen isotope fractionation between carbonate ion and water. *Geochim. Cosmochim. Acta* **73**, 5283–5291.

Zerkle A. L., Farquhar J., Johnston D. T., Cox R. P. and Canfield D. E. (2009) Fractionation of multiple sulfur isotopes during phototrophic oxidation of sulfide and elemental sulfur by a green sulfur bacterium. *Geochim. Cosmochim. Acta* **73**, 291–306.

Zerkle A. L., Kamyshny A., Kump L. R., Farquhar J., Oduro H. and Arthur M. A. (2010) Sulfur cycling in a stratified euxinic lake with moderately high sulfate: Constraints from quadruple S isotopes. *Geochim. Cosmochim. Acta* **74**, 4953–4970.

Zhang J.-Z. and Millero F. J. (1993) The products from the oxidation of H2S in seawater. *Geochim. Cosmochim. Acta* **57**, 1705–1718.

Zhang Z. and Ewing G. E. (2002) Infrared spectroscopy of SO2 aqueous solutions. *Spectrochim. Acta - Part A Mol. Biomol. Spectrosc.* **58**, 2105–2113.

Zmolek P., Xu X., Jackson T., Thiemens M. H. and Trogler W. C. (1999) Large Mass Independent Sulfur Isotope Fractionations during the Photopolymerization of 12CS2 and 13CS2. *J. Phys. Chem. A* **103**, 2477–2480.

Zopfi J., Ferdelman T.G. and Fossing H. (2004) Distribution and fate of sulfur intermediates—sulfite, tetrathionate, thiosulfate, and elemental sulfur—in marine sediments. In Sulfur Biogeochemistry – Past and Present (eds. J.P. Amend, K.J. Edwards, T.W. Lyons). GSA Special Papers 379, pp. 97-116.